Final Report

Skymaster Flying Propulsion Testbed

AE3200: Design Synthesis

DSE Group 25

Delft University of Technology

TU Delft

Final Report
Skymaster Flying Propulsion Testbed

by

DSE Group 25

Student Name	Student Number
Andrea Sepulcri	4803493
Chiel van Baardwijk	4652347
Eilidh Radcliff	4667549
Famke Wilmink	4545958
Fredrik Rhenman	4791576
Max Mckenzie	4845730
Ondřej Dvořák	4782798
Stijn van den Heuvel	4864670
Victor Petit	4858522

Instructors: Dr. ir. A. C. in 't Veld, G. van Helden, Ir. L. J. Castellanos
Institution: Delft University of Technology
Place: Faculty of Aerospace Engineering, Delft

Project duration: April 19, 2021 – July 2, 2021

Cover Image: Cessna Skymaster N4207X, DEAC

TU Delft

Preface

This report was written by a group of nine aerospace engineering students at the Delft University of Technology. As part of the Design Synthesis Exercise (DSE), we designed the modifications to a Cessna 337F Skymaster so that it may be retrofitted with an experimental engine and data acquisition system for research into sustainable propulsion systems. The Dutch Electric Aviation Centre (DEAC)'s goal is to use the modified Cessna Skymaster in collaboration with the Delft University of Technology and other research and education institutions.

Readers are assumed to have a basic understanding of flight performance, structural analysis and algebra. For those who are particularly interested in the analysis of different designs are suggested to read Chapter 10. Those who are more interested in the results of the final design are referred to Chapter 11.

We would like to express our gratitude towards Dr. Alexander in 't Veld for sharing his wisdom and continuous support as well as offering us the opportunity to visit the aircraft in Teuge, as well as to our coaches, Leonardo Castellanos and Gitte van Helden, who have been invaluable in providing feedback on reports and steering us in the right direction. The enthusiasm and sincerity of all three has been a consistent source of motivation throughout the project and working with them was a genuine pleasure. We would also like to mention Fred den Toom, Menno Klaassen, Joris Melkert and Bieke von den Hoff who have guided us by sharing their hands-on experience, for which we are very thankful. Their knowledge and intuition allowed us to overcome obstacles when other sources failed. Finally, we would like to thank Fernando Corte Vargas for his extremely pragmatic and useful insights. On many occasions it helped us to clear up doubts and regain focus.

DSE Group 25
Delft, June 2021

Nomenclature

Abbreviation	Definition
A/C	Aircraft
AC	Alternating Current
ACS	Aerodynamics, Stability & Control department
ADAHRS	Air Data, Attitude and Heading Reference System
AMC	Acceptable Means of Compliance
ATC	Air Traffic Control
AWG	American Wire Gauge
BD	Block Diagram
BMS	Battery Management System
CAD	Computer Aided Design
CH	Chairman
CVT	Continuously Variable Transmission
D&D	Design & Development
DC	Direct Current
DEAC	Dutch Electric Aviation Centre
DOA	Design Organisation Approval
DOT	Design Option Tree
DSE	Design Synthesis Exercise
DSM	Structures & Materials department
EASA	European Aviation Safety Agency
EUR	Euro's
FAA	Federal Aviation Agency
FBS	Functional Breakdown Structure
FFBD	Functional Flow Block Diagram
GPS	Global Positioning System
HE	Heat exchanger
H/W	Hardware
ICAO	International Civil Aviation Organisation
ICE	Internal Combustion Engine
ILT	Inspectie Leefomgeving en Transport
INST	Instrumentation department
ISA	International Standard Atmosphere
MAC	Mean Aerodynamic Chord
MIG	Metal Inert Gas
MNS	Mission Need Statement
MSL	Mean Sea Level
MTOW	Maximum Take-Off Weight
NAA	National Aviation Authority
NLR	The Royal Netherlands Aerospace Centre
OFBD	Operational Flow Block Diagram
OPS	Operations, sustainability & certification department
PERF	Flight performance department
PDS	Power Distribution System
PM	Project Manager
PMAD	Power Management and Distribution System
POB	Persons On Board
POS	Project Objective Statement
PROP	Propulsion department
PtF	Permit to Fly
QCM	Quality Control Manager
RDT	Requirement Discovery Tree
RM	Risk Manager
S/W	Software
SE	Systems Engineer
SEC	Secretary
SFPT	Skymaster Flying Propulsion Testbed
SM	Sustainability Manager
SMTB	SkyMaster TestBed
STC	Supplemental Type Certificate
SWOT	Strength, Weakness, Opportunity, and Threat
TBD	To Be Determined
TCDS	Type Certificate Data Sheet
TIG	Tungsten Inert Gas
US	United States
V&V	Verification & Validation
WBS	Work Breakdown Structure
WFD	Work Flow Diagram

Contents

Executive Overview

Preliminary Analysis - The report starts with a preliminary analysis which serves to summarise the result of previous phases of the project. First a market analysis is performed to identify stakeholders and participants of the project, as well as to establish their needs and expectations. This is followed by an initial list of prospective propulsion solutions. Finally, the chapter is concluded by listing a refined list of requirements that govern the design and the trade-off results of the previous phase of the project.

Design Methodology - The design methodology includes an introduction to the project approach. Next, there is an introduction to the three technical departments and the budget breakdown is included as this was used to allocate resources to the technical departments during the design process. Lastly, the verification and validation procedures used throughout the project are detailed.

Sustainable Development Strategy - Sustainability is a very diverse matter including financial, environmental and social sustainability. Circularity has been at the core of the sustainable development strategy, in which lean manufacturing, reuse and recycling are key. Noise, modifications and emissions were all considered in the design choices as well as the application of sustainable materials. An end-of-life and maintenance plan have been created as a basis for the continuation of the sustainable approach to the project.

Technical Risk Assessment - A technical risk assessment is conducted on the aircraft with respect to the modified parts. This includes operational, schedule and design risks. From the determination of risk, mitigation strategies are implemented and the effect of those are studied to determine if the risks are suitable enough to proceed. The effect of the mitigation strategies are also considered, to implement impactful strategies. Thirteen risks where identified in total and a couple of risk requirements stem from these risk which will influence the design.

Propulsion System Selection - The propulsion selection is driven by the endurance requirement, namely that the experimental engine should be able to operate for one hour of cruise, and the maximum rated power to be tested by the engine. First, the two most promising engines are selected from a preliminary list of engines that would be able to meet a specified climb requirement. This leads to the Emrax 348 and Magni250, for which plans exist in the near future to be implemented in electric aircraft. These engines are respectively rated at $210\ kW$ and $280\ kW$ continuous power. It is chosen to analyse both a battery- and hydrogen fuel cell-powered system. The systems are sized assuming cruise occurs at $5000\ ft$ altitude, at $150\ mph$ and $2500\ RPM$ and using 75% of available front propeller power.

It is found that the aircraft would require six PB345V124E-L battery packs to operate for at least an hour. This limits the maximum engine power to be tested to $250\ kW$, lower than that of the Magni250. The maximum total mass of the battery-powered electrical system then becomes $548\ kg$. It could be possible to add more batteries but this adds considerable complexity and at least $72\ kg$ of mass per battery. The extra batteries would have to be stored in the wings.

The sizing of the hydrogen propulsion system is driven by both the maximum continuous output power of the experimental engine and the endurance requirement. By using the maximum continuous output power of the experimental engine the subsystems can be sized. It is noted that a compressor is required to input ambient sea level pressure air into the fuel cell to maximise its performance. The endurance requirement in combination with the hydrogen required for take-off and climb is used to size the hydrogen tank. It is decided to use cryogenic hydrogen storage due to its good storage performance. In the end two PowerCellution P-Stack fuel cells are integrated into the design, giving a total electric motor output power of $220\ kW$. It is recommended to do additional research into the compressor and cryogenic versus cryo-compressed hydrogen storage. Furthermore, due to its lightweight design, the hydrogen propulsion system can be used to test lower powered electric motors for which a lower MTOW is required.

For the cooling of the components, a liquid cooled system is chosen. This system is split up into two separate cooling system. This is because the hydrogen fuel cell produces tremendously more heat than the engine does in the battery electric configuration. As a result two separate heat exchangers are sized which are implemented in a conventional type liquid cooling system. The system that is used for the battery electric configuration is fixed in the aircraft and the heat exchanger is placed inside a newly designed air duct. This airduct is positioned at the same location of the existing air duct - on top of the aircraft, above the rear engine compartment. The second cooling system is detachable and only used for the hydrogen fuel cell configuration. The heat exchanger for this system is place inside the belly pod on the bottom of the aircraft. Through the use of these two systems the propulsion components can be cooled sufficiently for cruising an hour at 5000 ft altitude.

Structures - The structural modifications focus on two aspects; the motor mounting and the fuel storage. For the motor mounting, it is decided that the structure is divided into two parts; a permanent structure attached to the firewall frame and removable sub-structure that is specific to the motor being tested to allow for a flexible testbed. To achieve this, first, 23 load cases are analysed for various combinations of scenarios taken from EASA Certification Specification (CS23). Next, from research into existing engine mounts, the material steel 4130 is selected for the mounting structure.

An analytical model using a finite element method, specifically the matrix stiffness method, is used to find the stresses and displacements of the elements in the structure. In parallel, this process is verified through unit and solution tests. For validation, the engine mount is modelled in CATIA and finite element analysis is performed to compare the loading of the truss elements and the displacements from the analytical model. Once the model is verified and validated, two new engine mount configurations are modelled and a sensitivity analysis is performed to find the most efficient within the material limitations. From this, engine mount 3 is selected weighing $13.04\ kg$, with a diameter tubing of $2.5\ cm$ and wall thickness, $4.8\ mm$.

For fuel storage two designs of fuel mounts are proposed, one for batteries and the other for hydrogen tanks. The mounts consist of two aluminium plates supported by a steel truss structure. For the battery two rows of three batteries are mounted each on top of the aluminium plate, whereas for hydrogen a single tank is sized an mount to fit between the two aluminium plates. This tank is kept in place by two vertical dividers and the truss structure at either ends of the mount.

To analyse the loads imposed by the fuel mount three types of analysis are performed. The first looks at the effect of the additional weight of the fuel on the entire cross section of the fuselage. Thereafter a local bending analysis is performed on the bottom plate, consisting of two keel beams, to evaluate local normal stresses. Finally, the connection between the fuel mount and the keel beams is analysed by considering a crash load-case in which the fuel is subjected to $19\ g$ forward acceleration. Based on this, the aluminium plates are sized.

Data Acquisition - The panel upgrade that will be implemented in the Skymaster will allow for more sophisticated data acquisition. The data handling is split into the categories of attitude, global positioning, air data and propulsion. Although the first three are very important for safe operations, the latter is critical for the nature of the aircraft being a testbed. Detailed data flow diagrams for the two different possible experimental engine types show that in terms of data handling the hydrogen fuel cell is more complicated. The operating windows and requirements for the data acquisition have been listed as a starting point to work together with an expert on the detailed design of the system.

Final Design - Taking the maximum mass of each component that could be used by both a battery- and hydrogen fuel cell powered system for interchangeability, this leads to a total mass of $1923\ kg$ when using batteries and $1593\ kg$ when using hydrogen fuel cells.

Future Project Development - The operations are separated into two domains, that of the ground station and then that of the Skymaster itself. From there it is further divided into 3 phases: the pre-flight, flight and post-flight operations. Since DEAC are partnered with various companies those connections will be taken advantage of for the operation of the testbed. The modification and maintenance will be conducted by partners Aircraft Maintenance Netherlands and Hangar One. If the need for hydrogen fuel arises due to the installation of hydrogen fuel cells in the testbed, this can be provided by Cleantech Regio partners GldH2. Moreover, an off-the-shelf charging station will be used to charge the batteries.

1 Introduction

Aviation is one of the most challenging sectors to decarbonise due to the stringent mass, volume and safety requirements as well as the necessary certification procedures. The International Civil Aviation Organization (ICAO) forecasted that by 2050 international aviation emissions could triple compared with 2015.[1] To achieve climate neutrality, deals, such as the European Green Deal, have stated the need to reduce transport emissions by 90 % by 2050 (compared to 1990-levels). Regardless, it is apparent that the aviation sector will have to contribute to this reduction.

In collaboration with the Dutch Electric Aviation Centre (DEAC), the aim of this project is to design the necessary modifications to the Cessna Skymaster so that it can be retrofitted with an experimental engine and a data acquisition system for research into alternative propulsion systems. The Cessna Skymaster is a suitable aircraft for our flying testbed due to its unusual configuration, where the two engines are on the centreline of the aircraft, thereby eliminating any yawing tendency of the aircraft in case of an engine failure as experienced by aircraft with conventional on-wing engine installations.

The aim of this report is to detail the process and result of the detailed design phase. This process starts with the results of the trade-off that has been performed in *The Midterm Report* [2]. Added to this, the report also builds on the *Baseline Report* and the *Project Plan* [1], [3]. For the conversion of a Cessna Skymaster into a testbed for experimental engines, the chosen concept was designed in more detail. The Project Objective Statement is to design modifications to the Cessna Skymaster to make it into a testbed for research into alternative propulsion systems by a group of 9 students in the span of 10 weeks.

The report as a whole should be considered in three parts: I) Design Approach, II) Detailed Design and III) Future Development. The first part considers the general methodology of the project and describes the necessary context for the detailed design process. The second describes the actual detailed design process, followed by future development in part III. In Chapter 2 an overview is given of the initial approach to the project. A preliminary design is generated after a concept trade-off has been performed. This is followed by Chapter 3, in which the design methodology is elaborated on in terms of a budget breakdown and defining the technical departments. Chapter 4, in which the certification process is considered, is followed by Chapter 5. In this chapter a detailed analysis is performed on the approach to sustainability after which the eventual design is analysed for its sustainable character. In Chapter 6 a technical risk assessment has been performed in which the risks involved with designing, modifying and operating a test bed are analysed. Following this, in Chapter 7 several subsystems are identified and sized in order to select two specific propulsion systems to be analysed in further detail. These systems is include an experimental engine and several other modifications to the aircraft, which has an effect on the structures, that is discussed in Chapter 8. In Chapter 9 a preliminary outline is given of the data acquisition system in which the application of both engines is considered. The analytical models used to estimate the designs performance will be elaborated on in Chapter 10 after which in Chapter 11 the final design is established by means of resource allocation and cost break-down. The adherence to the project goal and requirements is analysed by using the results of the design tools for a compliance matrix. Finally, in Chapter 12 an overview is given of the work that still needs to be performed before the aircraft can operate as an actual testbed.

[1] https://ec.europa.eu/clima/policies/transport/aviation_en [Accessed June 2021]

Part I

Design Approach

2
Preliminary Analysis

The goal of this chapter is to summarise the steps that were taken in earlier stages of this project, thereby laying a foundation for the detailed design phase described in this report. The previous phase of the project concluded with a preliminary design concept, which was selected through a multi-step process. First a market analysis is described in Section 2.1, which helps to identify important design characteristics for a competitive stake in the market. Thereafter, the identified prospective propulsion solutions are detailed in Section 2.2. In Section 2.3 the required functionalities of aircraft are described, followed by a requirement analysis in Section 2.4. Finally, the concept trade-off and the selected configuration are presented in Section 2.5.

2.1. Market Analysis

This section focuses on performing research into the hybrid flying testbed market. Stakeholders are identified and the market is defined. This is followed by an identification of market participants, as well as a brief case study of a potential competitor. Then, a list of potential clients is identified. Lastly, the aircraft's position in the market is analysed by use of a SWOT analysis and by considering what capabilities the market would require from a flying testbed.

Stakeholder Identification

Before getting an overview of the market it is important to define who the stakeholders are. First and foremost the aircraft is designed for the Dutch Electric Aviation Centre (DEAC). This makes DEAC the most important stakeholder, as they own the aircraft and intend to perform research with it. Furthermore, the TU Delft is a stakeholder as it partners with DEAC for Cessna Skymaster related research projects such as this one.

Other educational institutions are also currently collaborating on this project with DEAC. Firstly, students from the Deltion College will perform the practical work of manufacturing the aircraft.[1] For them the technical contents of this report, in particular regarding production, must be as detailed and accurate as possible. Furthermore, students from the Hogeschool van Amsterdam are researching how the infrastructure at Airport Teuge must be adapted to accommodate aircraft using alternative propulsion systems, including the SFPT.[2] Therefore, the operations phase of the project must be detailed. Lastly, students at Veluws College Walterbosch are performing research into how hydrogen distribution can be optimised at airfields [3]. As such, their research is independent of this project and they are not direct stakeholders. Nevertheless, their research will be relevant for future development of this project.

Other stakeholders are external research parties developing an alternative propulsion system that may be interested in testing this in the SFPT. A closer look on their potential needs is taken in the following sections.

Market Definition

The SFPT serves to fill the need for an aircraft able to perform research into alternative propulsion systems. The market can therefore be defined as follows:

[1] https://deac-teuge.nl/nieuws/artikel-over-bouw-elektrisch-vliegtuig-in-magazine-van-deltion-college-zwolle/ [Accessed June 2021]

[2] https://www.hva.nl/kc-techniek/gedeelde-content/nieuws/nieuwsberichten/2020/01/hva-maakt-stappen-richting-elektrisch-vliegen.html [Accessed June 2021]

[3] https://www.veluwseonderwijsgroep.nl/apeldoorns-technasium-en-deac-gaan-samenwerken/ [Accessed June 2021]

The alternative propulsion system market is considered to be the collection of buyers and sellers who are involved in performing research or acquiring test systems for sustainable propulsion.

The motivation for the project stems from large scale challenges the industry is facing with respect to sustainability and climate change. As a consequence of the widespread growth of air travel future aircraft will be required to be more efficient, a goal that may require the use of radically different propulsion systems. The global pressure for sustainability and reversal of climate change is the driving force behind an increasing amount of research and funding into sustainable air travel.

These driving forces are likely to characterise the industry for the foreseeable future. However, it is still important to to verify that the research to be performed by the SFPT will be worthwhile and contribute to tackling the problems at hand. From 2009 to 2016 the number of electric aircraft increased by 21%. From 2016 until 2019 this grew by 54%. Since then the number of experimental electric aircraft has boomed with new players such as H55 BRM Aero, Ampaire and Magnix setting out to explore the limits of electric propulsion.[4]

Although current technology does not allow for the power-to-weight ratio required to propel full-fledged airliners, sustainable propulsion is increasingly making its way into the world of general aviation. Given these trends, the SFPT's future as a research platform is secure and promising.

Market Participants

The vast majority of the market is dominated by educational and research institutions, such as the Delft University of Technology and the German Aerospace Centre (DLR). These organisations may develop test facilities themselves or have an interest in acquiring systems developed by external parties. In turn, their research facilities are used both for their own research as well as by external parties (clients) to test their own alternative propulsion systems. Note that the definition of the market is not limited to flying testbed systems; among other possibilities for testing alternative propulsion systems are ground-based test facilities such as Rolls Royce's 'Testbed 80' in Derby, UK. These must also be taken into account as market competitors, because a potential client may opt for ground-based facilities if flying testbeds offer no apparent (cost-effective) benefits.

In the lists below, the left-hand side is composed of major European institutions which could have an interest in a flying testbed (as clients) or may look into developing testing facilities themselves (as competitors). The right-hand side list includes existing testbeds/demonstrators that would act as competitors. An analysis of the potential competitors shows that unlike ground-based test facilities, the flying testbeds currently in the market do not allow simple interchangeability of the experimental propulsion system. Therefore, this is a huge gap in the market that the Skymaster Flying Propulsion Testbed (SFPT) can fill. Furthermore, it should be noted that the development of the SFPT is mainly for research purposes. Whereas for the development of a sustainable aircraft with the intention of selling it, an estimation of the market share would be very interesting, it is not relevant for this project. Next to that, there is also no definite way to quantify a market that performs scientific research.

Major European institutions in market
Delft University of Technology
Netherlands Aerospace Centre
German Aerospace Centre
Airbus
Rolls-Royce
Thales
BAE Systems
University of Cambridge

Demonstrators for alternative propulsion
Testbed 80 (Rolls-Royce) - Ground-based
EAS House (Airbus) - Ground-based
SibNIA SuperOx - Flying
E-fan (Airbus) - Flying
Pipistrel Velis Electro - Flying
magniX eCaravan - Flying
VoltAero Cassio - Flying
Ampaire Electric EEL - Flying

Case Study - Airbus EAS House

In this section a closer look is taken at a potential market competitor. As identified in Section 2.1, there are currently no flying testbeds in the market that allow for quick interchangeability. Therefore, a small case study is conducted into a ground-based testbed, namely the Airbus E-Aircraft Systems House

[4] `https://solarimpulse.com/news/electric-planes-how-the-industry-is-preparing-for-the-future` [Accessed April 2021]

(EAS) House. This is a $2500\ m^2$ facility opened in 2016 designed for testing hybrid-electric powertrains. A distinction is made between medium- and high-voltage testing, for helicopter-size and passenger-size aircraft hybrid-electric power systems respectively. At first, the EAS house was used exclusively for Airbus-related projects, such as the since discontinued E-Fan X. However, it has been announced that this will change.[5]

The EAS House offers the advantage of very simple interchangeability, since for example testing of an electric motor can be done by "mounting [it] on one of the EAS test rigs, applying the required sensors and installing cameras to monitor progress".[6] When comparing this to a flying testbed, the entire aircraft system will have to undergo more complicated mounting as well as various (safety) tests and certification procedures before the motor can be tested in flight. To match the advantages of a ground-based testbed, it is therefore imperative that the experimental propulsion system can be mounted on the testbed quickly with few required structural modifications and that ground-based testing procedures do not take too long to go through. These differences between ground-based and flying testbeds are accompanied by higher costs for interchangeability. However, this may be off-set by the advantages of obtaining test data in a real flight profile. Also, as a commercial company Airbus may charge equally high rates regardless. Therefore, it is important that costs are competitive. Although costs of using the EAS house are not published, making comparison of costs very difficult, it is worth noting that the development of the EAS house was a 50 million EUR investment.[6]

Potential Clients

As part of the market analysis it is important to get a scope of any potential customers that might be interested in making use of the SFPT for research purposes. The identified potential customers can be split up into two categories.

The first type of potential customers identified are research institutes currently working on alternative propulsion in aviation. In the section above, a list of major institutes researching this topic is identified. These organisations are all potential clients that might be interested in testing multiple types of propulsion systems in the SFPT, as it allows for relatively fast interchangeability. A closer look is taken at the TU Delft and DLR. At the TU Delft, many research projects are being performed into battery- and hydrogen- powered systems, both using hydrogen fuel cells and internal combustion engines. A large ongoing project is AeroDelft, who are developing a hydrogen powered 2-seat aircraft as a part of Project Phoenix. This aircraft will use a liquid hydrogen fuel cell in combination with an electric motor for propulsion [7]. A smaller prototype of this aircraft will take its first flight July 2021, but the first full-scale flight using liquid hydrogen is planned for 2024. Therefore, the SFPT could provide AeroDelft with the opportunity to test their propulsion system in flight before the full-scale flight to identify potential hazards beforehand.

Furthermore, DLR is considered. The DLR has specialised departments performing research into experimental propulsion systems, namely Component Technologies, Architecture of Propulsion System and Control of Propulsion System which focuses on researching all components of a hybrid-electric powertrain, their interrelations and how they can optimally be controlled. [8] The SFPT could provide these departments with a real environment to validate their theoretical research, as well as providing the opportunity for practical, in-flight research. The DLR also has an ongoing project in this sector, namely the 4-seat HY4 aircraft. Like AeroDelft, this aircraft features an electric motor powered by a hydrogen fuel cell. It has an additional battery to generate extra power if necessary. This year it received a Permit to Fly, many years after its kickoff in 2015 [16]. If the SFPT can offer test flights within weeks or even months of receiving an experimental propulsion unit, it already offers a serious advantage compared to such projects as the DLR HY4. This could be even an interesting option for DLR, as they have plans for developing larger hydrogen-powered aircraft in the future. Also, the HY4 currently uses gaseous

[5] https://www.airbus.com/newsroom/stories/world-class-alternative-propulsion-testing.html [Accessed May 2021]

[6] https://www.airbus.com/newsroom/news/en/2019/10/new-airbus-facility-will-help-zero-emission-technologies-to-take-flight.html [Accessed May 2021]

[7] https://aerodelft.nl/project-phoenix/ [Accessed June 2021]

[8] https://www.dlr.de/el/en/desktopdefault.aspx/tabid-15660/25340_read-64671/ [Accessed June 2021]

hydrogen but plans to switch to liquid hydrogen, which could be tested on the SFPT.[9]

The second type of potential customers considered are engine manufacturers that are developing or have developed an electric engine. These companies might be interested in using the SFPT for in-flight testing of the engine or for certification purposes. Some engine manufactures and engines are listed below along with the reason for their potential interest. A full list of potential engines can be found in Table 2.2.

1. MagniX - MagniX has developed the Magni250 and Magni500 electric engines. Whereas the Magni500 has been implemented in several aircraft, its smaller version, the Magni250, has not been. Since in the SFPT, switching out the engine could be done in relatively short time, this could save time and hence costs for MagniX in the process of in-flight testing. Eviation Alice. It is planned for FAA certification in 2022.
2. Siemens - Siemens SP260D Was originally planned for
3. H3X - H3X has is in the development stage of the HPDM250 engine. For this engine they still have a patent pending and it has no record of being used in any aircraft. H3X claims that the HPDM250 can deliver $250\ kW$ of power while only weighing $15\ kg$.[10]. Since this is a relatively small engine with high potential H3X could benefit from the SFPT. This engine technology is patent pending and not yet used in actual aircraft.

It is found that most research is currently being performed in hydrogen powered systems and battery powered systems. Batteries are designed for use with electrical motors. For hydrogen, most projects currently underway use hydrogen fuel cells connected to hydrogen but there is also some research into ICE engines. Cryogenic hydrogen appears to be the most interesting option. This future potential has also been recognised by a number of companies and organisations, like Airbus with their ZeroE program and student team AeroDelft with their Phoenix program, and CleanSky predicts that liquid hydrogen is the most viable option and is in need of additional research.[11][12][13] Therefore, if these most promising systems can be incorporated into the SFPT design, this greatly expands the list of potential clients.

Market Position

The SFPT competes in a niche market segment of extremely unique products. Almost per definition, test aircraft or facilities are not produced on a large scale and do not provide direct financial gains. Since their value is more abstract and is to be found in the research possibilities that they provide, determining the project's exact profitability is a difficult task. That being said, key features of successful testbeds can be identified. Some of these key features are already given by the user requirements, which mostly coincide with the market requirements (for example, the user has specified the requirement for a data acquisition system, something that is highly desirable in any testbed). In general, the market has two types of requirements:

1. Capability requirements: The testbed will be able to meet the needs of the user.
2. Cost requirements: The testbed will be cost-effective relative to its research output. Although this is difficult to quantify, a cost estimate is made to estimate the required financial resources for the project.

For cost, in general a budget is determined for such a project and research would be financed by the institution funding the project. This budget is then broken down into components following a cost breakdown structure as is later elaborated upon in Section 3.3. For this project, the preliminary budget was not specified, so the budget is estimated based on required costs per lowest level of the cost breakdown.

Due to the relatively easy interchangeability of the SFPT, switching out the engine is a more time effective process, hence reducing the costs. Now the requirements related to cost are highly dependant

[9] https://h2fly.de/ [Accessed June 2021]
[10] https://www.h3x.tech/ [Accessed May 2021]
[11] https://www.airbus.com/innovation/zero-emission/hydrogen/zeroe.html [Accessed June 2021]
[12] https://aerodelft.nl/project-phoenix/ [Accessed June 2021]
[13] https://www.cleansky.eu/news/hydrogen-powered-aviation-preparing-for-take-off [Accessed June 2021]

on the aforementioned institution that is funding the project in the sense that they determine the budget for such a project. As a results of this, the maximum cost of the modifications to the aircraft as well as the the process of interchanging the engine is still to be determined. These market requirements related to cost can be found in Table 2.9 and are denoted by MKT-COST.

As the SFPT project is mainly focused on research, it's priority is not to obtain a large market share. Because of this an estimation of the obtainable market share is omitted. However, it is worth noting that the global more electric aircraft market was valued at $1,809.20 million in 2019, and is projected to reach $4,612.69 million in 2027.[14] This predicted growth suggests an increased demand for testbeds for electric alternative propulsion systems.

The capability requirements stemming from the market depend on the needs of DEAC and on the needs of potential clients. The requirements shown in Table 2.9 are derived from the market analysis performed in this section, and indicate what the SFPT must be capable of to satisfy DEAC and expand the list of potential clients. These requirements supplement the user requirements provided directly by DEAC, which can be found throughout Section 2.4. The requirements in Table 2.9 also include the cost requirements.

Now, to analyse the product-market fit, the strengths, weaknesses, opportunities and threats (SWOT) are identified through means of a SWOT analysis. This is shown in Figure 2.1. Internally, the strengths of a flying testbed include the fact that it produces highly valuable data relative to numerical models. A flying testbed also allows for the aircraft's performance to be measured in real time, something ground-based facilities cannot do. The internal disadvantages are the fact that special pilot training is required and that test aircraft inherently involve more risk than traditional aircraft.

An external advantage of the project is that the aircraft is able to serve as a technology demonstrator. This could lead to government subsidies and commercial investment, putting DEAC at the forefront of a growing industry. External disadvantages are for example that certification may impose additional obstacles and costs on the project (e.g. not being able to fly abroad), and that specialised maintenance is required due to the aircraft's unique configuration. Another potential harmful factor of external origin is the possibility of the research being done leading to a technological dead-end.

	Helpful	Harmful
Internal origin	1) Produces more accurate data than numerical models 2) Performance of the entire aircraft can be measured (e.g. compared to a ground-based engine test facility)	1) Experimental aircraft are inherently more dangerous 2) Special pilot training required
External origin	1) Potential for government subsidies 2) Successful modified design could attract commercial investment 3) Design could lead the way in a growing industry	1) Certification requirements may oppose development 2) Specialised maintenance required to maintain the aircraft

Figure 2.1: SWOT Analysis of the Skymaster Testbed

[14] https://www.alliedmarketresearch.com/more-electric-aircraft-market-A06228 [Accessed June 2021]

2.2. Prospective Propulsion Solutions

To obtain a competitive stake in the market, it is important to identify the range of possible propulsion solutions that the aircraft should be able to test. Namely, this imposes requirements and limitations on the testbed and allows for identification of possible clients. In this section the available energy source options are identified in Section 2.2.1 and an overview of several existing propulsion systems is given in Section 2.2.2.

2.2.1. Energy Source Selection

Several different promising fuel options are recognised for use in aviation [7]. The recognised combinations of engine and energy source are listed in Table 2.1. The use of different fuel has major implications on engine type selection and general aviation is dominated by propeller aircraft due to their high efficiency at low speeds. Therefore only electric motors, reciprocating engines and turboprops are considered further.

Table 2.1: Prospective propulsion solutions

Engine type	Energy source	Converter
Electric	Battery	-
Electric	Hydrogen	Fuel cell
Reciprocating (ICE)	Hydrogen	-
Reciprocating	Bio/Synfuels	-
Turboprop	Hydrogen	-
Turboprop	Bio/Synfuels	-

The potential energy sources shown in Table 2.1 are detailed further in the subsections below.

Batteries

Use of batteries to power electric motors in aircraft is a quickly emerging trend in aviation. For the implementation of electric flight fuel tanks would have to be replaced by batteries. Even though electric flight seems very promising, battery capacity and specific energy specifications have proven to be a limiting factor within the progress of e-flight.

Whereas older aircraft often make use of Nickel Cadmium type batteries, newer ones tend to use Lithium-Ion batteries. One example of this is the Boeing 787 Dreamliner. The battery pack used in the Boeing 787 has a mass of $28.6\ kg$ and a energy capacity of $75\ Ah$ [39]. This means that the battery pack has a specific energy of around $83\ Wh/kg$.[15] This might not be enough to power a large passenger aircraft but it might be an interesting option to look at for the SFPT. One of the benefits of using this battery pack is that is is already certified for use in aircraft. Another Lithium-Ion type battery pack that might be of interest is the Pipistrel PB345V124E-L, which is the best certified battery pack on the market in terms of specific energy ($143.75\ Wh/kg$).[5]

The fact that both the aforementioned battery packs are certified is a great advantage, however battery packs currently used for other applications could also be of interest. The battery pack used for the Tesla Model-S could for instance be considered. The complete battery pack has has a capacity of $85\ kWh$ and a mass of $540\ kg$, giving it a specific energy of $157\ Wh/kg$.[16] For aeronautical application this is rather heavy but the single battery module does have a specific energy of $212\ Wh/kg$ which is higher than battery packs currently being used in the industries. However with corresponding necessary subsystems for integration this energy density decreases. Furthermore, a large downside is of course the fact that these battery packs are not certified for use in aviation.

Hydrogen

The second alternative energy source considered is hydrogen. Hydrogen is a highly promising energy source for aviation, due to its high energy density combined with the fact that it causes very low emissions. Hydrogen can either be used to provide electric power through the use of a fuel cell or it can be used in a reciprocating internal combustion engine (ICE) or turboprop.

[15] https://787updates.newairplane.com/787-Electrical-Systems/Batteries-and-Advanced-Airplanes [Accessed May 2021]

[16] https://en.wikipedia.org/wiki/Tesla_Model_S [Accessed May 2021]

An example of fuel cell use in aviation is the HY4 aircraft. The aircraft flies using an electric engine together with a Lithium Polymer battery and four PEM fuel cells converting hydrogen into electric power.[17] Gaseous hydrogen is stored in fuel tanks which is then led to $42\ kW$ liquid cooled fuel cells. The electricity is then stored in a battery and used for propulsion. An example of a hydrogen ICE in aviation is the Boeing Phantom Eye. For this particular project two 2.3 litre Ford Fusion combustion engines were modified for the use of hydrogen as fuel. Modifying existing conventional fuel engines to run on hydrogen is therefore recognised as an interesting option for the testbed. The hydrogen turboprop is eliminated as a viable option, as turboprops are generally excessive in terms of performance and mass for an aircraft of this size.

Bio/Synfuels
Lastly, biofuels and synfuels are considered. Currently, there is already widespread use of biofuels and synfuels in aviation as drop-in fuels. It is often blended into conventional aircraft fuel and in some countries it is even mandated to use a minimum ratio of bio/synfuels to conventional fuel.[18] Generally, it is preferable to use a blend over pure biofuels and use of this requires no or minimal modifications to the existing aircraft engine and fuel tanks [32]. Furthermore, use of biofuels reduces greenhouse gas emission, but does not eliminate it.[18] As such, biofuels cannot provide the large leaps in sustainability that aviation requires. Therefore, it is recognised that this is not the most interesting option for the flying testbed. Also, it would likely be more economical to test this on another aircraft, such as for example an original Cessna 337 with minor modifications to the existing engines, instead of replacing it in its entirety.

2.2.2. Engine Selection

Using the remaining options for energy sources, prospective engines can be identified and analysed. Currently, several organisations are developing engines that could be suitable for use in aviation. By obtaining an overview of their promising concepts, potential future customers can be identified. Therefore, the specifications of these engines should be taken into account for interchangeability of the design, as these organisations may want to test their propulsion systems on the SFPT.

An overview of prospective engines and several important specifications is shown in Table 2.2. It should be noted that some specifications are missing as they were not disclosed by the company. This is to be expected considering the high degree of competition involved in developing alternative propulsion systems. Furthermore, due to this same reason it can be expected that the actual power-to-weight ratio of the included engines is slightly lower than the ratio deduced from Table 2.2.

Table 2.2: Prospective engines

Project/Company	Engine	Mass [kg]	Continuous power [kW]	Peak power [kW]	RPM
Emrax [19]	Emrax348	42	210	380	1840 - 4500
H3X [20]	HDPM-250	49	200	250	unknown - 20000
Siemens [5]	SP260D	50	260	-	-
eFlyer [21]	SP70D	26	70	92	2600
Pipistrel Velis Electro[22]	E-811-268MVLC	30.8	49.2	57.6	unknown - 2500
MagniX[23]	Magni250	71	280	-	1900-3000
MagniX[23]	Magni500	133	560	-	1900-2600
Ampaire Electric EEL Skymaster[24]	-	-	130	-	-
DLR HY4[25] [15]	DLR HY4 electric engine	170	80	120	-
Boeing Phantom Eye [26]	modified 2.3L Ford Fusion engine	151	111	-	-

[17] https://de.zxc.wiki/wiki/HY4 [Accessed May 2021]
[18] https://www.reutersevents.com/sustainability/long-haul-getting-aviation-biofuel-ground [Accessed May 2021]
[19] https://emrax.com/e-motors/emrax-348/ [Accessed May 2021]
[20] https://www.h3x.tech/#motor [Accessed May 2021]
[21] https://www.bbaa.de/fileadmin/user_upload/02-preis/02-02-preistraeger/newsletter-2019/02-2019-09/02_Siemens_Anton.pdf [Accessed May 2021]
[22] https://www.pipistrel-aircraft.com/aircraft/electric-flight/ [Accessed May 2021]
[23] https://www.magnix.aero/products [Accessed May 2021]
[24] https://www.ainonline.com/aviation-news/business-aviation/2020-10-12/ampaires-electric-eel-skymaster-makes-longest-flight-yet [Accessed May 2021]
[25] https://www.dlr.de/tt/en/desktopdefault.aspx/tabid-10743/ [Accessed May 2021]
[26] https://www.escortfocus.com/html/2_3_duratec.html [Accessed May 2021]

In the previous stage of design, a tool was developed to help determine the feasibility of several propulsion systems. Using this tool, the engines could be plotted on a power-weight graph to estimate achievable minimum rates of climb. For more information on this model and the associated assumptions, refer to [2]. By implementing requirement PROP-PERF-2.2.2, which states that the aircraft shall, with all engines operative, be able to climb at a rate of $700\ fpm$ at ISA/MSL, an envelope of engines can be identified that could be tested on the SFPT. Note that the full list of requirements can be found in Section 2.4. Assuming that besides the modifications currently designed for the SFPT only the auxiliary tanks in the wings are removed, this envelope is defined by the two cases listed in Table 2.3.

Table 2.3: Limiting cases

Case	Engine + Fuel Weight [kg]	Power [kW]	MTOW [kg]	Climb rate [m/s]
Case I	883	145	2100	5.4
Case II	533	80	1750	5.4

By entering the selected prospective engines into this envelope, the preliminary engine selection can be defined. This is shown in Table 7.2. In Chapter 7 the final selection of two engines is explained and a detailed sizing of propulsion subsystems is performed.

Table 2.4: Preliminary engine selection

Engine	Power [kW]	Engine Weight [kg]	MTOW [kg]	Max. fuel weight [kg]
Magni250	280	71	2100	812
SP260D	260	50	2100	833
Emrax 348	210	42	2100	841
HPDM-250	200	15	2100	868
Phantom Eye	111	151	1750	382
DLR HY4	80	170	1750	363

2.3. Functional Analysis

The Functional Flow Block Diagram (FFBD) is shown in Figure 2.3 and depicts the chronological order of functions the aircraft will perform throughout the mission lifespan. Identifier codes are used to group the functions into classes. An accompanying colour-coding scheme is applied to denote the level of detail per function with extra clarity. The top level of detail is broken down into three sub-levels, namely: 1.1 - Produce aircraft, 1.2 - Operate aircraft and 1.3 - Dispose of aircraft. This distinction is made because these phases should all be taken into account while designing the aircraft. The design phase is not included, as Figure 2.3 is one of the tools used to derive the design phase in sufficient detail. Arrows are used to indicate the directional flow of functions. A clear distinction is made in the types of junctions between lines. Regular intersections with no words or arcs indicate AND statements. OR statements are indicated by the word "OR" and apply in the direction of arrows flowing through them. For example, the OR statement after function 1.2.2 applies to function 1.2.5 and 1.2.6 only. This means that function 1.2.3, 1.2.4 and 1.2.5 or 1.2.6 are performed. Arcs indicate that the intersecting arrows are unrelated. Furthermore, an arrow in combination with the word "ITERATE" denotes an iterative function. In Figure 2.3 this is used to indicate that it is intended to perform function 1.2 Operate Aircraft multiple times before the aircraft is disposed. Note that the functional flow block diagram continues across two pages. On the first page all reference boxes are connected to the original function by arrows. This is not done for the reference boxes on the second page for readability purposes.

The Functional Breakdown Structure (FBS) shows the complete set of functions provided by the Skymaster testbed. This includes one greater level of detail compared to the FFBD. It is shown in Figure 2.4. The same identifier codes and colour-coding scheme are applied. The identifier codes for the additional detailed functions contain an appended number, these functions are denoted by a new colour. Note that all functions shown are not yet quantified, so as not to unnecessarily constrain the design of the aircraft.

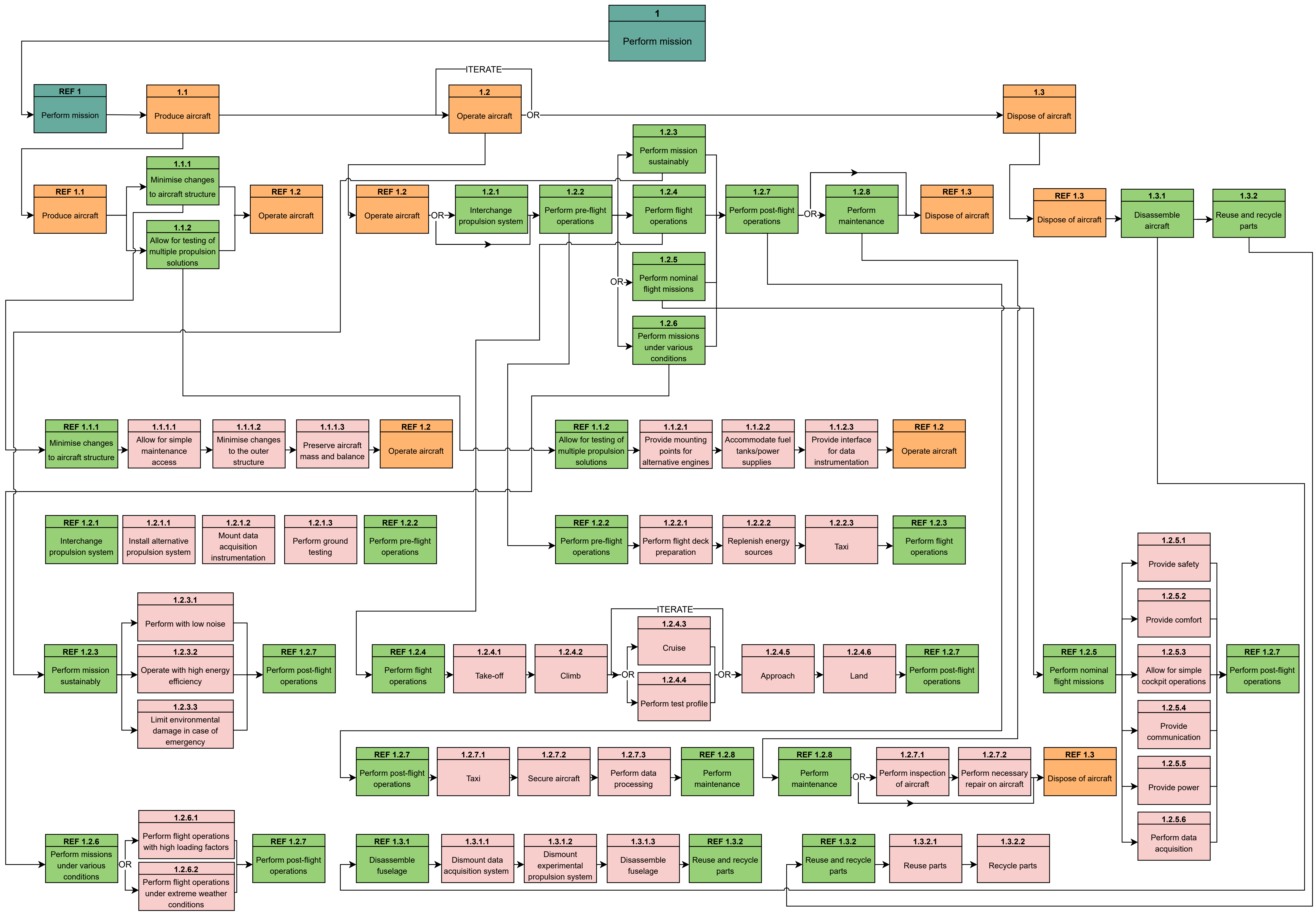

Figure 2.2: Functional Flow Block Diagram - Page 1 *Colour Code: Detail Level (low to high) - turquoise, orange, green, pink, blue*

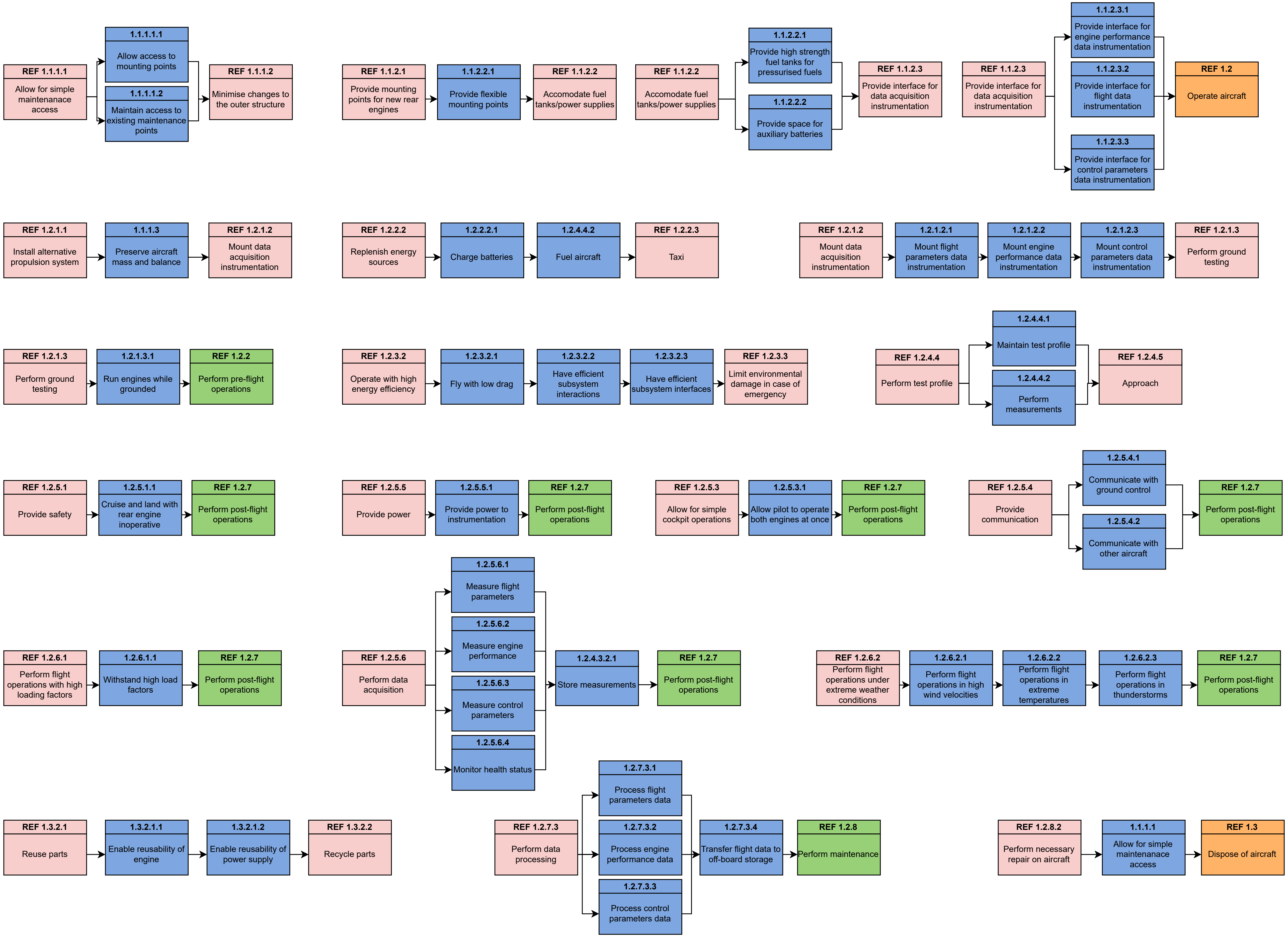

Figure 2.3: Functional Flow Block Diagram - Page 2 *Colour Code: Detail Level (low to high) - turquoise, orange, green, pink, blue*

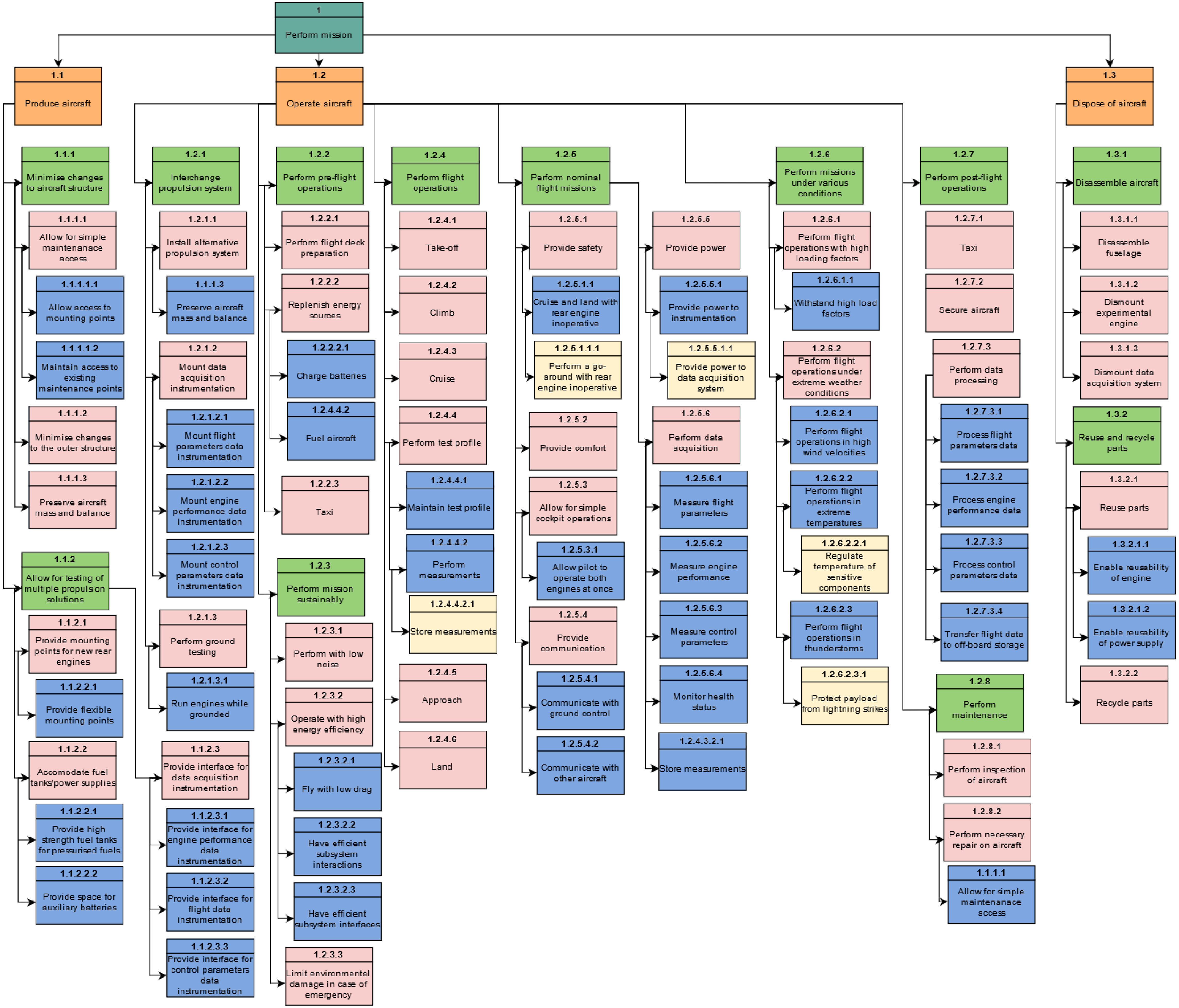

Figure 2.4: Functional Breakdown Structure Colour Code: Detail Level (low to high) - turquoise, orange, green, pink, blue

2.4. Requirements

Requirements are crucial in defining what the design should be able to do in order to fulfil its mission. They specify in clear terms what the desired end goals of the design are and thereby drive the design process. If the final design can be proven to meet these requirements then the mission and project is considered a success. Note that this assumes that the requirements accurately reflect the mission, an assumption which in itself must be proven and validated.

In this section the requirements that were derived in the *Baseline Report* are refined and listed together with their verification procedure [1]. This list serves to be a complete summary of *all* requirements that are applicable design. Requirements that have been identified to influence the design the most and are critical for the success of the project are classified as 'driving requirements'. These driving requirements are indicated in grey in the subsequent tables.

Preserve Existing Design Requirements - At the core of the project is the predefined use of the Cessna Skymaster as the basis for the testbed. From this stems a list of requirements as formulated in Table 2.5. These requirements define what characteristics of the original design should be preserved as a basis for the modified testbed design. The last column of Table 2.5 lists how each requirement is verified, i.e. how the design's adherence to the requirement will be checked. Parent requirements are defined in terms of their constituents/children, driving requirements are indicated in grey.

Table 2.5: Preserve existing design requirements (driving requirements in grey)

Requirement ID	Requirement	Verification
PED-1	The existing fuel tanks shall not be reduced in size so that their capacity is less than 46 US gallons.	Analysis/Inspection
PED-2	The design shall respect existing mass and balance limitations.	Analysis
PED-2.1	The take-off weight shall not exceed the MTOW of 2100 kg.	Inspection
PED-2.2	The CG shall be within 3.50-3.63 from the nose.	Analysis
PED-3	The design shall seat three people including the pilot.	Inspection
PED-4	The data acquisition system shall not interfere with existing systems.	Demonstration

Performance and Propulsion - Flight performance plays a key role in ensuring the design's ability to adhere to safety and mission requirements. Better flight performance means that the testbed will be able to fulfil its mission more effectively and efficiently. However, unrealistic flight performance requirements may constrain the design in ways such that it becomes infeasible (killer requirements). Early on in the project it was identified that a balance must be struck between flight performance and feasibility of the design. The minimum performance required for the testbed to achieve its goal are listed in Table 2.6. These stem from user specifications, the market analysis and safety considerations.

Table 2.6: Performance and propulsion system requirements

Requirement ID	Requirement	Verification
PROP-PERF-2.1	The experimental engine shall operate for one hour at an altitude of $5000\ ft$.	Analysis
PROP-PERF-2.2	The aircraft shall be able to depart at MTOW with three POB.	Analysis
PROP-PERF-2.2.1	The aircraft shall take off in a distance of $1199\ m$ at MTOW.	Analysis
PROP-PERF-2.2.2	The aircraft shall, with all engines operative, be able to climb at a rate of $700\ ft/min$ at ISA/MSL.	Analysis
PROP-PERF-2.2.3	The aircraft shall, with single engine operative, be able to climb at a rate of $200 ft/min$ at ISA/MSL.	Analysis
PROP-PERF-3	The aircraft shall, with all engines operative, maintain a climb gradient of 5.0 percent.	Analysis

Data Acquisition - Collecting data during flight is one of the core missions of the testbed, if not *the* goal of the project. The required performance of the data acquisition system is listed in Table 2.7.

Table 2.7: Data acquisition requirements

Requirement ID	Requirement	Verification
DA	The aircraft shall have a data acquisition system.	Inspection
DA-M-1.1	The sensors shall record all the relevant flight performance parameters (as shown in the RDT, [1]).	Demonstration
DA-M-1.2	The sensors shall record engine parameters.	Demonstration
DA-M-1.3	The sensors shall record control parameters.	Demonstration
DA-M-2	The sensors shall be able to output data to the data collection system.	Test
DA-S-1	The data collection system shall be able to store data throughout one flight.	Demonstration/Test

Safety and Certification Requirements - Table 2.8 lists requirements pertaining to certification and safety. Certification guidelines set by EASA (CS23) were used as guidance [20].

Table 2.8: Safety and certification requirements

Requirement ID	Requirement	Verification
SAF-ENG-1	The design shall be able to tolerate failure of the existing engine.[27]	Analysis
SAF-ENG-1.1	The non-experimental engine failure shall not cause an unsafe condition in accordance with EASA requirements.	Inspection
SAF-ENG-2	The design shall be able to tolerate failure of the experimental engine.	Analysis
SAF-ENG-2.1	The experimental engine failure shall not cause an unsafe condition in accordance with EASA requirements.	Inspection
SAF-ENG-2.2	The design shall be able to cruise at 5000ft at max gross weight, ISA and experimental engine inoperative.	Analysis
SAF-ENG-3	The structural design shall include a factor of safety of 1.5	Analysis
SAF-ENG-2.2.3	The design shall be controllable in accordance with CS23 with experimental engine being inoperative.	Analysis
SAF-CRASH	The modifications shall be crash-worthy (for further breakdown EASA certification requirements are consulted).	Inspection
CER-1	The design shall adhere to EASA CS 23 certification requirements as much as possible	Inspection

Market Analysis Requirements - The requirements listed in Table 2.9 followed from the market analysis in Section 2.1, which considers stakeholder's of the project and user expectations. Stakeholders desire a testbed that can operate a range of propulsion systems efficiently. This implies that experimental engines can be interchanged in a relatively short time-frame. Furthermore, stakeholders are interested in acquiring data yielded by flight tests. The specific performance and data acquisition requirements related to this are listed in Table 2.6 and Table 2.7 respectively.

[27] Although requirements SAF-ENG-1 and SAF-ENG-1.1 are already covered by the existing certification of the aircraft they are still included as modifications to the aircraft might have an effect on performance with respect to this requirement.

Table 2.9: Market analysis requirements

Requirement ID	Requirement	Verification
MKT-COST-1	Permanent modifications to the aircraft shall cost no more than [TBD] EUR.	Inspection
MKT-COST-2	Interchanging experimental propulsion system shall cost no more than [TBD] EUR.	Inspection
MKT-PROP-1	Fuel storage and distribution capabilities shall be provided for two fuel types.	Inspection/Demonstration
MKT-PROP-2	The experimental propulsion system shall be able to be interchanged within 10 working days.	Demonstration
MKT-PROP-3	The aircraft shall be able to perform nominal flight missions within a determined envelope of engine power and mass.	Analysis
MKT-PROP-4	The aircraft shall be able to house the experimental propulsion system without damaging it under the loads specified in the flight envelope.	Analysis
MKT-PROP-5	The aircraft shall provide mounting availability for external data acquisition systems	Demonstration

Structural Requirements - Below in Table 2.10, the requirements for the design of the engine mount are listed. These will drive the design of the mounting truss structure that will attach the engine to the aircraft, while reducing engine vibration and also introduce the loads safely into the aircraft. The use of an engine mount also increases the interchangeability of the engines and therefore, creating a more flexible testbed. In Table 2.11, the requirements generated for the design of the fuel mounting are listed.

Table 2.10: Engine mount requirements

Requirement ID	Requirement	Verification
STRUC-MOUNT-1	The engine mount shall use the same four installation nodes as for the mounts of the Continental IO-360 engine.	Inspection
STRUC-MOUNT-2	The engine mount shall be constructed from readily available materials for aircraft structures.	Demonstration
STRUC-MOUNT-3	The engine mount shall be able to sustain load cases according to CS-23.	Analysis/Demonstration
STRUC-MOUNT-4	The engine mount shall isolate vibrations with a maximum frequency of 50Hz.	Analysis/Demonstration
STRUC-MOUNT-5	The engine mount shall be capable of housing a variety of engines.	Demonstration

Table 2.11: Fuel mount requirements

Code	Requirement	Verification
FUEL-MNT-1	The structural mount shall weigh no more than 30kg.	Demonstration
FUEL-MNT-2	The structural mount shall introduce loads into the existing structure in a way that maintains its integrity.	Analysis
FUEL-MNT-3	The structural mount shall accommodate connections between the engine and fuel cells such as cabling or fuel lines.	Demonstration
FUEL-MNT-4	The structural mount shall prevent the fuel from moving around in the cabin.	Analysis/Test

Risk management requirements - In Table 2.12 the requirements stemming from the technical risk assessment are listed. These requirements are put in place for the possible situation if the system may fail to achieve performance requirements [23].

Table 2.12: Requirements stemming from risk

Requirement ID	Requirement	Verification
RISK-TECH-1	A ground test regime shall be used to verify the engine integration.	Test
RISK-TECH-3	The fuel cells shall be cooled to prevent overheating.	Analysis

Requirement Verification

The process of product verification is in order to check that the testbed meets the requirements. For this there are four possible methods to use: 1) inspection 2) analysis 3) demonstration 4) test. Selecting a verification method for each requirement is decided on by the designer and often more than one method is possible.

Inspection involves the review of the design documentation or visual inspection of the product to check that the product meets the requirements. An example of this is for the requirement PED-3, it is possible to inspect that the aircraft contains three seats for the passengers. Inspection is the most time and cost effective method of production verification. Analysis involves mathematical analysis of the system which itself also requires model verification and validation. Analysis is often used when flight conditions cannot be accurately simulated on the ground or when it is not economically feasible to test the system. For example, it is possible to verify requirement STRUC-MOUNT-4 by analytical analysis or finite element methods. Other verification process such as inspection, demonstration or testing are eliminated due to safety and cost.

Demonstration is the process of physically showing that the system is capable of meeting the requirement. Requirement MKT-PROP-2 may be verified through demonstration - proving that the experimental propulsion system may be interchanged within 10 working days. Finally, testing is a formal demonstration method, often requiring a testing environment. Requirement PROP-PERF-1 may verified through testing.

Requirement Validation

Requirement validation is a process to check whether the requirements are correct. This can be done through the 'VALID' method. Ensuring that the requirements are: **V**erifiable, **A**chievable, **L**ogical, **I**ntegral, **D**efinitive.

Firstly, verifiable requirements will be checked using the method outlined above. Achievability refers to the attainability of the requirements within the law of physics. A logical requirement does not arbitrarily limit the design and is relevant to the mission. Integral requirements are structured in a way that is complete and consistent. Finally, definitive requirements are specific in describing what the design shall do or be.

2.5. Concept Trade-Off

As a starting point for the design process a variety of concepts and configurations were considered. This included options such as solar panels or adding a third engine to the aircraft. After discarding options reasoned to be infeasible, a list of six potential configurations was established:

- **Configuration I** - Front engine as experimental engine, experimental fuel in fuselage, experimental fuel in wings if necessary.
- **Configuration II** - Rear engine as experimental engine, experimental fuel in fuselage belly-pod, experimental fuel in wings or fuselage if necessary.
- **Configuration III** - Rear engine as experimental engine, experimental fuel in fuselage, experimental fuel in wings if necessary.
- **Configuration IV** - Front engine as experimental engine, experimental fuel in wing or wing strut external pods, experimental fuel in fuselage if necessary.
- **Configuration V** - Rear engine as experimental engine, front engine upgrade/modification, experimental fuel in fuselage, experimental fuel in wings if necessary.
- **Configuration VI** - Same as configuration V except engines are swapped.

These six concepts were evaluated against four trade-off criteria, as listed in Table 2.13.

Design feasibility considered cost, interchangeability of the propulsion system and engineering effort required for design and implementation.

Certification looked at how difficult a concept would be to certify in terms of proving its safety.

Performance determined one engine inoperative (OEI) performance, climb rate, endurance and c.g. limitations. This criteria was graded the heaviest as flight performance will determine a large part of the design's effectiveness and adherence to the requirements.

Finally, sustainability considers a concept's impact on the environment. This receives the lowest weight since the ultimate goal of the project is not to be in itself sustainable, but to research sustainable propulsion for future aircraft. The goal of the testbed is to have a long-term impact on the industry which far outweighs any short-term benefit of making a single aircraft itself more sustainable.

Table 2.13: Trade-off weights

Criterion	Weight (+/- Margin)
Design Feasibility	30 (+/- 5)
Certification	20 (+/- 3)
Performance	40 (+/- 5)
Sustainability	10 (+/- 2.5)

The results of the trade-off process are given in Table 2.14

Table 2.14: Final trade-off table. Scores are rounded.

	I	II	III	IV	V	VI	Weights
Design Feasibility	19	19	23	14	14	12	/30 ($\pm$ 5)
Certification	16	12	15	12	13	14	/20 ($\pm$ 4)
Performance	27	26	26	26	36	34	/40 ($\pm$ 5)
Sustainability	9	8	9	7	6	6	/10 ($\pm$ 2.5)
Total	**71**	**65**	**73**	**59**	**69**	**66**	**/100**

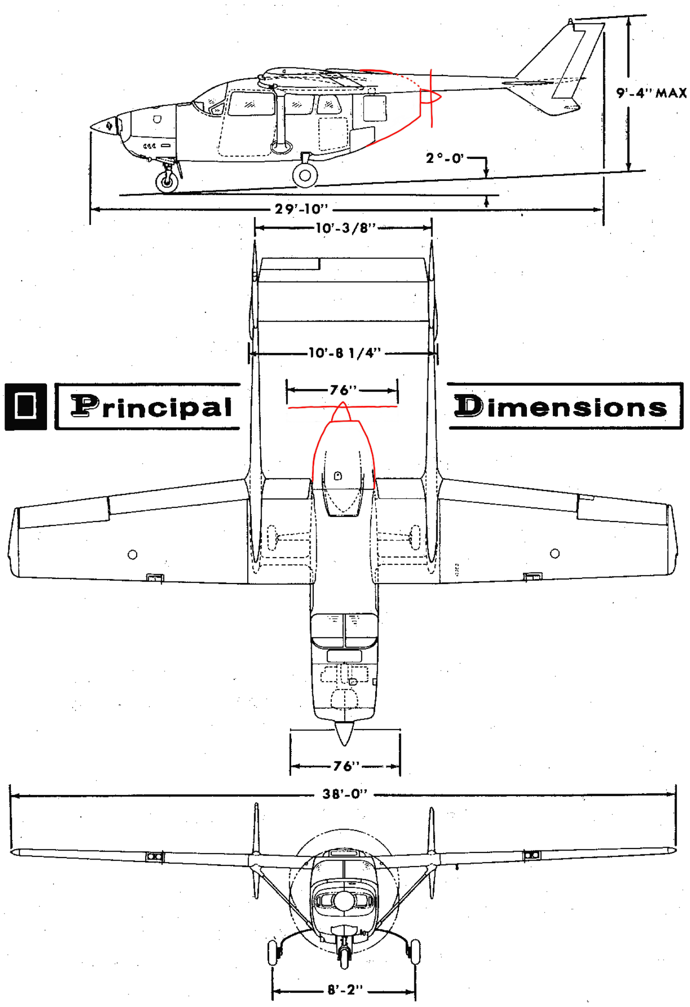

Figure 2.5: Selected Concept III

3
Design Methodology

In this chapter the applied design methodology and structure of the report is explained. This chapter begins with a top-level introduction into the project approach, including the project management. Next, Section 3.2 presents how the detailed phase of design is carried out by several main technical departments and gives an introduction into their applied methodologies. The budget breakdown and preliminary resource allocation is presented in Section 3.3. The synthesis of the technical departments into a coherent final design is explained in Section 3.4. Lastly, the project approach to verification and validation is explained in Section 3.5.

The goal of this report is to present a final detailed design of the aircraft for two chosen engines and corresponding propulsion systems. This is done by working on three main technical departments in parallel, namely propulsion system, structures and data acquisition. The design processes are each driven by separate requirements, as explained in Section 3.2. Also, a common project approach is applied is applied to all three design processes, driven by the future certification of the aircraft and taking into account a sustainable development strategy and technical risk assessment. Working in parallel brings with it several complications due to the interdependence of the technical departments. Therefore, a top-level iterative process is applied. First, a preliminary resource allocation is applied, which all technical departments design towards. The design is then frozen at several predetermined dates, and compliance with the requirements and defined budgets is checked each time. Based on this, the resource allocation is adjusted. With each iteration, the design becomes more detailed until in the end it is synthesised into a final design.

3.1. Project Approach

To structure the final design phase of the project, a variation of the project management method 'Scrum' is implemented. This is suitable for small teams working in a limited time-frame and allows for rapid development in which the project is divided into several phases known as sprints. Below in Figure 3.1 the process is visualised.

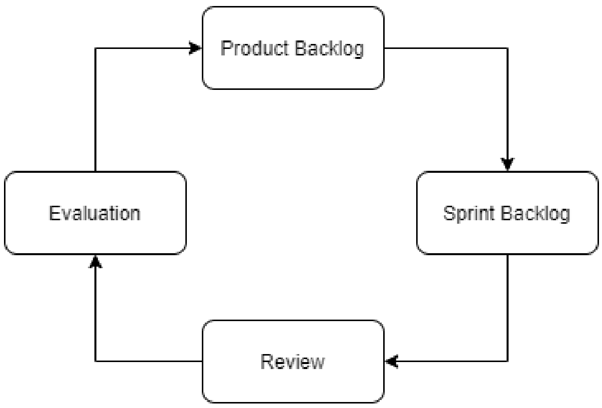

Figure 3.1: Project Approach

The product backlog includes the list of deliverables as well as the requirements generated for the project design - this is the 'to-do list' of the entire project and documented in Excel sheets, accessible by all team members. For the sprint backlog, tasks are transferred from the product backlog into the form of a visual timeline that is sent to all members at the beginning of the sprint. During the sprint review, it is ensured that each technical department has estimations for the required mass, volume and power budgets as well as an idea of the placement of components. These parameters, along with requirement compliance, are then checked by the systems engineers. The design is then iterated upon in the following sprint. Lastly, evaluation meetings are conducted for feedback and open discussion to ensure that the team can move to be as self-organising and efficient as possible.

3.2. Technical Departments

The work is divided into three core technical departments. First, changes to the propulsion system are delegated to the propulsion department. The other two are structures and data acquisition. In doing so, individuals can become more specialised over time in their specific fields in their specific fields and the work can be broken down into more manageable tasks. By regularly checking synthesising this work and checking compliance, this can be done without compromising the integration into the final design.

Propulsion System

The aim of the propulsion department is to select the two engines to be tested and to size the energy sources and corresponding electrical subsystems, including the cooling system. For this design process the performance requirements are driving. Namely, the preliminary engine selection is identified using the climb rate requirement. The final two engines are then selected based on their relevance for future aviation and technology readiness level. Furthermore, the batteries are sized using the endurance requirement for one hour of cruise. Lastly, the corresponding subsystems are sized using the maximum rated continuous power to be tested by the engines, with the purpose of maximising the engine envelope. This is necessary to obtain a competitive stake in the market and maximise the relevance to research parties, as explained in Section 2.1. The relevant requirements can be found in Table 2.6 and Table 2.9.

Structures

The structures department aims to design the necessary structural modifications to the aircraft, in particular the engine mount and fuel mount. For the design, a number of requirements are considered, based on the interchangeability, the existing structure and loading cases.

For the engine mount, a literature study is first conducted to gather information on existing engine mount structures. This is followed by a load case analysis based on the EASA Certification Specification (CS23). Following a material selection, an engine mount concept is analysed using two models for the loading cases identified with a safety factor of 1.5 applied. The engine mount design is then optimised for weight. For the fuel mounting, the existing fuselage structure is analysed to ensure the addition weight may be carried safely. This is done through an analysis of the local and global bending of the section. The requirements for the engine mounting can be found in Table 2.10 and the fuel mount requirement can be found in Table 2.11. Another specific requirement that applies to the structural design is **SAF-ENG-3**, which includes the safety factor for the structural design.

Data Acquisition

The data acquisition department aims to identify the most relevant parameters for detailed data acquisition on the testbed, as well as determine the mass and power budget required for the data acquisition system. This is done to ensure compliance to the available budgets and more importantly to ensure that the aircraft can carry out its primary purpose, namely to perform research on alternative propulsion systems.

3.3. Budget Breakdown

Requirements pertaining to mass and centre of gravity limits are particularly challenging due to the fact that they can not be delegated to one specific technical department. To ensure that the integrated design does in fact meet these requirements requires co-operation and co-ordination between technical departments, as each technical department has an influence on the mass and balance of the aircraft.

The structures and propulsion department make the most drastic changes in terms of mass and volume. The creation of a mass budget follows from this realisation, and serves to keep a track of how much mass each department may use. It must be kept in mind that this budget is meant to be descriptive rather than instructive, in that it does not set any hard limits on how much mass a particular technical department uses, but attempts to describe how mass is being 'spent' during the design process.

The mass budget of the original design is given in Table 3.1.

Table 3.1: Original mass budget

Component	Mass $[kg]$
Fuel front	129
Fuel back	125
6x people	6×90
Empty weight	1036
3x seats	3×22
IO-360	150
Structural mount	13
Removables	270
MTOW	2100

The mass budget for the modified design considers the original aircraft minus three people and seats, the back fuel, removables and one IO-360 and mount. This lead to a new take-off weight of only $1194\ kg$. This leaves a total of $906\ kg$ for modifications.

For case I, as per the baseline report (i.e., heavy and powerful engine), the mass budget was broken down as in Table 3.2.

Table 3.2: Mass budget breakdown

Component	Mass $[kg]$
Engine mount	20
Fuel mount	25
DAS & mount	39
Propulsion system	826
Total modifications	906

Note that the IO-360 is a relatively heavy engine compared to the engines that the Skymaster will be equipped with. This means that the c.g. of the aircraft will shift forward due to mass being removed in the back. There is little that can be done about this, other than to extend the arm of the engine by increasing the length of the mount. This would lead to significant changes in the design and increase the weight of both cables and the mount itself. It is therefore decided that adding ballast in the rear of the aircraft is a more effective solution, and offers more flexibility in terms of mass and balance requirements. The systems engineers continuously keep track of changes to either the mass or c.g. location, and co-ordinate the appropriate measures to ensure adherence to requirements.

3.4. Design Synthesis

In design synthesis the results of all three technical departments are combined to form one coherent design concept. In this process the technical departments work together to place their systems within the aircraft, hereby ensuring there is enough space for each system and that they do not conflict with each other (in terms of location). During this process systems engineers take data from each department to ensure that the integrated design adheres to all requirements.

3.5. Verification & Validation

Throughout the design process, various models and tools are developed. To ensure that they function as intended extensive verification and validation of these tools is required.

Verification

Verification is an integral part in developing models with the design process and aims at answering the question ”Are we building the model correctly?”. This is ensured through several common practices as well as model-dependent methods, as explained in the corresponding sections.

For all developed models unit tests are implemented. Unit tests are software tests for small components of the model. To aid in efficient unit testing, written code is always separated into clearly defined units such as classes and functions. For the models used in this project, these unit tests are written for each function and for each class method of the code. To implement the unit tests in an efficient manner, the python library ”pytest” is used to allow for automated testing of the code. This allows for comparisons of the input and output of constructed functions to values acquired from an external source. Such as comparing a mathematical function computed by the code to a hand computed value.

Another python library used is ”Coverage”, which allows for the generation of coverage reports. These reports show in detail what parts of the code are covered by the unit tests. This allows for confidence in the model as each step of the model can be checked and verified.

To allow for correct and appropriate unit testing of the code and a complete coverage of the models, unit testing is applied as an integral part of the workflow while developing the models. Unit tests are written at the same time as the functions and methods which they are testing. This allows for the creation of unit tests which accurately cover all the inputs and outputs of the function. It also allows for discovery of bugs immediately when they are written. This saves time, as it prevents having to sift through the entire code at the end to find small bugs.

Lastly, a distinction is made between code verification and calculation verification. Code verification is the process of finding and fixing programming errors in the written code [18]. Calculation verification is the process of determining whether the numerical model contains errors or inaccuracies from the applied numerical methods [18]. Throughout this project, code verification is always applied and calculation verification is applied where possible. The latter is performed by comparing the results to that of a simplified model in order to find for example linearisation errors.

Validation

Validation aims at answering the question ”Are we building the right model?”. One of the applied methodologies is that properties of the original Skymaster are entered into the developed models. The outputs are then compared to real results from for example the Owner’s Manual in order to validate the results. Furthermore, when sizing subsystems the obtained weight, volume and required power is compared to properties of existing components in the market. Where no off-the-shelf components exist with the required properties, the results are scaled accordingly. This gives an indication of the expected order of magnitude. Other model-specific validation techniques are used where possible.

Another important form of validation is the use of sensitivity analysis. For that, parameters that are uncertain within a certain range are entered in the model at various values within that range to observe the effect on the final results. This is especially important for trade-offs to identify whether another concept may turn out to be best under other realistic conditions. Also, it is applied to the sizing of methodologies to identify certain risks. For example, if due to a slightly lower real specific energy the batteries would have much lower endurance, the number of batteries may have to be increased accordingly.

4
Certification

The certification of the testbed is an important process which will be discussed in this section. By developing a certification strategy a clear plan is laid out for how certification will be performed once the aircraft is introduced into service. This chapter pertains mainly to the requirement CER-1: *The design shall adhere to EASA CS 23 certification requirements as much as possible*.

First, certification classification and the original certification of the DEAC Cessna Skymaster is introduced in Section 4.1. Next, an elaboration on registration options for the SFPT is in Section 4.2. After this the options for certifying the SFPT will be discussed, and a certification strategy will be chosen in Section 4.3.

4.1. Certification Classification

In order for an aircraft to be considered airworthy it should be certified within a specific category based on various technical aspects of the aircraft such as complexity and age of design. [1]

The certification process generally consists of two stages; type certification and certificate of airworthiness issue. The type certification involves the process of establishing that the generic type design meets applicable design and safety requirements. While the certificate of airworthiness recognises that an individual aircraft meets any additional requirements and is physically airworthy. It is the responsibility of the local National Aviation Authority (NAA) to issue the certification, after which the design of the aircraft cannot be altered. The Federal Aviation Authority (FAA) and European Aviation Safety Agency (EASA) are the two main regulating bodies which set rules to govern certification and are generally accepted by all other NAAs. The certification structures are identical, apart from some minor details. Within the documentation the categories are divided into Parts as follows;

Focusing on Part 21-29:

- Part 21: Certification Procedures
- Part 23: Normal Category Aircraft
- Part 25: Transport Category Aircraft
- Part 27: Normal Category Rotorcraft
- Part 29: Transport Category Rotorcraft

For the Parts, there is guidance material to help with interpreting the regulations, known within the FAA as 'Advisory Circular (AC)' and for EASA 'Acceptable Means of Compliance (AMC)'. These detail conditions and load cases that the aircraft is advised be tested within to ensure compliance with the set mandatory regulations. The guidance material aids the negotiation process between the manufacturer and the regulator to agree on a method to prove compliance of the rules. Deviation from the AMCs is acceptable with valid argumentation.

Original Cessna 337F Certification

The Cessna 337F, to be used for the SFPT, is currently certified by the FAA. The FAA's certification process consists of reviewing a proposed design, ground and flight tests, an evaluation of required

[1] https://rgl.faa.gov/Regulatory_and_Guidance_Library/rgMakeModel.nsf/Frameset?OpenPage [Accessed May 2021]

maintenance and finally in collaboration with other civil aviation authorities on their approval for aircraft import [2].

After certification, a document containing a formal description of the aircraft is created, this is known as the Type Certificate Data Sheet (TCDS). Included in the TCDS are the limitations and information required for type certification including airspeed, weight, and thrust limitations [3]. For an existing Cessna 337F, the TCDS includes details on the engines, propellers and flight limitations. As the engine and propellers are both changed for the SFPT, the aircraft is outside of the Type Certificate and so should be re-certified for the large scale modifications.

4.2. Aircraft Registration

The certification of an aircraft is dependent on where the aircraft is registered. There are 162 [3] NAAs and so to coordinate them the International Civil Aviation Organization (ICAO) exists, a sector within the United Nations. Each country involved with ICAO has a NAA to oversee, regulate and coordinate airport, airspace and aircraft airworthiness. The Cessna Skymaster owned by DEAC is currently registered in the United States through the FAA. However, for re-certification of the aircraft post-modification it may be beneficial to re-register the aircraft as the regulations vary for each NAA. The three options for registration of the Skymaster are; FAA registration, Dutch registration as EASA certified, and Dutch Annex-1 registration.

Although FAA registration is from the NAA of the United States, normal category aircraft are permitted to fly in other areas that are also ICAO member states, as stated by Article 33 [40]. FAA registration is the most popular, with approximately 75% of the world's aircraft. The advantage of FAA registration is that it requires less administration and is focused on the required safety measures. Another benefit is the accessibility of Supplemental Type Certificates that other NAAs do not recognise. In addition, the FAA maintenance regulations are more relaxed than other's (i.e. EASA) and so the cost is lowered [4]. U.S. registered aircraft are permitted to fly in Europe so long as the correct documentation is on board the aircraft [5].

However, the United States law requires that all FAA registered aircraft must be under the name of a U.S. entity or citizen. Therefore, a European company such as DEAC must employ a Trust to act on behalf of the company to facilitate the registration. However the main problem is if the aircraft is then certified through the Special Airworthiness Certificate (e.g. experimental category), it is only valid in U.S. airspace [6].

A second possibility is to register the aircraft in the Netherlands as an EASA certified aircraft. This does require a type certificate from EASA and is therefore a very unlikely option, since receiving a type certificate requires full certification on the aircraft which will not be possible for the experimental propulsion systems.

The third possibility, that of registering the Skymaster in the Netherlands, is under a section known as Annex-1. These are known as 'non-EASA aircraft' that are not required under the EASA Basic Regulation to hold an EASA certificate of airworthiness, an EASA restricted certificate of airworthiness or an EASA permit to fly, and therefore are out of the scope of EASA regulation [7]. Included in Annex-1 aircraft, are aircraft built or modified for scientific purposes.

4.3. Testbed Certification

In this section, certification strategies for the SFPT will be investigated. When re-certifying the Skymaster there are a few options to consider. The certification strategy options include the possibilities of a Supplemental Type Certificate (STC) either within FAA or EASA regulations, applying for a Design Organisation Approval (DOA) at EASA, or getting a temporary 'permit to fly' within the Annex-1 registration at the Dutch NAA. Finally, the final certification strategy will be elaborated on.

[2] https://www.faa.gov/aircraft/air_cert/airworthiness_certification/ [Accessed May 2021]
[3] https://en.wikipedia.org/wiki/National_aviation_authority [Accessed May 2021]
[4] http://www.faa-aircraft-registration.com/N-Registration_Advantages.html [Accessed May 2021]
[5] https://basic6aviation.com/questions_page.html [Accessed May 2021]
[6] https://www.faa.gov/aircraft/air_cert/airworthiness_certification/sp_awcert/ [Accessed May 2021]
[7] https://www.caa.co.uk/General-aviation/Pilot-licences/Introduction-to-licensing/What-is-a-non-EASA-aircraft-/ [Accessed May 2021]

Supplemental Type Certificate

For a FAA certified aircraft a STC may be issued when an applicant has received FAA approval to modify an aeronautical product from its original design, thus including a new certified mass and power envelope that differs from the original type certificate. Not only is the isolated modification considered but also the effect on the original design.[8] However, for multiple major aircraft modifications this process is not recommended due to the large engineering effort and cost. It should be noted, that a FAA database includes a repository of approved STCs for the Cessna 337F which may be used for certification.[9] However, supporting data including drawings, instructions and specifications are property of the STC holder and are thus not publicly available.

Design Organisation Approval

Another option to certify the aircraft is to apply for a DOA. A DOA is an approval issued by EASA, stating that the design organisation is able to design and construct parts, within their field of expertise, without any further certification and apart from EASA.[10] This means the design organisation is thus able to modify the aircraft, and thus for example its performance or mass, outside of the original type certificate.

The advantage of certifying via a DOA is that the design organisation, DEAC in this case, is continuously able to design and implement major alterations to the aircraft, without further verification from EASA. Disadvantages are the continuous documentation required, as an active design assurance system is required to receive a DOA from EASA. Other requirements for the DOA include a design organisation handbook and procedures, and the qualifications and experience of management staff personnel. Any major changes to any of these documents need to be issued to EASA.

Permit to Fly

One of the most viable options for the certification of the SFPT is to register for a Permit to Fly (PtF) in the Annex-1 registration at the Inspectie Leefomgeving en Transport (ILT). This means the aircraft is not able to prove its airworthiness via a type certificate, however is still deemed safe to fly by the governing authority. This gives greater freedom to alter the aircraft in any way required [8].

A PtF has the advantage that any modification to the aircraft, within reason and keeping safety in mind, will be accepted to let the aircraft perform its flights. A PtF can thus be issued even when for example new power or mass envelopes are outside of the original type certification, however the PtF is received more easily when the aircraft stays within its type certificate as much as possible. A disadvantage of a PtF is the fact that it is temporary. The amount of flights the aircraft is permitted to perform is defined, together with an exact scope of what will happen during each flight. This means that for performing multiple different mission envelopes, multiple PtFs need to be requested [8].

Final Certification Strategy

To conclude, a certification strategy has been chosen. The first step of the certification strategy is to register the aircraft in the Netherlands. This means it will be registered as an Annex-1 experimental aircraft in the ILT. This includes admission into the civil aircraft register in the Netherlands [11].

The next step would be to apply for a PtF at the ILT. This permit to fly is based on the Netherlands Civil Aviation Act [13], specifically parts 3.8 and 3.21, and the Normenkader Ontheffing Luchtwaardigheid [12]. This is possible since the aircraft will be nationally registered as an Annex 1 aircraft. For the PtF the aircraft needs to be in a special circumstance according to the Normenkader Ontheffingen Luchtwaardigheid [14]. The special circumstance our aircraft would use is the execution of experiments in Dutch airspace serving a social purpose for which the aircraft is an essential instrument in the experiment. The social purpose can be defined as the development of more sustainable propulsion systems.

[8] https://www.smartbrief.com/original/2019/07/understanding-supplemental-type-certificate-process [Accessed May 2021]

[9] https://rgl.faa.gov/Regulatory_and_Guidance_Library/rgSTC.nsf/MainFrame?OpenFrameSet [Accessed May 2021]

[10] https://www.easa.europa.eu/domains/aircraft-products/design-organisations/design-organisations-approvals[Accessed June 2021]

[11] https://wetten.overheid.nl/BWBR0005555/2021-01-01#Hoofdstuk3 [Accessed May 2021]

This would make it legal to fly the aircraft in Dutch airspace.

4.4. Design Certification

Now that a certain strategy has been chosen, the process of certificating the aircraft including its modifications can be looked at. As is stated above, it is more straightforward to receive a PtF when the aircraft is inside its original certification as much as possible, or otherwise be inside FAR/CS 23 regulations. Since the aircraft will fly in the Netherlands, this design will base itself on the CS 23 regulations [20]. The main parts that will be discussed are the required tests proving that the newly designed engine mount and fuel mount are complying with the regulations, compliance with fire safety regulations, and whether the design of the experimental propulsion system is able to be mounted and operated inside a part of the existing regulations.

Structural Certification

First of all, the requirement SAF-ENG-3: The structural design shall include a factor of safety of 1.5 stems from CS 23 requirements, and will be adhered to in Chapter 8.

To prove that the structural modifications designed in Chapter 8 are compliant with the regulations, the structures need to be tested or simulated on the most critical load cases in compliance with regulations CS 23.307: Proof of Structure. Complying with CS 23.307 means proving that the design is in accordance with CS 23.305: Strength and Deformation, which states that the structure must be able to withstand limit loads without detrimental permanent deformation or withstand ultimate loads for a duration of at least three seconds without failure. This must thus be done for both the engine mount and the fuel mount.

This proof of structure should be done using substantiating load tests for both static and dynamic cases. For the static load cases structural analysis may be used only if the structure conforms to those for which experience has shown this method to be reliable. Since the engine mount is a simple truss structure, it may be interesting to research whether it needs substantiating load tests or whether just the structural analysis is enough to proof it is strong enough.

The proof of structure is required to comply with requirement STRUC-MOUNT-3: The engine mount shall be able to sustain load cases according to CS 23. Other structural tests that usually need to be performed on new aircraft will not be applicable to this design, since it does not alter the subsystems that need to be tested. This goes for example for the wing structure or the landing gear.

Fire Safety Regulations

The design must comply with fire protection regulations from CS 23, which include regulations on for example the location and type of fire extinguishers and the flame resistance of the compartment interiors, which is assumed to be in place for the original skymaster inside the passenger compartment. It also includes regulations on the fire protection on engine mounts and other flight structures in CS 23.865. This will thus be included in the future development of the engine mount [20].

Other fire safety regulations that can be complied with is the powerplant fire protection, which states that a designated fire zone must be in place for the propulsion system. However the regulations are based on regular reciprocating and turbine engines, which is not the case in this design. Even so, putting the experimental propulsion system inside designated fire zones behind firewalls greatly improves the safety of the SFPT and is also included into the design. According to CS 23.1191, a firewall must be able to withstand $1093 \pm 83°C$ for at least 15 minutes. Next to this the firewall must be made from listed materials with determined thicknesses to be used without the need to test the firewall. Openings in firewalls must also be sealed in accordance with the CS 23 regulations [20].

Inside both the designated fire zones, a fire extinguisher is required by the regulations CS 23.1195 which must be adequate to distinguish fires. This is a combination of the fire extinguishing system used, the quantity of the extinguishing agent, and the discharge distribution inside the fire zone [20].

[12] https://www.ilent.nl/documenten/publicaties/2016/01/15/normenkader-ontheffingen-luchtwaardigheid-2015 [Accessed May 2021]

Propulsion System Regulations

The first important regulation CS 23.903 (c) that this design will comply with is that, in case of failure of one of the propulsion systems on board, the other propulsion system is not affected in any way and is able to continue operations [20]. This is very important since this is the basis of the design, where if the experimental propulsion system fails the aircraft is still able to operate in a safe manner. This is included in the requirements as SAF-ENG-1 and SAF-ENG-2 which state that the design will be able to tolerate failure of either of the engines on board without causing unsafe conditions.

In accordance with the same CS 23.903, parts f and g state that an altitude and airspeed envelope must be established for in-flight engine restarting, including the fact that each engine must have restart capabilities within that envelope [20]. This is imperative in case of a OEI performance test, or any other reasons why a propulsion system is shut off without suffering fatal damage.

Furthermore the design must comply with CS 23.939 stating that the operating characteristics of the propulsion systems must be investigated in flight to determine that no adverse characteristics are present. This is dealt with by the data acquisition system, which allows for continuous monitoring of the experimental propulsion system [20]. Again this regulation is officially applicable to turbine or reciprocating engines only, however it improves the safety of the design and is thus important to comply with. This is in compliance with requirements DA-M-1.1, DA-M-1.2, and DA-M-1.3 stating that the sensors shall record flight performance, engine performance, and control parameters.

Any regulations stating that the propulsion system must be installed according to its type certificate cannot be complied with due to the experimental nature of the propulsion systems. These regulations will thus be ignored during the implementation of the experimental propulsion system into the SFPT.

5

Sustainable Development Strategy

The mission of the project is to test new sustainable propulsion systems with the project objective of modifying a Cessna Skymaster into a propulsion testbed. Hereby, by definition the purpose of the project is focused very much on environmental sustainability. Nevertheless, within the development and execution of the project, extra effort can be put in to optimise the sustainability of the project. In this chapter the approach to sustainability is motivated in Section 5.1. The sustainable engineering strategy is outlined inSection 5.2. The sustainable characteristics of the design is analysed in Section 5.3. Finally, in Section 5.4 plans to ensure future project sustainability are outlined, including a materials analysis and and end-of-life plan.

5.1. Project Sustainability Approach

While sustainability is accounted for in the design of the SFPT, it should be noted that the overall contribution is low due to the fact that it is an old air frame being adapted to be utilised as a research facility for sustainable alternative fuels. Although the testbed may be considered unsustainable in the short term relative to novel experimental aircraft, the goal of the project is to research propulsion systems to make *future* aircraft more sustainable. By being unsustainable in the short term, the testbed may provide research possibilities that will make aviation as a whole more sustainable, offsetting any short term deficiencies in sustainability.

Sustainability Phases

To be able to assess the sustainability of the technical development, the project life-cycle can be split into three phases:

- Development
- Operation
- End-of-Life

In the development phase, plans will already be put in place for the later phases of the project. Therefore sustainable engineering will have to be practised throughout this phase as well as all later phases to maintain the sustainability of the design and the project as a whole.

Sustainability Types

In the *Baseline Report* [1] it was discussed how the sustainability of a project can be assessed in terms of financial, social, and environmental sustainability. A lot of the sustainable approaches and developments are difficult to be quantified. Therefore, sustainability is only partially included in the requirements and mainly in the form of environmental sustainability as this is at the core of the project objective. Nevertheless, all financial, social and environmental sustainability aspects play a big role in the development of the product.

A sustainable project can, among others, be identified by its ability to run from one project phase to another smoothly and the opportunity to circulate through the project loop multiple times. The latter is called circularity. Applying circularity in engineering has a direct impact on the environmental and financial sustainability as can be seen in Figure 5.1. Circularity is often thought of in terms of environmental sustainability. Nevertheless, while circularity focuses on efficiency, reuse and waste minimisation, this has a direct impact on financial sustainability.

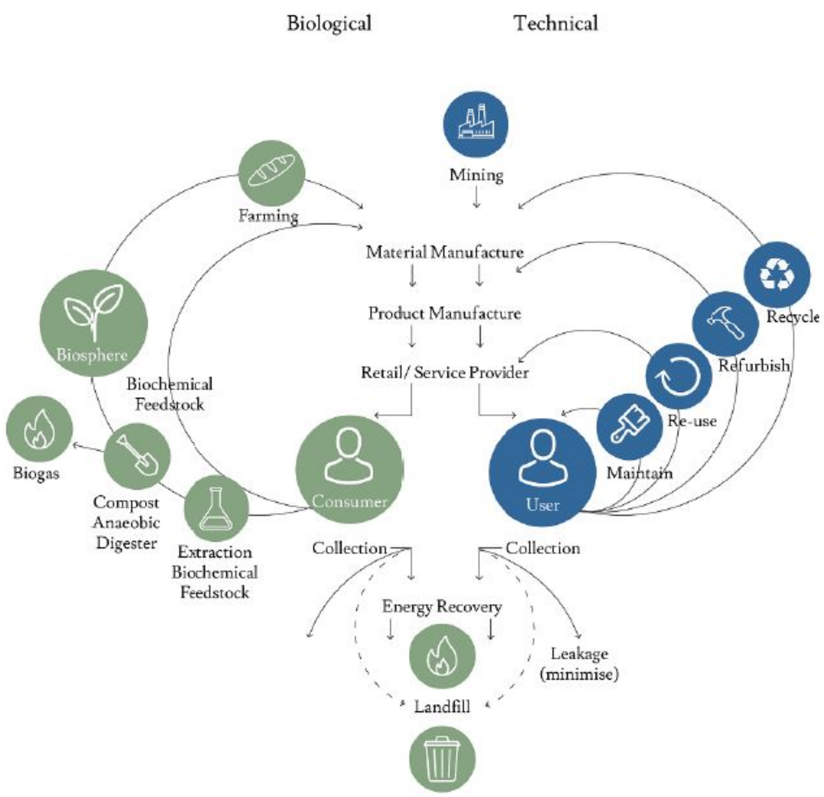

Figure 5.1: Butterfly diagram of how environmental and financial sustainability by practising circularity in engineering [38]

5.2. Sustainability Engineering

The aspects and actions that are considered differ in terms of influence on the specific pillars of environmental, financial, and social sustainability.

Environmental Sustainability Approach

Ultimately the major values that have been considered in the sustainable development approach are listed below:

- **Reuse and Recycle** - Reusing and recycling shall be implemented as much as possible in parts of the design.
- **Emission and Carbon Footprint** - As a bare minimum the aircraft and its propulsion system should at all times adhere to laws and regulations. Something that is not always regulated, but should clearly be considered in the design choice is the environmental impact in case of a critical failure.
- **Alternative propulsion system choice** - The direct application of the testbed is to conduct research on alternative sustainable propulsion systems.
- **Material choice and manufacturing** - Whenever there is an opportunity to choose between different materials during the development, all aspects like recyclability, durability, hazard, waste, efficiency, and resource should be considered.

Social Sustainability Approach

In terms of social sustainability specifically, the clients happiness is of major concern . During the entire development of the product, the desires and requirements of the client should always be key. Continuous communication with the client will therefore always be maintained. Adherence to laws and regulations at all times is a direct example of improving the social sustainability.

Minimising noise is one of the aspects of social sustainability that can easily be considered in this project. Noise will be generated mainly during the operational phase and in a minor extent for a short period during the production phase. During the development, minimising noise therefore is an important selection criterion for the design trade-off. Next to this, specific measures should be put in place to reduce noise during production. In this, the standard noise generation and handling regulations in the hangar should be clearly established and complied with for the sake of employees and surroundings.

Financial Sustainability Approach
Added to the earlier mentioned strategy with regards to reusing and recycling, for the financial sustainability of the project, general project management is of high importance. Accurate planning and administration of the project should therefore always be in place throughout each different project phase. Production, operational and maintenance costs should be considered.

Strategy Implementation
From what has been discussed an action plan was set up as part of the strategy to ensure sustainability at the start of the development phase. Generally, sustainable developmentis one of the core values and should be taken into account during the approach over every part of the design. Nevertheless, specific analysis are done to optimise the sustainability.

1. First of all, for the financial sustainability the *Project Plan* has been written [3]. The team has approached this as a living document and kept having a close look at this document to prevent unnecessary (financial) consequences. A Functional flow diagram, Functional breakdown, Budget Breakdown, Risk Assessment and Market Analysis have been performed which are all included in Chapter 2. A cost breakdown is presented in Section 11.3.
2. In the *Midterm Report*, during the design trade-off, sustainability has been included in the design trade off and was analysed in detail in a sub-trade off [2]. The results of the final trade-off are discussed in Section 2.5. A more detailed analysis on the sustainability of the final concept chosen is given in Section 5.3.
3. Regarding noise, an analysis has been done on the noise characteristics in which there has been a collaboration with experts in that field doing research on the Skymaster specifically. This analysis resulted in the desire to analyse the possibility of replacing the propeller blades as is discussed in Section 5.3.
4. To complete the development phase, once the detailed design is accomplished, an accurate analysis of the chosen materials is performed in Section 5.4. In this analysis the main focus is on finding alternative materials that are more durable, recyclable and less harmful for the environment.
5. A Production Plan has to be put in place to optimise the sustainable execution of the design as is presented in Section 12.1. The existence and execution of such plan ensures unnecessary waste of materials is prevented.
6. Finally, a plan is set up for the end-of-life and maintenance procedures, also including the processing of waste as can be found in Section 5.4. This ensures there is easy and approachable documentation of these procedures for the entire life-cycle of the aircraft.

5.3. Sustainable Design Characteristics
As part of the design trade-off, a more detailed trade-off between the individual aspects contributing to sustainability is performed. The criterion of sustainability has been split into several different aspects which are noise, modifications, emissions and materials.

Noise Analysis
There has been a collaboration with Bieke von den Hoff, a PhD candidate working on the noise assessment of DEAC's Cessna Skymaster. From the first phase of her research, she has analysed the noise levels of the original configuration for the Skymaster [26]. From this, it was concluded that the main noise sources of the Skymaster are the propellers and engines. DEAC owns two pairs of propellers for the Skymaster - a two-blade and three-blade set. As part of the more detailed design, awaiting the results from von den Hoff's further research, the choice could be made to install a different propeller.

This increases the amount of modifications which in turn reduces the environmental sustainability of the aircraft. However, the noise generated by the propellers would decrease when using a three-blade during every iteration of operation and as DEAC already owns the propeller, it would be advised for it to be installed if it turns out to be beneficial for the noise generation. From a financial sustainability point of view, the variable cost as are discussed in Table 11.3, might be reduced by fitting a new propeller as well.

The noise caused by the aerodynamics around the body is minor to that of the engine and propeller blades. Another aspect considered, is that newer engines generally have better performance regarding noise and therefore replacing one engine is expected to improve the noise levels significantly.

Modifications and Emissions

To optimise sustainability, as many of the original Cessna Skymaster's parts should be used as possible. Minimising modifications also decreases emissions during the production phase. Generally, even though some modifications to the structure will be required, using the wing and fuselage as space to store fuel will require minimal modifications. One engine will have to be replaced including its mounts, which requires new parts.

Emissions are also taken into account by considering the fuel flow of the existing engine. For the purposes of this section, emissions are considered to be proportionate to the fuel flow of the (existing) engine. The fuel flow in turn is a function of engine power.

For commercial aircraft, weight has a substantial impact on emissions due to the snowball effect. This is because these aircraft are designed to travel distance in the most efficient way possible over many years. Thus, a marginal improvement in efficiency culminates over a large period of time. For testbeds these effects are of far less concern, if any. Testbeds do not have the goal of flying from A to B in the first place and one of the core goals of research provided by the testbed is to reduce emissions in *other* aircraft.

This being said, by considering the power required from the existing engine for each design option, an effort could be made to lower emissions in the short term. Additional weight required to turn the Cessna Skymaster into a testbed is marginal and is assumed to not have an impact on emissions since the goal of the testbed is to test engines at a range of different power settings, regardless of weight. Weight may however have an impact on endurance or speed, as discussed in other sections.

5.4. Materials Analysis and End-of-Life

The more material that is required, the harder the aircraft will be to recycle and the more emissions will be produced for production of the parts. For the manufacturing there is a strong focus on the application of lean manufacturing. In this, the manufacturing process should be optimised to minimise the waste of resources and energy. Also, by centralising production and choosing for local suppliers, carbon emission due to transportation are minimised for the production phase. Once the detailed design is established, more sophisticated analyses can be done regarding the material sustainability. Therefore, for the detailed design, a detailed analysis regarding the individual aspects of durability, recyclability, hazard and resource is done to optimise the sustainability of the design on its most detailed level as is found in Section 5.4.

To optimally facilitate this, the planning of the production should be done during the development phase by means of creating a detailed production plan and a production flow diagram as discussed in Section 12.1, which is also further put into context in Chapter 12. Added to this a plan is set up for the end-of-life and maintenance procedures including the processing of waste as can be found in Section 5.4

Materials Plan

Battery Materials - The batteries to supply the electric engines of energy are chosen to be the Pipistrel PB345V124E-L. This is a lithium ion type battery that uses the nickel manganese cobalt chemistry. Even though all batteries are very hazardous, lithium ion batteries are categorised as non-hazardous waste as opposed to batteries containing lead or cadmium. Even though the production of batteries is very energy-intensive, batteries are fairly well recycleable. Even though the possibilities for battery recycling are still limited at the moment, at the expected end-of-life of the aircraft, more opportunities to apply circularity are expected. Pipistrel being a very established organisation in Europe, with multiple different production sites, unnecessarily excessive transport of the product can also be minimised. In general batteries have a decreasing performance over its lifespan. This is a general characteristic of the use of batteries and the sustainable contribution of using electric energy as an energy supply for engines outweighs this negative aspect.

Engine Mount Materials - For the engine mount, steel material (Chromoly 4130) is chosen as will be discussed in Section 8.1.2. Although composites generally have a higher specific strength, Chromoly 4130 has shown to be easily weldable and machinable. Specifically this characteristic contributes to the sustainability of the use of this material. Even though the manufacturing and maintenance process involves high emission processes, the modifiability and recoverability of Chromoly 4130 makes that it is a very durable material. With the use of sustainably resourced energy for the manufacturing, the negative impact on the sustainability of this process can be minimised. Another added benefit of using this material is that is is widely recycleable. For that reason it will be very much possible to apply circularity at the end-of-life as is discussed in Section 12.1. As the material is produced at multiple different location within Europa, also the fairly local resourcing and limited required transport, contribute to sustainability.

Hydrogen Tank Materials - For the hydrogen tank a type IV tank was chosen. These tanks will be build from either aluminium or of carbon fibre with a polymer liner. For aluminium the same considerations hold as for steel as has been discussed. Fibre-reinforced plastics have much improved in their sustainability by the adoption of alternative materials and technologies such as closed mould processes, natural fibres and low-styrene resins. Although recycling of composites is not yet optimised, much effort is put in the availability of recycling sites and the improvement of recycling methods like shredding, collection and milling or energy recovery through incineration [21]. By the time the hydrogen tank will reach its end-of-life this is expected to be much better. Although the energy required for production is quite high, like any manufacturing process, the use of sustainably resourced energy reduces the negative impact on the sustainability of this process.

End-of-Life Plan

The final phase is the end-of-life of the testbed. This is most likely to occur if at some point the aircraft is either deemed unsafe to fly or there is no purpose for it anymore by DEAC.

Looking back at Figure 5.1 the end-of-life phase can be approached in five different ways. In Figure 5.2 it is shown that one could decide to use circularity to come back to different points in the product life-cycle.

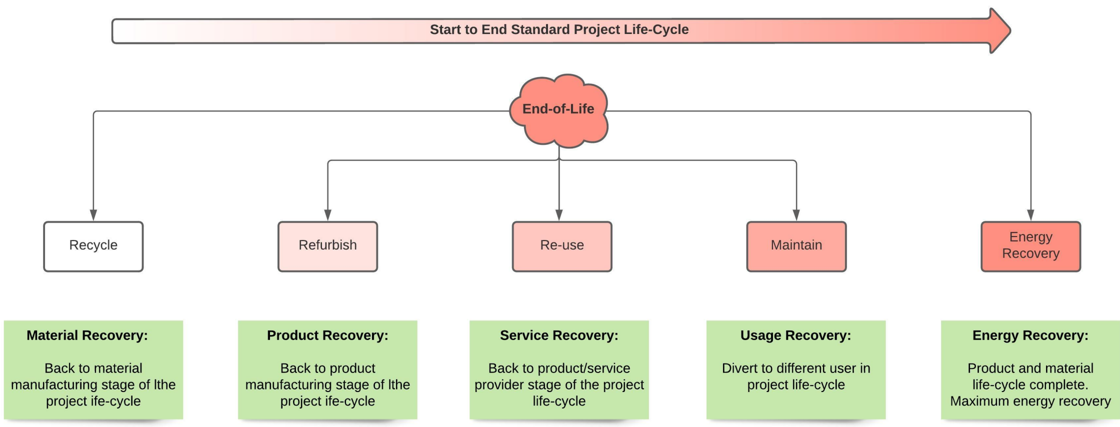

Figure 5.2: End-of-Life Action Option Tree

Material Recovery - The choice could be made that as many of the original materials as possible should be recovered. This way the materials could be used in any new application. The disadvantage of this approach is that not all materials can be recycled as easily in which case only a part of the original product can be circulated while the rest might be wasted.

Product Recovery - In the same way as the original Cessna Skymaster is being converted into a testbed by Group 25, the aircraft could be modified for a new purpose. The advantage of this is that less work will have to be done regarding disassembly. Nevertheless, new materials will most likely be used and some of the original parts will become redundant.

Service Recovery - In this case another organisation will continue providing the a different service with the same product. In terms of both financial and environmental sustainability this is a very beneficial option. DEAC will not have to pay for disposal and no materials will be wasted.

Usage Recovery - In this case another organisation will continue providing the a similar service with the same product. As discussed above this is very beneficial for both financial and environmental sustainability.

Energy Recovery - The last option would be to completely dispose the aircraft. In this case energy can be recovered out of the materials of the aircraft. No physical parts of the aircraft will re-enter a life-cycle and circularity is only minimally applied in terms of recovering some energy. The efficiencies of such processes are very low and can be expensive as well. This option is therefore the least advisable due to its minimal financial and environmental sustainability.

From the options explained above it is clear that depending on the situation that the order of best end-of-life approaches would be:

1. Maintain
2. Re-use
3. Refurbish
4. Recycle
5. Energy Recovery

The sustainable efficiency is highest when the aircraft could be reused in as much of its original configuration as possible. It is not a given that this is an option at the end-of-life of the testbed and (financial) resources should be put aside for this.

6
Technical Risk Assessment

This chapter outlines the functions and elements that introduce risk into the project. Risk mitigation is approached through two strategies, looking at the total effect of the mitigation and their impact on probability and consequence. Section 6.1 defines consequences and probability of the risk. The definitions of effectiveness of the mitigation strategies are also included in this section. Thereafter risks are identified in Section 6.2, where mitigation strategies are implemented and the change in probability and consequence are determined. From this a risk map (Table 6.4) is made to visualise their impact. Thereafter the risk map is updated (Table 6.5) to reflect the changes in risk after mitigation is implemented. A table to show the effectiveness of each risk mitigation strategy is also shown in Table 6.6.

6.1. Definitions

Technical risk is the possibility that a technical requirement of the system may not be achieved in the system life cycle. Technical risk exists if the system may fail to achieve performance requirements [23]. Before a risk assessment can be done definitions of both probability and consequence needs to be given. For probability of occurrence, five probability categories were used. These five states are, in order of increasing probability of occurrence; very low, low, medium, high and very high. The definitions of these probabilities are found in Table 6.1.

Table 6.1: Probability definitions

Very High (5)	Event will almost always occur during the mission
High (4)	Event has a strong likelihood of occurring during the mission
Medium (3)	Event might occur during the mission
Low (2)	Event has a low likelihood of occurring during the mission
Very Low (1)	Event will almost never occur,

The effectiveness of each mitigation strategy will also be evaluated. The definitions of the effectiveness is given in Table 6.2. Effectiveness is also included in the risk analysis since estimating probability and consequence after mitigation is subjective. Therefore, introducing an aspect which looks at the quantity of mitigation strategy introduces confidence that a risk is mitigated.

Table 6.2: Effectiveness Definitions

Not Effective	No risk control measure available
Minimal	Only one risk control measure available
Limited	Only two risk control measures available
Effective	More than two risk control measure available

The consequence of a risk is defined in relation to its impact on the mission and external effects. The definitions of severity can be seen in Table 6.3. Three aspects of the mission defines the consequence, effect on the aeroplane, effect on flight crew and effect on the test flight.

Table 6.3: Severity Level [41]

	Effect on aeroplane	Effect on flight crew/occupants	Effect on test flight
Catastrophic	Normally with hull loss. Damage beyond repair	Fatalities or injury	Failure of the test flight. Objective of the test flight not achieved.
Hazardous	Large reduction in functional capabilities or safety margins. Repair of aircraft structure or engines required.	Serious injury. Physical distress or excessive workload impairs ability to perform tasks.	Partial failure of the test flight. Objective of the test flight is partly achieved
Major	Significant reduction in functional capabilities or safety margins. Repair of aircraft parts or systems required.	Physical discomfort or significant increase in workload.	Degraded flight test results, objective of flight test achieved with limitations.
Minor	Slight reduction in functional capabilities or safety margins. Repair of aircraft parts or systems according to normal schedule	Slight increase in workload. Physical discomfort for occupants	

6.2. Technical Risk Determination

This section presents the methodology of choosing the elements to include into the risk map and present the different types of risk. At the end, a risk map is constructed to show the impact of these risks on the project. To generate the technical risks, a functional analysis was completed in [1]. The analysis finds elements which have high probability of failure and/or have high consequences for the mission. From this analysis the following list of risks are identified, where the FFBD code is shown from the elements stemming from it.

Note that for the purposes of this analysis the following list only considers risks that are unique to the project. For example, for every aircraft there exists the risk of the undercarriage not deploying. Since the design will not change the undercarriage, this risk is not considered. The most important risks relate to the engine failing or the fuel supply causing damage to the aircraft. In these cases the safety of the pilot is at stake, which far outweighs any other risk posed to the mission.

The risk are presented in categories depending on the phase which with the risk is present. The first part take into the account the design of the aircraft. This is followed with risks which are present during the operational phase.

Design Phase Risk

Techn-2	Probability 2	Consequence 1
Risk: Not enough power is available to power the data acquisition system. *Probability:* Since a certain level of redundancy will be built into the design (i.e. multiple power sources which power the main bus), the probability of this occurring is low (2/5). *Consequence:* The effect is negligible (1/4), since this would only be an inconvenience and could be rectified after the flight.		
Mitigation: A margin will be introduced when the sizing the electrical system. *Effect:* This reduces the probability of the data acquisition system not being able to run due to a lack of power (1/5)		
Effectiveness Minimal	Probability 1	Consequence 1

Techn-6	Probability 4	Consequence 2
Risk: The propulsion system cannot be interchanged in the required/desired amount of time. *Probability:* The probability that this will occur is linked to accuracy of estimates on how much time will be required and the expertise of maintenance personnel. Since there will likely be unforeseen hurdles during the process of interchanging the propulsion system which are impossible to predict, the chances of this occurring are high (4/5). *Consequence:* Depending on exactly how much extra time is needed, the effect of this may vary between negligible and critical (1-3/4) as it would disrupt test programmes.		
Mitigation: To mitigate this risk margins should be set in place to ensure realistic time-frames. *Effect:* This reduces the probability to (3/5).		
Effectiveness Minimal	Probability 3	Consequence 2

Techn-7	Probability 2	Consequence 3
Risk: The additional modifications do not fit into the allocated spaces inside the aircraft. If incorrect dimensions are used during the design process or there is a lack of contingency measures, then the data acquisition may not be compatible with the aircraft. *Probability:* The chances of this occurring are estimated low (2/5). *Consequence:* Estimated as critical (3/5) as it is driving requirement of the mission will not be met.		
Mitigation: In order to reduce the risk of the data acquisition system from not being able to be introduced into the aircraft a volume budget and contingency is used. *Effect:* Decreases the probability of occurrence (1/5).		
Effectiveness Minimal	Probability 1	Consequence 3

Techn-8	Probability 2	Consequence 4
Risk: Structural support around the experimental engine fails. *Probability:* The probability is low (2/5) as the structure will be designed to accommodate the experimental engine within set limits. *Consequence:* If the mounting around the experimental engine fails the engine can impact the performance of the aircraft and might cause serious damage to the air frame. Therefore the consequence of this risk is judged catastrophic (4/4).		
Mitigation: **1.** To reduce the occurrence of a structural failure a safety factor of 1.5 will be used. **2.** For the first couple of flights strain gauges can be placed on the engine mount to measure internal forces. *Effect:* This will reduce the probability of the structural failure of the engine mount (1/5).		
Effectiveness Limited	Probability 1	Consequence 4

Techn-9	Probability 3	Consequence 3
Risk: Battery pack overheats. *Probability:* The chances of this occurring depend on power setting and flight conditions and may vary, but for now are given a (3/5). *Consequence:* This risk has critical (3/4) consequence since it may result in fire or damage to the aircraft, as well as a reduction in flight performance.		
Mitigation: An investigation into the required cooling needed for both in flight and during ground operations will be done. *Effect:* This will decrease probability of occurrence as a design which can cool the batteries will be implemented. Furthermore weather conditions may need to be taken into account, as operating the engine at high power during the take-off on a hot day will likely be a critical scenario. By specifying an envelope of operational limits probability (2/5) and consequence (2/4) are both reduced.		
Effectiveness Minimal	Probability 2	Consequence 2

Techn-13	Probability 3	Consequence 4
Risk: Cooling system is not adequate enough to cool the propulsion system (Fuel cell or batteries and electrical motor). *Probability:* This has a medium chance of occurrence, since other electrical aircraft, pipistral electro, this has been a problem. *Consequence:* This would cause a catastrophic risk as this would prevent the objective of the test flight from being achieved.		
Mitigation: **1.** A safety factor will be added to the cooling system to ensure that the system is properly cool. **2.** Installation of temperature sensors and annunciator panel to warn the pilot of any overheating of the propulsion system. *Effect:* Allows the pilot to take faster action in case of overheating and introducing a safety factor both allow for a decrease in probability.		
Effectiveness Limited	Probability 2	Consequence 4

Operational Phase Risk

Techn-12	Probability 3	Consequence 4
Risk: Experimental propulsion system fire or explosion. *Probability:* The risk of this occurring is deemed medium (3/5), as risk may be heightened during impact situations such as a rough or emergency landing, or situations where a high power output is required. *Consequence:* Potentially catastrophic consequence (4/4) since the pilots or the structure of the aircraft may be damaged.		
Mitigation: **1.** A second fire wall will be placed in between the battery/hydrogen compartment and the cockpit. **2.** A fire suppressant system can be installed in the battery/hydrogen storage area. *Effect:* This will will reduce the consequence of the fire as the pilot will have time to safely land. Despite these measures, the probability and consequence are still (2/5) and (3/4), respectively.		
Effectiveness Limited	Probability 2	Consequence 3

Take-Off

Techn-3	Probability 2	Consequence 4
Risk: Experimental engine fails during take-off or climb. *Probability:* The probability is low (2/5) as the engine is usually tested extensively before being implemented on the aircraft, and the climb phase is a relatively small portion of the flight. *Consequence:* If the experimental engine fails during take off or climb this may result in catastrophic (4/4) consequences to the mission since the aircraft may struggle to maintain altitude and crash.		
Mitigation: The mitigation strategy for this is very similar to RISK-TECHN-1: ensuring that the pilot is appropriately trained, and considering flight performance. The effects of an engine failure on flight performance should be considered at each point during climb and take-off to determine the most critical case. There will likely be a point after lift-off where aborting the take-off (i.e. landing on the remaining available runway) is unsafe and the climb must be continued despite marginal performance. For engine failure during climb, there might be a decision altitude at which point making a 180-degree turn back to the runway is the best option as opposed to landing straight ahead in a field. *Effect:* By evaluating and communicating these options to the pilot, preparation and contingency measures can be put in place to ensure the best outcome for every situation. Selecting an airfield with a larger runway, or in a less populated area (more fields) also play a large roll in reducing the consequence. Despite these measures, an engine failure in the early climb will be a critical scenario and therefore has a critical consequence (3/4). The probability can again be reduced by ground tests (1/5).		
Effectiveness Minimal	Probability 1	Consequence 3

<table>
<tr><td>Techn-10</td><td>Probability 2</td><td>Consequence 4</td></tr>
<tr><td colspan="3">Risk: Aircraft overruns the runway in the case of an aborted takeoff.
Probability: There is a low probability (2/5) of this occurring as the mass and balance are the same or lower than the pre-modified Cessna, and the brakes are assumed to be original.
Consequence: There is a catastrophic (4/4) consequence if this occurs as severe injury and loss of aircraft may occur.</td></tr>
<tr><td colspan="3">Mitigation: 1. Operating from a long runway. 2. Regular maintenance and extensive ground testing
Effect: Would reduce the probability to (1/5).</td></tr>
<tr><td>Effectiveness Limited</td><td>Probability 1</td><td>Consequence 4</td></tr>
</table>

Cruise

<table>
<tr><td>Techn-1</td><td>Probability 3</td><td>Consequence 3</td></tr>
<tr><td colspan="3">Risk: Engine failure during cruise.
Probability: As the engine is of experimental nature and majority of flight-time will be spent at cruise, the probability of this occurring is medium (3/5).
Consequence: If not taken into account, the consequences are potentially critical (3/4).</td></tr>
<tr><td colspan="3">Mitigation: 1. OEI performance is taken into consideration during the design process by ensuring that the aircraft has to be able to achieve a marginally positive climb rate in the case of OEI. 2. Implement a ground testing regime.
Effect: Ensures that the aircraft is capable of returning to the airfield in theory. In practice, pilots should be trained to deal with the consequences of this reduction in performance and should be aware of the aircraft's limitations. For example, for OEI flaps and gear should be deployed tactically once the pilot is certain that the runway is within range (although the aircraft may be able to maintain altitude in clean configuration, this may no longer be the case in landing configuration). This would reduce the consequence to marginal (2/4). Testing the engine extensively on the ground could reduce the probability to (2/5). This can only be done to an extent, and the engine is still experimental after all.</td></tr>
<tr><td>Effectiveness Limited</td><td>Probability 2</td><td>Consequence 2</td></tr>
</table>

<table>
<tr><td>Techn-11</td><td>Probability 2</td><td>Consequence 2</td></tr>
<tr><td colspan="3">Risk: The experimental propulsion system cannot meet the one hour cruise requirement. The probability of this is low (2/5) as the aircraft is going to be designed to meet at least 1 hour of cruise. The consequence of this risk is marginal (2/4) as the aircraft may have to perform multiple flights instead of one.</td></tr>
<tr><td colspan="3">Mitigation: Performance calculations should take margins into account. The aircraft could be flown at lower speeds for longer endurance, and the current charge can be monitored during the flight to gauge performance.
Effect: This would reduce the probability to (1/5). Arrangements could be made on the ground to ensure quick charging and turnarounds times for the aircraft, reducing consequence (1/4).</td></tr>
<tr><td>Effectiveness Minimal</td><td>Probability 1</td><td>Consequence 1</td></tr>
</table>

Post-Flight

<table>
<tr><td>Techn-7</td><td>Probability 2</td><td>Consequence 3</td></tr>
<tr><td colspan="3">Risk: The data acquisition does not fit into the plane. If incorrect dimensions are used during the design process or there is a lack of contingency measures, then the data acquisition may not be compatible with the aircraft. The chances of this occurring are estimated low (2/5) and the consequences are estimated critical (3/4) as a driving requirement of the mission will not be met.</td></tr>
<tr><td colspan="3">Mitigation: In order to reduce the risk of the data acquisition system from not being able to be introduced into the aircraft a volume budget and contingency is used.
Effect: This mitigates the risk as the probability of occurrence is reduced (1/5).</td></tr>
<tr><td>Effectiveness Minimal</td><td>Probability 1</td><td>Consequence 31</td></tr>
</table>

Table 6.4 shows the risk map as a result of the previous list. Evidently RISK-TECH-5 and RISK-TECH-13 are the most prominent: that mass and c.g. limits are exceeded and that the cooling system would be adequate.. Risks that are mildly severe are the following:

- RISK-TECH 6: propulsion system cannot be interchanged in required amount of time
- RISK-TECH 1 and 9: engine failure during cruise, battery overheat

- RISK-TECH 3, 8 and 10: engine failure during take-off or climb, structural failure of support, over-run

Table 6.4: Technical risk map prior to abatement

Probability \ Consequence	Minor	Major	Hazardous	Catastrophic
Very High				
High		6		
Medium			1,9	5, 13
Low	2	11	7	3,8,10
Very Low				4

6.3. Technical Risk Mitigation

Table 6.5 shows the risk map after mitigation, for which three strategies have been applied:

- Change design: e.g. upgrade existing engine
- Setup operational limits/strategies: e.g. train pilot, set c.g. margins/limits
- Execute tests: e.g. test engine on the ground

Table 6.5: Technical risk map after abatement

Probability \ Consequence	Minor	Major	Hazardous	Catastrophic
Very High				
High				
Medium		6		
Low		1,5,9	3	13
Very Low	2,11	4	7	8,10

Table 6.6 shows the effectiveness of the mitigation strategies implemented.

Table 6.6: Risk Mitigation Effectiveness

Effectiveness \ Severity	Minor	Major	Hazardous	Catastrophic
Not Effective				
Minimal	2	1, 3, 5		
Limited		9, 4, 6	3, 7	12, 13, 8, 10
Effective				

6.4. Risk Requirements

From the mitigation strategies outlined in Section 6.3 risk requirements can be generated. The risk requirements can be seen in Table 2.12. Only some of the mitigation strategies will be translated into requirements, since these are the ones that are going to be needed for the design phase.

6.5. Risk Item Tracking

Throughout the project small meetings where held with the technical departments to discuss new risks and evaluate the progress of mitigating identified risks. This helped introduce risk into the project, and made it an integral part where all departments where implementing risk mitigation strategies.

Table 11.13 shows the compliance with the technical risks requirements which stem from technical risk requirements.

The last step is to update the maps with new risks that may present themselves in the future. As the design process develops changes may be made which affect risks and their mitigation. During the detailed design phase additional risks may need to be considered, or some discarded. Special attention will be paid to the risks identified in this chapter by ”tracking” the, i.e. re-evaluating as the design develops.

Part II

Detailed Design

7 Propulsion System Selection

In this chapter the propulsion system sizing is explained and the selected subsystems are presented. First, the methodology is introduced in Section 7.1. Secondly, the selection of two motors to be used in the detailed design is treated in Section 7.2. Thirdly, the subsystem sizing of both a battery- and a hydrogen-powered system is presented in Section 7.3. Lastly, the cooling system is considered separately from the other subsystems. This is treated in Section 7.4. The integration of the propulsion system into the aircraft structure is analysed in Chapter 8.

7.1. Methodology

In the previous stage of design, two envelopes were identified for the propulsion systems. The model used to determine this was based on requirement PROP-PERF-2.2.2: The aircraft shall, with all engines operative, be able to climb at a rate of $5.4\ m/s$ at ISA/MSL. The tool provides an estimate of what minimum rated power is necessary to meet the climb required for a specific max take-off weight (MTOW). Also, a list of motors that may be relevant for testing on the SFPT is plotted on the graph. Note that the zero point of the horizontal axis coincides with an estimate of the total mass budget available for the propulsion system. By combining this with an estimate of the acquired mass per propulsion system source considered this acts as the starting point for the propulsion system sizing. A detailed explanation on the equations and assumptions applied in developing said model and mass estimations may be found in the Midterm Report [2].

Combining these results, the limiting cases shown in Table 7.1 are identified. At the original MTOW, the electric motor would need to provide $145\ kW$ of continuous power to meet the climb requirement. By lowering the allowable MTOW to $1750\ kg$, the aircraft would meet this requirement with minimum $80\ kW$ continuous power. Note that this is a preliminary estimate, the range of testing capabilities for the final design is analysed in Chapter 11. Furthermore, from this a list of six feasible motors are identified for testing on the SFPT, as listed below in Table 7.2. The first four motors are electric motors that either have been used with battery packs or for which plans exist for use with battery packs. The Phantom Eye uses a hydrogen internal combustion engine (ICE). Lastly, the DLR HY4 uses an electric motor in combination with a hydrogen fuel cell.

Table 7.1: Limiting power envelope cases

Case	Engine + Fuel Weight [kg]	Power [kW]	MTOW [kg]	Climb rate [m/s]
Case I	883	145	2100	5.4
Case II	533	80	1750	5.4

Table 7.2: Preliminary motor selection

Motor	Power [kW]	Weight [kg]	MTOW [kg]	Max. available weight [kg]
Magni250	280	71	2100	812
SP260D	260	50	2100	833
Emrax 348	210	42	2100	841
HDPM-250	200	15	2100	868
Phantom Eye	111	151	1750	382
DLR HY4	80	170	1750	363

In this stage of design, the two most relevant motors on this list are identified in Section 7.2. Using these motors, the remaining subsystems are then sized in Section 7.3 in accordance with the maximum capabilities of the motor and endurance requirement PROP-PERF-2.1: "The experimental engine shall operate for one hour at an altitude of $5000\ ft$". As the subsystems generate a certain power loss in the form of thermal heat, a cooling system is required to keep the subsystems within their operating temperature limits. The subsystems are all sized through an iterative process. The first iteration of the subsystems is performed using theoretical properties. With each iteration the acquired results are implemented in the structural design, and compliance with budgets and requirements is checked. At these intermediate steps, it is also re-evaluated what maximum output power can feasibly be tested for the motors. Where applicable, off-the-shelf products are selected that match what is theoretically required by the system. Some subsystems do not exist with the exact properties that are required and are therefore sized theoretically. As such, the design becomes more detailed and more accurate with each iteration.

The system is designed such that the selected motors and energy sources can be plugged into the same system with only minor modifications required. Furthermore, the entire analysis of the propulsion system assumes the aircraft weight is at the original MTOW of $2100\ kg$. At the end of Section 7.3 a discussion is included on lowering the MTOW in order to test motors with lower rated power.

The batteries and hydrogen tanks are sized for the endurance requirement by starting at the required output power of the propeller and working backwards. However, the other subsystems must be designed by taking into account the maximum power to be delivered by the motor. Namely, subsystems will have to be able to operate under these most 'extreme' conditions. Since the required output power of the propeller in cruise conditions can be calculated and the maximum continuous power of the electric motor is known, they represent a good starting point for the sizing of all the subsystems and the power generation systems. It is assumed that both the battery powered system and the fuel cell should be able to produce enough power to fly at the maximum continuous power setting of the electric motor, and fly for an hour at a cruise speed of $V = 150\ [mph]$, at $5000\ [ft]$ altitude with an assumed propeller speed of $2500\ [RPM]$. Furthermore, an estimate of the total energy required to perform taxi, take-off and climb is subtracted from the available experimental energy available for cruise.

7.2. Motor Selection

In this section the final motor selection is detailed, following from the preliminary list of motors which were identified using quantitative analysis of the climb rate requirement. Now, qualitative argumentation is used to identify which two motors are the most interesting options to implement in the SFPT. The six motors considered are listed in Table 7.2. In the text below, the elimination of discarded options is explained and the two final motors are elaborated upon in further detail.

Firstly, the Boeing Phantom Eye motor is discarded. This is a hydrogen ICE designed specifically for military drone purposes. First of all, a hydrogen ICE is at the moment 2 to 3 times less efficient than a hydrogen fuel cell. Due to this, it is assumed a hydrogen ICE is a less prospective propulsion system than a hydrogen fuel cell. Furthermore, due to this design being military, there is very little information on the layout and technical details of the propulsion system making it very difficult to implement it in the design.

Secondly, the DLR HY4 electric motor is discarded. This is, similarly to the Boeing Phantom Eye, due to the large lack of information to work with. The mass of the engine identified in the Midterm Report is found to be incorrect and no correct mass has been found [2]. This fact makes it impossible to implement this in the SFPT.

Thirdly, the H3X HPDM-250 electric motor is discarded. The company designing this motor claims it is possible to reach a power to weight ratio of $13\ kW/kg$, which is 2.5 times higher than the other electrical motors selected. When comparing it to a Formula E electric motor, which is considered to be at the top of electrical motor technology with a power to weight ratio of $7.7\ kW/kg$, a power to weight ratio of $13\ kW/kg$ seems unrealistically high. Next to this H3X have only recently begun with the design of this motor, which probably means the motor will be outside of the timeline of the project.

This leaves three options on the motor selection. To support the two definitive choices, the technology readiness level of the remaining motors is considered. Motors are deemed particularly interesting if there are plans for use in commercial aviation that are at a stage close to in-flight testing. Namely, this would allow the SFPT project to begin manufacturing immediately after finishing the design phase. This resulted in choosing the Magni250 and the Emrax 348 as the two engines the design will be made for. The Magni250 and Emrax 348 are attractive options due to several reasons. The Magni250 can provide up to $280\ kW$ maximum continuous power, and by designing for this the testbed can greatly expand its envelope compared to the original continental IO-360 engine it is replacing, which can provide approximately $157\ kW$ output power [31]. Furthermore, the Magni250 is planned for FAA certification in 2022, and is set to be used in the Eviation Alice 9-seat commercial aircraft. [1] This aircraft aims to achieve its FAA type certification by 2023.[2]. Originally, the SP260D was going to be used but this was replaced by the Magni250 because it was further in development.[3] This is also why the SP260D is discarded for detailed design of the SFPT. Namely, it is currently not very far along with ground tests, which would cause delays in the project. The Magni250 is further in development but has also not been tested in flight, and the SFPT provides a great opportunity to do so.

The Emrax 348 can provide up to $210\ kW$ max continuous power if air and liquid cooled, or $189\ kW$ if liquid cooled. This is closer to the output power of the original continental IO-360, making it a suitable replacement. This engine has been classified at Technology Readiness Level (TRL) 9, meaning that the system can be used in its operational environment, and EASA certification is currently in progress [24]. Also, it is worth noting that earlier, smaller models of this series are already implemented in several successful electric aircraft.[4]

Therefore, this selection boils down to the Magni250 and the Emrax 348. An overview of several important parameters including, power, efficiency and weight are given in Table 7.3. Note that maximum continuous power of the Emrax 348 is decreased from $210\ kW$ to $189\ kW$, as the engine is to be liquid cooled. By using a combination of liquid and air cooling the Emrax 348 could deliver $210\ kW$.

Table 7.3: Properties of selected motors

Motor	Power [kW]	Efficiency [-]	Motor Weight [kg]	MTOW [kg]	Max. available weight [kg]
Magni250	280	0.93	71	2100	812
Emrax 348	189	0.92	42	2100	841

7.3. Subsystem Sizing

Two possible energy sources considered are a battery pack and hydrogen in combination with fuel cells. Both energy sources deliver direct current (DC) power to the system, which also contains components running on alternating current (AC). In Section 7.3.2 and Section 7.3.3, the sizing of the two specific systems is elaborated upon further. To be able to perform this analysis, the required subsystems are identified and the methodologies used to size these specific subsystems are introduced in Section 7.3.1.

7.3.1. Subsystem Identification

Propeller

The efficiency of the propeller must be obtained to compute the required power output of the electric motor and thus the required power output of either the batteries or fuel cell. The efficiency is estimated using the rule of thumb of Rogers [13]. This estimation uses the propeller advance ratio J as a function of cruise speed V in m/s, propeller rotational speed n in RPS, and the propeller diameter D in m as can be seen in Equation 7.1. Equation 7.2 is a quadratic estimation of $\eta_{prop} = f(J)$.

$$J = \frac{V}{n \cdot D} \tag{7.1}$$

$$\eta_{prop} = -0.75 \cdot J^2 + 1.5 \cdot J + 0.15 \tag{7.2}$$

[1] `https://www.futureflight.aero/news-article/2020-11-19/faa-seeks-input-special-conditions-certify-magnix-electric-propulsion` [Accessed June 2021]

[2] `https://airwaysmag.com/innovation/eviation-alice-maiden-flight/` [Accessed June 2021]

[3] `https://www.flightglobal.com/airframers/eviation-receives-alices-first-magnix-electric-propulsion-unit/143760.article` [Accessed June 2021]

[4] `https://emrax.com/references/aviation-aerospace/` [Accessed June 2021]

Electric motor

The electric motors have been chosen in Section 7.2. As is stated in Section 7.1 the power generation systems are sized for the maximum continuous power output of both the Magni250 and Emrax 348. The performance parameters of these electric motors can be found in Table 7.3.

Inverter

Another subsystem to consider is an inverter. An inverter changes the direct current output power of the DC-DC converter to an alternating current to input into the electric motor, the coolant pump, the cooling fan, or the compressor. It was decided to use the specifications of the MagniDrive for both the Magni250 and the Emrax 348. This means the efficiency of the inverter is $\eta_{inverter} = 0.989$, and the mass for an output power of $170\ kW$ is $12\ kg$.[5] It has to be taken into account that this inverter is not able to handle the maximum continuous power required by the electric motor, and is therefore sized to the theoretical power output it should be able to handle, as can be seen in Equation 7.3.

$$m_{inverter} = \frac{m_{MagniDrive}[kg]}{P_{MagniDrive}[kW]} \cdot P_{req_{out}} = \frac{12}{170} \cdot P_{req_{out}} \tag{7.3}$$

DC-DC converter

Furthermore, DC-DC converters are also considered. The input voltage required by the motor is assumed to be different than the output voltage of the battery or fuel cell. This requires the voltage to be changed to the required voltage by the electric motor, which is done by a DC-DC converter. The DC-DC converter is sized using a verified and validated method by Mueller et al. [37]. Noting that the output power of the DC-DC converter is directly used by the inverter, the mass is given by Equation 7.4. The DC-DC converter has an efficiency of $\eta_{DCDC-conv} = 0.98$

$$m_{DCDC-conv} = 0.016 \frac{[kg]}{[kW]} \cdot P_{inverter} \tag{7.4}$$

Power distribution system

In order to minimise the number of modifications when switching propulsion systems, the power distribution system is to be shared by both types of propulsion systems. Since this system is in between the power generation system (batteries or fuel cell) and the electric system and cooling, it will be used in the sizing computations in Section 7.3.2 and Section 7.3.3. The power distribution system (PDS) is to be sized using Vonhoff [44]. In Vonhoff it is stated that the power management and distribution system (PMAD) is responsible for both converting the DC power as well as inverting it to ac power and distributing and controlling the power to the electric motor, the compressor, and the cooling system. Since a DC-DC converter and inverter will be sized separately in this report, the PDS will be sized using an adapted method, which can be seen in Equation 7.5 and Equation 7.6, where $\hat{\rho}_{pds} = 10\ kW/kg$ is the specific power density and $\eta_{PMAD} = 0.9$ is the assumed efficiency of a PMAD system according to Vonhoff [44]. The efficiency is divided by the inverter and converter efficiency to the power three due to the three outputs of the PMAD system assumed by Vonhoff [44].

$$m_{pds} = \frac{P_{pds}}{\hat{\rho}_{pds}} - m_{DCDC-conv} - m_{inverter} \tag{7.5}$$

$$\eta_{pds} = \frac{\eta_{PMAD}}{(\eta_{DCDC-conv} \cdot \eta_{inverter})^3} \tag{7.6}$$

Cooling

The cooling system ensures that either the batteries or the fuel cell together with all the other subsystems remain within their required operating temperatures. Since the size and power requirement of the cooling system is dependent on the power output of the batteries or the fuel cell and on whether it is

[5] `https://www.magnix.aero/products`[accessed May 2021]

cooling batteries or a fuel, the sizing of the cooling system is done in Section 7.4. As the cooling system draws relatively little power (in the order watts, not kilowatts), it is connected to the aircraft alternator power bus. This is also better for safety concerns, so that the cooling system can still operate in case of failure of the experimental energy source.

Cables

As this system requires very high power transmission, the cables represent a considerable part of the mass budget. For this analysis, the focus lies on cables estimated to be over $0.1\ m$ in length. For these longer cables, a safety factor of 1.5 is applied to the length, to account for corners and differences in height between subsystem components. As some subsystems are placed close together, the contribution to the mass budget of the cables interlinking them is considered negligible. Some short cables will be required to connect these subsystems, but it is assumed that their effect is taken into account in the safety factors applied.

Currently, there are no cables commercially available in aviation certified to carry the combination of high voltage and high current required by the components in the system. Due to this, no off-the-shelf products can be selected, and the cables must be sized theoretically, for which no verification step-by-step plan exists. Therefore, a methodology is developed for this purpose by combining properties of existing aviation cables with theoretical insights using a statistical approach.

Usually, cables are selected by choosing a cable that best matches several properties such as the required efficiency, available mass budget and current rating. A cable consists of a conductor enclosed in a sheathing of insulation. It is important to note that the current rating depends mainly on the conductor, whereas the maximum voltage depends mainly on the insulation. The conductors are available in various diameters as dictated by the American Wire Gauge (AWG) system. In aviation, the most used conductors consist of copper or aluminium cores with a metal plating such as nickel, tin, or silver. The main purpose of coating the core with another metal is to increase corrosion resistance and increasing allowable operating temperature. For this project, it is decided to use nickel plated copper cables. Copper is chosen for the conducting material because of its superior conductivity and ductile strength compared to aluminium.[6] Also, copper has greater thermal properties than aluminium, which is beneficial for potential energy inefficiencies for high power transmission in an experimental system. Aluminium would have the advantage of having lower weight, but since the cables are all relatively short their contribution to the mass budget is limited regardless. Nickel plating is selected because this allows for high operating temperatures and resistance to corrosion at extremely low temperatures. [7] It is noted that a weight ratio of nickel to copper of 27% is common for aviation wires. This ratio is assumed for the remainder of the design analysis.

As stated before, commercially available cables do not fit the required properties for the SFPT. Namely, available ampacities (current ratings) range to slightly upwards of $300\ A$ and most cables are at best insulated for a voltage of $600\ Vrms$. It is assumed that the ampacity and voltage rating can be sized independently. Focusing first on ampacity, by plotting the ampacity and conductor cross-sectional area using values from the Handbook of Electronic Tables and Formulas for AWG size cables, a linear relation between these values is found, as can be seen in Figure 7.1 [46]. The current ratings used to generate this statistical estimate are conservative; in reality this is likely to be higher for a given AWG size. Now assuming ampacity scales linearly with cross-sectional area, Equation 7.7 is obtained. This ratio of required area over initial area is used to estimate the increase in conductor weight required. It is used in combination with statistical averages from reference cables. The final conductor radius r is obtained using Equation 7.8, where A is area and I indicates current. Whenever the reference wires have larger ampacities than required, the conductor diameter is not modified and standard off-the-shelf sizes are used.

$$r_{A_{cond}} = \frac{A_{cond_{new}}}{A_{cond_{ref}}} = \frac{I_{new}}{I_{old}} \tag{7.7}$$

[6] `https://www.anixter.com/content/dam/anixter/resources/wire-wisdom/anixter-aluminum-versus-copper-wire-wisdom-en.pdf` [Accessed June 2021]

[7] `https://www.nassauelectrical.com/pages/good-reasons-why-nickel-plated-copper-cables-perform-well-in-harsh-environments` [Accessed June 2021]

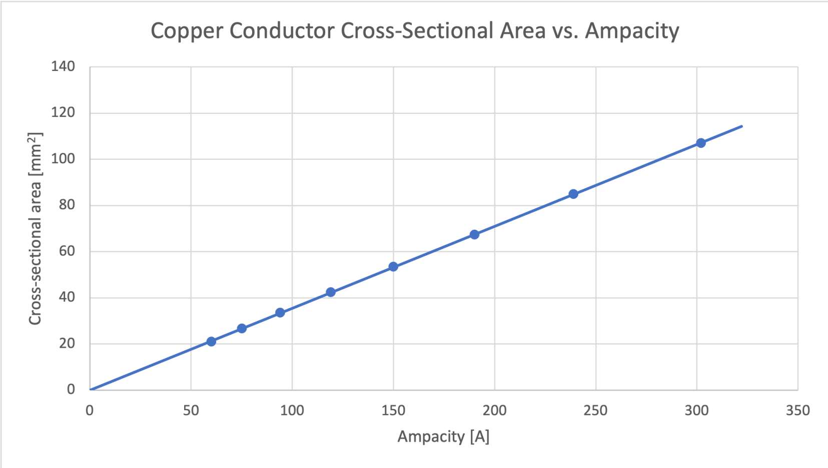

Figure 7.1: Cross-sectional area of copper conductor for various current ratings [46]

$$d_{cond_{new}} = \sqrt{\frac{A_{cond} \cdot 4}{/pi}} \tag{7.8}$$

As the original conductor weight per meter of reference cables used is not directly specified (only the finished cable weight per meter is given), some assumptions must be made. The conductor mass is assumed to consist solely of a commonly used copper wire mass for the specified AWG size. This assumption is reasonable for nickel plated copper because the densities of nickel and copper are very close, namely $8908\ kg/m^3$ and $8940\ kg/m^3$.[8] The power loss for each cable can be calculated using the current flowing through the conductor, using Equation 7.9.[9] For preliminary iterations, a total cable efficiency of 0.98 is assumed, as this cable efficiency is commonly sized for in aviation. Also, it is assumed that return cables do not contribute any power loss as in an optimally engineered electrical system the return cables carry only negligibly low voltage. In Equation 7.9 the $\rho_{(\Omega-m)}$ is the resistivity of the wire.

$$P_{loss_{(kW)}} = 1000 \cdot \frac{I^2_{(A)} \cdot \rho_{(\Omega-m)} \cdot L_{(m)}}{A_{(sqmm)}} \tag{7.9}$$

In continuation, using the calculated conductor area the required insulation can be determined. For this, again the same reference cables are used. It is noted that the main contribution to insulation depends on the dielectric strength of the material, given in V/m, and sufficient thickness is required to prevent corona discharge. Therefore, the reference thickness of the insulation, which equals outer finished cable diameter minus conductor diameter, must be increased by the ratio $r_V = \frac{V_{new}}{V_{old}}$. This gives in an increase in insulation area as shown in Equation 7.11. The reference insulation thickness is taken to be $d_{insu_{ref}} - d_{cond_{ref}} = 2.5\ mm$, equal to the largest insulation thickness observed across the reference cables. Coincidentally, it also equals the average insulation thickness times a safety factor of 1.25 for redundancy. The reference thickness is assumed constant, as no apparent trends are observed between conductor sizing and insulation thickness. This is a logical result, verifying the applied assumption that the required insulation thickness only depends on voltage. Similar to the conductor analysis, the calculated area ratio can be multiplied by the reference insulation weight per meter to give the new required insulation weight per meter. The reference insulation weight is taken to equal the weight of the cable minus the weight of conductor. The total cable diameter (of outer insulation) is obtained using Equation 7.10. Whenever the reference wires have larger voltage ratings than required, the insulation thickness is not modified and reference values are used.

[8] `https://www.engineeringtoolbox.com/metal-alloys-densities-d_50.html` [Accessed June 2021]
[9] `https://www.electrical4u.net/calculator/cable-power-loss-calculator-formula-calculation/` [Accessed June 2021]

$$d_{insu_{new}} = d_{cond_{new}} + \frac{V_{new}}{V_{ref}} \cdot (d_{insu_{ref}} - d_{cond_{ref}}) = d_{cond_{new}} + \frac{V_{new}}{600} \cdot 2.5 \tag{7.10}$$

$$r_{A_{insu}} = \frac{A_{insunew}}{A_{insu_{ref}}} = \frac{d^2_{insu_{new}} - d^2_{cond_{new}}}{d^2_{insu_{ref}} - d^2_{cond_{ref}}} \tag{7.11}$$

Together, this leads to Equation 7.12. Here $m_{cond_{AWGx}}$ denotes the average copper conductor mass per meter and $m_{insu_{AWGx}} = m_{tot_{AWGx}} - m_{cond_{AWGx}}$ denotes the reference insulation mass per meter. The values used in Table 7.4 below are used to size the new theoretical cables [4][46].

$$m_{cable} = r_{A_{cond}} \cdot m_{cond_{AWGx}} + r_{A_{insu}} \cdot m_{insu_{AWGx}} \tag{7.12}$$

Table 7.4: Properties of reference power transmission cables, rated at $600\ Vrms$ [4][46]

AWG	Conductor diameter $d_{cond_{ref}}[mm]$	Outer diameter $d_{insu_{ref}}[mm]$	Ampacity $I_{ref}[A]$	Conductor mass $m_{cond_{AWGx}}[g/m]$	Total mass $m_{tot_{AWGx}}[g/m]$
0000	15.9	18.4	302	954	1235
000	14.4	16.9	239	756	980
00	12.5	15	190	600	775
0	11.3	13.8	150	475	615

7.3.2. Battery Powered System Sizing

Using the identified subsystems, the batteries can be sized. As stated before, the subsystems are sized by working backwards from the propeller to size for endurance and from the motor to account for maximum rated motor power. This is done by dividing each component output power by its efficiency to find the required input power. To help visualise this process, an electrical block diagram of the battery-powered propulsion system is included in Figure 7.2 below. As indicated in the legend, also a section of the alternator power bus is included. Namely, the battery management system (BMS) integrated in each PB345V124E-L battery must be powered by an auxiliary system.[10] This BMS has several functions, namely automatic cell over-voltage protection, cell under-voltage protection and cell over-temperature protection. Also, it calculates the battery pack state of charge.[11] The power distribution system is also directly connected to the controller, to set required power of the batteries based on pilot input. Furthermore, note that the cooling system is not included in this diagram as that system is connected to the separate power bus and does not directly influence the system. This choice is made purposefully as a means of risk mitigation, so that if the batteries are shut off due to overheating of a component the cooling system can continue to operate. This mitigates the risk of for example thermal runaway occurring. Furthermore, for the cables the maximum expected voltages and currents are included. These values are independent and not expected to occur simultaneously, but are rather included to give an indication of the most extreme conditions for cable sizing.

Battery Packs

Starting with the propeller, the required output power of the experimental engine can calculated. This is done using an adaptation of the performance model explained in Section 10.3. To use this model to size for the endurance requirement PROP-PERF-2.1, "The experimental engine shall operate for one hour at an altitude of $5000\ ft$", several assumptions must be made. Firstly, the desired true airspeed must (TAS) be selected. It is chosen to cruise at $150\ mph$ TAS. This choice is made because it falls within the cruise speed range of the original Skymaster and still leaves room for further acceleration or deceleration. Furthermore the propeller rotations per minute (RPM) must be identified. For this $2500/RPM$ was assumed. Lastly, to calculate the required power of solely the rear (experimental) engine, an assumption must be made on the power consumption of the front engine. For this, the Skymaster Owner's

[10] https://www.pipistrel-aircraft.com/aircraft/electric-flight/batteries-systems-and-bms/ [Accessed June 2021]

[11] https://www.pipistrel-aircraft.com/aircraft/electric-flight/batteries-systems-and-bms/ [Accessed June 2021]

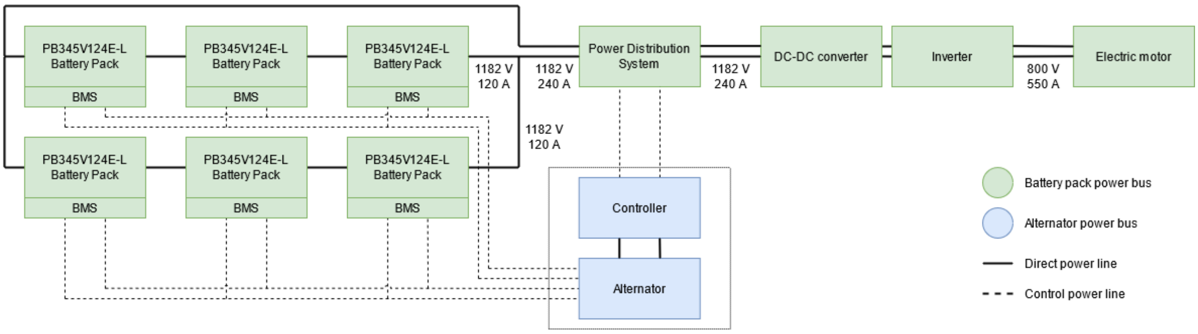

Figure 7.2: Electrical block diagram of battery-powered propulsion system

Table 7.5: Energy required for taxi, take-off and climb

Phase	Energy [kWh]
Take-off	1.48
Climb	7.71
Total	9.19

manual is used. In this manual, it is stated that cruise of the original Skymaster usually occurs between 65-75% of rated power [9]. To maximise endurance of the alternative propulsion system, it is decided to cruise using a fixed 75% of available output power from the front propeller. The output power required from the rear propeller is then the total required power to cruise (at $5000\ ft$, $150\ mph$ and 2500 RPM) minus 75% of available front propeller output power. Applying these assumptions to the model yields a required power output of $41.78\ kW$ from the rear propeller.

Furthermore, the power required from the experimental propulsion system to perform taxi, take-off and climb to $5000\ ft$ must be taken into account in calculating the endurance of the SFPT. As there are countless possible conditions under which this can occur, several assumptions are made. The assumptions are derived from performance of the original aircraft. To begin with, taxi is assumed to be occur using only the front engine. If the aircraft must taxi over loose gravel it is recommended to use the rear engine, but since this is a testbed it is assumed the aircraft will take-off from well maintained runways [9]. In the Owner's Manual it is stated that take-off occurs at full throttle of the original engines [9]. Therefore, the rear engine is assumed to deliver IO-360 peak power for a duration of 30 seconds, after which the aircraft commences the climb phase. In the Owner's Manual regular climb is stated to occur at $1100\ ft/min$, under which conditions it would take 4 minutes and 33 seconds to reach $5000\ ft$ altitude from $0\ ft$ [9]. This rate of climb is possible using 75% of original peak power of both engines [9]. To increase experimental propulsion system endurance, the maximum continuous power of the front engine is used, which decreases the power required by the rear engine to achieve the same total power. By multiplying the power by time and dividing the result by the total electrical efficiency from battery output to engine output, the required energy is calculated. The results are presented in Table 7.5. Note that the results are estimates due to the assumptions applied and will vary depending on take-off procedure, but serve as an indicator for expected order of magnitude.

By applying the process outlined in Section 7.3.1 above and working backwards using the assumed efficiencies, the required power output from the batteries can be identified for the specified cruise conditions. As explained before, note that for preliminary iterations the cable efficiency of 98% was used across the total length. Using the calculated required battery output and the state-of-the-art battery specific energy, the required battery mass can be found. Currently, the best battery pack certified for use in aviation is the PB345V124E-L. This battery pack can be found on the Pipistrel Velis Electro, the world's first type certified electric aircraft. One battery pack weighs $72\ kg$ and provides a power capacity of $11\ kWh$, according to the Velis Electro type certificate. This results in a specific energy of $152.78\ Wh/kg$. This value can be used to calculate the theoretical required mass of batteries to be used. However, as opposed to other subsystems, namely the cables, the power distribution, the DC-DC converter, and inverter, the choice is made to use the PB345V124E-L battery packs instead of theoretically sizing them. Namely, the other subsystems are available in many sizes and are often tailored to specific purposes while the development and certification of a battery pack is much more complex and expensive. Therefore, also taking into account the energy required for take-off and climb, the required number of battery packs is determined. Using the calculated battery power it is found that between five and six PB345V124E-L batteries would be needed to meet the endurance requirement of one hour of cruise.

The same process can be applied from the electric motor to calculate whether the motors could be tested at their maximum rated capacity. This depends on the electric motor selected and therefore varies between the Emrax 348 and Magni250. As is explained in Section 7.4, liquid cooling is used as opposed to either air cooling or a combination of both. This limits the maximum continuous power of the Emrax 348 to $189\ kW$, where the Magni250 is still rated at $280\ kW$ continuous power. As higher power is more demanding for the batteries and subsystems, this is used for the sizing. The chosen PB345V124E-L can deliver a maximum of $394\ V$ and $120A$ resulting in a maximum output power of $47.28\ kW$ per battery. Taking this into account along with the efficiencies of the subsystems it is found in all iterations that it would require more than six batteries to test $280\ kW$ engine output power. Therefore the choice must be made between using six or seven batteries in the final design.

For the rest of the propulsion system design, six batteries are used for several reasons. Firstly, this is decided due to volume constraints. The batteries are stored in the fuselage between the rear firewall and a new firewall as explained in Section 8.3. There is enough volume in this compartment available for the six batteries to be safely integrated into the aircraft structure. However extra batteries would not fit here and would have to be incorporated into the wings. Secondly the mass is considered. Each battery adds a minimum of $72\ kg$ of mass to the system, along with more structural support, cabling, and cooling. Third, incorporating these batteries into the wings would lead to increased structural, electrical, and cooling complexity. Fourth, the rated power that can be tested is still far above original rated power of the motor, so this still allows for testing a considerably large envelope. For the final system presented in Table 7.6, the power of motors that can be tested is now limited to $252\ kW$. A discussion on the effect of choosing six, seven or eight batteries is included in Equation 7.3.2. For sizing of the cooling subsystem in Section 7.4 a thermal efficiency of 0.99 is assumed for the batteries. This value is conservatively assumed using the thermal efficiency of reference batteries [29]. Note that this efficiency is not applied to the nominal capacity of the batteries, as it is assumed they are already derated to account for this.

Subsystems

With the choice to use six batteries, the rest of the subsystems can be sized using the maximum power that the batteries can supply at once. This is done using the weight estimation techniques outlined in Section 7.3.1. The results are outlined in Table 7.6.

For the cables, some further assumptions are made, firstly for the cable length. Note that a safety factor of 1.5 is used for the cable length, as mentioned before. In order to limit the current through the cables while still allowing for a redundant configuration in case of single battery failure, the batteries are placed in two parallel rows of three batteries in series. For each row, the cables are assumed to run along the width of the fuselage at the new firewall ($0.98 \cdot 1.5\ m$ each). Then, there is a cable junction before the cable enters the power distribution system in the corner of the fuselage wall and new firewall. From here, a cable runs to just aft of the rear firewall ($0.7 \cdot 1.5\ m$). Then the power flows through the DC-DC converter and inverter before entering a cable that runs from the rear firewall to the aft propeller ($1.37 \cdot 1.5\ m$). To size the cables the individual maximum current and maximum voltage that could flow through them are used. This explains why in Table 7.6 cable 1 and cable 2 have the same weight estimate for both motors. Cable 3 on the other hand depends on the maximum current and maximum voltage that the motor could require. As these values differ, the cable weight differs per motor [31] [33].

As for the one hour endurance requirement in cruise, the final endurance is calculated using by dividing the total power capacity of the batteries minus the energy required for take-off and landing by the required battery output power for both motors. With six batteries the aircraft can provide $E_{bat} = 66\ kWh$ of energy, and take-off and climb is found to require $E_{req_{cruise}} = 9.19\ kWh$. Using the Emrax 348, the aircraft requires a continuous power of $P_{req_{cruise}} = 54.03\ kW$ from the batteries. For the Magni250, the system requires $P_{req_{cruise}} = 53.45\ kW$ of continuous power. Therefore, using Equation 7.13, the

Table 7.6: Overview of subsystem sizing for battery-powered system

Subsystem	Mass [kg]	
	Emrax 348	Magni250
Motor	42	71
Cable 3	9.22	8.75
Inverter	14.51	19.13
DC-DC converter	3.32	4.39
Cable 2	3.25	3.25
PDS	3.37	4.45
Cable 1	4.57	4.57
Battery	432	432
Total	508.74	547.54

Table 7.7: Propulsion system endurance, testable engine power and total propulsion system for 6, 7 or 8 batteries

Number of batteries	Endurance [min]	Engine power [kW]	Total mass [kg]
6	64	252	548
7	76	294	619
8	88	336	691

aircraft has an endurance $T_{endurance}$ of 1 hour and 3.1 minutes for the Emrax 348 and 1 hour and 3.8 minutes for the Magni250.

$$T_{endurance} = \frac{E_{bat} - E_{req_{climb}}}{P_{req_{cruise}}} \tag{7.13}$$

As interchangeability is one of the goals of this design the subsystems with the highest power-carrying capacity, and thereby the highest weight, are used for both motors. This increases the total mass for the Emrax 348 system to approximately $518.54\ kg$. The total mass for the Magni250 system remains $547.54\ kg$.

Future Possibilities

In this subsection several future possibilities for the battery-powered propulsion system are introduced. The viability of these options depends both on external scientific development and DEAC's ability to implement these ideas.

Also, the use of extra batteries can be considered. As explained in the previous section, using more than six batteries comes with several drawbacks. It adds considerable complexity to the design, but nevertheless it could be possible in terms of mass budget. Namely, the current total aircraft mass equals $1923\ kg$, which is still $177\ kg$ below the MTOW. The mass budget breakdown can be found in Section 11.2. As explained before, the extra batteries would need to be stored in wings. Auxiliary tanks including fuel weighed $49\ kg$ each [9].However, this would require using different batteries to the ones installed in the fuselage due to dimensional constraints. If the full volume would be filled with batteries a structural analysis of the wings would be required, since the density of batteries are larger than that of fuel. For this, new battery packs could be developed or an off-the-shelf product could be selected. However for both options, a lower specific energy would be expected, considering that the PB345V124E-L battery pack specific energy is among the current state-of-the-art. Furthermore, this would add considerable complexity to the electrical system as it likely generates a different current and voltage. Momentarily neglecting mass from extra cables and structural support, this would result in the properties shown in Table 7.7. The results shown are calculated for the Magni250, as this engine is currently limited in its maximum testable power, and are rounded to whole numbers.

Furthermore, in the future batteries are expected to achieve far greater power densities. Lithium-Ion batteries are slowly reaching their maximum potential, but initial developments in other technologies are very promising. A particularly interesting option is the use of Lithium-Sulphur battery packs, which are expected to reach $500 - 600\ Wh/kg$ specific energy on cell level in the coming years. Even if it is assumed that $30-40\%$ of specific energy is lost due to packaging, this results in a worst case $300-420\ Wh/kg$ specific energy, which is still far above that the $152.78\ Wh/kg$ specific energy of the PB345V124E-L battery pack that is currently designed for. In this case, the aircraft could fly for one hour of cruise under the specified conditions and require only $147-209\ kg$ of batteries, a considerable improvement from the current battery mass of $432\ kg$. Therefore, much longer missions could be designed for. Also, as this allows to carry more batteries on board which can together provide a larger amount of power, higher rated motors could be tested. Another option would be to decrease the MTOW further and still meet the endurance requirement, allowing for further expansion of the motor envelope to lower rated motors as the climb requirement can still be met.

Verification and Validation
Verification and validation is applied as defined in Section 3.5.

For code verification, unit tests are applied using the 'unittest' module in Python and a coverage report indicates a coverage of 79% of the written code. Furthermore, all intermediate results for functions and classes are checked to determine whether results are as expected. For example, the calculated efficiencies of cables must be below 1, as otherwise they would be giving extra power to the system instead of losing power due to thermal inefficiency. Also, several systems tests are applied to verify accurate integration of the different units. An example of this is verifying whether the calculated total electrical system efficiency times required battery power equals motor power, which it does.

For validation, the calculated results are compared to real off-the-shelf products where possible. For some subsystems, no products exist on the market with the required power transmission abilities, so the model is validated using lower input powers. As an example, for validation of the cabling sizing, an existing $600\ Vrms$ AWG0 cable is scaled to cable sizes up to a $600\ Vrms$ AWG0000 cable and results are compared. The estimate is closest to the real cable for smaller size changes but even when scaling the AWG0 to AWG0000 the diameter approximation error is smaller than 1%. The same process is applied for cables with the same AWG size scaled from different lower voltages to $600\ Vrm$. It is found that the calculated required thickness slightly overestimates compared to the average. This is considered good, as it ensures the insulation thickness is sufficient and has only a very small influence on estimated weight.

It is recognised that further validation is required in the future. Namely, sizing of individual components is validated but this is not yet done for the total system. A good way to do this would be by applying the model to existing electric aircraft using as input the required cruise power and maximum power to be transmitted. This is not yet done as such detailed information is generally not disclosed, but if this can be obtained it would serve as a great means of validation. If any estimates of mass of efficiencies are off significantly, and this cannot be attributed to major system differences, the methods used can be adjusted accordingly.

Furthermore, several sensitivity analyses are performed. An example of this is checking possible variations on the specific energy of the battery pack, perhaps the most important value in this analysis. In the Pipistrel type certificate an $11\ kWh$ power capacity per $72\ kg$ battery pack is quoted, while on the Pipistrel Velis Electro website this is stated as $12.4\ kWh$ specific energy per battery pack [19].[12] For this, it is calculated that $4.99-5.05$ battery packs would be required. Also, from PB345V124E-L website the specific energy can be deduced. Using the nominal nominal energy capacity of $30\ Ah$ and nominal voltage $345\ V$ a power capacity of $10.35\ kWh$ is obtained.[13] This would result in needing $5.98-6.04$ battery packs. Therefore in a worst case scenario the aircraft could still cruise for almost one hour. The likelihood of the power capacity being lower than $11\ kWh$ is assumed low, since the aircraft was likely type certified using conservative numbers. Other examples of performed sensitivity analyses include checking a wider range of found efficiencies and power transmission densities of subsystems. The motor efficiency would have to be reduced to below 0.88 before more than six batteries are required to meet the endurance requirement.

[12] https://www.pipistrel-aircraft.com/aircraft/electric-flight/velis-electro-easa-tc/ [Accessed June 2021]
[13] https://www.pipistrel-aircraft.com/aircraft/electric-flight/batteries-systems-and-bms/ [Accessed June 2021]

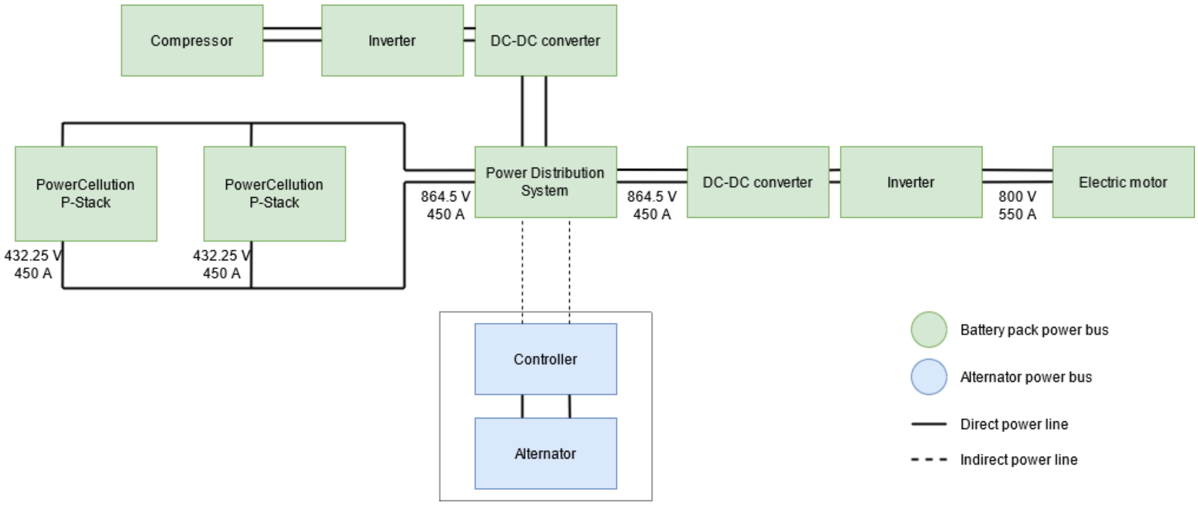

Figure 7.3: Electrical block diagram of hydrogen fuel cell powered propulsion system.

7.3.3. Hydrogen System Sizing

In this subsection, both the hydrogen fuel cell system as well as the hydrogen storage will be sized in both mass and volume, using the methodology developed by Vonhoff [44]. A presentation of the electrical system can be seen in the form of an electrical block diagram in Figure 7.3. Equal to the electrical block diagram for the battery-powered system the power distribution system is directly connected to the controller, to set required power of the batteries based on pilot input. The cooling system is not included in this diagram as that system is connected to the separate power bus and does not directly influence the electrical system. This choice is made for risk mitigation purposes, so that if the hydrogen fuel cells are shut off due to overheating of a subsystem or drying out of the fuel cells the cooling system can continue to operate.

Hydrogen Fuel Cell

To size the hydrogen fuel cell, the methodology from Vonhoff was adopted [44]. This method assumes any fuel cell consists of 5 components: The fuel cell, a compressor, a cooling system, a power management and distribution system, and an electric motor [44]. For cables and other minor subsystems the method assumes a factor of 1.2 to be added to the mass, however since the cables are sized specifically for this design and the mass of other subsystems is assumed to be negligible, it was decided to neglect this factor in the calculations. The DC-DC converter, inverter, cables, and electric motor will be sized using the methods described in Section 7.3. The cooling will be separately sized in Section 7.4. The fuel cell is assumed to be a Low Temperature Proton Exchange Membrane Fuel Cell, due to the technology being more developed compared to other types of fuel cells [44].

For the cables, some further assumptions are made which correspond to the assumptions made in Section 7.3.2. Firstly for the cable length, note that a safety factor of 1.5 is used for the cable length. It is assumed one large cable runs along the new firewall ($0.98 \cdot 1.5\ m$), one large cable runs from the new firewall to the rear firewall ($0.7 \cdot 1.5\ m$), and one large cable runs from the rear firewall to the aft propeller ($1.37 \cdot 1.5\ m$). To size the cables the maximum current and maximum voltage that could flow through them are used, which for the electric motor is $I_{max} = 550\ A$ and $V_{max} = 800\ V$ respectively. For the cables leading from the fuel cell to the pds and the DC-DC converter the maximum current and voltage are determined using the PowerCellution P-Stack fuel cell, with $I_{max} = 450\ A$ and $V_{max} = 432.25\ V$ per fuel cell stack.[14] This explains why in Table 7.8 cable 1 and cable 2 have the same weight estimate for both motors, but cable 3 does not as it depends on the maximum current and maximum voltage that the motor could require. As these values differ, the cable weight differs per motor [31] [33].

The total power the fuel cell should be able to generate is the sum of all the subsystems it is powering throughout the flight, which is the output of the PDS, for which the power goes through cable 1 and the PDS. How to compute the power required for the electrical motor has been covered in Section 7.3,

[14] `https://powercellution.com/p-stack` [Accessed June 2021]

where P_{cable_2} is the required output power of the cable into the DC-DC converter for the electric motor. To size the compressor correctly, it needs to be taken into account that as well as for the electric motor the compressor needs an AC power input assumed to be on a different voltage than what the fuel cell is producing. Therefore another inverter and DC-DC converter is required. Since the compressor is very close to the fuel cell, the length and thus mass and influence of the cables is assumed to be negligible. $P_{DCDC-comp}$ is thus the required output power of the DC-DC converter for the compressor.

$$P_{FC} = \frac{P_{pds}}{\eta_{cable_1} \cdot \eta_{pds}} \tag{7.14}$$

$$P_{pds} = \frac{P_{cable_2}}{\eta_{cable_2}} + \frac{P_{DCDC-comp}}{\eta_{DCDC-conv}} \tag{7.15}$$

The required power to compress the incoming air before entering the fuel cell can be computed using the required mass flow into the fuel cell and the change in total air temperature before and after compression, as can be seen in Equation 7.16. The stoichiometric ratio λ_{O_2} is the ratio of oxygen supplied over the oxygen necessary for the electrochemical reaction with hydrogen, which usually is between 1.5 and 2.0 to ensure the entire fuel cell has sufficient oxygen partial pressure resulting in optimal fuel cell performance [44]. In Equation 7.20 the total air temperature is derived using the first law of thermodynamics to calculate the total enthalpy $h_{tot} = h + (V^2/2)$ and implementing, by assuming a constant specific heat capacity at constant pressure, that enthalpy is $h = Cp \cdot T$. The required mass flow is computed using the required power and the efficiency of the fuel cell [44]. Using the pressure ratio at altitude p_{alt}/p_0 times a factor of 1.05 to account for pressure losses after the compressor, the total temperature after compressing can be computed together with the total air temperature T_{tot1}, the compressor efficiency η_{comp}, and the heat capacity ratio of air γ. Together with the mass flow of the air $\dot{m}_{air}$, which is computed using the stiochiometric ratio λ_{O_2} and the power and efficiency of the fuel cell P_{FC} and η_{FC} respectively, the power used by the compressor P_{comp} can be computed. For this also the difference between the total temperatures before and after compression divided by the efficiency of the electric motor $(T_{tot2} - T_{tot1})/\eta_{em}$ and the specific heat capacity at constant pressure C_p are used. In $(T_{tot2} - T_{tot1})/\eta_{em}$ it is assumed the electric motor driving the compressor has the same efficiency as the electric motor used for propulsion.

$$P_{comp} = \dot{m}_{air} \cdot C_p \cdot \frac{T_{tot2} - T_{tot1}}{\eta_{em}} \tag{7.16}$$

$$\dot{m}_{air} = 2.856 \cdot 10^{-7} \cdot \lambda_{O_2} \cdot \frac{P_{FC}}{\eta_{FC}} \tag{7.17}$$

$$T_{tot2} = T_{tot1} \cdot \left(1 + \frac{1}{\eta_{comp}}\right) \cdot PR_{comp}^{\frac{\gamma-1}{\gamma}-1} \tag{7.18}$$

$$PR_{comp} = \frac{p_{alt}}{p_0} \cdot 1.05 \tag{7.19}$$

$$T_{tot1} = T_{alt} + \frac{V^2}{2 \cdot C_p} \tag{7.20}$$

It may be noted that the required fuel cell power depends on the required power for the compressor, but also that the required power for the compressor depend on the fuel cell power. In order to estimate both of these an iterative process is required and a model is built to size the system. For this the compressor power is taken to be the output power of an inverter - this uses the output power of a DC-DC converter connected to the PDS. The efficiencies of these components are taken into account according to the subsystems and their sizing introduced in Section 7.3. Note that there are different inverters and DC-DC converters sized for the compressor compared with the electric motor.

It is known how much power is required from or for each main subsystem, so next the specific power density of each major subsystem is required from literature to get to the mass. Again these assumptions were based the method from Vonhoff for fuel cell sizing [44]. The specific power densities for the compressor and the fuel cell are assumed to be $\hat{\rho}_{comp} = 2.0\ kW/kg$ and $\hat{\rho}_{FC} = 125/42\ kW/kg$ respectively, where that of the compressor is based on Vonhoff and that of the fuel cell is based on the PowerCellution P-Stack [44].[15] The mass of both the fuel cell m_{FC} and the compresser m_{comp} can thus be estimated using Equation 7.21 and Equation 7.22. The mass of all the inverters, DC-DC converters, and cabling is also estimated using the sizing methods explained in Section 7.3.

$$m_{FC} = \frac{P_{FC}}{\hat{\rho}_{FC}} \tag{7.21}$$

$$m_{comp} = \frac{P_{comp}}{\hat{\rho}_{comp}} \tag{7.22}$$

In Table 7.8 an overview is given of all the subsystems and their masses for both the Emrax 348 and the Magni250 at maximum continuous power.

Table 7.8: Overview of subsystem sizing for hydrogen fuel cell

Subsystem	Mass [kg]	
	Emrax 348	Magni250
Motor	42	71
Cable 3	9.46	8.99
Inverter$_{em}$	13.07	19.15
DCDC-conv$_{em}$	3.32	4.87
Cable 2	4.81	4.81
Cable 1	6.74	6.74
Compressor	0.57	0.83
Inverter$_{comp}$	0.16	0.24
DCDC-conv$_{comp}$	0.04	0.05
PDS	4.85	7.10
Fuel cell	72.93	106.83

Hydrogen Storage

The hydrogen storage sizing is performed by computing the amount of hydrogen required the endurance requirement PROP-PERF-2.1, "The experimental engine shall operate for one hour at an altitude of $5000\ ft$", and adding the hydrogen used during take-off and climb. Using Section 10.3, for cruise it was determined approximately $P_{em_{cruise}} = 41.8kW$ of output power was required from the propeller using 75% output power of the front engine. The endurance of one hour is $E_{cruise} = 1\ h \cdot 60\ min/h \cdot 60\ sec/min = 3600\ sec$. For taxi, it is assumed only the front engine will be used, thus not requiring the use of any hydrogen. Next, for the take-off it is assumed peak power level of the original IO-360 is used for $E_{TO} = 30\ sec$ as was stated in Section 7.3.2, with $P_{em_{TO}} = 210\ hp \cdot 0.7457\ kW/hp$ the output power of the electric motor. Finally for climb, it is assumed that to have a climb rate of $1100\ fpm$ a total power using both engines of 75% of the original IO-360 engines is used. This results in a total of $315\ hp$, which is divided between the front engine running at maximum continuous power of $195\ hp$ and the electric motor thus delivering $P_{em_{climb}} = 120\ hp \cdot 0.7457\ kW/hp$. Climbing at $1100\ fpm$ to an altitude of $5000\ ft$ gives $E_{climb} = 5000/1100 \cdot 60\ sec/min$. Using this, the required power from the fuel cell for cruise, take-off, and climb respectively are computed using the method described above.

Using Equation 7.23, the mass of the hydrogen m_{H_2} itself can be computed, which is a summation of the hydrogen masses for cruise, take-off, and climb. The Lower Heating Value of hydrogen is assumed to be $LHV_{H_2} = 120\ MJ/kg$ [44].

$$m_{H_2} = \Sigma \frac{P_{FC} \cdot 10^3 [W] \cdot E[sec]}{LHV_{H_2} \cdot 10^6 [J/kg]} \tag{7.23}$$

[15] https://powercellution.com/p-stack [Accessed June 2021]

From this, the mass and size of the tank are determined. However there are multiple types of storage that can be used for the testbed. These include; compressed at 300 bar, compressed at 700 bar, or cryogenic at 20 Kelvin. An overview of the three storage methods and their performances can be found in Table 7.9, where they are compared to kerosene for reference [44].

Table 7.9: An overview of storage parameters per storage method of hydrogen compared to kerosene [44].

Parameter	Kerosene	300 Bar H_2	700 Bar H_2	Cryogenic H_2
$\rho_{H_2}[kg/m^3]$	800	20	40	70
$\eta_{storage}[-]$	0.95	0.05	0.10	0.20
$\eta_{vol}[-]$	0.95	0.5	0.5	0.5
$LHV[MJ/kg]$	43	120	120	120

Using this, the mass and volume of the different storage types can be computed. The mass of the tank and hydrogen combined can be computed using Equation 7.24. The mass of the hydrogen is used to compute the volume of the hydrogen in Equation 7.25. The volume of the hydrogen is than combined with the volumetric efficiency to find the volume of the hydrogen tanks in Equation 7.26 [44]. The results of these equations for the three different types of storage can be found in Table 7.10.

$$m_{tank} = \frac{(1-\eta_{storage}) \cdot m_{H_2}}{\eta_{storage}} \tag{7.24}$$

$$V_{H_2} = \frac{m_{H_2}}{\rho_{H_2}} \tag{7.25}$$

$$V_{tank} = \frac{V_{H_2}}{\eta_{vol}} \tag{7.26}$$

Table 7.10: Results for mass and volume sizing for three different types of hydrogen storage [44].

Parameter	300 Bar H_2	700 Bar H_2	Cryogenic H_2
$m_{H_2}[kg]$	3.29	3.29	3.29
$m_{tank}[kg]$	65.78	32.89	16.45
$V_{H_2}[m^3]$	0.164	0.082	0.047
$V_{tank}[m^3]$	0.329	0.164	0.094

It is clear that cryogenic has the best storage performance, and is also the preferred choice for testing as it has the most future potential for aviation purposes. This future potential is elaborated on in the market analysis in Section 2.1. Therefore cryogenic tanks will be used in future computations and the structural design.

It is assumed the design will use a cylindrical tank which gives the easiest storage inside the aircraft, even though it is not the most efficient. Now using the width determined by the structural design to store the hydrogen tanks as the length of the tank, the diameter of the tank can be computed using Equation 7.27.

$$D_{tank} = 2 \cdot \sqrt{\frac{V_{tank}}{L_{tank} \cdot \pi}} \tag{7.27}$$

Final Design

After sizing the hydrogen tank, it can be combined with the subsystem sizing to finalise the design of the system. Again, using the PowerCellution P-Stack as a reference, using the required power to meet the maximum continuous power from the Magni250, it can be computed that at least 3 fuel cells will be required to generate the amount of power required for the Magni250, and at least 2 fuel cells will be required to generate the amount of power required for the Emrax 348.[9] This means that the mass, and the maximum output voltage and current can be computed to fit into the design. As is discussed in Section 7.4 the fuel cells are very difficult to cool down to their low thermal efficiency of $\eta_{FC} = 0.5$. This means that it is almost impossible to cool the fuel cells when they are running at the maximum continuous power of the Magni250. For this reason it is decided that the design will include 2 PowerCellution P-Stack fuel cells generating a power of $P_{FC} = 250\ kW$ in total, delivering a total of $P_{em} = 220\ kW$ to the electric motor. Using this a new subsystem sizing can be determined which is shown in Table 7.11, using the mass of two P-Stacks $m_{FC} = 84\ kg$ and the lower voltage in cable 1 and 2 of $V_{max_{cable_{1/2}}} = 864.5\ V$.[9]

The masses computed for the hydrogen system are used for the cooling design in Section 7.4 and structural design in Chapter 8.

Table 7.11: Overview of subsystem sizing for hydrogen fuel cell

Subsystem	**Mass [kg]**	
	Emrax 348	**Magni250**
Motor	42	71
Cable 3	9.46	8.99
Inverter$_{em}$	13.07	15.05
DCDC-conv$_{em}$	3.32	3.83
Cable 2	4.16	4.16
Cable 1	5.82	5.82
Compressor	0.57	0.65
Inverter$_{comp}$	0.16	0.19
DCDC-conv$_{comp}$	0.04	0.04
PDS	4.85	5.58
Fuel cell	84	84
Full hydrogen tank	17.27	17.08
Total	184.25	216.39

Future Possibilities

There are a number of assumptions made during the sizing of the hydrogen propulsion system and so it is important to evaluate the effect of these and highlight aspects that can be improved in further detailed design.

The first aspect that is interesting to look at is the compressor subsystem. Currently, the compressor is sized using the assumption that the aircraft will always be at an altitude of $5000\ ft$, and the design right now does not include the inlet of the air to the compressor or any electrical properties of the compressor. It has also been sized using the assumptions made by Vonhoff [44], and not using any existing compressor for reference as was done for the inverter, DC-DC converter, or the fuel cells.

A second aspect that requires additional research is into the hydrogen storage. In this design the choice is made to use cryogenic hydrogen. However this does require additional care while inside the aircraft that have not been taken into account, like for example the need to vent hydrogen when the pressure inside the tank increases due to the heating of the hydrogen. A recommendation that can be made is to research the possibility of cryo-compressed hydrogen storage. This new technology is invented to use the best of both compressed and cryogenic hydrogen and stores the liquid hydrogen in a pressure vessel for up to 350 bar, which would reduce the need to vent any boil-off hydrogen.

A final recommendation for the future would be to use the hydrogen system for a mission envelope using a lower MTOW, thus allowing engines with a lower power rating to be tested. The MTOW could be lowered significantly for hydrogen-powered systems, as the current total mass budget adds up to $1593\ kg$, which is $507\ kg$ below the current MTOW of $2100\ kg$. By lowering the MTOW, the climb requirement outlined in Section 2.4 can still be met with lower engine power. For example, it was found that by lowering MTOW to $1750\ kg$ engines with at least $80\ kW$ continuous power could be tested. The MTOW could in no scenario be reduced by so much that engines with maximum continuous power of $41.78\ kW$ could be tested, as this power is required to fly under the the specified cruise conditions.

Verification and Validation
For verification and validation the methods described in Section 3.5 are used.

To start the functions and classes used in the hydrogen system sizing model are all unit tested using the unittest module in python. This resulted in a coverage of 78% of the model. Furthermore the intermediate results of all functions and classes that are inside the model are checked, also for whether the results are as expected. For example, the efficiencies of subsystems should be below one. The loop to compute compressor and fuel cell power can be verified by using their respective required powers as inputs into the equations to compute the required power of the fuel cell and the compressor respectively. The results are confirmed to be correct.

Furthermore the model was validated as much as possible using existing subsystems or sizing methods for reference. For example the basis of this hydrogen system sizing model is the model built by Vonhoff [44], which has been verified and validated. Further validation was performed as described in Section 7.3.2 for the cable sizing methodology.

It is noted that for this model further validation is required for subsystems like the compressor, and for the entire model itself. Since there are very few examples of hydrogen fuel cell powered aircraft of which information is available, validating the model right now is difficult. It is recommended to contact AeroDelft, also working on a hydrogen fuel cell powered aircraft, as a potential collaboration partner for model validation.

7.4. Cooling System Design

As the electrical system heats up during operation due to inefficiencies, a cooling system is necessary to keep temperatures to a reasonable level and thus maximise performance. For the design of the cooling system, two cases are considered. This is because there are significant differences in the cooling system requirements between the battery and the hydrogen fuel cell options. The two configurations considered are as below:

- Configuration A: Battery-electric system with an engine operating at 280 kW
- Configuration B: Hydrogen fuel cell with an engine operating at 145 kW powered by fuel cells

As cruise is the only flight regime which is expected for prolonged periods, it will also be chosen as a basis for cooling system design. This method is typical for general aviation aircraft [22]. Therefore, the design for both cases is evaluated for cruising at an altitude of 1000 m MSL at 150 MPH.

Air vs. Liquid Cooling

For the cooling system design, both air cooling and liquid cooling systems were considered. Both types are viable for the implementation of an electric engine in the SFPT. However, in order to enable interchangeability properly, a liquid cooling system is far more advantageous. This is due to the modifications that would have to be made for switching out the engine if using air cooling. Air cooling would require specific air flow channels for different engines. On the other hand, using a liquid cooling system allows for good interchangeability since one system can be designed that can be applied to a range of electric engines by simply connecting the tubes to the engines and other components. The downside of this is that the engines to be tested in the SFPT have to allow for liquid cooling and hence have a built in liquid cooling system. As liquid cooling is chosen, no ram-air inlet for air cooling will be proposed. However, air cooling can still be provided if needed by means of a cooling fan. In such a case it is imperative that there is sufficient air circulation in the engine compartment.

Liquid Cooling Method Selection

In the design of a liquid cooling system, many things have to be considered. First of all, the type of coolant is chosen. Since the engine manual for the Emrax 348 as well as the cooling system in the Pipistrel Velis Electro use a 50% water %50 glycol mixture, this mixture will also be used for the SFPT cooling system design. The water-glycol mixture has the advantage that it has a higher boiling point than normal water enabling the cooling system to operate at higher temperatures. Next to the coolant, the cooling system also has to be chosen for which there are two options. Firstly, there is a conventional liquid cooling system where the coolant flows through components extracting heat. The coolant then flows through a heat exchanger where it is cooled down by the incoming stream of air. Such liquid cooling systems may be pressurised and the pressurisation of the cooling system allows for the boiling point of the coolant to rise. As an increased temperature difference between the coolant and air flow leads to a smaller heat exchange, increasing the boiling point of the coolant is advantageous.

Another option is an evaporative cooling system. The idea behind evaporative cooling is that if a fluid is taken to its boiling temperature, it still takes an immense amount of heat to evaporate. In such a system, coolant is taken to a temperature higher than the boiling point of the boiler fluid. Then coolant is passed through a heat exchanger in a boiler. This vessel contains boiling fluid and the exchange of heat between the coolant and the boiler fluid, results in the boiler fluid vaporising while it maintains its temperature. The vapour may either be expelled from the aircraft (open-loop system) or condensed in an air cooled condenser (closed-loop system).

The primary option considered for the SFPT is a conventional heat exchanger in contact with air flow. Pressurisation will not be beneficial, due to the fact that a 50% water 50% glycol mixture is used, the boiling point of the liquid will already be higher and above the temperature at which the cooling system operates due to maximum temperatures of the involved components. Looking at evaporative cooling must also be considered, closed loop systems have historically proved to be very complicated systems with large volumes. There is no clear reason why such a system should perform better than the conventional option. An open loop evaporative cooling system is much more interesting due to its relative simplicity. Its main advantages are its neutral contribution to the drag performance and the ability to function when the aircraft is not moving. Its main disadvantages lie in the need to contain large amounts of the boiler fluid while not exceeding mass or balance limits during the flight. For this project a heat exchanger in contact with airflow is primarily studied. However, estimations are made on an evaporative cooling system to show whether it has any practical meaning to a similar project.

Cooling System Requirements

In order to size the cooling system, an overview of the rejected heat per component is given in Table 7.12 for the all electric configuration and in Table 7.13 for the hydrogen fuel cell configuration.

Table 7.12: Power rejected per component for the configuration A

Component	Power rejected [kW]
Engine	18.9
Inverter	3
DC-DC converter	5.6
Power distribution system	3.3
Battery	2.9
Total	33.7

Table 7.13: Power rejected per component for the configuration B

Component	Power rejected [kW]
Engine	12.6
Inverter 1	1.8
DC-DC converter	3.3
Compressor	0.5
Inverter 2	0.02
DC-DC converter 2	0.04
Fuel cell	166.5
Power distribution system	1.9
Total	186.6

As specified in the manual for Emrax motors, the minimum coolant flow necessary for the Emrax 348 engine is $6\ l/min$ and the maximum temperature at the engine inlet is $50\ °C$ [33]. From here, the assumption is made that all other components have the same maximum inlet temperature and the flow rate in each component is scaled proportionally to its rejected power. The scaled minimum flow rates are shown in Table 7.14. These minimum coolant flow rates for configuration A are easily achievable through the use of an off-the-shelf pump such as the Pierburg CWA50 [16]. However, a second pump could be added to the system in order to reduce risk in case the first pump fails. The necessary flowrates for configuration B are also easily achievable by making use of the Pierburg CWA400 pumps in series [17]. As for power, the coolant pumps are the only components that require power in the cooling system. In case of configuration A, the use of two CWA50 pumps would need $112\ W$ and in configuration B, two much more powerful CWA400 pumps are used which need $568\ W$ of power.

Table 7.14: Minimum coolant flow rate

Configuration	Flow rate [l/min]
A	10.7
B	110.7

Heat Exchanger Core Characteristics

While liquid cooled piston engines became one of the two prominent cooling options in the 1930s and 1940s, today they are restricted to special cases in aviation. During that time, many radiator core configurations were tested. While some of the configurations can be found in many high performance aircraft of the era (eg. finned tube or honeycomb cores), there is no clear, dominant option. Nowadays liquid cooling can be mainly seen on aircraft with diesel or electric engine and finned tube cores are the predominant option. Piancastelli et al. discusses high-altitude piston-powered flight and recommends the use of finned tube cores in such an application [30]. Drela discusses a very similar topic with the same choice of radiator core [17].

The automotive industry uses liquid cooled engines very frequently. Especially racing cars such as the ones used in Formula 1 operate under conditions that are not dissimilar to a cruising Cessna Skymaster. Piancastelli et al. shows arguments for why most car radiators evolved into a finned tube configuration in modern times [30]. These usually have a significant frontal area and a comparatively low flow length through the core. Increasing the flow length results in a considerable drag penalty with limited benefits in thermal performance. An interesting thing to note is that this is in contrast with choices on high performance aircraft in the past. However, this can be explained by very high operating velocities of these aircraft where the emphasis on a compact design is larger. If other options proved unfeasible, using a thicker core may be of great interest.

Based on the reviewed sources, the decision was made to choose a louvered finned flat tube core. To reduce the number of free variables and aid optimisation in this first order estimate, multiple design variables will be fixed based on the current standards in the automotive industry. A survey was conducted for typical automotive radiators that are currently available and a representative case can be found in Assanis et al. [28]. Important geometrical values for this case are shown in Figure 7.4 and are chosen as values for preliminary sizing. These values may indeed be very far from optimal in this case, but they should serve as a good representation of a modern heat exchanger core. Moreover, as recommended aluminium was chosen as the heat exchanger material rather than copper and brass [30]. The tubes will be oriented horizontally so they can be made longer while fitting into the aircraft contours better. Longer tubes will be beneficial for cooling [28].

[16] `https://www.tecomotive.com/en/products/CWA50.html` [Accessed June 2021]
[17] `https://www.tecomotive.com/en/products/CWA400.html` [Accessed June 2021]

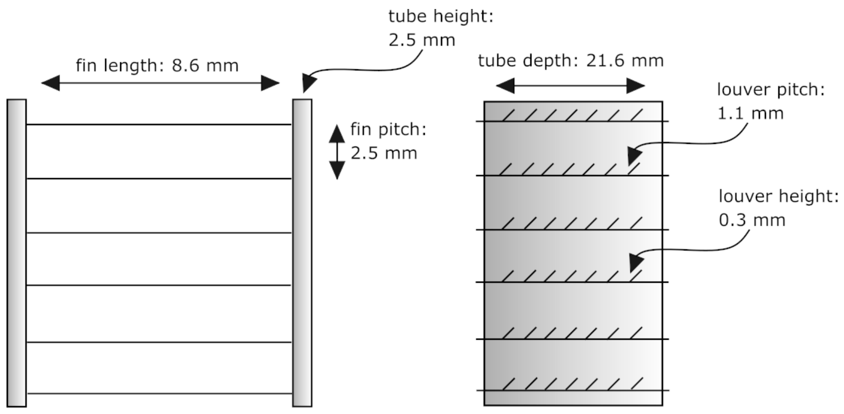

Figure 7.4: Chosen HE core geometry

Heat Exchanger Thermal Model

The temperature of the coolant entering the heat exchanger $T_{c,i}$ is expressed by Equation 7.28 with $T_{c,o}$ being the coolant temperature at the heat exchanger outlet and with $\dot{m}_c$ being the coolant mass flow and $c_{p,c}$ its specific heat capacity. For the airflow the method is analogical.

$$T_{c,i} = T_{c,o} + \frac{\dot{Q}}{c_{p,c}\dot{m}_c} \tag{7.28}$$

To calculate the heat rejection performance, the NTU method was chosen [45]. In the NTU method, first the theoretical maximum heat flow $\dot{Q}_{max}$ between the coolant and the air is first calculated as found in Equation 7.32.

$$\dot{Q}_{max} = C_{min}(T_{c,i} - T_{a,i}) \tag{7.29}$$

$$C_{min} = min(\dot{m}_a c_{p,a}, \dot{m}_c c_{p,c}) \tag{7.30}$$

$$C_{max} = max(\dot{m}_a c_{p,a}, \dot{m}_c c_{p,c}) \tag{7.31}$$

To find the real heat flow, the maximum theoretical value is then multiplied with an efficiency factor.

$$\dot{Q} = \epsilon \dot{Q}_{max} \tag{7.32}$$

The efficiency factor ϵ is dependent on the heat exchanger configuration. In this case, flow passes through fins and multiple tubes and neither of the fluids consequently has a chance to mix in the direction normal to its motion. Therefore, from [14] a relation is chosen as in Equation 7.33 since the heat exchanger can be characterised as a cross-flow heat exchanger with both flows unmixed.

$$\epsilon = 1 - \text{exp}\left\{\frac{NTU^{0.22}}{C_r}\left(\text{exp}\left\{-C_r NTU^{0.78}\right\} - 1\right)\right\} \tag{7.33}$$

$$C_r = \frac{C_{min}}{C_{max}} \tag{7.34}$$

The number of thermal units NTU is defined as in the Equation 7.35 with A and U being the heat transfer area and overall heat transfer coefficient for either the coolant side or the air side.

$$NTU = \frac{UA}{C_r} \tag{7.35}$$

The overall heat transfer coefficient of the core U is a necessary input for the NTU method and thermal characteristics of the core are modelled using a way found in [45]. The heat transfer coefficient U_a for the air side is expressed as in Equation 7.36.

$$\frac{1}{U_a A_a} = \frac{1}{h_a \eta_a} + \frac{A_a t_t}{k_t A_w} + \frac{A_a}{A_c h_c} \tag{7.36}$$

$$A_w = \frac{A_a + A_c}{2} \tag{7.37}$$

In this equation t_t is the tube thickness and k_t its thermal conductivity. The factor η_a stems from the non-homogenous temperature distribution on the radiator fins and is evaluated using a method found in [45]. Convective heat transfer coefficients h_a and h_c are found using correlations found in [28]. They are not listed here in their full extent but their limitations and influencing variables are taken into account.

$$h_c = f(k_c, D_h, Re_D, c_{p,c}, \mu_c)\ with\ 3000 < Re_D < 5 \cdot 10^6\ and\ 0.5 < Pr < 2000 \tag{7.38}$$

D_h is the hydraulic diameter of the tubes, Re_D the Reynolds number in the tube flow, D_h the characteristic dimension, μ_c is the coolant dynamic viscosity and Pr the Prandtl number of the coolant.

$$h_a = f(k_a, Re_{pl}, c_{p,a}, \mu_a, core\ geometry)\ with\ 100 < Re_{pl} < 3000 \tag{7.39}$$

With Re_{pl} being the Reynolds number of the air flow and the louver pitch being the characteristic dimension.

It should be noted that use of the correlations outside their bounds of validity can be very misleading. However based on the heat exchanger flow properties commonly found in literature, there is a belief that the expressions should sufficiently cover the region of interest. All the results are validated to not exceed these limits.

In the case of modelling a thick core the method described above becomes insufficient as air temperature increases significantly along the air stream in the heat exchanger (HE). This harms the heat transfer capabilities as the temperature difference between the air and the coolant grows smaller. Distributing coolant flow along the thickness of the core also becomes non-trivial and may have a significant impact on results. Using a number of considerations stemming from the radiator geometry, relations can be produced relating required HE frontal area to air flow velocity in the core.

Heat Exchanger Aerodynamic Model

Two main contributors to cooling drag are considered. Drag coming from the cooling system internal flow and external drag of the cooling system housing. As [25] shows, the largest heat transfer to drag ratios may be achieved at very low flow velocities through the core. This may however not be practical on aircraft installation as the drag in the HE housing might cancel the achieved benefits.

[25] provides a relation for pressure drop on a typical radiator core. Although it is known that this data is rather outdated, the relation for pressure drop is extrapolated in first order sizing. q_{core} is the dynamic pressure in the core and v_{core} is the airflow velocity in the core.

$$\frac{\Delta p}{q_{core}} = 0.017 v_{core}^2 - 0.671 v_{core} + 12.69\ with\ 3.5m/s < v_{core} < 25m/s \tag{7.40}$$

Drag coefficient of internal flow is then expressed assuming that the duct outlet pressure is equal to the ambient air pressure using a relation from [25] with A_f being the core frontal area.

$$C_{d,int} = 2\frac{v_{core}}{V_{TAS}}\left(1 - \sqrt{1 - \frac{\Delta p}{q_{core}}\left(\frac{v_{core}}{V_{TAS}}\right)^2}\right)\frac{A_f}{S} \tag{7.41}$$

External drag of the radiator is evaluated using a value typical for similar installations found in [25] with $A_{f,ext}$ being the external area of the radiator housing.

$$C_{d,ext} = 0.1\frac{A_{f,ext}}{S} \tag{7.42}$$

One way to mitigate the overly large radiator housing protruding from the aircraft external structure is with the installation of a radiator under at an angle to the free stream flow. Rough relations for an increase in radiator pressure drop due to being at an angle are given in [36]. The upper bound is expressed in Equation 7.43 and the meaning of angle α is shown in Figure 7.5.

$$\frac{\Delta p}{q} = \frac{\Delta p_0}{q} + tan(\alpha)^2 \tag{7.43}$$

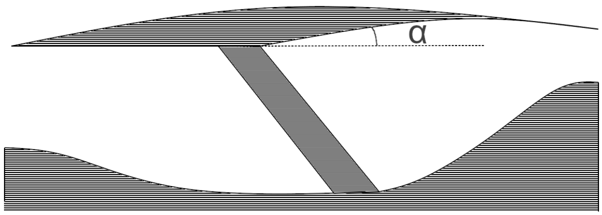

Figure 7.5: Possible duct geometry with an angled radiator

As Equation 7.41 essentially reflects change in momentum, possible positioning of the duct nozzle at an angle β to the undisturbed airflow would result in Equation 7.44. In many cases it may be beneficial for angles β and α to be roughly equal as it helps to reduce the external frontal area.

$$C_{d,int} = 2\frac{v_{core}}{V_{TAS}}\left(1 - \sqrt{1 - \frac{\Delta p}{q_{core}}\left(\frac{v_{core}}{V_{TAS}}\right)^2 cos(\beta)}\right)\frac{A_f}{S} \tag{7.44}$$

Modern aerodynamics allow for design of very efficient ducts and inlets and in the first order analysis, this factor is neglected. This may lead to an underestimation of the internal drag, but as [25] and [22] show, the losses in both can be made quite low with careful design.

While sources such as [35] imply that the waste heat may be used to significantly reduce net drag of the HE installation, they recommend its use mainly at higher airspeeds. Therefore it is neglected in this first order analysis.

Open Loop Evaporative Cooling

Typical boiler fluid used in evaporate cooling systems is 50 percent mixture of methanol and water [11]. It definitely has advantageous properties for such application, eg. lower boiling point then typical coolant at atmospheric pressure. [11] also mentions that almost all applications of such system are piston engine racing aircraft and they use the same fluid to prevent detonation in the engine during combustion. This is not applicable to SFPT, and for simplicity only pure methanol is used as an example.

The necessary amount of fluid for a flight of length t_{flight} is expressed in Equation 7.45 with ΔH_{vap} being the enthalpy of vaporization and M being the molar mass. This equation neglects the fact that some of the fluid will be carried away with the vapor. Real necessary amount will be higher to a certain extent and careful design of the outlet is necessary to minimize this type of losses.

$$m_{fluid} = \frac{M\dot{Q}t_{flight}}{\Delta H_{vap}} \tag{7.45}$$

HE in the boiler fluid will act in a way similar to a HE described in Figure 7.4 and will not be further elaborated upon.

Verification and Validation of the Cooling System

The HE model was compared with results coming from a validated FDM model of automotive radiator presented in [28]. While staying in the range of validity of correlations used in the model, maximum error of +23 percent in the heat transfer rate was found. This can be explained by the assumptions as effects of non-homogenous distribution of the flow and temperature along the HE are neglected in our model. Therefore the model can hardly be considered validated, but it still may be used for preliminary sizing. This gives rise to a 1.25 safety factor in rejected heat for radiator sizing.

Due to a lack of validation data, the mostly empirical models for aerodynamic drag were only verified for correct function.

All code was verified by use of unit tests and by testing larger blocks of code, before they were integrated.

Cooling system design

In this section integration of cooling into the airframe will be elaborated upon.

Figure 7.6 shows required core frontal areas with safety factor included for case A and case B for multiple air and coolant flow rates, which were found to give reasonable results by trial and error.

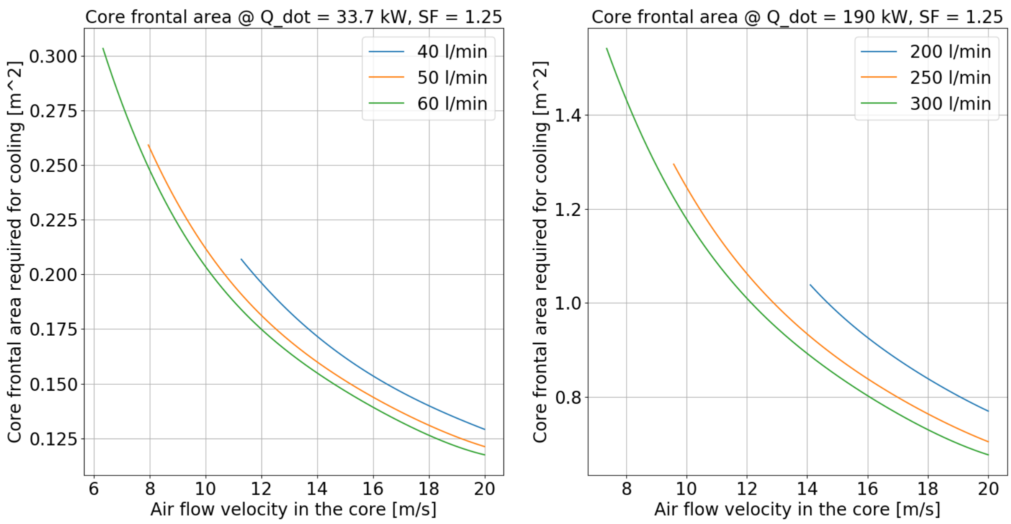

Figure 7.6: Relation between necessary HE frontal area and core air flow velocity

It is possible to observe that the necessary HE frontal areas for both cases are vastly different. The aircraft will almost always flown with components from configuration A and testing fuel cells as in configuration B will not happen during every flight. Larger HE is detrimental to flight performance, adds unnecessary mass, takes up available volume and requires larger coolant flow. A good solution to this is having a fixed smaller HE capable of cooling all components in configuration A and a removable larger HE for cooling the fuel cell in configuration B. In such case coolant can be kept in two separate circuits. Properties for such coolant circuits are listed in the table 7.15 with chosen coolant flow rates. These have been found by trying many possibilities and reaching a point where increasing the coolant flow rate stops yielding a significant frontal area reduction for a given air mass flow.

Table 7.15: Description of coolant circuits

Circuit	Heat transfer rate [kW]	Coolant flow rate [l/min]
Smaller HE	33.7	50
Larger HE	166.5	250

There are many places on the aircraft where HEs may be positioned. Options will be discussed qualitatively.

In case of the smaller HE it can be seen that its frontal area is rather small and it can be placed on many places in the aircraft. To keep the modifications to a minimum a self evident option is a position of former rear engine cooling duct. Figure 7.7 shows that such a HE can be comfortably contained within the fuselage contours at such position. This way the length of the coolant carrying tubes is also reduced as all the cooled components would be rather close to the HE. Many other positions can be considered such as wings, tailbooms or other position on the fuselage, but they hardly offer any significant advantage. Therefore a position overhead of engine mount is chosen.

The larger removable HE positioning is more restricted as it is much larger. Main options lie in placing it on the wings or the fuselage. Wings are indeed an option, but they would require an amount of structural modifications, long coolant tubes, use of two HEs to keep symmetry and not induce yawing effects and they offer a very limited duct length. Top of the fuselage and its sides offer significantly lesser amount of space than its bottom side. By using top of the fuselage favourable choice of placing small HE there would also have to be rejected, due to a flow obstruction. Bottom side of the fuselage is on the other hand quite compelling. Figure 7.7 shows that there is enough space for a pod with an angled HE. There are existing structural mounts for external cargo pods and the HE would be very close to the actual fuel cell. Based on this argumentation a belly mounted HE pod is chosen.

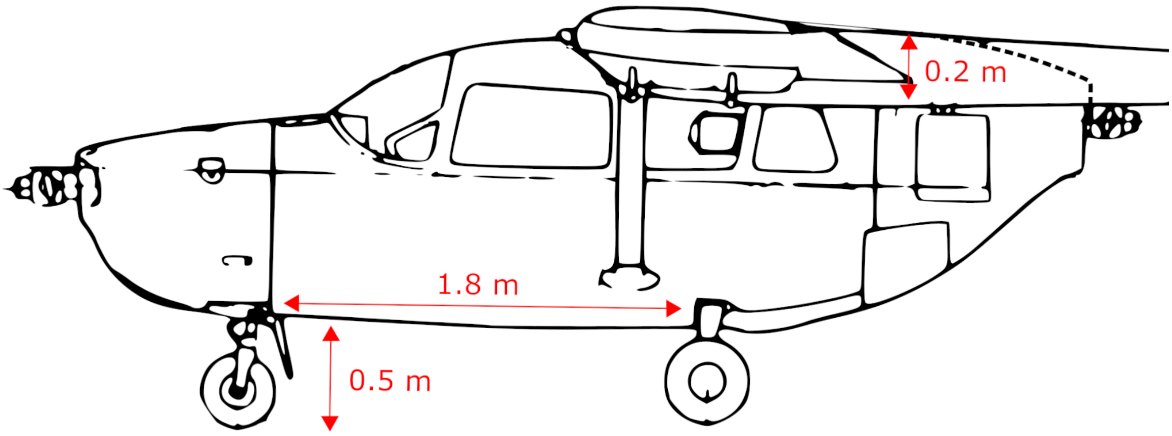

Figure 7.7: Available space for HEs

Note is taken with regards to mass flow through the HEs. [25] explains that due to a complex flow field around an intake to a duct, mass flow through the intake is independent of its cross sectional area to an extent. Mass flow through the HE will be regulated by pilot changing the flow field inside the duct using a cowl flap. Therefore combinations of core air flow velocity and frontal area are assumed to be physically achievable at the given flight condition. Intake design is a highly complex problem and it will not be elaborated upon further as it adds only a little value to this first order estimate.

Using relations for drag developed in the section 7.4 and the geometric considerations from Figure 7.7 an estimate is made for both options. In the case of the large radiator, the model heavily favours angling the radiator more to reduce the frontal area of the external structure. This may however, lead to extreme duct shapes and possibly completely incorrect solutions as the HE core is at a very high angle of attack. Therefore, for the purpose of the analysis a maximum angle α is considered to be 45 degrees. The results are presented in the Figure 7.8. With regards to drag it is stated that the drag coefficient of the former installation was likely close to 0.005 [36].

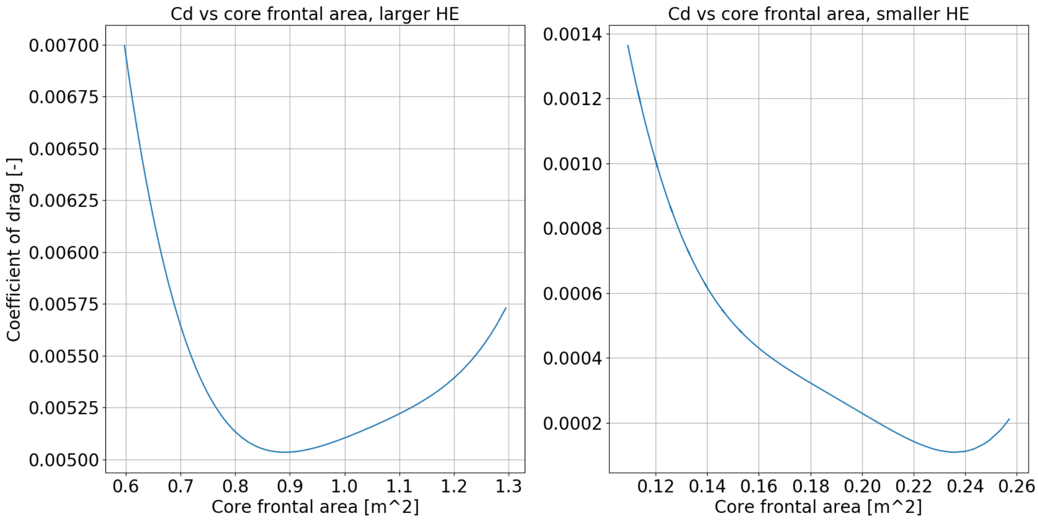

Figure 7.8: Relation between HE frontal area and the drag coefficient of installation

From Figure 7.8, the sizes of both radiators are estimated and listed in Table 7.16. Note that the larger HE size is chosen slightly suboptimally as there must be a sufficient clearance between the ground and the radiator. The size of the smaller HE can easily be varied as its impact on the drag coefficient is low.

Table 7.16: Description of the HEs

HE	width [m]	height [m]	angle [deg]	mass [kg]	Cd of installation [-]
Smaller HE	0.9	0.2	0	1.6	0.0003
Larger HE	1.4	0.54	45	6.8	0.0053

The larger HE would not fit under the fuselage if it was not placed under an angle. Placing it under an angle of 45 degrees results in a 12 cm buffer for the duct structure and ground clearance. The layout is illustrated in Figure 7.9.

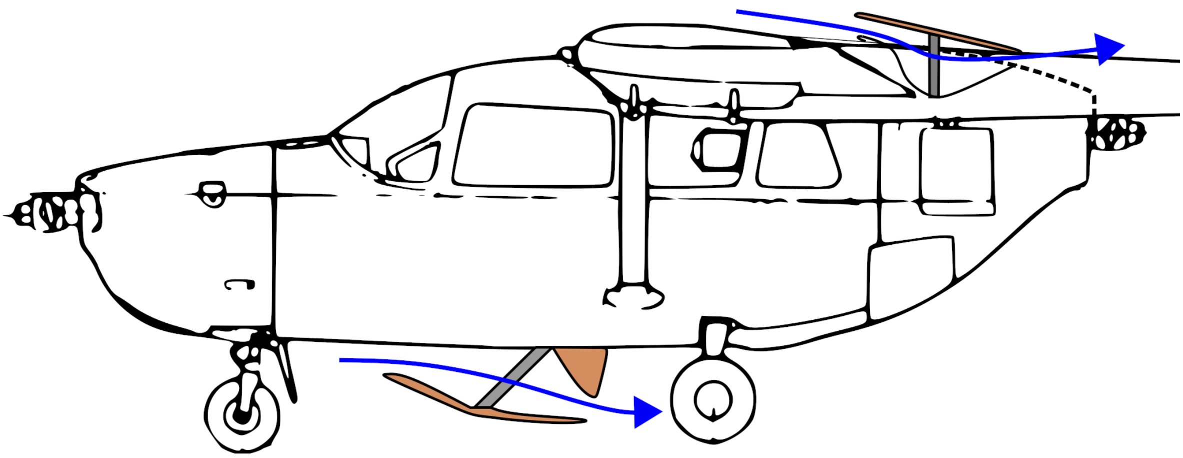

Figure 7.9: Chosen configuration - sizes, positioning and inlet and duct design are purely illustrative

While this result is indeed useful, further study on the possibility of using a thicker core on the larger HE is recommended. As mentioned above, a coherent HE and inlet design has to be achieved. This makes the process inherently iterative. Here only a part of the first iteration has been shown, but the optimal design may differ significantly. The above result shows that cooling performance for the considered cases can likely be made sufficient using solely HEs without an overly large drag penalty. On the other hand, it also shows that further increasing the cooling performance if necessary would be problematic both in terms of drag and available space. As a measure of further increasing this performance, a boiler is considered. Figure 7.10 shows the necessary mass of methanol for an hour flight as a function of transferred heat. Unfortunately the mass of such system is quite high and therefore evaporative cooling is not elaborated further.

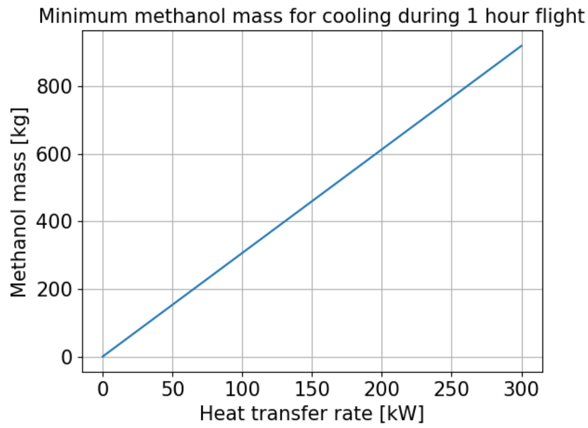

Figure 7.10: Evaporative cooling system minimum methanol mass

8 Structures

This chapter discusses the detailed design of structural modifications. These modifications are divided into two parts: the design of the engine mounting system to allow for a flexible testbed as will be discussed in Section 8.1 and Section 8.2 and the storage of fuel within the fuselage as will be discussed in Section 8.3.

8.1. Engine Mount

The engine mount, as discussed in the *Midterm Report*, is important for securing the engine and reducing the vibrations as well as introducing the loads safely into the fuselage [2]. In this section, the loads experienced by the engine mount are first identified and computed for the various loading cases as set in Certification Specification 23 (CS23). The vibration isolation of the mount is also discussed and a material is selected.

From research into existing engine mounts a concept is designed for which an analytical model is developed and verified through unit and solution tests. A model is then created in CATIA, where it is simulated using Finite Element Analysis for validation purposes. After verification and validation, two more engine mount concepts are designed and a sensitivity analysis is performed to find the most suitable one for the SFPT.

For the SFPT, it is important that the new engine mount is as universal as possible - allowing a variety of engines to be installed for testing. To allow for engines of different dimensions to be tested there are two options; the truss structure may either be fixed or adjustable. Due to the fact that the engines will not be interchanged every day, the adjustable engine mount adds unnecessary complexity to the design with many moving parts. This will increase the stress on the aircraft operator while the testbed is in use. In addition to this, existing engine mounts have been proven to be reliable and safe. While an adjustable mount is theoretically feasible, it is advised to use traditional engine mount design techniques.

A fixed engine mount consists of a permanent structure with various sub-structures, specific to each engine, that may be interchanged to allow for a flexible testbed. In this design phase, the testbed is designed for research into two specific engines (Magni250 and Emrax 348), however for the load case analysis the mount is designed so that DEAC may test different engines in the future.

To consider fixed engine mounts for the SFPT, research is conducted on existing mounting structures for four aircraft using electric engines. The first example, studied from images is the Extra 330LE aircraft which uses the Siemens SP260D engine. It has a sub-structure bolted directly to the permanent truss structure and the engine is held in the front by extending the mounting structure over the corners of the engine. Another example is the Pipistrel Hypstair aircraft, in which the Siemens electric engine is held in the front by a machined metal structure. The third engine mount researched is the MagniX's Magni500, for this the engine is also supported at the front. Lastly, the Emrax 348 engine mounted in an aircraft is inspected and found to often be mounted on its rear side. It is assumed that these are the specified mounting points for the selected engine.

From these examples, it is deduced that the options for mounting can be divided into the attachment of the sub-structure and the mounting points of the engine. In the examples listed above, for mounts that include a sub-structure use bolts to join with the permanent mount. However, it is also a possibility to use a metal sheet in which attachment points can punched into. This sheet could then be mounted with various sub-structures, however it would increase the weight.

8.1.1. Design Concept

From investigation into existing engine mounts such as the Cessna 172, numbers for dimensions including the diameter and thickness of the mount are estimated for an initial design for the permanent engine mount. The existing firewall points are known from measurements at DEAC, the width is $98cm$, a height of $38cm$ and the distance from the firewall to the propeller is $137cm$. Combining these, the first design that is then used for the permanent mounting structure is designed and modelled in CATIA. It is shown below in Figure 8.1.

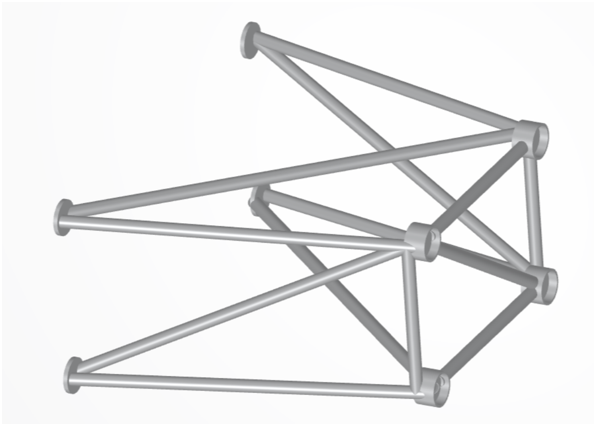

Figure 8.1: Engine Mount Initial Concept

Below in Table 8.1 the thickness and diameter of the tubes are listed as well as the mass of this design. These parameters are will later be analysed further in a sensitivity analysis for the chosen design.

Table 8.1: Dimensions of initial engine mount concept

Parameter	Value	Unit
Mass	18.8	kg
Diameter	2.5	cm
Thickness	2	mm

8.1.2. Load Cases

Firstly, the load cases that must be analysed are identified. The engine is assumed to be a rigid body and the first load case to consider is the weight of the engine for the maximum and minimum load factor scenarios. It is also assumed that the engine is subjected to inertial, thrust, torque and gyroscopic loads. There is also the p-factor, this is an aerodynamic loading experienced by a moving propeller due to the flow being asymmetric to its axis of rotation. However, it has been shown through experience that the effects of on the engine mount are relatively small and can be neglected for propellers with a diameter less than 2.74 m [20]. Below in Figure 8.2 a free body diagram of the engine is shown.

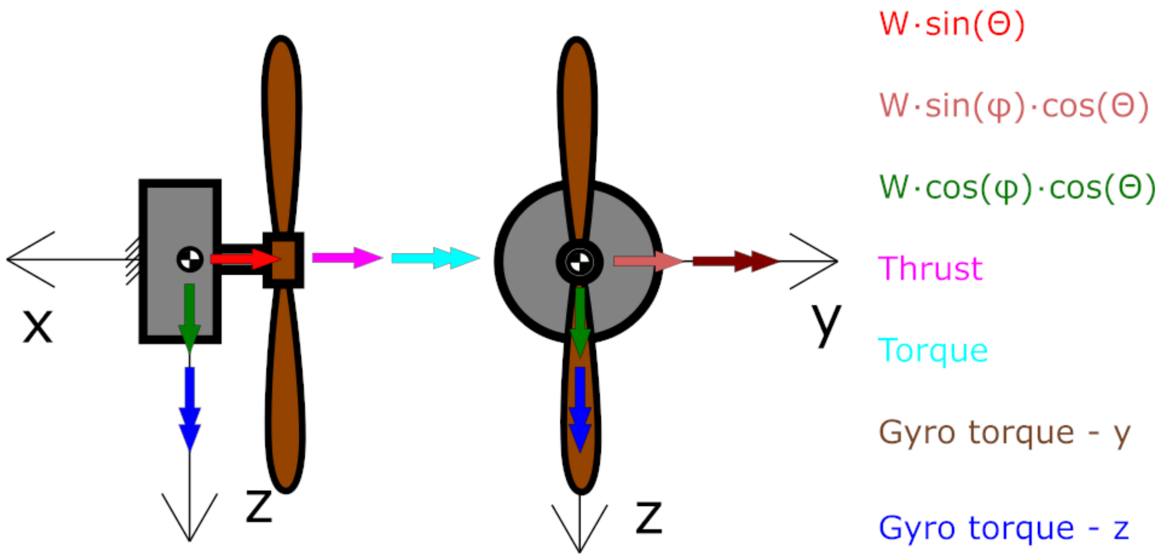

Figure 8.2: Engine Mounting FBD

Load Calculation

Analysing the loads acting on an aircraft engine is not a trivial task as an aircraft follows various trajectories and full three dimensional equations of motion are necessary.

A coordinate system with an origin in the engine c.g. is chosen as shown in Figure 8.2. An inertial reference frame is considered where the velocity vector of the aircraft c.g. is $v = [U, V, W]^T$ and vector of the angular rates of the aircraft is $\omega = [p, q, r]^T$. From literature, the equations of motion 8.1 and 8.4 are constructed for the engine [10]. Vector $r = [x, y, z]^T$ is a position of the c.g. of the aircraft while $F = [F_x, F_y, F_z]^T$ and $M = [M_x, M_y, F_z]^T$ are the total reaction forces and moments acting on the engine mount respectively.

$$Thrust - Wsin(\theta) + F_x = m\dot{U} - rV + qW + x\left(q^2 + r^2\right) - y(pq - \dot{r}) - z(pr + \dot{q}) \tag{8.1}$$
$$Wsin(\phi)cos(\theta) + F_y = \dot{V} - pW + rU - x(pq + \dot{r}) + y\left(p^2 + r^2\right) - z(qr - \dot{p}) \tag{8.2}$$
$$Wcos(\phi)cos(\theta) + F_z = \dot{W} - qU + pV - x(pr - \dot{q}) - y(qr + \dot{p}) + z\left(p^2 + q^2\right) \tag{8.3}$$

$$Torque + M_x = I_x\dot{p} - (I_y - I_z)\, qr \tag{8.4}$$
$$Gyro_y + x_{mount}F_z + M_y = I_y\dot{q} + (I_x - I_z)\, pr \tag{8.5}$$
$$Gyro_z + x_{mount}F_y + M_z = I_z\dot{r} - (I_x - I_y)\, pq \tag{8.6}$$

This system of equations is solved for specific flight scenarios which will be explained in Section 8.1.2, using expressions for thrust, torque and gyroscopic moments.

The thrust is calculated using a method found in literature, specifically from the book titled 'General Aviation Aircraft Design' [22]. In this, the thrust is calculated by interpolating between the static thrust and the maximum velocity thrust.

$$T_{max} = \frac{P}{\eta_{prop_{max}} V_{max}} \tag{8.7}$$

$$T_0 = \left(P^2 \eta_{prop_{static}} \pi \frac{d_{prop}^2}{2} \rho_0\right)^{\frac{1}{3}} \tag{8.8}$$

The torque is also calculated using a method found in 'General Aviation Aircraft Design' [22].

$$Torque = \frac{P}{2\pi \cdot RPM} \tag{8.9}$$

The gyroscopic moment is calculated using an equation found in [20] for where ω is the pitch or the yaw rate of the aircraft.

$$Gyroscopic\ torque = 2\pi \cdot \omega \cdot RPM \cdot I_{prop_x} \tag{8.10}$$

Load case selection
The specific flight scenarios analysed for the load cases stem from the Certification Specification (CS23). Firstly CS.371a, which includes details of the gyroscopic and aerodynamic loads that a engine mount must be design for, at maximum continuous rpm for all combinations of the following;

- A yaw velocity of 2.5 radians per second
- A pitch velocity of 1.0 radians per second
- A normal load factor of 2.5
- Maximum continuous thrust

The second scenario is for manoeuvring loads, taken from CS 23.423 [20]. Two conditions are analysed and calculated using the numbers shown in Table 8.2;

- For a sudden movement of the pitching control, at the speed V_A to the maximum aft movement, and the maximum forward movement, as limited by the control stops, or pilot effort, whichever is critical.
- A sudden aft movement of the pitching control at speeds above V_A, followed by a forward movement of the pitching control resulting in the following combinations of normal and angular acceleration

Table 8.2: Normal and angular acceleration for manoeuvring loads

Condition	Normal Acceleration (n)	Angular Acceleration [rad/s^2]
Nose-up pitching	1.0	$-(\frac{39}{V})n_m(n_m - 1.5)$
Nose-down pitching	n$_m$	$-(\frac{39}{V})n_m(n_m - 1.5)$

Where n_m is the positive limit manoeuvring load factor and V, the initial speed (kts).

The third scenario stems from CS 23.363 and defines the side load factor on the engine mount as 1.33 in this case.

The fourth scenario, taken from CS 23.361, describes the loading on the engine mount that must be possible to withstand at the design manoeuvring speed. These include the following;

- 75 % of the limit load at the design manoeuvring speed and limit torque and propeller speed corresponding to take-off power
- Full limit load at the design manoeuvring speed and limit torque and propeller speed belonging to maximum continuous power

Using combinations of these loading case requirements, 23 load cases are analysed. With Case 19 as the maximum load case. Note that, although the load case analysis is extensive, crash loads are no included. It is recommended for future development that these are included for the engine mount analysis.

Through research into multiple electric motors, values for the limiting engine are decided upon. These include a maximum engine mass, power, rpm as well as propeller dimensions and efficiencies. These are included below in Table 8.3.

Table 8.3: Limiting electric motor for load case analysis

Parameter	Value	Unit
Engine Mass	150	kg
Power	280	kW
RPM	3000	-
Propeller Mass	15	kg
Prop I	4	
Eta prop static	0.6	-
Eta prop max speed	1	-
Propeller Diameter	2	m

Vibration Analysis
Another important role of the engine mount is vibration isolation. Electric motors transmit less vibration than combustion engines. This is mainly due to the large asymmetric moving parts in a combustion engine that are not present in electric motors. However, it is still important to achieve low vibration transmission to the aircraft structure and occupants to ensure that the natural frequency of the air-frame is higher than that produced by the engine so that resonance is avoided. Resonance describes the phenomenon in which an object with a natural frequency, receives a forced vibration of the same frequency, resulting in a vibration of a larger amplitude. It is important to avoid this as it may initiate cracks in the structure which my propagate to cause failure.

Passive isolation systems use techniques such as rubber pads or mechanical springs. Isolation is achieved by limiting the ability of vibrations to be coupled to the structure being isolated. The mechanical connection, dissipates the energy of the vibration. Passive systems, in comparison to active systems, are simple and therefore generally more reliable and safe. The most widely used passive isolaters are elastomers.

To assess the need of a damping system, the frequency of the original IO 360 engine as well as the natural frequency for the air-frame are both estimated. The IO 360 engine has a maximum rpm of 2800, equal to a frequency of 47 Hz. However, the combustion engine is a hive of mechanical activity with many moving and spinning parts and so in reality, the frequency is estimated to be higher. Therefore, it is assumed that the air-frame must have a natural frequency higher than this. To validate this assumption, a literature study is performed into the natural frequencies of aircraft fuselage vibrations. One paper found, includes details of an experiment performed on a single engine light aircraft with the aim of 'quantitatively determining the relative importance of engine induced structure-borne noise' [27]. The resonant (natural) frequencies of the specific fuselage panels for Figure 8.3 are listed in Table 8.4.

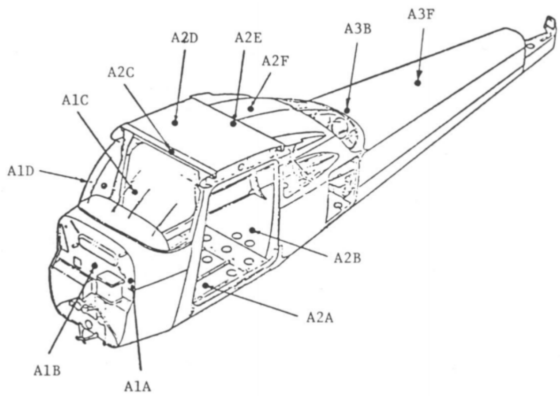

Figure 8.3: Fuselage Panel Sections [27]

Table 8.4: Table of resonant frequencies for Figure 8.3 [27]

Panel	Resonant Freqency [Hz]
A2A	215
A1C	200
A3C	47
A2D	220
A3D	61
A1E	92
A1F	30
A2F	98
A3F	200
A1G	125

From these numbers it is deduced that the Skymaster aircraft body also has a higher natural frequency than 47Hz. For electric engines, the rotor and propeller rotate at the same speed and so it is assumed to act as one vibration at the same frequency. Below in Table 8.5, various electric motors and their frequencies are listed. The first two engines listed, are the selected engines for the design of this project however, to ensure that the SFPT is as flexible as possible other electric engines are assessed too.

Table 8.5: Electric engines and frequencies

Engine	Max RPM	Max Frequency [Hz]
Emrax 348	4500	75
Magni-250	3000	50
SP70D	2600	43.3
E-811-268MVLC	2500	41.7

As discussed in the load cases, the limiting RPM is set at 3000 and this translates to a frequency of 50Hz. While it is estimated that the air-frame has a higher natural frequency than this it is recommended that a rubber bushing is fitted as a damper. It is not possible size the damper as the amplitude of the vibrations are currently unknown. It is recommended that through testing of the engines and their specific mounts it is possible to size the damper accurately. For the purposes of the design analysis, dampers were researched in the Lord catalogue - a technology and manufacturing company that develops specific parts for the aerospace industry, among others. [1] The damper housing in the design is assumed to have a radius of 4cm. This number may change in further investigation into the required damping for each engine.

Material Selection

Steel is most often used in engine mounting as the mount is a relatively small component in the aircraft. Specifically, 4130 Chromoly steel is most commonly used in the light aircraft industry.[2]. Chromoly steel is categorised as a low alloy steel, the ’30’ in ’4130’, indicating the percentage of carbon included (0.30%). The combination of the other elements, chromium and molybdenum produces a material with excellent hardenability and toughness, it is also easy to weld. In line with requirement **STRUC-MOUNT-2**, it is readily available from aviation parts suppliers such as Wicks, however the cost is dependent on the quantity purchased. [3] Below, in Table 8.6 the properties of steel 4130 are listed.

[1] https://www.lord.com/ [Accessed June 2021]

[2] https://www.voestalpine.com/blog/en/mobility/capabilities-that-aircraft-engine-mounts-must-possess/ [Accessed June 2021]

[3] https://www.wicksaircraft.com/c/channels-angles/ [Accessed June 2021]

Table 8.6: Properties of Chromoly 4130 [4]

Property	Value	Unit
Density	7850	kg/m^3
Ultimate Tensile Strength	560	MPa
Yield Tensile Strength	460	MPa
Modulus of Elasticity	190-210	GPa
Bulk modulus	140	GPa
Shear modulus	80	GPa
Poissons ratio	0.27-0.30	-

One other consideration for the material choice is the coefficient of thermal expansion. Materials expand with temperature increase and for the fuel mount this possibility must be considered. It is found that the coefficient of thermal expansion of steel 4130 is $1.2e-05(1/K)$.[5] The change in dimensions of the engine mount is not analysed in depth for this project due to the fact that the engine mount itself will not withstand high temperatures due to a) the cooling of components and b) the small contact points of the material with heated components. However, for future analysis it is recommended that an research is conducted on the temperature change the truss structure is exposed to in various regions. The thermal displacements are calculated using $\delta_T = \alpha \Delta T L$, where α is the coefficient of thermal expansion (1/K), ΔT is the temperature change (K) and L is the length of the truss member. For statically indeterminate members, thermal displacements are constrained by the supports, therefore producing thermal stress.

8.2. Engine Mount Model

In this section, the analytical model for the engine mount is described and an analysis is performed for an initial engine mount design concept. The verification procedure is then detailed and for the validation a finite element analysis model is simulated in CATIA. Following this, two additional engine mount concepts are modelled and a sensitivity analysis is performed to compare mass and cross-sectional area.

8.2.1. Analysis

In order to choose a design an analysis has to be done on the performance of each design. This can be done using a finite element method, specifically the matrix stiffness method. This section will present the theory, an example and the implementation to the initial engine mount design.

The matrix stiffness method relates the displacement of each element to the forces applied to them. The relationship between displacement and force applied can be seen in Equation 8.11.

$$F = \frac{AE}{L}\sigma \tag{8.11}$$

For a simple one dimensional case, seen in Figure 8.5, we can construct a linear relation between the three locations where force is applied an their displacements. The linear relation can be seen in Equation 8.12.

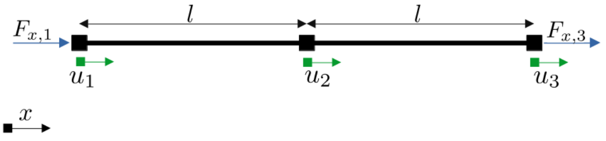

$$\begin{bmatrix} F_{x,1} \\ F_{x,2} \\ F_{x,3} \end{bmatrix} = \frac{AE}{L} \begin{bmatrix} 1 & -1 & 0 \\ -1 & 2 & -1 \\ 0 & 1 & -1 \end{bmatrix} \begin{bmatrix} u_1 \\ u_2 \\ u_3 \end{bmatrix} \tag{8.12}$$

Figure 8.4: One Dimensional Stiffness Matrix Example

In order solve this at least one node has to be constrained and the forces of the other nodes need to be known. This trivial as the internal node, node 2, will have a resultant force of zero and the force $F_{x,3}$

[3] `https://www.azom.com/article.aspx?ArticleID=6742` [Accessed June 2021]
[4] `https://www.azom.com/article.aspx?ArticleID=6742` [Accessed June 2021]
[5] `https://matmatch.com/materials/song001-aisi-4130-annealed` [Accessed June 2021]

is the external forces. With this, the displacements can be solved and in turn the internal stresses of the beams.

A thorough example will follow, here a two beam truss statically indeterminate structure is presented, seen in Figure 8.5. From this we can construct two linear relations between the displacements and forces on each node of the two elements. This can be seen in Equation 8.13 and Equation 8.14.

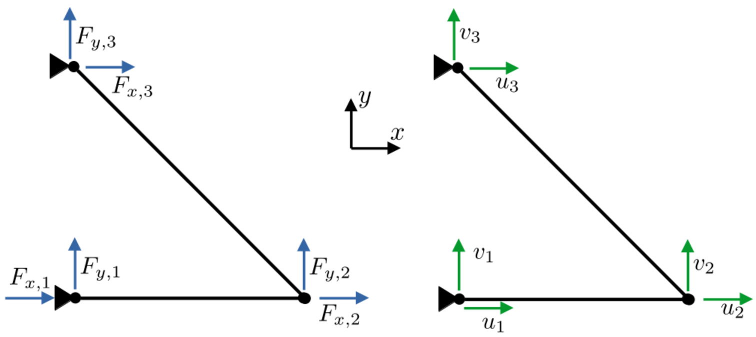

Figure 8.5: Truss Structure Example

$$\begin{bmatrix} F_{x,1} \\ F_{y,1} \\ F_{z,1} \\ F_{x,2} \\ F_{y,2} \\ F_{z,2} \end{bmatrix} = \frac{AE}{L} \begin{bmatrix} 1 & 0 & 0 & -1 & 0 & 0 \\ 0 & 0 & 0 & 0 & 0 & 0 \\ 0 & 0 & 0 & 0 & 0 & 0 \\ -1 & 0 & 0 & 1 & 0 & 0 \\ 0 & 0 & 0 & 0 & 0 & 0 \\ 0 & 0 & 0 & 0 & 0 & 0 \end{bmatrix} \begin{bmatrix} u_1 \\ v_1 \\ w_1 \\ u_2 \\ u_2 \\ w_2 \end{bmatrix} \tag{8.13}$$

$$\begin{bmatrix} F_{x,2} \\ F_{y,2} \\ F_{z,2} \\ F_{x,3} \\ F_{y,3} \\ F_{z,3} \end{bmatrix} = \frac{AE}{L} \begin{bmatrix} \frac{1}{2\sqrt{2}} & -\frac{1}{2\sqrt{2}} & 0 & -\frac{1}{2\sqrt{2}} & \frac{1}{2\sqrt{2}} & 0 \\ -\frac{1}{2\sqrt{2}} & \frac{1}{2\sqrt{2}} & 0 & \frac{1}{2\sqrt{2}} & -\frac{1}{2\sqrt{2}} & 0 \\ 0 & 0 & 0 & 0 & 0 & 0 \\ -\frac{1}{2\sqrt{2}} & \frac{1}{2\sqrt{2}} & 0 & \frac{1}{2\sqrt{2}} & -\frac{1}{2\sqrt{2}} & 0 \\ \frac{1}{2\sqrt{2}} & -\frac{1}{2\sqrt{2}} & 0 & -\frac{1}{2\sqrt{2}} & \frac{1}{2\sqrt{2}} & 0 \\ 0 & 0 & 0 & 0 & 0 & 0 \end{bmatrix} \begin{bmatrix} u_2 \\ v_2 \\ w_2 \\ u_3 \\ u_3 \\ w_3 \end{bmatrix} \tag{8.14}$$

From these two local systems of equations we can combine them to describe the whole relationship of the truss structure. This produces a global linear system, seen in Equation 8.15. Since two edges are clamped and we assume this system not to move in the z-plane, the columns and rows corresponding to these displacements can be removed. This leads to the simplified Equation 8.16.

$$\begin{bmatrix} F_{x,1} \\ F_{y,1} \\ F_{z,1} \\ F_{x,2} \\ F_{y,2} \\ F_{z,2} \\ F_{x,3} \\ F_{y,3} \\ F_{z,3} \end{bmatrix} = \frac{AE}{L} \begin{bmatrix} 1 & 0 & 0 & -1 & 0 & 0 & 0 & 0 & 0 \\ 0 & 0 & 0 & 0 & 0 & 0 & 0 & 0 & 0 \\ 0 & 0 & 0 & 0 & 0 & 0 & 0 & 0 & 0 \\ -1 & 0 & 0 & 1-\frac{1}{2\sqrt{2}} & -\frac{1}{2\sqrt{2}} & 0 & \frac{1}{2\sqrt{2}} & \frac{1}{2\sqrt{2}} & 0 \\ 0 & 0 & 0 & -\frac{1}{2\sqrt{2}} & \frac{1}{2\sqrt{2}} & 0 & \frac{1}{2\sqrt{2}} & -\frac{1}{2\sqrt{2}} & 0 \\ 0 & 0 & 0 & 0 & 0 & 0 & 0 & 0 & 0 \\ 0 & 0 & 0 & -\frac{1}{2\sqrt{2}} & \frac{1}{2\sqrt{2}} & 0 & \frac{1}{2\sqrt{2}} & -\frac{1}{2\sqrt{2}} & 0 \\ 0 & 0 & 0 & \frac{1}{2\sqrt{2}} & -\frac{1}{2\sqrt{2}} & 0 & -\frac{1}{2\sqrt{2}} & \frac{1}{2\sqrt{2}} & 0 \\ 0 & 0 & 0 & 0 & 0 & 0 & 0 & 0 & 0 \end{bmatrix} \begin{bmatrix} u_1 = 0 \\ v_1 = 0 \\ w_1 = 0 \\ u_2 \\ v_2 \\ w_2 = 0 \\ u_3 = 0 \\ u_3 = 0 \\ w_3 = 0 \end{bmatrix} \tag{8.15}$$

$$\begin{bmatrix} F_{x,2} \\ F_{y,2} \end{bmatrix} = \frac{AE}{L} \begin{bmatrix} 1+\frac{1}{2\sqrt{2}} & -\frac{1}{2\sqrt{2}} \\ -\frac{1}{2\sqrt{2}} & \frac{1}{2\sqrt{2}} \end{bmatrix} \begin{bmatrix} u_2 \\ v_2 \end{bmatrix} \tag{8.16}$$

By inverting the simplified matrix we can solve for the displacements of the non clamped nodes, Equation 8.17. Using the full columns of the global matrix, Equation 8.15, all the forces on the system can be determined, Equation 8.18.

$$\begin{bmatrix} u_2 \\ v_2 \end{bmatrix} = \frac{L}{AE} \begin{bmatrix} 1 & 1 \\ 1 & 1+2\sqrt{2} \end{bmatrix} \begin{bmatrix} F_{x,2} \\ F_{y,2} \end{bmatrix} \quad (8.17)$$

$$\begin{bmatrix} F_{x,1} \\ F_{y,1} \\ F_{z,1} \\ F_{x,2} \\ F_{y,2} \\ F_{z,2} \\ F_{x,3} \\ F_{y,3} \\ F_{z,3} \end{bmatrix} = \begin{bmatrix} -1 & 0 \\ 0 & 0 \\ 0 & 0 \\ 1-\frac{1}{2\sqrt{2}} & \frac{1}{2\sqrt{2}} \\ -\frac{1}{2\sqrt{2}} & \frac{1}{2\sqrt{2}} \\ 0 & 0 \\ -\frac{1}{2\sqrt{2}} & \frac{1}{2\sqrt{2}} \\ \frac{1}{2\sqrt{2}} & -\frac{1}{2\sqrt{2}} \\ 0 & 0 \end{bmatrix} \begin{bmatrix} 1 & 1 \\ 1 & 1+2\sqrt{2} \end{bmatrix} \begin{bmatrix} F_{x,2} \\ F_{y,2} \end{bmatrix} \quad (8.18)$$

The forces and displacements of each node is now computed. To obtain the internal stress of the elements of the truss, the strain of each element is solved. Strain is the measure of the change of the length of an element to its original length, Equation 8.19. Using the strain of each element the stress of the element can be determined using the young-modulus relation, Equation 8.20.

$$\epsilon = \frac{\Delta L}{L} \quad (8.19) \qquad \sigma = E\epsilon \quad (8.20)$$

Using this method of generating a stiffness matrix for the truss structure, a python module was produced to analyse the design concepts. In Listing 8.2.1 a pseudo code representation of the module is shown

```
node_coords = [List of all the coordinates of each nodes]

for node_coord in node_coords:
    nodes.append(Node(node_coord))

elements_connectivity = [node-node connectivity]

elements = []
for element_connect in element_connectivity:
    elements.append(element(element_coonect, nodes))

k_matrix = []

for element in elements:
    k_matrix.add_sub_matrix(element.submatrix)

k_reduced = k_matrix.remove_no_displacement_all()
k_tall = k_matrix.remove_no_displacement_col()

displacement = Invert(k) * known_forces
forces = k_tall * Invert(k_reduced) * known_forces
```

8.2.2. Verification

In parallel to creating the model for the truss analysis, verification is performed to ensure that the model accurately represents the underlying mathematical model and its solution. The verification process consists of calculation verification to check that the numerical model does not contain errors or inaccuracies from numerical methods. The verification test are conducted using the PyTest module in

Python, which also generates a coverage report, indicating that 78% of the analytical model is tested and verified.

Unit tests are performed to check separate parts of the code to ensure they are independently correct. The following four tests are included.

The first unit test takes the input for two nodes of an element and checking that the distance between them is as expected. This is checked for a simple input of a node at position (0,0,0) and another at (1,0,0). The output distance between these two is checked to be 1 and therefore the test is passed.

The second unit test checks the angle between two elements. The vector [1,0,0] and [$\frac{\sqrt{3}}{2}$, 1/2,0] are used and then using the equation $a \cdot b = |a||b|cos(\theta)$, it is checked that the output is 30 degrees.

The third unit test, checks that the transformation matrix, X, is singular. For a singular matrix is is known that; $X \cdot X^T = I$, where I is the identity matrix. This test is passed.

The last unit test checks that that the local k matrices can be constructed from the global $9x9$ stiffness matrix. For this, a worked solution is used from the textbook 'Aircraft Structures for Engineering Students' is used to verify the solution from the model [34]. The worked-out example included is for a 2D structure, so it is also adapted for 3D and verified again.

Next, solution tests are performed and checked using the solved problems in the textbook 'Aircraft Structures for Engineering Students' [34]. This includes, the global matrix and the forces acting on the nodes and their displacements for a simple scenario.

8.2.3. Validation

The validation process uses the finite element analysis feature in CATIA 3DExperience. A simulation is created of the engine mount for various mesh sizes which vary from 0-100 (coarse to fine), however due to restricted computer power the maximum mesh size simulated is 20. Mesh sizes are often the largest source of error in a finite element analysis simulation and are often undetectable by an inexperienced engineer. A few problems may result in simulating with the wrong mesh size. For too coarse meshes, the elements are larger and therefore, while the stress patterns of the elements are correct, the magnitudes on the peak stresses are not. This is a safety issue for structural design as the areas of peak stress are usually the point of failure. There is also the possibility of using a too fine mesh; while this is not a safety concern it adds unnecessary cost and time. The meshes simulated for the purposes of the engine mount design are considered 'coarse' and therefore it is recommended for further research, to perform a mesh independence study to compare the variation of finite element analysis simulation results depending on the mesh size. Currently, mesh sizes 10, 15 and 20 are tested but for further comparison it is advised to simulate up to 60-75. It is also a possibility to refine the mesh in regions with known high deformations or stresses.

For the simulation restraints are first applied to the firewall bolt points, these are the boundary conditions. It is assumed that the firewall frame (attachment point) has a high stiffness such that it does not deform under the loads and therefore a clamp restraint is applied. Next, for the maximum load case (Case 19), the forces exerted at nodes 4,5,6 and 7 are applied as point forces using the assumption that the force will be applied through the bolt directly to the truss elements. This set up is shown below in Figure 8.6. The forces applied are are adjusted by a safety factor of 1.5, in line with the requirement **SAF-ENG-3**.

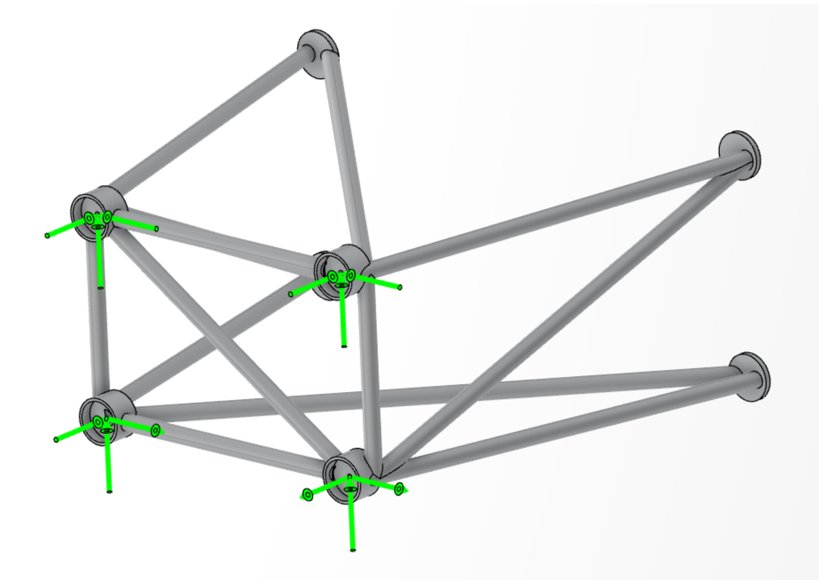

Figure 8.6: Simulation load application

The first result to be validated is a figure of the compression and tension within the truss elements. Below, in Figure 8.7, this is represented by blue (compression) and red (tension) areas. The sign of the stresses through the truss elements are then compared with those from the analytical model.

The compression and tension in the primary load carrying elements are visually inspected. As can be seen, the elements connecting nodes 0 & 4 and 1 & 6 are in tension and elements connecting nodes 3 & 4 and 2 & 6 are in compression. Elements, such as the one connecting nodes 6 & 7, are in bending and so have tension and compression (as can be seen in Figure 8.8) are shown as white areas in the analytical model.

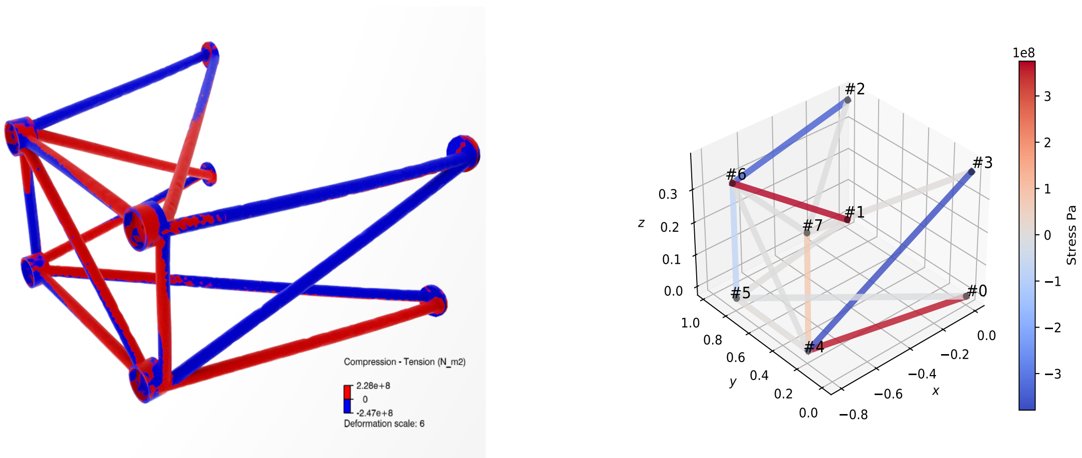

(a) CATIA simulation: compression and tension

(b) Analytical Model: compression and tension

Figure 8.7: Validation comparison: compression and tension of truss elements

The second result of the simulation is shown below in Figure 8.8, in which the displacement of the points on the truss are shown for the critical loading case (Case 19). The maximum displacement occurs in the middle of the inner rectangle. From this simulation the displacements of the nodes 4,5,6,& 7 are measured.

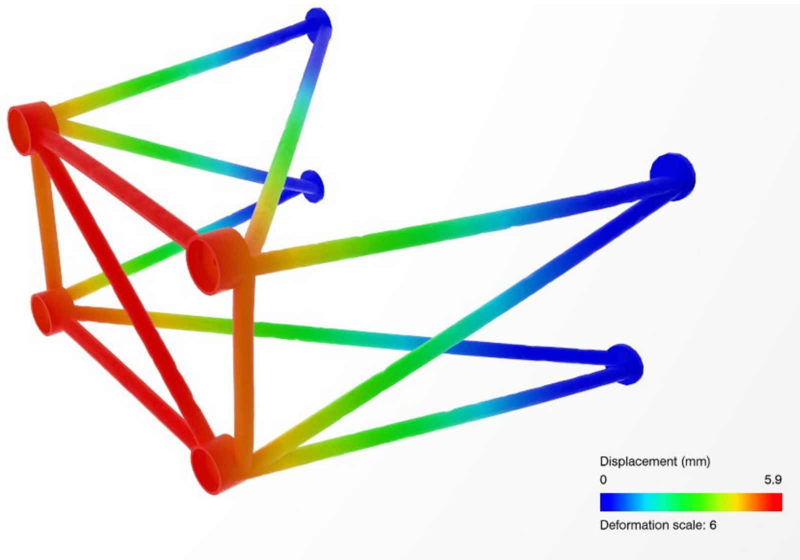

Figure 8.8: Engine mount displacement simulation: load case 19, mesh size 20

Below, in Table 8.7 the values for the displacement of the four nodes for the analytical model are compared with the FEM simulations on CATIA for three different mesh sizes. There is approximately a 2 mm difference between the analytical model and the CATIA simulation, this is due to a three main reasons which are identified below.

- In the analytical model the structure is assumed to be linear-elastic while for the simulation bending is also accounted for.Instead of deflecting instantly, the truss structure will bend first.
- The damper housing strengthens the structure. The damper housing is a larger area than the nodes in the analytical model and so the stress is reduced.
- The joining of the truss elements.The truss elements are welded to the damper housing at different locations to allow access to the bolt for the sub-stricture, this however introduces torsion due to asymmetric bending.

Table 8.7: Displacement data for analytical model, CATIA simulation with mesh size 10, 15 and 20

Node	Model	Displacement [mm]
Node 4	Analytical	7.20
	CATIA (mesh 10)	5.41
	CATIA (mesh 15)	5.37
	CATIA (mesh 20)	5.25
Node 5	Analytical	7.05
	CATIA (mesh 10)	5.28
	CATIA (mesh 15)	5.25
	CATIA (mesh 20)	5.24
Node 6	Analytical	7.04
	CATIA (mesh 10)	5.31
	CATIA (mesh 15)	5.29
	CATIA (mesh 20)	5.26
Node 7	Analytical	7.21
	CATIA (mesh 10)	5.29
	CATIA (mesh 15)	5.24
	CATIA (mesh 20)	5.23

8.2.4. Design Concepts and Sensitivity

After the verification and validation of the analytical model, two new engine mount designs are created. These designs are shown below in Figure 8.9 and Figure 8.10.

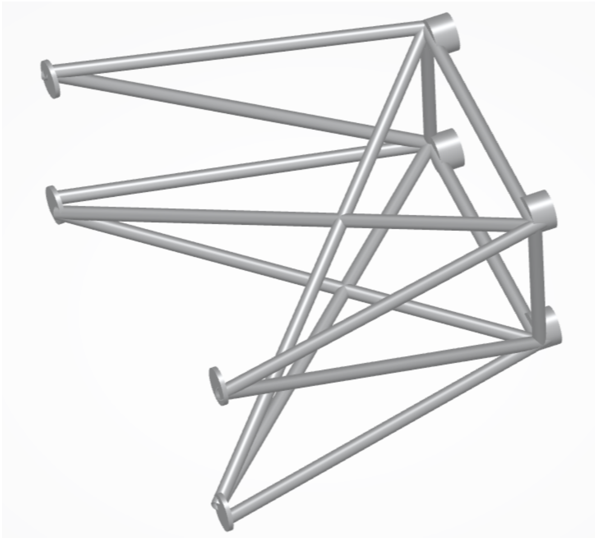

Figure 8.9: Engine Mount Concept 2

As can be seen in Figure 8.9, the truss structure consists of 13 elements. However, there are two large elements through the centre of the structure, limiting accessibility and adding weight.

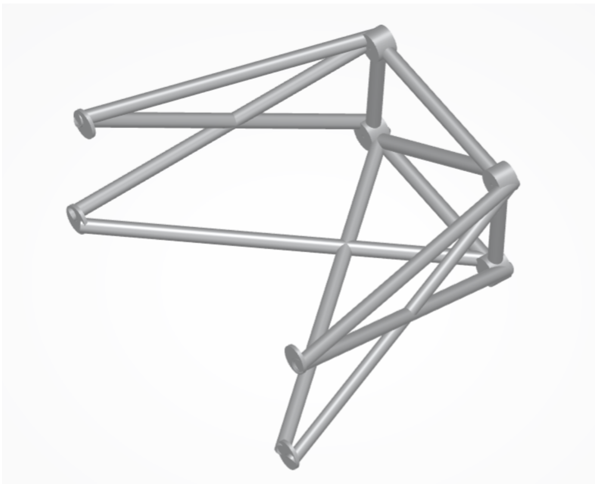

Figure 8.10: Engine Mount Concept 3

The third design concept, is a symmetric design in the z axis. It also has the advantage of being highly accessible through the top of the structure which allows for potential storage of fuel or data acquisition components. The available volume within this area is 0.168 m^3.

A sensitivity analysis is performed for the three engine mount design concepts in which a graph of the maximum stress (Pa) in the truss against mass (kg) is plotted to find the most 'efficient' concept. To vary the mass, the cross-sectional area of the truss is changed. A dotted line is included to indicate the maximum tensile strength. This is shown below in Figure 8.11.

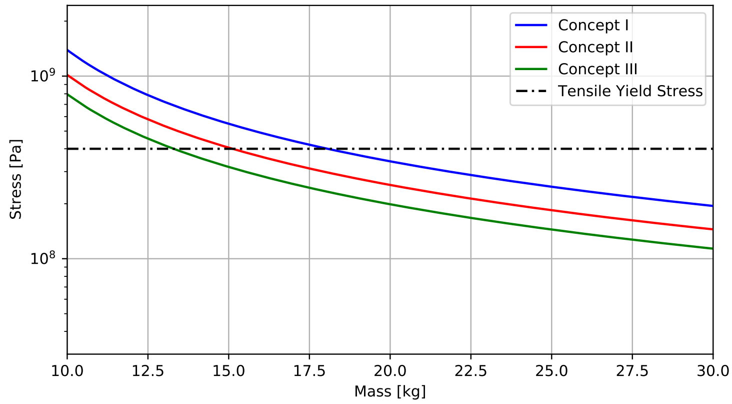

Figure 8.11: Graph of stress [Pa] against mass [kg]

As can be seen above, the third engine mount option is the most 'efficient' and is therefore selected. The minimum mass is 13.04 kg, with a cross-sectional area of $6.8 \cdot 10^-4m^2$. For this cross-sectional area, a table of possible thickness and diameter combinations is found and included below in Table 8.8.

For the maximum compressive loads it is important to consider the expected failure mode, namely, column buckling. For this, the truss elements may be modelled as slender beams that are subjected to axial compressive loads. Using Equation 8.21, the force exerted on the truss for each thickness and diameter combination is found.

Table 8.8: Thickness, radius and critical stress for column buckling maintaining a cross-sectional area of $6.8 \cdot 10^-4m^3$

t [mm]	R [cm]	σ_{cr} [MPa]
3.9	2.90	578
4.2	2.80	519
4.4	2.70	468
4.8	2.50	374
5.4	2.30	284
5.7	2.20	243
6.0	2.10	206

$$P_{cr} = \frac{\pi^2 E(Ar^2)}{L^2} \tag{8.21}$$

where E is the Young's Modulus (taken from Table 8.6 to be $205GPa$, r is the radius of gyration, calculated using the equation $r = \frac{\sqrt{(2}}{2} \cdot radius$ and L is the length of the longest element in the truss (for concept 3, this is 1.05m). From the critical load P_{cr}, the critical stress, σ_{cr} is calculated using $\sigma = P/A$. It is required that σ_{cr} < $\sigma_y = 460MPa$.

8.2.5. Results and Recommendations

Combining these parameters, option 3 is selected. Below in Table 8.9, the details of the engine mount are listed.

Table 8.9: Permanent engine mount parameters

Parameter	Value	Unit
Mass	13.04	kg
Wall thickness	4.8	mm
Radius	2.50	cm
Material	Steel 4130	-
Tensile Strength	460	MPa
Compressive Strength	374	MPa
$x_{c.g.}$ (from rear firewall)	521	mm

For the substructure, the attachment points of the selected motors are researched. For the Emrax 348 there are two options for mounting. Either on the front with 6x M10 threaded holes or on the back with 10x M8 threaded holes.The mounting points for the Magni 250 are not specified however, from technical drawings it is inferred that there are 9 bolts on the back and 6 on the front. While the hole size is unknown, from research into electric motors it is expected they are M8 or M10 holes. The manufacturing, assembly and integration of the engine mount with the aircraft is discussed further in Chapter 12.

8.3. Fuel Storage

The second part of structural modifications pertains to the fuel of the experimental propulsion system. Two types of fuel will be used for the aft engine: batteries and hydrogen tanks. Since the aircraft's current configuration is suited for storing fuel in the wings, structural modifications are required to be able to mount other types of fuel at other locations. The goal is to be able to mount fuel in the fuselage interchangeably.

The design process of the fuel mount starts by specifying a list of requirements as in Table 8.10. This will ensure that the operational limits of the mount are specified in clear terms and help steer the design process. In the subsequent requirements ”structural mount” refers to both the mount itself and its connections with the batteries and fuselage.

Table 8.10: Fuel mount requirements

Code	Requirement	Verification
FUEL-MNT-1	The structural mount shall weigh no more than 30kg.	Demonstration
FUEL-MNT-2	The structural mount shall introduce loads into the existing structure in a way that maintains its integrity.	Analysis
FUEL-MNT-3	The structural mount shall be able to sustain loads according to the flight envelope.	Analysis
FUEL-MNT-4	The structural mount shall accommodate connections between the engine and fuel cells such as cabling or fuel lines.	Demonstration
FUEL-MNT-5	The structural mount shall prevent the fuel from moving around in the cabin.	Analysis/Test

One of the key reasons for a fuel mount is to stop fuel from being able to move freely in the compartment, as this could damage the existing structure and even injure the pilot.

Mounting fuel within the structure of the fuselage has three main advantages:

1. The cabin is highly accessible.
2. The nominal centre of gravity is located between the landing gear and the main wing strut, towards the aft of the cabin. This means that the fuel will be mounted close to the centre of gravity.
3. The existing structure is already tailored towards sustaining relatively high loads as it was designed to accommodate passengers.

Design Concepts

The core of the existing fuselage structure is illustrated in Figure 8.12a. Element 4 in the figure indicates the part of the structure that is closest to the nose of the aircraft, element 2 is situated on towards the rear and coincides with the aft bulkhead. Figure 8.12b shows how the same structure fits into the larger aircraft. Note that not all of this space will be used to store fuel, as a part of the core structure will also be used to seat a passenger. The forward bulkhead will be placed accordingly to allow for this, as indicated in orange in Figure 8.12b

This part of the fuselage is heavily reinforced as can be seen by the number of beams and structural features in Figure 8.12a. The reason for this reinforcement is the fact that the main loads experienced by the aircraft come together at this location: the lift produced by the wings, the support provided by the landing gear, the weight of payload, and the weight of both the front and back engine. The wings attach to element 3 and the top part of the frame of element 4. The centre of gravity of the aircraft is located to the front (nose-ward) part of this core structure, which further proves that this area is the structural 'heart' of the aircraft.

The bottom of this core structure, i.e. the floor of the cabin, is supported by two keel beams upon which the seats are usually mounted. As will be discussed in the remainder of this section, these two beams play a critical role in the structural integrity of the fuselage and carry significant loads. For this reason it was decided to mount the fuel storage on top of these two beams, as they are already optimised to carry loads usually imposed by passengers and payload.

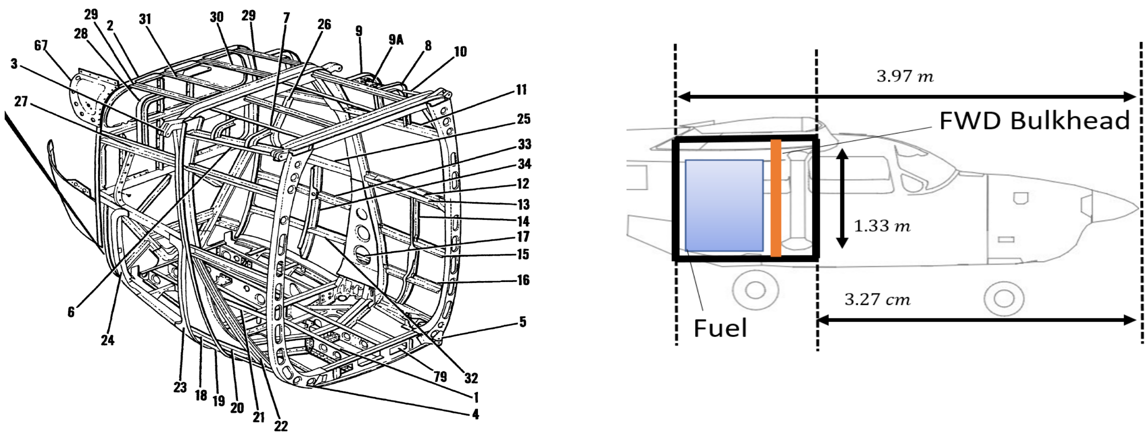

(a) Fuselage core

(b) Location of structural core

Figure 8.12: Structural core

Figure 8.13 shows the proposed concept for storing batteries. It consists of a truss structure (2) which supports two plates (4) upon which batteries (1) are mounted. This setup allows for easy wiring and cooling (requirement FUEL-MNT-4: The structural mount shall accommodate connections between the engine and fuel cells such as cabling or fuel lines), and is sized such that it fits through the existing door of the fuselage. The entire structure is connected to the aircraft by riveting the bottom plate to the two keel beams (3). An additional benefit of this is that there is some flexibility in the location along the keel beams at which the fuel mount is riveted. This could be beneficial in adhering to the c.g. requirements and could allow for the mount to be placed at different locations depending on its weight.

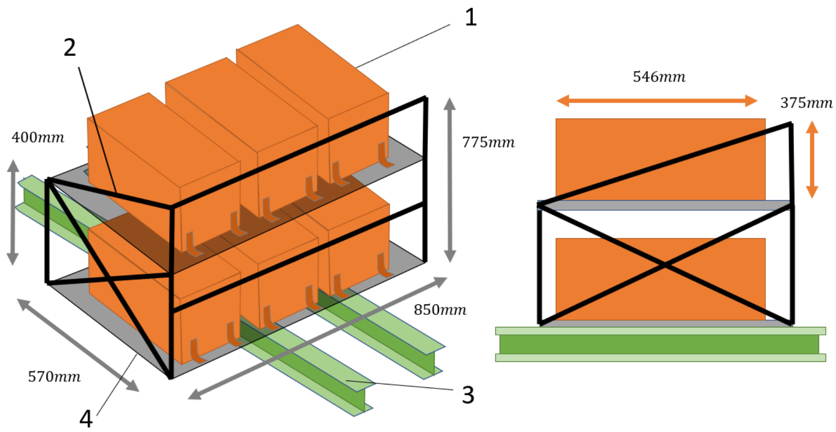

Figure 8.13: Battery storage

Figure 8.14 shows the same structure adapted for hydrogen tanks. The hydrogen tank itself (2) is kept in place through two vertical plates (1) which are to stop the tank sliding within the structure. The tank is kept from sliding through the holes in the vertical plates by the truss structure itself on either side.

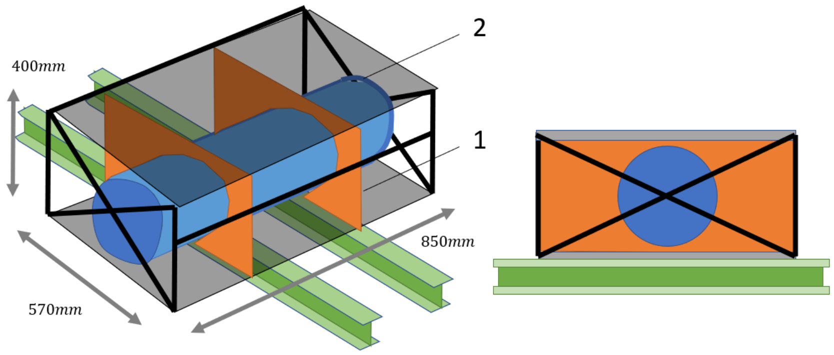

Figure 8.14: Hydrogen storage

Both of these concepts are analysed using the following methodology:

1. A global analysis of how the weight of the battery storage impacts the aircraft structure
2. Analysis of the connection between the fuel storage and keel beams to ensure the fuel mount is secure at all stages during flight

In doing these analysis adherence to requirement FUEL-MNT-5: *The structural mount shall prevent the fuel from moving around in the cabin* is proven.

Existing Aircraft Structure

The goal of this analysis is to evaluate the effect of adding fuel mounted to the floor of this structure. Figure 8.15a highlights the four sides that make up the structure. The top plate contains four stringers and the bottom plate makes use of two keel beams (stringers), as illustrated in Figure 8.15b. Although the walls do contain stiffeners, their contribution to bending is assumed to be negligible as their main function is to connect the top and bottom plates. Furthermore, it is assumed that the skin on the top and bottom of the fuselage does not take up any load (as it is approximately $1mm$ thick and only serves to separate the cabin from the outside world). This means that the effective cross section of the core structure is reduced down to six beams, distributed across the top and bottom plates, as in Figure 8.15b. This is relevant to calculations involving the flexural axis, y_{cent}, as well as the moment of inertia I. A_t and A_b represent the area of the top and bottom stringers, respectively.

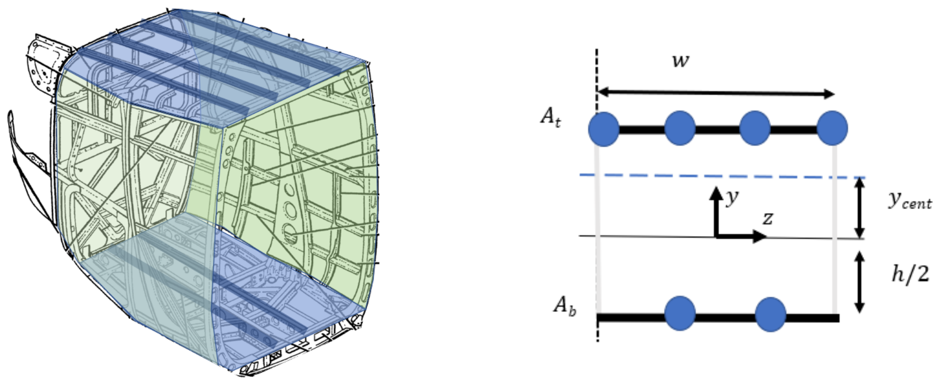

(a) Stringer location

(b) Idealised fuselage core

Figure 8.15: Fuselage section for fuel storage

These stringers ensure bending stiffness, with the bottom being in compression and top being in tension during flight since the entire structure bends around the wing as it lifts the fuselage. This is evident from the free body diagram, shown in Figure 8.16.

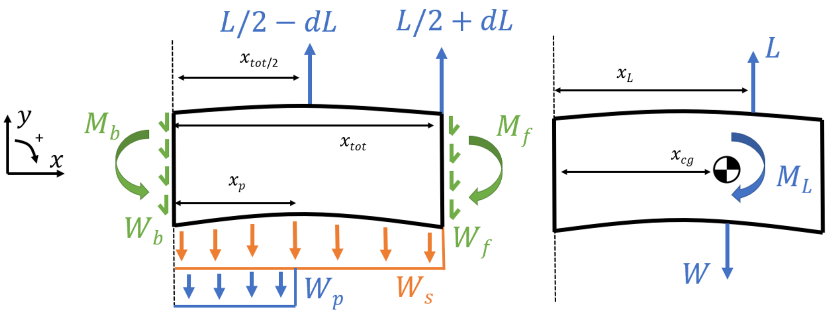

Figure 8.16: Free body diagram of core structure

The FBD isolates the core structure by considering the weight and moment of the front and back of the aircraft. L and dL are left as two degrees of freedom to ensure vertical and moment equilibrium. Note that $450kg$ is taken to be the maximum weight of the fuel and structural mount. It is assumed that the current design of the aircraft is equipped to handle $300kg$ (3 passengers and cargo) of payload over the same distance, meaning that it must be proven that the fuel does not weight more than $300kg$ or that the structure is capable of sustaining $450kg$. As an initial analysis steady flight is assumed, meaning both moment and vertical force equilibrium take place. Vertical equilibrium entails that:

$$\sum F_y : L = W_b + W_p + W_s + W_f = W \tag{8.22}$$

Note that this is therefore the net lift produced by the wings and empennage, i.e. the total lift minus the weight of the empennage and wing. dL accounts for the moment produced by the wing and the empennage. It is known that the internal moment beyond x_{tot} is equal to zero (boundary condition for moment equilibrium)[6]:

$$(CW+)\sum M_{x_f} = -M_b - W_b \cdot x_{tot} - W_p(x_{tot} - x_p/2) - W_s x_{tot}/2 + L \cdot 0.75 x_{tot} - dL \cdot x_{tot}/2 + M_f = 0 \tag{8.23}$$

This allows for the aerodynamic moment of the tail and wing to be calculated:

$$dL = [-M_b - W_b \cdot x_{tot} - W_p(x_{tot} - x_p/2) - W_s x_{tot}/2 + L \cdot 0.75 x_{tot} + M_f]/(x_{tot}/2) \tag{8.24}$$

[6]The program steps from left to right to calculate internal forces, so by default the internal forces are zero at the left hand side but not at the right hand side.

8.3.1. Bending Analysis

Global Bending Analysis

Figure 8.17a shows the resulting internal shear and moment diagrams for two load cases: $W_p = 450kg$ (fuel) and $W_p = 300$ (3 passengers). The figure shows that the maximum moment occurs at $x = x_{tot}$, i.e. the most forward part of the core structure. This makes intuitive sense as the this is the location around which the front part of the aircraft "hinges" and is supported by the wing. The actual maximum moment itself ($\approx -7kNm$) is constant for both cases since the moment M_f is constant. There is a marginal increase in both shear and moment for $x < x_p$. Positive internal forces are indicated in Figure 8.17b.

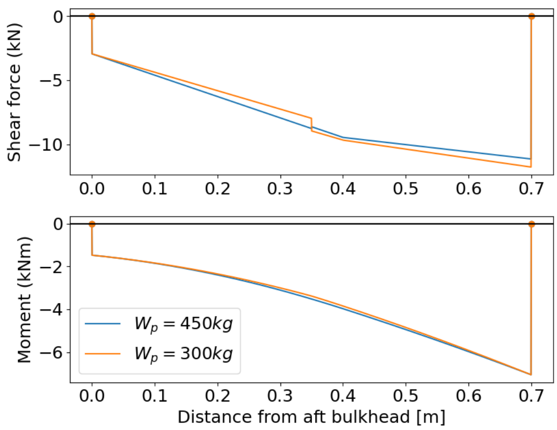

(a) Global internal shear and moment diagram

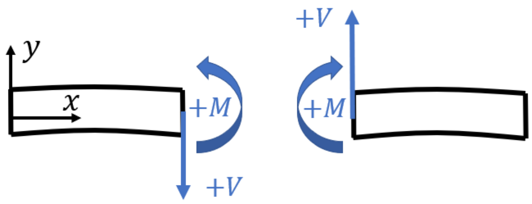

(b) Internal force convention

Figure 8.17: Global bending and shear analysis

Figure 8.17a also shows that the maximum shear along the beam is even marginally decreased for $W_p = 450kg$. This is because slightly more lifting force is provided at the centre frame ($x_{tot}/2$) than at the front to compensate for the additional moment. This centre vertical frame is the same reason for the jump in shear force at $x_{tot}/2$.

Table 8.11: Differences in global moment and shear per load case

$x_{tot/2}$ **(approaching from left)**	$W_p = 450$	$W = 300$	**RD**
Moment (Nm)	-3522.38	-3382.95	+4%
Shear (N)	-8764.77	-7968.10	+9%
x_{tot} **(approaching from left)**	$W_p = 450$	$W = 300$	**PD**
Moment (Nm)	-7059.29	-7059.07	0%
Shear (N)	-11139.39	-11769.54	-5%

Figure 8.18 shows how normal stress (σ) is distributed across the cross section. For this the flexure formula was used:

$$\sigma = -\frac{My}{I} \tag{8.25}$$

where M was taken to be the maximum moment along the x-direction as per Figure 8.17a. y is the distance from the neutral axis, y_{cent}, which is indicated in red in Figure 8.18. I is the moment of inertia of the cross section. These entities were determined using Equation 8.26 and Equation 8.27, using conventions established in Figure 8.15b. Note that for the moment of the inertia only the Steiner terms of the stringers are considered.

$$y_{cent} = \frac{4 \cdot A_t \cdot h/2 - 2 \cdot A_b \cdot h/2}{4 \cdot A_t + 2 \cdot A_b} \quad (8.26) \qquad I = 4 \cdot A_t(h/2)^2 + 2 \cdot A_b(h/2)^2 \quad (8.27)$$

Evidently the neutral axis is located nearer to the bottom plate than the top plate. This is because even though there are more stringers on the top plate, the two stringers on the bottom plate are more than three times larger. Therefore more mass is situated nearer to the bottom than the top of the structure. The reason for this is likely because the weight of payload is introduced into the structure through the bottom part of the fuselage, hereby warranting extra reinforcement. An additional motivation to move the neutral axis downward is due to the fact that the bottom plate will be in compression during flight which entails the risk of buckling, a problem the top plate does not have to contend with.

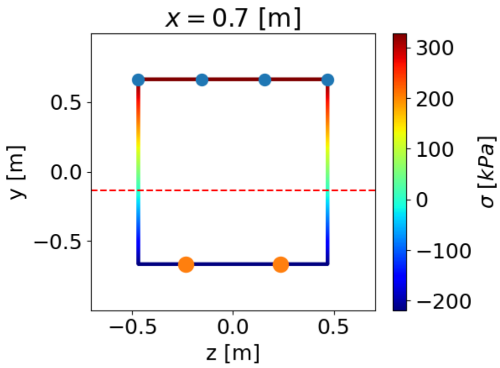

Figure 8.18: Maximum global normal stress

The results of this analysis are tabulated in Table 8.12. The key takeaway is that the bottom plate is in compression, and that in absolute terms the top plate experiences a higher normal stress. Since the maximum moment itself stays constant for both cases at $x = 0.7$, there is no additional normal stress due to the added weight of fuel relative to loading passengers.

Table 8.12: Maximum global normal stress results

Entity	Value	Units
Max compression	-218875.22	Pa
Max tension	328312.83	Pa
y_{cent}	-0.13	m
A_t	0.001	m^3
A_b	0.003	m^3
h	1.33	m

Local Bending Analysis

So far only the global picture of the core structure has been discussed, which is to say that the entire structure was idealised as one coherent beam. In reality the individual parts of the structure are also subject to their own bending and loads. In this section the bottom plate will be analysed, as this is the location which is in direct contact with the increased load ($W_p = 450kg$ instead of $W_p = 300kg$). A local analysis could have also been performed for the top plate, but the decision was made to focus on the bottom. The additional loads introduced will undoubtedly have an effect on the load distribution of the plate, but this effect will be relatively less as the top plate must also sustain the weight of the entire aircraft.

To explore this in more detail the bottom plate of the fuselage is considered as illustrated in Figure 8.19. This represents the 'local' picture, which is to be superimposed on top of the global picture. T_1 through T_3 represent the tensile forces imposed by the three vertical frames shown in Figure 8.12a. Vertical equilibrium necessitates that as the aircraft (bottom plate) is loaded with more weight, these three members will need to carry more loads to 'lift' the additional payload. This coincides with results shown in Figure 8.17a, where it was determined that the limiting factor would be shear, not bending. However, although the maximum *global* moment did not increase under the additional weight of fuel, the same may not necessarily be true for the local bottom plate. Furthermore, during bending analysis of the bottom plate normal stresses must be superimposed, meaning that the internal moment distribution in Figure 8.17a is still highly relevant.

Besides three tensile members, Figure 8.19 also considers the weight of the plate itself, W_s, and the load of passengers or fuel W_p. The condition for vertical equilibrium states:

$$T_1 + T_2 + T_3 = W_s + W_p \tag{8.28}$$

Additionally, the internal moment at the right-most edge is again set to zero (since the program steps from left to right):

$$(CW+) \sum M_3 = T_1 \cdot x_{tot} - W_p(x_{tot} - x_p/2) + T_2 \cdot x_{tot}/2 - W_s \cdot x_{tot}/2 = 0 \tag{8.29}$$

Since W_p and W_s are known, this leaves a total of three unknowns to be solved by two equations. Therefore the assumption is made that one-third of the load total vertical load is taken up by T_2:

$$T_2 = \frac{W_s + W_p}{3} \tag{8.30}$$

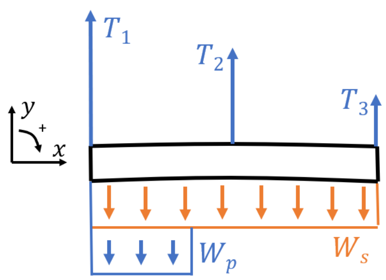

Figure 8.19: Local (bottom plate) free body diagram

The resulting local internal and shear moment diagrams are given in Figure 8.20. Numerical results are tabulated in Table 8.13. The internal force diagrams show that the maximum bending moment occurs at $x = 0.22m$ for both load cases, approximately in the centre of the payload. Conversely, the maximum shear force occurs at the beginning of the plate at $x = 0m$.

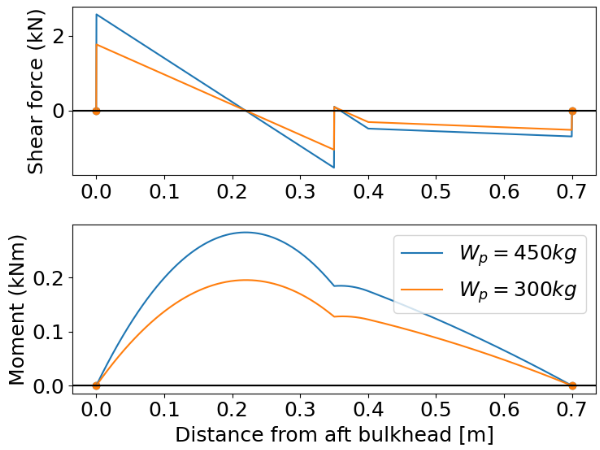

Figure 8.20: Local (bottom) internal shear and moment diagram

Table 8.13 indicates that both the maximum bending and shear increase by 31% for $W_p = 450kg$ relative to the nominal case. This is significant for the plate itself and is an important result of the analysis.

Table 8.13: Differences in bending and shear per load case

	$W_p = 450kg$	$W_p = 300kg$	**PD**
$T_1\ (N)$	2580.96	1775.14	+31%
$T_2\ (N)$	1635.00	1144.50	+30%
$T_3\ (N)$	689.03	513.85	+25%
Max bending (Nm)	283.77	195.52	+31%
Max shear (N)	2576.85	1772.32	+31%

Finally, Figure 8.21 shows the normal stress at the location of maximum *local* bending (Figure 8.20) for each load case. Since the beams are symmetric the neutral axis of the bottom plate coincides with $y = 0$. In this graph the residual global stress (compression, negative) has been superimposed uniformly across the cross section for both cases. At $x = 0.22$ the local bending moment is largest, but the global bending moment is relatively small (Figure 8.17a).

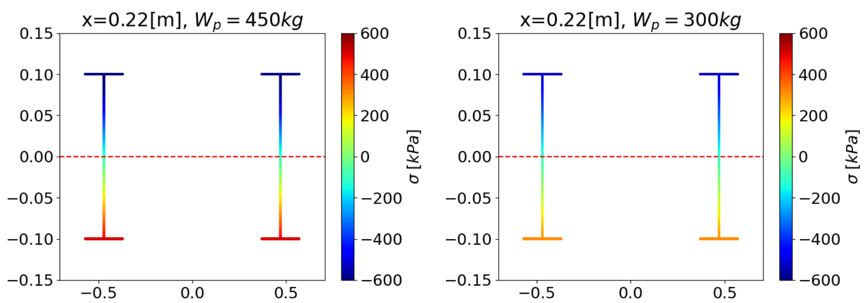

Figure 8.21: Maximum local normal stress

Table 8.14 numerically compares the two graphs in Figure 8.21 and lists the residual global stress in each case, which in itself is different (corresponding to Figure 8.17a).

Table 8.14: Cross section differences per load case

$x = 0.22m$	$W_p = 450kg$	$W_p = 300kg$	PD
Residual global (Pa)	-105372.52	-76460.26	+27%
Local max. compression (Pa)	-608094.99	-418977.80	+30%
Local max. tension (Pa)	608094.99	418977.80	+32%
Superimposed compression (Pa)	-713467.52	-495504.35	+30%
Superimposed tension (Pa)	502722.47	342451.26	+32%

Since the superimposed normal stress experienced by the beams is a function of both residual and local normal stress by definition, the maximum normal stress experienced by the bottom beams does not necessarily occur at the location of maximum local bending. Instead, it occurs at the location where the sum of residual and local normal stress reaches a maximum. This is explored by Figure 8.22, where the maximum superimposed stress is plotted along with its components. The left graph shows the normal stress at maximum compression, which occurs at the top of each beam. The right hand side shows tension, occurring at the bottom of each beam. Interesting to note is that for compression superimposition increases the maximum normal stress experienced, whereas for tension local stress is alleviated by the addition of residual stress. Therefore in this case the critical location becomes the top part of the beams which experiences the highest normal stress, as indicated in Table 8.14.

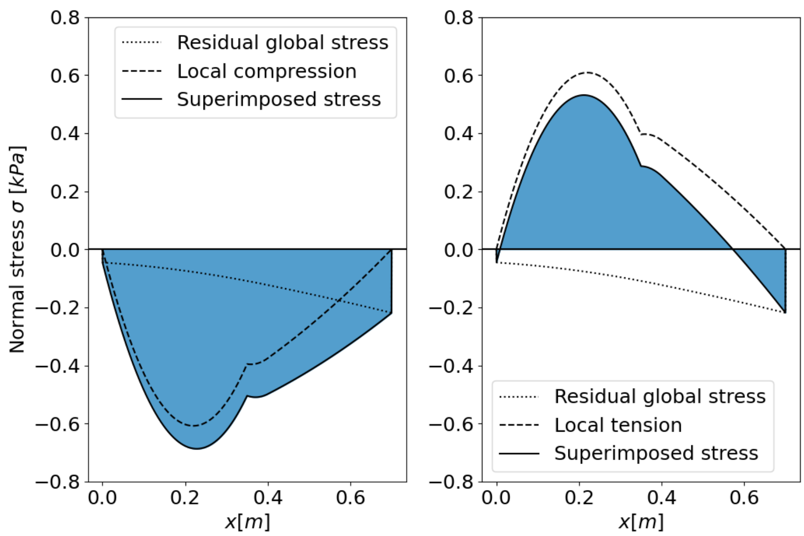

Figure 8.22: Superimposed normal stress variation along core structure

8.3.2. Results and Recommendations for Existing Structure

The most important results of the previous sections are summarised in Table 8.15. The key takeaway is that even though the global moment does not increase, the local maximum moment and normal stress experienced by the keel beams *does* increase. Should this lead to failure under extreme loading circumstances (high g scenario's) then the top flange of the two keel beam would most likely fail due to compression (assuming that no other structural elements fail before this). The maximum global shear along the beam decreases for $W_p = 450kg$.

Table 8.15: Summary of results

Criteria	Location	$W_p = 450kg$	$W_p = 300kg$	PD
Superimposed local compression (Pa)	$x = 0.22$	-713467.52	-495504.35	+30%
Max global compression (bottom) (Pa)	x_{tot}	-218875.22	-218875.22	0%
Max global tension (top) (Pa)	x_{tot}	328312.83	328312.83	0%
Max local shear (N)	$x = 0$	2576.85	1772.32	+31%

Finally, something that has not yet been considered is the fact that the three vertical frames (tensile members) will experience a higher amount of tension (+30% on average, Table 8.13). This increases their risk of failure under extreme load cases.

There are three solutions to alleviate loads:

1. Add another vertical frame at $x_{tot}/6$ to take up some of the global shear loads experienced by the tensile members
2. Add another keel beam or reinforce existing to be accommodate additional normal (compressive) stress
3. Limit flight envelope to prevent exposure to excessive loads, the recommendation would be to limit maximum loads by 30% as this is the amount of additional load which is experienced

Figure 8.23 shows the effect of adding an extra keel beam. This reduces the maximum superimposed compression stress from $-608.6kPa$ to $-305.5kPa$ (48%). Tensile stress is reduced from $502.7kPa$ to $200.3kPa$ (61%). Comparing with Table 8.15, the conclusion is drawn that by adding a keel beam stresses are reduced to approximately two-thirds of what they were for $W_p = 300kg$.

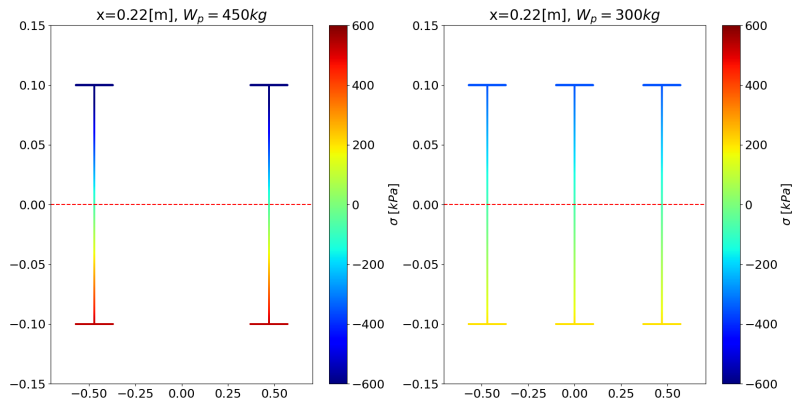

Figure 8.23: Effect of adding another keel beam

8.3.3. Verification and Validation

To verify and validate the model used to determine local and global loads multiple methods were used. The model itself was built to be as flexible as practically possible, meaning that it allowed for forces, moments, and distributed loads to be added as inputs. The program would then evaluate the effect of each of these inputs on the internal forces at each location along the beam by considering internal equilibrium of forces. In essence it would 'step' from left to right (increasing x), and each time the program encountered an additional force or moment it would incorporate its effects and continue to take it into account by apply beam theory and internal equilibrium of forces.

Verification

To verify the model it was checked that the internal shear and moment were in fact zero at the ultimate right hand side of the beam. Taking the last element of the discretized list of internal moments and shear (which includes moments and forces at x_{tot}) across the global beam yielded results shown in Table 8.16.

Table 8.16: Boundary condition internal forces

Criteria	Value
Internal moment (Nm)	$-1.81 \cdot 10^{-12}$
Internal shear (N)	$1.70 \cdot 10^{-13}$

The reason the internal forces are not exactly zero is due to the way that the beam is discretized into sections. The first step in the program is to split the beam into a set number of x locations. Since the last element of the beam itself is not exactly located at x_{tot}, but one step to the right of it (so that the program also incorporates the forces at x_{tot}), there is a negligible contribution of forces.

Figure 8.24 shows the effect of varying the number of points evaluated across the beam. It can be seen from the graph that the difference between $n = 80, n = 200$ and $n = 500$ is barely distinguishable, indicating that they have converged to the same solution.

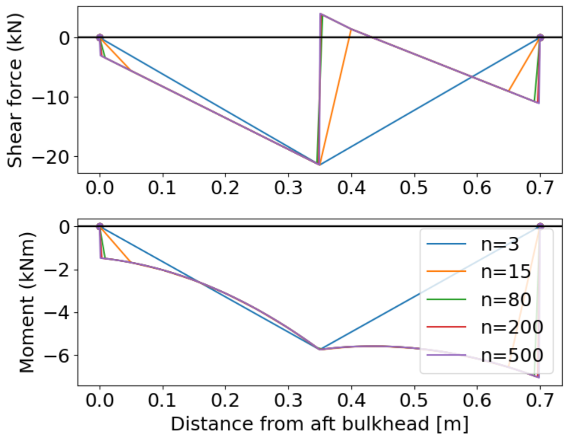

Figure 8.24: Convergence of fuel mount model

The last form of verification entails the use of an analytical model for a simple load case, shown in Figure 8.25a. Positive internal forces are shown in Figure 8.25b.

(a) Verification load case

(b) Internal force

Figure 8.25: Global bending and shear analysis

Setting the length of the beam to $1m$, $x_p = 0.5m$ and $w = 1000/0.5 = 2000N/m$, for $x < x_p$ the internal shear force is calculated by considering vertical equilibrium:

$$500 - 2000 \cdot x - V = 0 \Rightarrow V = 500 - 2000 \cdot x \tag{8.31}$$

Beyond x_p the shear force should be constant and equal to

$$V = 500 - 2000 \cdot x_p = -500 \tag{8.32}$$

The internal moment for $x < x_p$ is calculated according to

$$500 \cdot x - 2000 \cdot x^2/2 - M = 0 \Rightarrow M = 500 \cdot x - 1000 \cdot x^2 \tag{8.33}$$

For $x > x_p$ the moment is calculated by

$$500 \cdot x - 2000 \cdot x_p \cdot (x - x_p/2) - M = 0 \Rightarrow M = 500 \cdot x - 2000 \cdot x_p \cdot (x - x_p/2) \tag{8.34}$$

Table 8.17: Verification results

Analytical	$x = 0$	x_p	$x = 1$
V (N)	500	-500	-500
M (Nm)	0	0	-250
Numerical	$x = 0$	x_p	$x = 1$
V (N)	498.99	-500	-500
M (Nm)	0	-0.125	-249.74

These formulas are used to calculate analytical solutions at $x = 0$, $x = x_p$ and $x = 1$. These are given and compared with simulation results in Table 8.17. Again a small discrepancy is found between the analytical and numerical values, which is attributed to the way the beam is discretised. This simulation used 2000 discrete points.

Upon increasing the number of points from 2000 to 5000, $V(x = 0)$ became 499.59, $M(x_p) = -0.05$ and $M(1) = -249.89$, thus showing convergent behaviour.

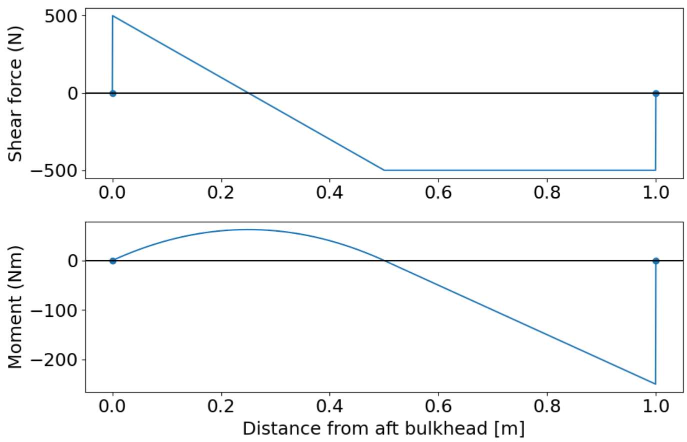

Figure 8.26: Shear and moment diagrams for fuselage section

Validation

Validation of the model is inherently difficult due to the lack of data available and extensive simplification of the structure. The idea behind the model is not to predict internal stresses with complete accuracy, but rather to gauge the effect of the additional weight of the fuel. The assumptions that govern the model include:

1. The skin of the fuselage has a negligible bending contribution
2. The entire structure can be idealised as a beam
3. The centre vertical frame takes up one-third of the vertical loads

The first validation method is to extrapolate the c.g. location based on the implied loads in Figure 8.16. Taking clockwise moments around an arbitrary location x_{cg} and rewriting:

$$(CW+)\sum M_{cg} = -W_b \cdot 0.5 - W_b \cdot x_{cg} - W_p(x_{cg} - x_p/2) - W_s(x_{cg} - x_{tot}/2) + W_f(1.2 + x_{tot} - x_{cg}) \tag{8.35}$$

$$\Rightarrow x_{cg} = \left[W_b \cdot 0.5 - W_p\frac{x_p}{2} - W_s\frac{x_{tot}}{2} - W_f(1.2 + W_f) \cdot x_{tot}\right]/(-W_b - W_p - W_s - W_f) \tag{8.36}$$

This yields $x_{cg} = 0.69714$, which is just behind wing strut. Since it is known that the nominal c.g. limits are between the wing strut and main landing gear (approximately $x_{tot}/2$), the load distribution is considered validated.

To validate the assumption that the skin of the fuselage contributes negligibly to bending, the moment of inertia of one skin flange is calculated:

$$I_{skin} = \frac{1}{12} \cdot 0.001 \cdot 1.33^3 = 0.001960m^4 \tag{8.37}$$

As this is only 1.1% of the total moment of inertia of the global cross section, the assumption is considered valid. The assumptions pertaining to the idealisation of the structure as a beam and that the centre vertical frame takes up one-third of the load are difficult to validate due to lack of data and their simplifying nature.

8.3.4. Fuel Mount Connection

The connection between the fuel mount and the fuselage will consist of two columns of rivets. In the event of a crash the most prominent risk is failure of the rivets or bottom sheet, which would mean that the whole construction would be free to slide forward and potentially injure passengers. CS23 specifies that the maximum g-load to be sustained in the forward direction in the event of crash is 19g. Figure 8.27 shows how loads are expected to be distributed in the event of a crash. It shows that the keel beams will experience both shear and normal forces.

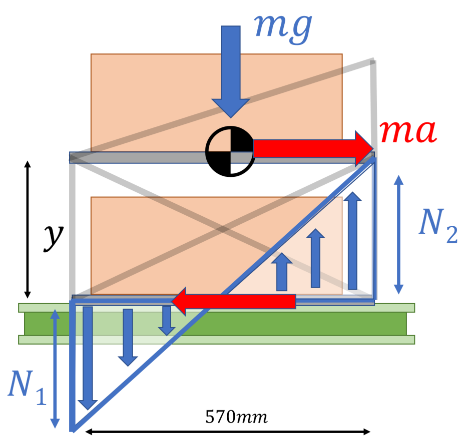

Figure 8.27: FBD of fuel mount in the event of a crash

During a crash the rivets will be responsible for producing a force that is able to decelerate the entire structure according to $F = ma$. Additionally, moments around the centre of gravity must equal to zero. Assuming that the total weight of the structure will not exceed $450kg$, moment equilibrium states:

$$(CW+)\sum M_{cg} = \int_0^{0.57} N(x)(x_{cg} - x)dx + ma \cdot y = 0 \tag{8.38}$$

Furthermore, vertical equilibrium requires:

$$\sum F_y : mg - \int_0^{0.57} N(x)dx = 0 \tag{8.39}$$

The normal force exerted by the beam is distributed linearly:

$$N(x) = a(x) + b \tag{8.40}$$

Filling Equation 8.40 in Equation 8.38 yields:

$$\int_0^{0.57} (a(x)+b)(0.285-x)dx + 19 \cdot 450 \cdot 0.3875 \cdot 9.81 \tag{8.41}$$

$$= \int_0^{0.57} [-ax^2 + (0.285 \cdot a - b)x + b \cdot 0.285]dx + 32501.756 \tag{8.42}$$

$$M_{cg} = -\frac{a}{3}[0.57^3] + \frac{(0.285a-b)}{2}[0.57^2] + 0.285 \cdot b \cdot [0.57] = -32501.756 \tag{8.43}$$

$$\sum F_y : 450 \cdot 9.81 - \int_0^{0.57} (a(x)+b)dx = 4414.5 - \frac{a}{2}0.57^2 - b \cdot 0.57 = 0 \tag{8.44}$$

$$\begin{bmatrix} -\frac{1}{3}0.57^3 + \frac{0.285}{2}0.57^2 & -\frac{1}{2}0.57^2 + 0.285 \cdot 0.57 \\ -\frac{1}{2}0.57^2 & -0.57 \end{bmatrix} \begin{bmatrix} a \\ b \end{bmatrix} = \begin{bmatrix} -32501.756 \\ -4414.5 \end{bmatrix} \tag{8.45}$$

$$\Rightarrow \begin{bmatrix} a \\ b \end{bmatrix} = \begin{bmatrix} 2.10 \cdot 10^6 \\ -5.92 \cdot 10^5 \end{bmatrix} \tag{8.46}$$

This results in the normal force distribution as shown in Figure 8.28. The maximum normal force occurs at $x = 0.57$, with a magnitude of $N_2 = +608kN$ in the upwards direction. This means that the front part of the fuel mount wants to push the keel beams downward. Since the fuel mount and keel beams are in direct contact, this does not impose any additional (vertical) forces on the rivets since the the bottom plate and top part of the keel beam will simply be pushing against each other. The same cannot be said for the rear part of the fuel mount ($x = 0$), which will be pulled downward by rivets since they are what connects the two plates. The maximum tensile force a rivet will be required to sustain is $N_1 = -592kN$.

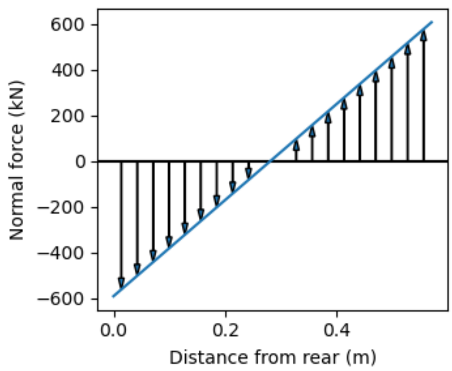

Figure 8.28: Normal force distribution along fuel mount

An individual rivet in tension is shown in Figure 8.29a. Three rows of fasteners will be used per keel beam, meaning that in the worst case scenario the maximum tensile load a rivet must endure is $592kN/(2 \cdot 3) = 98kN$. This force will result in the tendency for the bolt to shear away from the centre column in the vertical direction. This information is useful as a first estimate for what type or size of bolt would be required.

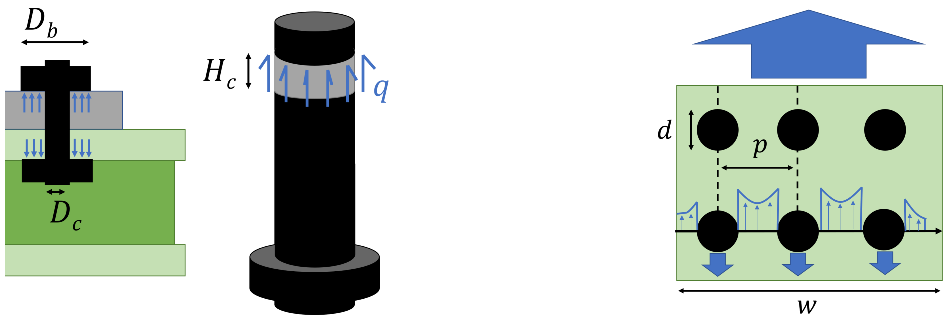

(a) Bolts in tension

(b) Bolts in shear

Figure 8.29: Global bending and shear analysis

For shear, Figure 8.29b shows how stresses are distributed throughout the panel. There are three ways the panel could fail:

1. The panel itself fails (Equation 8.47)
2. The rivets fail in shear (Equation 8.50)
3. The panel fails around fasteners (Equation 8.51)

The panel itself experiences a nominal stress between fasteners equal to:

$$\sigma_{nom} = \frac{F}{A} = \frac{F}{t(w - nd)} \tag{8.47}$$

Where t is the plate thickness and n is the number of bolts (across both keel beams). To account for stress concentrations around bolts (as seen in Figure 8.29b) a stress concentration factor is used[7]. Taking $w = 150mm$ and $d = 20mm$:

$$K_t = 3 - 3.13\left(\frac{d}{w/3}\right) + 3.66\left(\frac{d}{w/3}\right)^2 - 1.53\left(\frac{d}{w/3}\right)^3 = 2.23569 \tag{8.48}$$

Then, using the stress concentration factor to calculate the actual normal stress:

$$\sigma = \sigma_{nom} \cdot K_t = 2.23569 \cdot \frac{450 \cdot 9.81 \cdot 19}{t(0.150 - 6 \cdot 0.02)} = \frac{931950.0}{t} \tag{8.49}$$

For bolts in shear, the maximum shear stress τ is calculated by:

$$\tau = \frac{F}{A} = \frac{F}{6 \cdot (d/2)^2\pi} = \frac{450 \cdot 9.81 \cdot 19}{6 \cdot (0.02/2)^2\pi} = 44.49[MPa] \tag{8.50}$$

For the area of the plate next to each bolt the maximum stress is determined by:

$$\sigma = \frac{F}{A} = \frac{F}{6dt} = \frac{698692.5}{t} \tag{8.51}$$

In these equations the plate thickness t is left as a variable. To determine t a bending analysis was performed across the width of the plate (perpendicular to the direction of the keel beams). Figure 8.30a shows the internal shear and force across the bottom plate of the fuel mount. Figure 8.30b shows the force which were used as an input for the program. These include the two vertical ribs at the end of the mount, the normal force provided by the two beams keel beams, as well as one layer of batteries.

[7] https://www.amazon.com/Roarks-Formulas-Stress-Strain-8th/dp/0071742476/ref=as_li_ss_tl?ie=UTF8&linkCode=ll1&tag=mechanicalc-20&linkId=adf3407e8a8c5bdfa1b5d81af744008e [Accessed June 2021]

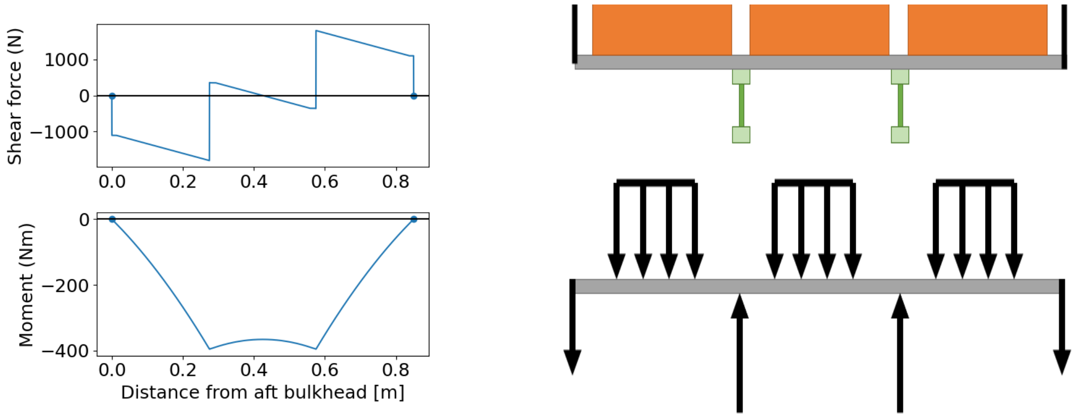

(a) Verification load case **(b)** Internal force

Figure 8.30: Global bending and shear analysis

In this case both the maximum moment and shear in the plate occur above the keel beams. Using Aluminium 6061 which has a yield stress of $276MPa$, and a load factor $n = 4.6$, the maximum normal stress in the plate is calculated as a function of sheet thickness t and maximum moment ($-395Nm$):

$$\sigma = -\frac{nMy}{I} = -\frac{nM \cdot t/2}{\frac{1}{12}0.57t^3} = \frac{19126}{t^2} \tag{8.52}$$

Using a maximum yield stress of $276MPa$ in combination with the previous equations allows for the calculation of required skin thickness, as given in Table 8.18. It is clear that the most prominent mode of failure is bending of the sheet in extreme load cases, which requires the sheet to have minimum thickness of $8.324mm$.

Table 8.18: Required sheet thickness per failure mode

Failure mode	Required skin thickness (mm)
Sheet yield inter-bolt	2.025
Sheet yield around bolt	1.518
Sheet yield due to bending	8.324

For the sheet thickness a number of stringers are recommended to reduce the required thickness to $\approx 2mm$, aligning with inter-bolt and around bolt yielding as in Table 8.18.

To estimate the weight of the entire structure the sheet thickness in Table 8.18 is used and no stringers are assumed. Using a density of $2700kg/m^3$ for Chromoly 4130, this results in a mass of $2700 \cdot 0.006448 \cdot 0.570 \cdot 0.850 = 8.4kg$. Since the top plate only has to sustain half the load (one row of batteries), it is assumed that the top plate weighs approximately $4.2kg$. Adding the truss structure and making the prediction that it weights $\approx 6kg$ (relative to the $13kg$ of the fuel mount), this puts the entire mount at a total weight of:

$$W_{fuel-mount} = 8.4 + 4.2 + 6 = 18.6 \quad [kg] \tag{8.53}$$

which adheres to the requirement that the fuel mount may not weigh more than $30kg$. Finally, it is worth noting that the fuel mount is able to fit through the existing door making this design advantageous for interchangeability.

Results and Recommendations for Fuel Mount Connection

This section briefly summaries the results of the fuel mount analysis. First, a global bending analysis was performed which proved that the maximum moment and shear across the core structure of the aircraft did not increase with additional fuel load. As a result, the global tension and compression ($32.8kPa$ and $-21.9kPa$, respectively) stayed constant in the top and bottom plate. This suggests that on a global scale the existing structure is able to sustain loads imposed by the additional fuel, which makes intuitive sense as the an additional $150kg$ is relatively little when considering the scale of the entire aircraft.

A subsequent local bending analysis was performed to evaluate the local effects of additional fuel on the bottom plate, which consists of two keel beams. This showed that the local bending was far more significant for stresses in the beams than global bending ($400kPa$ on average versus $100kPa$). This is likely because on a global scale the moment of inertia of the entire core structure is relatively large since the distance between the top and bottom plate is large. On a local scale, the moment of inertia is determined only by the height and width of the two keel beams. By performing a local bending analysis and superimposing global stresses it was ultimately found that the maximum local compression increased by 30%. Compression stress in the keel beams was found to be 3 The solution to this problem would be to either consider limiting the envelope of manoeuvring loads or adding a third keel beam. The latter would reduce the total compressive stress by 48%, allowing the structure to sustain the existing flight envelope.

Two things that need to be kept in mind which have not been analysed in this section are: 1) tensile members in the sides of the fuselage, 2) shear flow analysis in beams. Tensile forces were shown to increase by $25\% - 31\%$, although this is a very crude preliminary estimation. Further analysis would be required to determine the full extent of the impact on the sides of the fuselage. Likewise, shear flow throughout the core structure and keel beams has also not yet be considered and would be the logical next step in analysis.

The final step is to check compliance with the original requirements as done in Table 8.19. The structural mount weighs 18.6kg (FUEL-MNT-1), integrity of the existing structure has been verified (FUEL-MNT-2) and the truss structure accommodates cabling (FUEL-MNT-3). Finally, analysis of the connection showed that the connection prevents the fuel from moving around in the cabin.

Table 8.19: Fuel mount requirements

Code	**Requirement**	✓
FUEL-MNT-1	The structural mount shall weigh no more than 30kg.	18.6kg
FUEL-MNT-2	The structural mount shall introduce loads into the existing structure in a way that maintains its integrity.	✓
FUEL-MNT-3	The structural mount shall accommodate connections between the engine and fuel cells such as cabling or fuel lines.	✓
FUEL-MNT-4	The structural mount shall prevent the fuel from moving around in the cabin.	✓

9 Data Acquisition

As the flying propulsion testbed is designed for performing research on alternative propulsion systems, it is required that it has a data acquisition system for data to be extracted and analysed. Therefore, this section aims to provide an overview of the electronic components required for the data acquisition system design. Several block diagrams will be presented to visualise the data handling and a power budget will be provided.

9.1. Instrumentation Panel Upgrade

A panel upgrade will be implemented in the Skymaster for which the requisite components were provided by DEAC. From this list a block diagram of the electronic components was created which is shown in Figure 9.1. In the *Midterm Report* it was shown that the components as shown would fit inside the aircraft [2]. One important note to make is that whilst the panel upgrade consists of two engine monitors only one has been shown in the block diagram to save space.

Figure 9.1: A block diagram illustrating electronic components that will be brought aboard the testbed

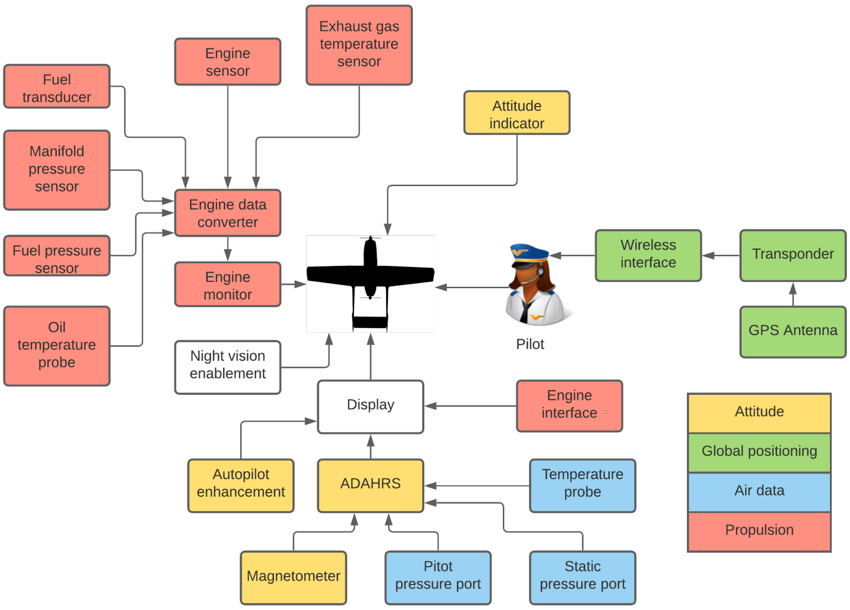

9.2. Data Handling

When creating the data handling structure of the testbed it is important to separate the data into several domains [12]. The domains with which the testbed will be working with is as follows:

- Attitude - The orientation of the aircraft with respect to the ground and air frame
- Global positioning - The geographic position and time information of the aircraft.
- Air data - The properties of the air (density, pressure, temperature and etc.)
- Propulsion - Properties of the engine (manifold pressure, cylinder head temperatures and etc.)
- Analogue vs digital - While this is not a domain in itself it is important to distinguish which sensors in the aircraft operate with analogue signals or digital signals

These domains and their constituent instrumentation are detailed below.

Attitude

The attitude instrumentation is similar to what was already in the Skymaster pre-modifications except that the analogue instrumentation is now digital. Firstly in the flight deck an attitude indicator will be installed alongside a display that is given data via an Attitude Determination And Heading Reference System (ADAHRS). A Garmin autopilot enhancement is also installed as well as a magnetometer to determine the orientation of the aircraft with respect to the Earth's magnetic field. Finally, the installation of an angle of attack vane can be considered; however since this is not critical instrumentation it does not necessarily have to be installed on the testbed.

Global Positioning

The global positioning instrumentation is the simplest to integrate as it does not require any modification from what is installed in the panel upgrade. The GPS antenna will simply connect to the transponder where the pilot can then receive global positioning data via the wireless interface installed in the transponder.

Air Data

Similarly the air data instrumentation is also quite simple in its nature. Currently, the setup consists of a temperature probe to measure the raw air temperature outside the aircraft as well as pitot pressure ports and static pressure ports which all feed into the ADAHRS.

Propulsion

The propulsion instrumentation is where the instrumentation is at its most complex as the design will have to be modular and flexible in order to be suitable for the multiple engine types that will be tested.

The propulsion monitoring equipment from the panel upgrade consisted of an engine monitor and an engine data converter taking in data from various sensors as can be seen in the red blocks in Figure 9.1. However, these are only applicable to the unchanged engine in the aircraft. Thus in addition to these existing sensors, there will have to be supplementary sensors to monitor the electric engine as well as a modular system to monitor the power supplies depending on if they are simply batteries or hydrogen fuel cells.

A crucial part of the testbed is monitoring the engine's performance. For this, various parameters such as the RPM and power output will need to be known. While for traditional internal combustion engines, engine monitors and their associated instrumentation are readily available with off-the-shelf components, no such equipment exists as of yet for electric engines. Therefore, a custom designed solution will have to be made to monitor the engine parameters.

The power for the engines will be supplied from 2 different types of power supply, including hydrogen fuel cell and electric batteries. Depending on the type of power supply that will be used different parameters will be of interest to monitor performance. These parameters can then be split up into what is required for safety monitoring and parameters that would be nice to know and of much added value knowing the nature of the aircraft is to be a testbed.

Electric engine & batteries: The setup of the electric engine and battery data acquisition system at its core is extremely simple and can be seen in Figure 9.2. The graph is a combination between a hardware/software diagram and a data handling diagram. The hardware/software part is shown by the flow of physical and electric control inputs. The data handling part of the graph shows how and what specific measurements are performed within the system, how and to what type of data these are processed and the eventual resulting data streams. The dashed lines represent essential parameters that should be acquired, while the dotted lines represent parameters that would be beneficial for the analytic nature of the test bed.

The battery data processor will receive data measured by an ammeter, voltmeter and temperature probe, which will eventually be processed to report the depth of discharge, temperature and power, voltage and current output of the batteries. The temperature will displayed to the pilot, allowing him to react by changing the amount of throttle in order to reduce heat production.The power data processor will receive the measured temperature of the entire electrical system as well as the voltage and current from the power converter. Since the temperature of the electrical system is not as critical as the temperature of the batteries and the power output of the power converter is also not likely to be the source of inefficiencies; the power, voltage current and temperature going to the engine monitor display are thus marked as an optional parameters. Finally, the engine data processor will receive the data from an accelerometer and temperature probe. These are then processed to have the RPM, torque and temperature of the engine. The RPM and torque are essential to calculate the performance and efficiency of the motor. The temperature of the motor is necessary not only for the efficiency of the motor but also for the pilot's safety as if it is over temperature the pilot can reduce power to mitigate the risk of an engine failure.

All data will come together and can (if desired) be displayed on the engine monitor display. This will then both be fed back to the pilot and be stored in data storage for post-flight analysis. In accordance with the risk mitigation strategy, non-volatile data storage as well as redundant storage will be utilised to minimise the risk of data loss in flight.

Electric engine & H_2 Fuel cells: The complete system of the hydrogen engine is more complex,

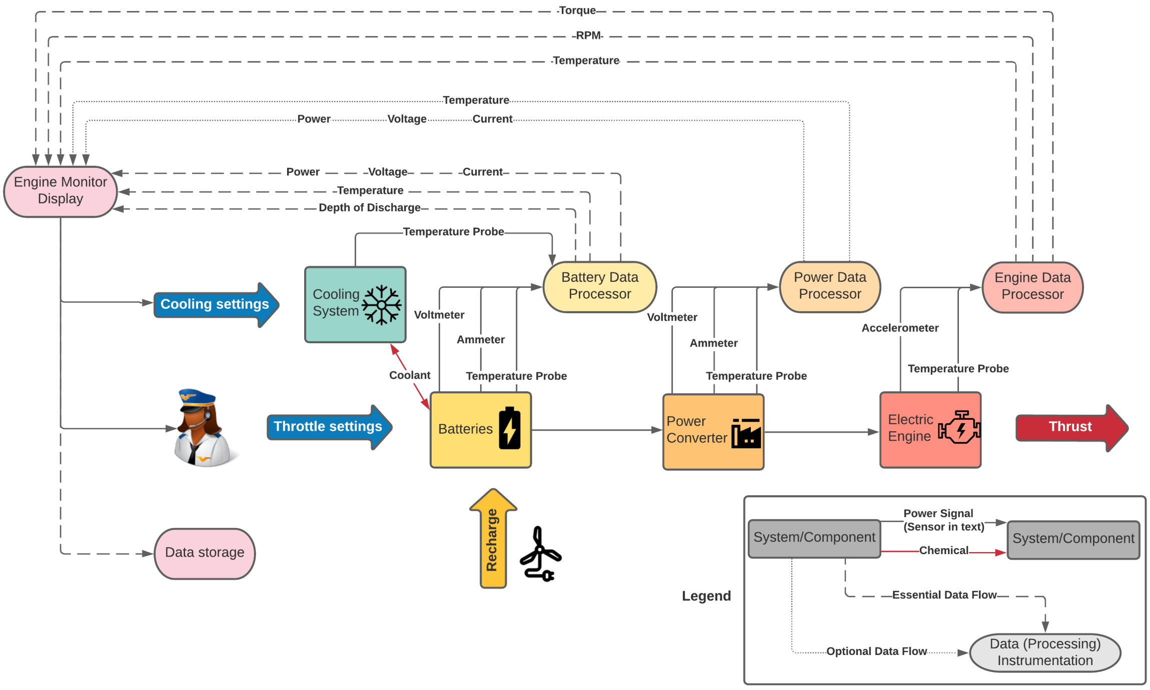

Figure 9.2: Electric engine data acquisition and hardware/software block diagram

although at the basis the same as the electric engine as can be seen from Figure 9.3. To be able to monitor all the relevant parameters, this time the measurement will be fed into a hydrogen data processor, fuel cell processor, added to the power and engine data processor as already seen for the electric engine. The cooling system is a bit more complex, but will still have the same data flow, although now working on both the humidifier and and the fuel cell.

The hydrogen data processor will receiver the conditions in the tank, compressor and humidifier. The pressure and temperature in the tank is measured by means of probes for safety and hydrogen level estimation purposes. The temperature in the fuel tank can also be monitored for performance purposes. The compressor will compress the air that will then enter the humidifier to be combined with the hydrogen. For performance monitoring purposes it can be useful to measure both inflow and outflow pressure and temperature. The humidifier is installed to keep the hydrogen (mixture) at the best operating humidity. For performance monitoring purposes it would therefore be beneficial to measure the humidity of the mixture at both ends of the humidifier by means of a hygrometer as well as the pressure and temperature. The fuel cell (battery), power and engine data processing will be the same as for the electric engine and will monitor the same safety and performance parameters.

In Table 9.1 a summary is given of the different sensors that will be minimally required for the forementioned safety parameter monitoring as well as an estimation of the required power and mass. For the different sensors the operating window is given. Added to this, there will be measurements shown in Figure 9.3 with a dotted line that could potentially be added. For the non essential parameters relevant sensors can partially be expected to be supplied by the client with the respective engine. Nevertheless storage and connectivity should be in place with the engine monitor display as well as the data storage is case it will be supplied. With this the most extreme case of all the parameters shown in the graph should be considered. On top of that there might be sensors related to propeller pitch and/or noise measurement that can be externally installed. These will be externally installed and no specific design considerations need to be internally except the availability of connectivity and data storage.

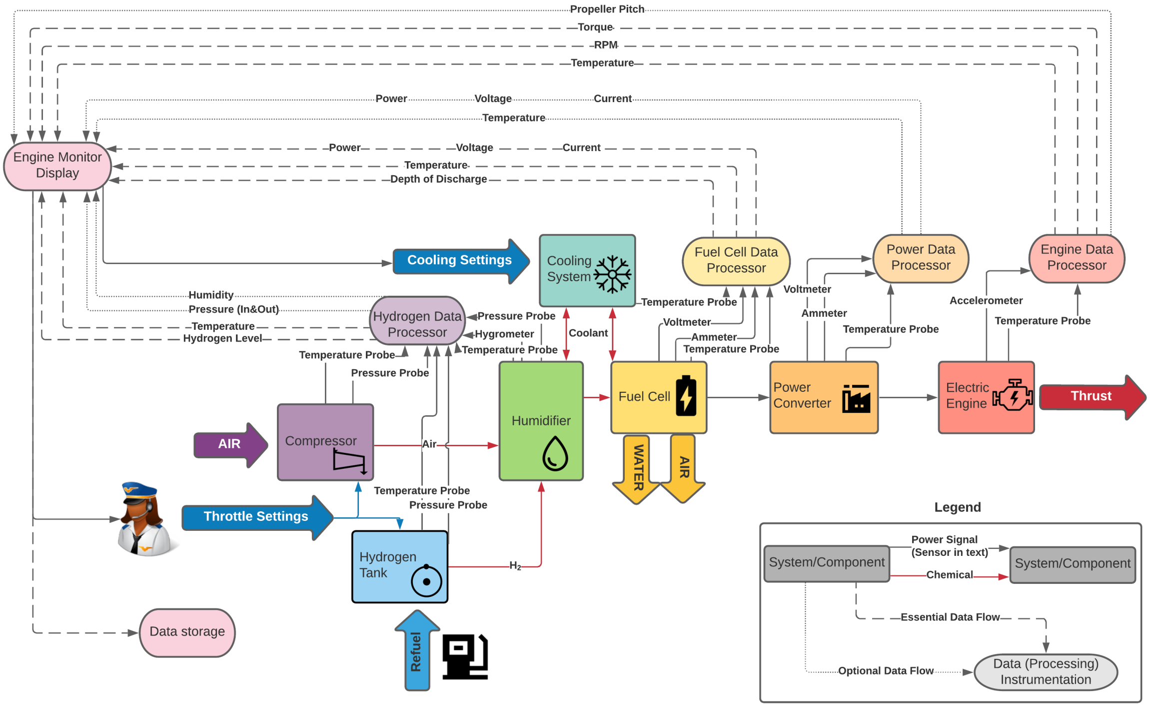

Figure 9.3: Hydrogen fuel cell data acquisition and hardware/software block diagram

Monitoring System	Parameter	Operating Window	Sensor Type
Engine Monitor	RPM Torque Temperature	1900-4500 [RPM] 0-1500 [Nm] 25-120 [° C]	Measured using accelerometer Calculated using RPM measurements Measured using a temperature probe
Battery Monitor	Temperature Voltage Current Depth of Discharge	0-45 [° C] 0-800 [V] 0-1100 [A] 0-100 [%]	Temperature probe Voltmeter Ammeter Calculated with voltage measurements
Fuel Cell Monitor	Temperature Voltage Current Depth of Discharge	60-95 [° C] 0-6 [V] 0-150 [A] -	Temperature probe Voltmeter Ammeter Calculated with Voltage Sensors
Fuel Tank Monitor	Pressure	0-700 [bar]	Pressure probe
Cooling System	*Temperature*	30-100 [° C]	Temperature probe

Table 9.1: Data acquisition design details. The optional parameters to be measured are in italics.

9.3. Experimental Engine Monitor Display

During the literature study phase, the NLR hangar at Rotterdam The Hague airport was visited where a Pipistrel Velis Electro was available to be referenced. From there, it was evident that a further step in the final design had to be taken and the additional engine monitor had to be designed. The additional monitor will be installed on the flight deck taking the place of one of the engine monitors from the panel upgrade in Section 9.1 and Figure 9.1. An off the shelf display can be used in conjunction with the new sensors and software to display the information. The new monitor would have to display critical warnings as well as the necessary information for performance and safety as listed in Table 9.1. A possible design for this display is shown in Figure 9.4 and Figure 9.5.

9.4. Instrumentation Power and Mass Budget

Since the data acquisition instrumentation that will be added to the aircraft do not exist as off-the-shelf components, the power budget cannot be given accurately. However, estimations can be made based

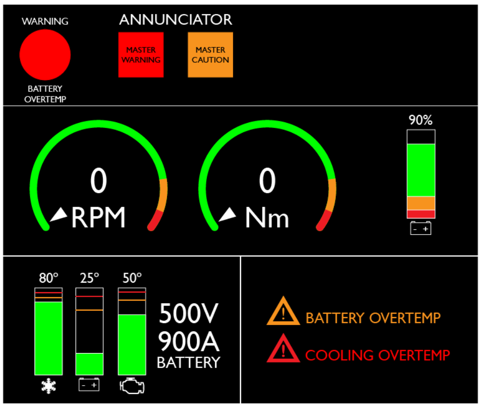

Figure 9.4: The engine monitor display for the engine-battery combination

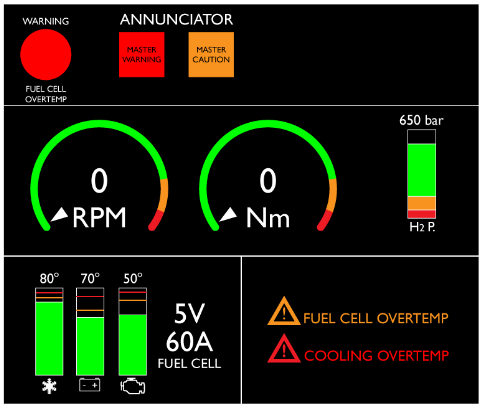

Figure 9.5: The engine monitor display for the engine-hydrogen fuel cell combination

on the power requirements of similar components. Using this estimation method a theoretical maximum power requirement from the instrumentation would be $375W$ easily within the $980W$ available from the alternator. In the same way an estimation can be made for the mass. This has resulted in $11.4kg$, also being far below the allocated $30kg$. For both power and mass this contingency in what was assigned to the data acquisition and what is expected to be used, will allow for extra sensors to be installed depending on the type of engine and the request of the client.

10
Performance Analysis

In this chapter the design tools that have been used in order to estimate the aircraft's performance are detailed. Section 10.1 details the c.g. shift due to modifications and proposes the addition of ballast to the design. An aerodynamic model is described in Section 10.2. This forms the foundation for performance calculations in Section 10.3. Finally, models are verified and validated in Section 10.4 and Section 10.5, respectively.

10.1. Stability and Control

To determine the centre of gravity shift due to all modifications the aircraft is divided into four compartments as shown in Figure 10.1. Components or modifications are mounted at the centre of any one of these compartments, or on one of the bulkheads (orange).

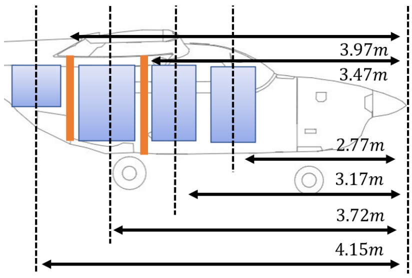

Figure 10.1: C.g. compartments

Table 10.1 first considers the mass and arm of the stripped aircraft according to a recent mass and balance report. Thereafter, the c.g. shift due to each component is considered by using

$$x_{modified} = \frac{m_{old} \cdot x_{old} + m_{new} \cdot x_{new}}{m_{old} + m_{new}} \tag{10.1}$$

The configuration required to support the Emrax 348 is given in Table 10.1. The replaced engine mount is assumed to not have an effect on the c.g., since both engine mounts are located at the same location and are assumed to weigh the same. The original c.g. limits of the aircraft are $3.50\ m - 3.63\ m$ from the nose.

Table 10.1: Modified aircraft mass and balance for Emrax 348 - Battery

Component	Mass [kg]	Arm from nose [m]
Stripped aircraft	1038	3.556
IO-360	-150	4.15
Cable 3	9.22	4.15
Cable 2	4.16	3.72
Cable 1	5.82	3.47
Battery	432	3.72
DCDC Converter	3.32	4.15
Power distribution	3.37	4.15
Inverter	14.51	4.15
Fuel mount	18.6	3.72
FWD firewall	3.6	3.47
Emrax 348	42	4.15
Original fuel	129	3.47
Two people (front)	200	2.77
One passenger (rear)	100	3.17
Modified aircraft	1793.21	3.457752

Table 10.1 shows that with three people (two passengers, one pilot) loaded, for the Emrax 348 configuration the c.g. is outside limits ($3.46\ m, 3.5\ m$). If only one the pilot is seated in the front, then the c.g. is at $3.51\ m$. As fuel is burnt in the wings the $c.g.$ moves aft by a maximum of $0.01\ m$. This means that as long as the pilot weighs less than $100\ kg$ and is the only person in the plane (no cargo), then the aircraft will operating at its FWD c.g. limit for the situation outlined in Table 10.1.

The option exists to add ballast in the tail ($x = 9\ m$). To accommodate two passengers in the front row and one in the back, $15\ kg$ of weight would be needed at $x = 9\ m$. This would bring the c.g. to $3.5\ m$, therefore ideally $40\ kg$ of ballast would be optimal to bring the c.g. to a comfortable $3.57\ m$. These two situations are shown in Figure 10.2. The main reason the modified aircraft is outside the c.g. limits of the original design is due to the fact that the relatively heavy IO-360 is replaced with lighter engines, shifting the c.g. forward significantly.

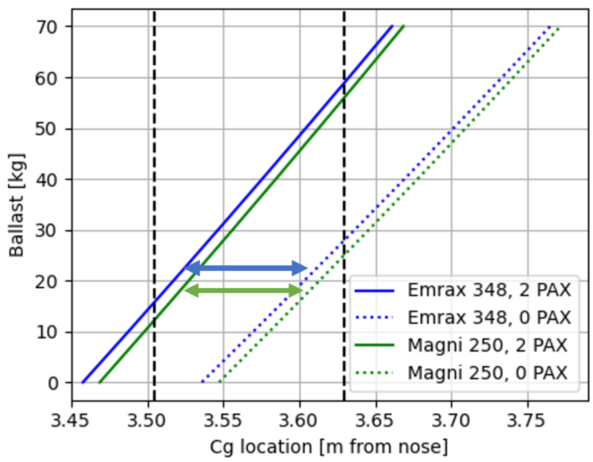

Figure 10.2: Effect of adding ballast

For the Magni250 all weights and arms stay the same, except for the weight of the engine itself which increases to 72. Figure 10.2 shows that for the Magni250, a minimum of $11\ kg$ of ballast would be required with the optimum ballast would being $18\ kg$ (green envelope). For the Emrax 348 a minimum of $16\ kg$ is required with an optimum of $22\ kg$. The maximum ballast for both engines is around $25\ kg$. In this figure the 0 PAX scenario entails that the pilot weighs a minimum of $60 kg$.

The hydrogen system for the Magni250 and Emrax 348 is broken down as in Table 10.2. It shows that c.g. is even more forward than previously, this is due to the fact that the hydrogen fuel cells weigh significantly less than batteries.

Table 10.2: Modified aircraft mass and balance for Emrax 348 - Hydrogen

Component	Mass [kg]	Arm from nose [m]
Stripped aircraft	1038	3.556
IO-360	-150	4.15
Hydrogen tank	17.27	3.72
Fuel cell	84	3.72
Cable 3	9.46	4.15
Cable 2	4.16	3.72
Cable 1	5.82	3.47
Inverter 1	13.07	4.15
Converter 1	3.32	4.15
Compressor	0.57	3.72
Inverter 2	0.16	3.72
Converter 2	0.04	3.72
PDS	4.85	3.72
Two people (front)	200	2.77
One person (rear)	100	
Firewall	3.6	3.47
Emrax 348	42	4.15
Fuel mount	18.6	3.72
Original fuel	129	3.47
Two people (front)	200	2.77
One passenger (rear)	100	3.17
Modified aircraft	1361.91	3.388

Performing the same analysis as for the batteries yields Figure 10.3. In this case more ballast is required ($\approx 28\,kg$), which exceeds the limit for the previous analysis which set $25kg$ as an upper bound. Figure 10.3 also shows that the envelope has now become 'tighter'. This means that the minimum, optimal and maximum ballast for each engine now coincide at $25\,kg$ for the Magni 250 and $30\,kg$ for the Emrax 348.

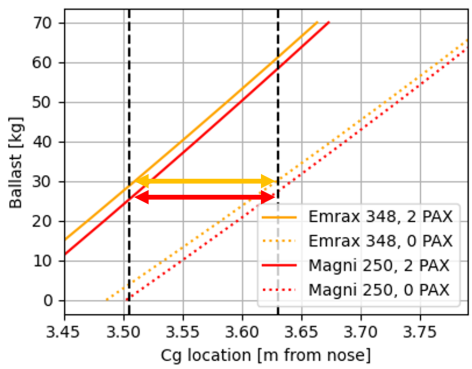

Figure 10.3: Effect of adding ballast (hydrogen)

The previous results are summarised in Table 10.3. It shows the optimal ballast for each propulsion system, *assuming* that the pilot weighs at least $60\,kg$ and the maximum load is two passengers and one pilot who each weigh $100\,kg$, with two people in the front and one in the back. For batteries a ballast of $20\,kg$ would suffice for both engines. For the hydrogen Magni 250, $26\,kg$ would be required and $30\,kg$ for the Emrax 348.

Table 10.3: Summary of weight and balance results

Ballast at $x = 9m$	Minimum [kg]	Maximum [kg]	Optimum [kg]
Emrax 348 Battery	16	29	22
Magni 250 Battery	11	25	18
Emrax 348 Hydrogen	30	30	30
Magni 250 Hydrogen	26	26	26

To stop the need for interchanging ballast what a limit can also be set on pilot weights. Setting the minimum pilot weight to be $70kg$ leads to Figure 10.4. Orange and red indicate hydrogen systems, green and blue traditional electric. It shows that by setting the ballast to $28kg$ all possible propulsion system combinations can be accounted for. In this case the advantage is that the ballast does not have to be interchanged when an engine or fuel cell is swapped, the disadvantage is that ballast may need to be added in the case of a light single pilot. Although, it may be more convenient to add ballast in the front of the aircraft (in the form of cargo in the cabin) than to retrofit ballast in the tailplane.

For a forward c.g. the most limiting case is the Emrax 348 with hydrogen fuel and three people in the cabin, each weighing $100\ kg$. The hydrogen Emrax 348 is the lightest propulsion system, thus when combined with maximum payload in the front it results in the maximum forward c.g (yellow line). This sets a lower limit for the ballast to be at least $28\ kg$. On the other hand, the most limiting aft c.g. case is the Magni250 with batteries and a single $70\ kg$ pilot. This will result in the most aft c.g. since the aircraft is now equipped with the heaviest propulsion system in the rear and the lightest payload in the front. This sets a limit for the ballast to not be larger than $28\ kg$. All other combinations of payload and propulsion system are between these two cases, as shown in Figure 10.4.

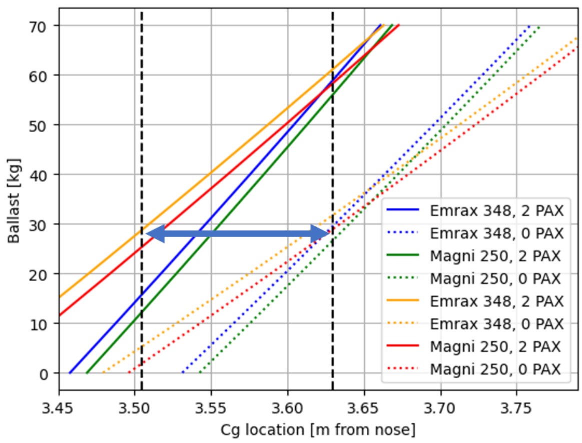

Figure 10.4: C.g. envelope for minimum pilot weight

To summarise, there are two options for weight and balance:

1. A fixed ballast of $28\ kg$ is mounted at $x = 9\ m$. The minimum weight for the pilot is $70\ kg$, the maximum payload is $2 \times 100\ kg$ in the front row and $1 \times 100\ kg$ in the back row.
2. Ballast is changed according to configuration. The minimum weight for the pilot is $60\ kg$, the maximum payload is the same as (1) and ballast must be loaded according to Table 10.3.

10.2. Aerodynamic Model

For the design of the modification to the Skymaster, the external changes that are made of the aircraft are for the hydrogen propulsion system, for a which a cooling system is fitted to the belly of the fuselage. For this, a comparison of the drag polars for the clean configuration and the modified aircraft is shown below.

Drag Polar Estimation

For the clean aircraft, data is extracted from the flight manual including cruise settings at different engine settings and altitudes. In level flight assumption is made that the thrust acts in the flight direction. As the aircraft is in equilibrium, the equation 10.2 holds. The power available is calculated using Equation 10.3.

$$P_a - P_r = 0 \tag{10.2}$$

$$P_a = P_{br_{front}}\eta_{front} + P_{br_{rear}}\eta_{rear} \tag{10.3}$$

$$\tag{10.4}$$

The brake power of the engine is determined by multiplying the $\%BHP$ for each flight condition with the maximum brake power of the engine (210 HP for the Continental IO-360 engines). The propeller efficiency is assumed to be a function of its advance ratio. In the case of a pusher propeller however, the incoming air to the propeller disk is not undisturbed flow and this effect also plays a role. Extrapolated from rule of thumb described in the [13] as a first order estimate the propeller efficiency is expressed by the equation 10.5. In this first order analysis the propeller efficiencies are assumed to be the same for front and rear engine.

$$\eta = -0.75J^2 + 1.5J + 0.15 \tag{10.5}$$

The required power is defined in the equation 10.6 the equilibrium equation is described in the 10.7.

$$P_r = \frac{1}{2}\rho V^3 SC_d \tag{10.6}$$

$$P_{br_{front}}\eta_{front} + P_{br_{rear}}\eta_{rear} = \frac{1}{2}\rho V^3 SC_d \tag{10.7}$$

The drag coefficient is assumed to take the form shown in equation 10.8, where coefficients k_0, k_1 and k_2 are unknowns to be solved.

$$C_D = k_0 + k_1 C_L + k_2 C_L^2 \tag{10.8}$$

Coefficients of the drag polar are estimated using linear regression. The design matrix X takes form described by the equation 10.9

$$X = \begin{bmatrix} \frac{1}{2}\rho_0 V_0^3 S & \frac{1}{2}\rho_0 V_0^3 SC_{l_0} & \frac{1}{2}\rho_0 V_0^3 SC_{l_0}^2 \\ \frac{1}{2}\rho_1 V_1^3 S & \frac{1}{2}\rho_1 V_1^3 SC_{l_1} & \frac{1}{2}\rho_1 V_1^3 SC_{l_1}^2 \\ ... & ... & ... \\ \frac{1}{2}\rho_n V_n^3 S & \frac{1}{2}\rho_n V_n^3 SC_{l_n} & \frac{1}{2}\rho_n V_n^3 SC_{l_n}^2 \end{bmatrix} \tag{10.9}$$

The vector of the observed values y is expressed in the equation 10.10.

$$y = \begin{bmatrix} \eta(P_{br_{front_0}} + P_{br_{rear_0}}) \\ \eta(P_{br_{front_1}} + P_{br_{rear_1}}) \\ ... \\ \eta(P_{br_{front_n}} + P_{br_{rear_n}}) \end{bmatrix} \tag{10.10}$$

With the drag coefficients for the aircraft with both propellers running estimated using the least squares method, further analysis is possible. The drag polar for the Skymaster can be seen in Figure 10.5.

The drag polars of the original aircraft and the modified fuselage for the fuselage are compared. For the modified aircraft (hydrogen system), the original cooling inlet is removed and a belly pod is added housing the radiator, discussed in Section 7.4. The difference between the zero lift drag coefficient (ΔC_{D_0}) is -0.0012 for the two configurations. The slight difference is shown in below in Table 10.4. This indicates that the drag performance is better for the modified aircraft.

Table 10.4: Drag Polar Parameters

	C_{D_0}	k_1	k_2
Original Aircraft	0.024	0.025	0.048
Modified Aircraft	0.023	0.025	0.048

For a visual comparison between the drag polars, a graph of C_L against C_D is plotted for the original aircraft and the aircraft with modifications. This is shown below in Figure 10.5.

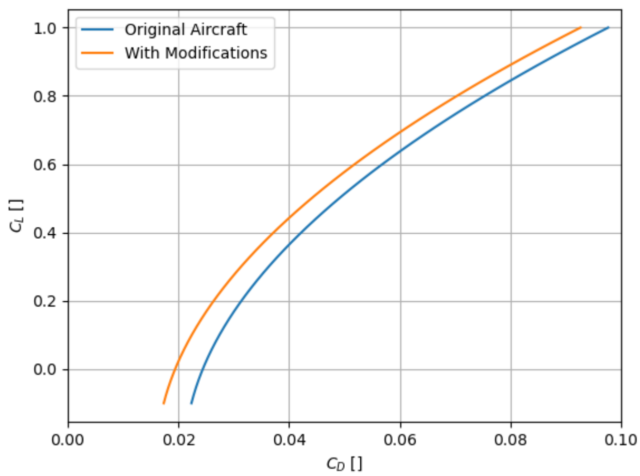

Figure 10.5: Drag polar estimation through cruise data

10.3. Performance Determination

This section will outline the method of developing a performance model of the aircraft and the steps taken to verify and validate the model.

Drag Contributions

With the drag polar of the clean aircraft known the effect of changes to the aircraft configuration on the drag can be estimated. All the considered cases are listed in Table 10.5.

Table 10.5: Drag contributions for considered cases

Case	$\boldsymbol{\Delta CD_0}$	**Remarks and source**
Flaps 1/3	0.0018	[22]
Landing gear deployed	0.0112	[6], -110 FPM reduction
Landing gear + doors during retraction	0.0245	[6], -240 FPM reduction
Feathered propeller	0.0033	[25]
Fuselage drag (rear engine inoperative)	0.0087	[9], -85 FPM reduction
Belly pod	0.0010	[9], -15 FPM reduction, 0.5 m^2 volume
Wing pods	0.0007	[25], 0.5 m^2 volume
Cowl flap fully open (one engine)	0.0034	[43]

For a number of these options there is a known effect on climb rate. In these cases it can be solved for ΔCD_0 using the equation 10.11.

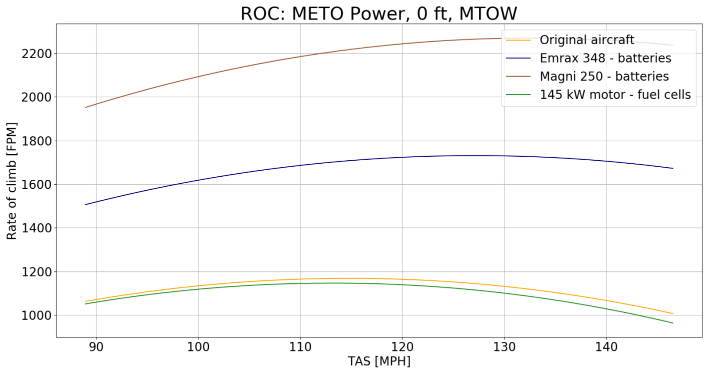

Figure 10.6: Climb rates of experimental engines at MTOW at takeoff power settings

$$\Delta RC = \frac{P_a - P_{r_2}}{W} - \frac{P_a - P_{r_1}}{W} = \frac{P_{r_1} - P_{r_2}}{W} \longrightarrow \Delta CD_0 = \frac{W \Delta RC}{\frac{1}{2}\rho V^3 S} \tag{10.11}$$

If this is not known the contribution to the zero-lift drag is estimated using literature. The drag contribution is assumed to vary linearly with the reference area.

As mentioned in [42] the effect of the rear propeller influences the flow field around the rear of the fuselage and reduces drag. With the rear engine inoperative this advantage disappears.

Another thing to be noted is the cooling drag of the engines. During cruise the cowl flap is assumed to be closed. This is the case for the engine out situations as closing the cowl flap is part of the procedure [9]. If the cowl flaps are open during climb, the reduction in performance may be substantial. For another similar twin engine installation in [43] a change in cooling drag from 7 percent to 13 percent of the total aircraft drag comes when fully opening both cowl flaps. There is a belief that the rear engine with a more complicated internal flow may perform worse in the terms of cooling drag than the front engine. It is however hard to tell to what extent this is.

Rate of Climb Estimation

Equation 10.12 represents the rate of climb calculation as implemented in the model. Figure 10.6 shows the new climb rates expected when installing the two different experimental engines at takeoff settings at MTOW with battery packs installed. When considering the hydrogen fuel cell, the limiting factor of the system will be the power supplied by the fuel cell. Since the hydrogen fuel cell is rated for 145 kW, which is similar to the IO-360 configuration comparable climb rates to the original aircraft will be expected.

$$RC = \frac{P_a - P_r}{W} \tag{10.12}$$

Take-Off Performance

From [22] empirical relations for ground run, rotation distance, transition distance and distance to clear an obstacle after transition were taken. The height of the obstacle is chosen to be $50ft$.

The take-off distance for the Emrax 348 was determined to be 450m. For the Magni 250 analysis yielded 447m. This would allow for the aircraft to take-off comfortably from Teuge airport, where it is currently stationed (hereby adhering to requirements).

10.4. Model Verification

By applying unit tests while writing the code, the time spent finding and fixing bugs, this occurred multiple times as small mistakes where found at the time of writing the code. Overall the experience of creating unit tests at the same time as writing the functions and methods of the model was beneficial as less time is wasted. The coverage report for the applied unit tests of the aerodynamic and performance models indicated a 71% coverage.

10.5. Model Validation

To validate the models presented in this report, the performance data of the original design is used to validate the new designs. Parameters including the climb rate, maximum speed, and take-off distance that are calculated in the performance model are compared with the values stated in the flight manual [9].

Firstly, the rate of climb performance comparison is shown below in Table 10.6. It can be observed that the rate of climbs are similar with only small to moderate difference ($65 ft/min$). The speeds are also validated due to the minimal difference between the model and the flight manual.

Table 10.6: Rate of climb comparison between flight manual and performance model

	Both Engine Operative		**Rear Engine Inoperative**		**Front Engine Inoperative**	
	Climb Rate [ft/min]	IAS [mph]	Climb Rate [ft/min]	IAS [mph]	Climb Rate [ft/min]	IAS [mph]
Flight Manual [9]	1100	114	235	101	320	101
Performance Tool	1165	115	125	89	193	96

Next the take-off distance comparison is shown below in Table 10.7. The values shown are for the performance model and the flight manual. The difference between the two is 35 ft. This is a difference of 2 % which is considered acceptable for validation.

Table 10.7: Take-off distance comparison between flight manual and performance model

	Take-off distance [ft]
Flight manual [9]	1675
Model	1710

11 Design Synthesis

This chapter brings together the modifications by detailing the integrated design and result. Section 11.1 shows the internal configuration of the aircraft. A cost break down is given in Section 11.3. Finally, adherence to requirements is demonstrated in Section 11.4.

11.1. Final Design

Internal Configuration

The internal configuration of the testbed is designed to comply with centre of gravity and volume limitations. The panel upgrade instrumentation as well as the additional engine monitor will replace the existing instrumentation on the flight deck of the aircraft, the new flight deck of the testbed will then be as shown in Figure 11.1 with the blacked out blocks being original instrumentation that does not necessarily need to be replaced.

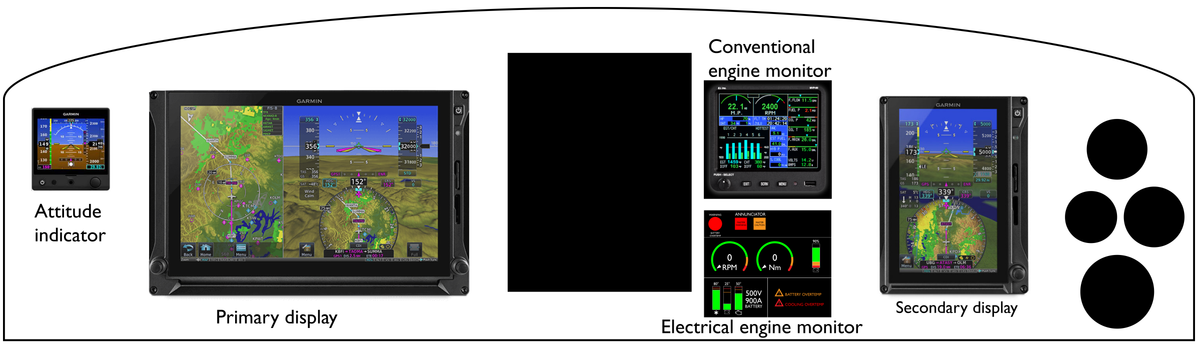

Figure 11.1: The upgraded flight deck containing the new digital instrumentation

As stated in requirement **PED-3**, three of the original six seats will remain in the aircraft cabin. Therefore, the additional data acquisition instrumentation such as the data storage can be installed in the place of the missing seats. Performance sensors such as the engine monitor or battery monitor can be assumed to be negligible in terms of their space requirements. The batteries or fuel cells will be installed behind a secondary fire wall after the second row of seats. The new engine mount truss structure is mounted behind the current fire wall with the radiator mounted above it behind the rear air intake. Taking reference again from the Pipistrel Velis Electro, the inverter and converter will be installed inside the truss structure and the motor at the end of the structure. This design is shown in Figure 11.2 and Figure 11.3 where the orange blocks are components, the blue lines are cooling tubes and the yellow lines are power lines.

Firewall

For safety, it is necessary to isolate the fuel from the rest of the cabin by placing a second firewall between the fuel and the passengers. For this a number of requirements are generated - in line with the driving requirement **CER-1**.

- SAF-FIRE-1 The firewall shall resist a flame of temperature no less than 1093 ± 83°C
- SAF- FIRE - 2 The firewall material and fittings shall resist flame penetration for at least 15 minutes.

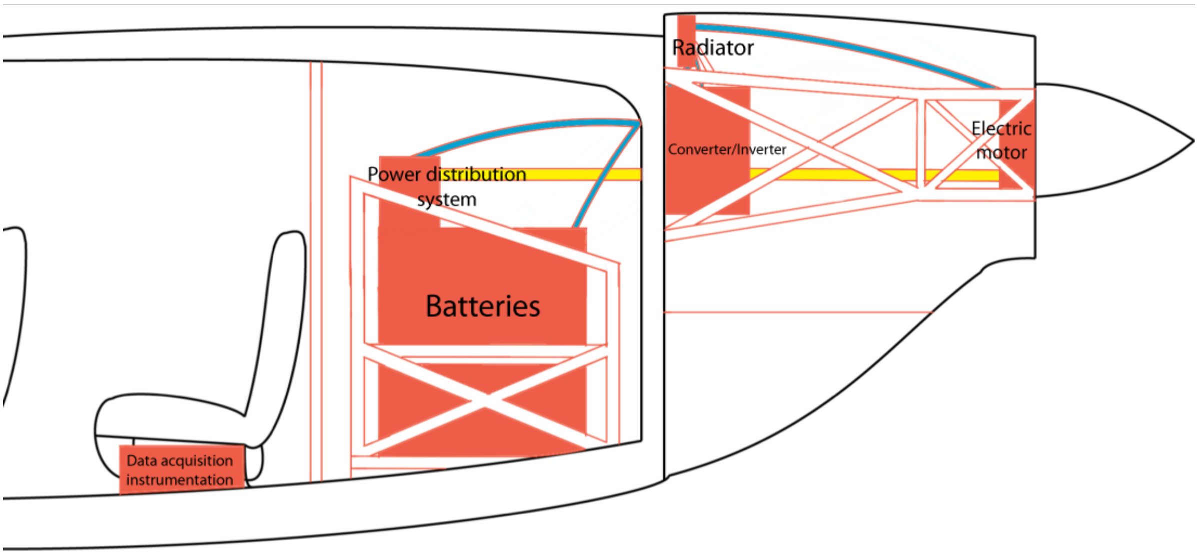

Figure 11.2: A drawing illustrating the internal configuration of the testbed with batteries installed.

- SAF-FIRE-3 The firewall shall be removable to allow for accessibility for interchanging the engine and fuel types.

To meet theses requirements, CS23 lists optional materials and specifies the required thicknesses. These include a stainless steel sheet with 0.38 mm thickness, a mild steel sheet (coated with aluminium or otherwise protected against corrosion) with a 0.45 mm thickness or a titanium sheet with a 0.41 mm thickness. Stainless steel is alloyed with chromium and is therefore more resistant to corrosion than mild steel which is alloyed with carbon. For this reason a mild steel sheet is coated with aluminium which is more expensive.

The fuselage dimensions at the location of the second firewall include a height of 1.33 m and width of 0.94 m, resulting in an area of 1.25 m^3. For a comparison, in Table 11.1, the possible material choices, their thicknesses, mass calculation and estimated costs are included.

Table 11.1: Comparison of materials for firewall

Material	Thickness [mm]	Density [kg/m^3]	Mass [kg]	Cost [€/kg] [1]
Stainless steel	0.38	7,500	3.6	3.74
Mild steel with coating	0.45	7,850	4.4	-
Titanium sheet	0.41	4510	2.3	87

Due to the small variation in mass but large variation in cost, a stainless steel firewall is selected. It is fitted behind the second row of seats and is easily removable to allow for access to the fuel.

11.2. Resource Allocation

In this section the final resource allocation is explained, including the final power, mass and volume budgets. This excludes the cost breakdown structure, which can be found in Section 11.3.

Power Budget

To begin with, for this detailed design two separate power buses were considered. Firstly, the experimental propulsion system is connected to a separate power bus, in line with the risk mitigation strategy introduced in Chapter 6. A detailed analysis of the electrical systems for both battery- and hydrogen-

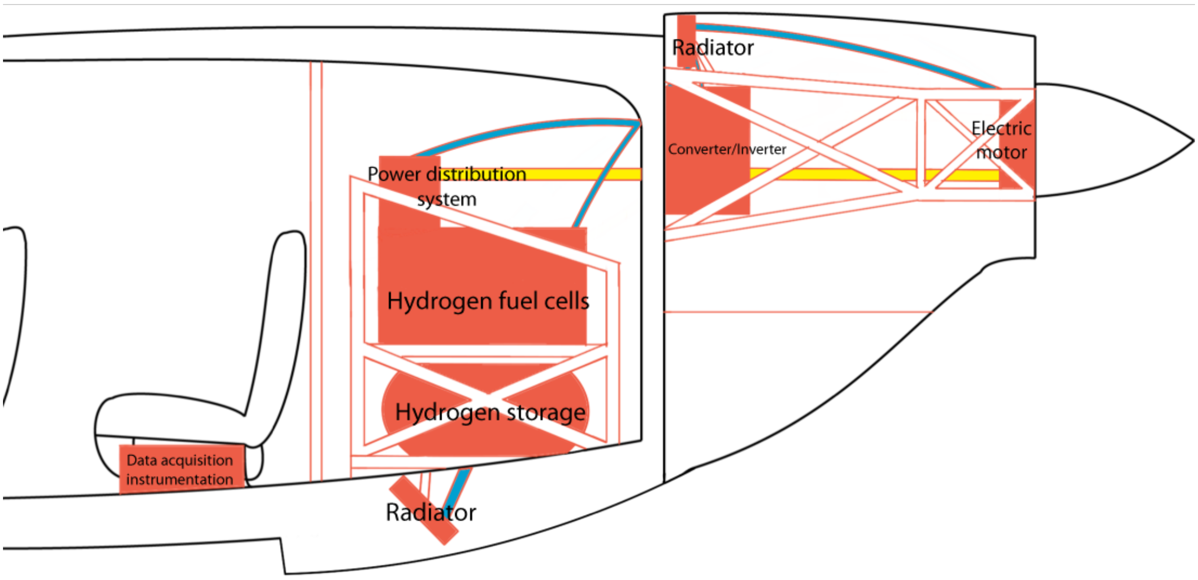

Figure 11.3: A drawing illustrating the internal configuration of the testbed with hydrogen fuel cells installed.

Table 11.2: Power budget

Component	Power required [W]	
	Battery	Hydrogen
Glass cockpit	214	214
Data acquisition	84	84
Fuel management	180	0
Cooling	112	568
Total	590	766

powered systems can be found in Chapter 7. The second power bus is that of the rest of the aircraft. This power is generated by an alternator connected to the front non-experimental engine, the continental IO-360. The power available from this alternator is $28\ V$ at a current of $35\ A$, resulting in $980\ W$ of available power.

This is used to power the glass cockpit, data acquisition, power management system and the cooling system. A breakdown of the required power for these subsystems is included in Table 11.2. For this, peak required power is used. The power required for the glass cockpit was derived by reviewing the data sheets of the included instrumentation. The power required for data acquisition is calculated in Chapter 9. The power required for fuel management is derived by first considering the battery packs. These have an integral battery management system which requires $30\ W$ peak power per battery, using auxiliary power. For six batteries, this results in $180\ W$ total being required. For hydrogen-powered systems, it is assumed that no auxiliary power is necessary for fuel management. Lastly, the power required for cooling is calculated in Section 7.4. This results in $390\ W$ extra power for battery-powered systems and $214\ W$ for hydrogen-powered systems. This could be used to power additional instrumentation or larger/more energy sources. Also, this is more than sufficient to power lights and other electronics in the cabin.

Final Mass Budget

Here an overview is given of the mass budget of the final design, including the propulsion systems, engine and fuel mount, cooling system, and data acquisition system. In Table 11.3 the final mass budget for the battery powered system can be found.

Table 11.3: Final mass budget for the battery powered aircraft

Component	Mass [kg]	
	Emrax 348	Magni250
Stripped aircraft	1038	
Removed IO-360	-150	
Experimental engine	42	71
Propulsion subsystems	49	
Batteries	432	
Engine mount	20.4	
Fuel mount	18.6	
Firewall	3.6	
Data acquisition	11.4	
Pilot + passengers	300	
Original fuel	129	
Total	**1894**	**1923**

In Table 11.4 the final mass budget for the hydrogen fuel cell powered system can be found. For both the heaviest propulsion subsystems, which include for example the inverter or the pds, are used to improve interchangeability. Since, when an inverter can handle the maximum power that will ever go through the system, it is assumed it will be able to handle any power level below that. The same is done for the compressor and its subsystems for the hydrogen fuel cell powered system.

Table 11.4: Final mass budget for the hydrogen fuel cell powered aircraft

Component	Mass [kg]	
	Emrax 348	Magni250
Stripped aircraft	1038	
Removed IO-360	-150	
Experimental engine	42	71
Propulsion subsystems	49	
Fuel cell + hydrogen tank	101.3	
Compressor + subsystems	0.9	
Engine mount	20.4	
Fuel mount	18.6	
Firewall	3.6	
Data acquisition	11.4	
Pilot + passengers	300	
Original fuel	129	
Total	**1564.2**	**1593.2**

Volume Budget

The volume budget was calculated to be 2.5 m^3 this includes the area in the engine bay and the unused space in the fuselage, space left free after three occupants are in the aircraft. After installation of the required power system and engine mounting structure this is met. If additional endurance would be needed, placement of batteries where the auxiliary fuel tanks resided can be done. However this would require different types of batteries from the pipistrel ones since the airfoil dimensions are not sufficient to facilitate the pipistrel batteries.

11.3. Cost break-down structure

For an overview of the costs of realising the proposed modifications a cost breakdown structure is presented in Figure 11.4, where the letter H denotes the hydrogen fuel cell configuration and BE is used for the battery electric configuration. It should be noted that the cost breakdown structure tree only lists the overall costs of the main categories. A more detailed breakdown of the cost is provided in Table 11.5 and Table 11.6. The overall project costs can be divided into two types. Namely, fixed costs and variable costs. The fixed costs are defined as costs that do not variate with a higher or lower usage of the SFPT. On the other hand, variable costs are all costs that change as the SFPT is used more or less. An example of this is the operational cost that will come out higher if more flights are carried out. In the variable cost segment, the engine cost are stated separately as the engine does not have to be switched out every flight, while the other costs are applicable to every flight.

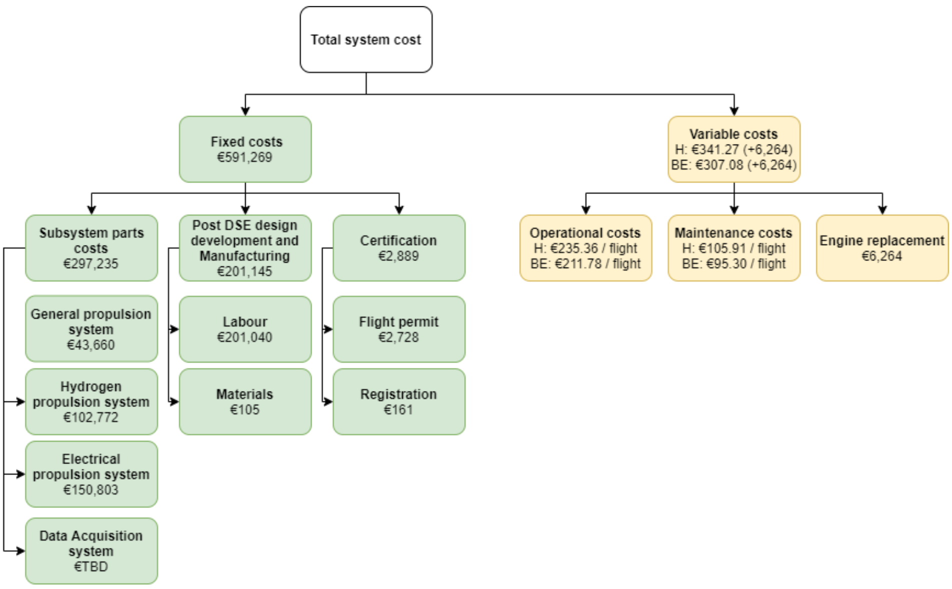

Figure 11.4: Cost break-down structure

Fixed Costs

A breakdown of the fixed costs is given in Table 11.5. The table is divided into the different categories corresponding to the structure shown in Figure 11.4.

The first category is the propulsion system. The specification column gives an overview of the necessary parts to be acquired for the general propulsion system. The first part is the engine. Since two engines are selected as described in Chapter 7, cost estimation is done based on these engines. For the Magni250 no price was found, however, the estimated costs for the Emrax 348 are €12,240. As inverters that can handle 300 kW already exist, a realistic price estimation can be given. Looking at prices of existing inverters of this type, the estimation results in a cost of around €7,900[2].

Unfortunately, no DC-DC converter capable of dealing with $280\ kW$ of power currently exists. Therefore, the estimation of the price is done using a scaling method. Under the assumption that the price of a DC-DC converter varies linearly with the amount of power that it can handle, a price estimate of €23,520 [3] was found.

The second category is the parts that are specifically required for the hydrogen fuel cell configuration. This differs from some of the parts necessary for the all electric propulsion configuration in the fact that the fuel cell and hydrogen fuel tank will be replaced by batteries. The cost of the fuel cell is estimated to be 693 €/kW [4]. As described in Section 7.4 the fuel cell will need to be able to produce a power of $145\ kW$. Therefore, the cost of the fuel cell will be roughly €101,000.

The hydrogen fuel tank need to be capable of storing at least $3.23kg$ of liquid hydrogen. As these types of tanks are usually not bought of the shelf but they are specifically designed for a certain purpose,

[2] https://www.digikey.com/en/products/detail/cree-wolfspeed/CRD300DA12E-XM3/11565363 [Accessed June 2021]

[3] https://nl.rs-online.com/web/p/embedded-switch-mode-power-supplies-smps/8762627/?cm_mmc=NL-PLA-DS3A-_-google-_-CSS_NL_NL_Power_Supplies_%26_Transformers_Whoop-_-(NL:Whoop!)+Embedded+Switch+Mode+Power+Supplies+(SMPS)-_-8762627&matchtype=&pla-478639249835&gclid=Cj0KCQjwlMaGBhD3ARIsAPvWd6gryf7wguaBwGxr_T31hvAYAjmA0sq0cuff1K1LBiDjzidzoP1YSJ4aAu1TEALw_wcB&gclsrc=aw.ds [Accessed June 2021]

[4] http://lma.berkeley.edu/posters/A%20Stack%20Cost%20Comparison%20of%20100%20kW%20Combined%20Heat%20and%20Power%20Fuel%20Cell%20Systems.pdf [Accessed June 2021]

the determination of the cost is done through scaling. The cost of a liquid hydrogen storage system is estimated be 300 €/kg [5]. This results in the cost of the fuel tank amounting to €969.

The main cost driving components for the cooling system are the pumps, the tubing, the expansion tanks and the radiator. For each of the cooling systems two pumps are to be installed for redundancy. At a price estimation of €219 per pump this puts the costs for the pumps at €438 for both systems[6]. The expansion tank has a cost of €45 [7]. The cost of the heat exchanger are estimated using a heat exchanger that has similar dimensions and performance characteristics to the one that is designed for the SFPT. This resulted in a cost of €320 per heat exchanger [8].

The batteries are estimated to cost around €19,000 per battery pack. Since no official prices on the pipistrel battery can be found, this estimation is based on a talk with Fred den Toom who has a lot of experience in aircraft modification and maintenance. For the proposed design a total of six battery packs are necessary. This results in a cost of €114,000. Next to the batteries, expenses also have to be made for the acquisition of a charging station. For the estimated cost of this the pricing of the charging station offered by pipistrel is used, resulting in the price of €36,000 [9].

Providing a cost estimation for the data acquisition components proves to be a bit more difficult as a lot of the components needed for this do not exist yet. The consequence of this is that these monitoring systems still have to be designed for the usage of an battery electric or a hydrogen fuel cell propulsion system in the SFPT. An external research party could design these system as it requires a lot of knowledge on electrical engineering. As no cost estimations for the design of such monitors could be found online, the costs for these components are denoted as TBD.

For the post-DSE activities an estimation could be made using Figure 12.4 in Section 12.3 in which the estimation completely consists of the development time put in post-DSE multiplied by the labour cost per hour to perform the work. From here it can be seen that the post-DSE activities have been split up in four categories of review, certification, modification and training taking up a total of 447 days of which approximately 280 working days. Even though multiple people will be involved with the continuation of the project, for estimation purposes of man hours it can be calculated as per amount of full time working weeks of 40 hours, Depending on the point in the timeline the density of man hours spend on the project will vary, but it is fair to assume an average of two people working on the project full time. With working weeks of 40 hours and on average 228 working days in a year, this adds up to approximately 22,338 hours ($\frac{228}{365} \cdot 447 \cdot 8 \cdot 2$). These hours are covered by employees with different wages including engineers, students and mechanics. Assuming one of the two people working on the project full time will be a student and knowing that mechanics' wages are significantly lower than that of engineers an average wage of €5,000 a month for an engineer will be assumed. Converting to a hourly wage of approximately €90 and having 2234 hours of work, this leads up to a total labour cost of €201,040. This estimate is taking into account contingencies [10], [11].

As the engine mount, the battery mount and the firewall have to produced, a cost estimate on the material is also included. Starting off with the engine mount, for which in total around $20\ kg$ of steel 4130 is needed. The price of steel 4130 is 1.69 €/kg, resulting in a total material cost of €33.80.[12] For the battery mount $6kg$ of steel 4130 is necessary as well as $12.5kg$ of aluminium 6061. With the price of aluminium 6061 being 3.90 €/kg it results in the material cost being €58.89.[13] Finally, for the firewall stainless steel is used which comes in at a price of 3.74 €/kg. This in combination with a necessary amount of 3.6 kg leads to the material costs being €13.47.

The final type of fixed costs that are considered are the one related to the certification of the aircraft.

[5] https://www.utwente.nl/en/tnw/ems/research/ats/chmt/m13-hendrie-derking-cryoworld-chmt-2019.pdf [Accessed June 2021]

[6] https://tecomotive.com/store/en/water-pumps/pierburg-cwa150-water-pump [Accessed June 2021]

[7] https://bearmach.com/product/expansion-tanks-coenenet/expansion-tank-lr024296?glCountry=NL&glCurrency=EUR&gclid=Cj0KCQjw5auGBhDEARIsAFyNm9EhENNQvBHteg-N7aJHGSQ2AwAEJc6eWa1YBZwejskbEi0ykuhtFiYaAs5YEALw_wcB [Accessed June 2021]

[8] https://csfrace.com/csfs-new-high-performance-dual-pass-universal-heat-exchanger/[Accessed June 2021]

[9] https://www.pipistrel-prices.com/configurator/configure/647/[Accessed June 2021]

[10] http://www.salaryexplorer.com/salary-survey.php?loc=152&loctype=1&job=22&jobtype=1 [Accessed June 2021]

[11] http://www.salaryexplorer.com/salary-survey.php?loc=152&loctype=1&job=68&jobtype=3 [Accessed June 2021]

[12] https://www.indiamart.com/proddetail/aisi-4130-tube-12919071830.html [Accessed June 2021]

[13] https://www.indiamart.com/proddetail/aluminium-plate-6061-20351968273.html [Accessed June 2021]

As the aircraft needs to be permitted to fly, getting a permit for this creates additional expenses. The cost of a permit for this is €2,728. Next to that registration of the aircraft adds another €161 to the total expenses[14]. Taking into account all of the aforementioned expenses the total amount of fixed cost is estimated to be €501,269.27.

Table 11.5: Overview of fixed costs

Category	Specification	Estimated cost in €
Propulsion system	Engine	12,240
	Inverter	7,900
	DC-DC converter	23,520
Hydrogen fuel cell specific	Fuel cell	101,000
	Fuel tank	969
	Cooling system	
	Pump x2	438
	Expansion tank	45
	Heat exchanger	320
Electric flight specific	Batteries	114,000
	Charging station	36,000
	Cooling system	
	Pump x2	438
	Expansion tank	45
	Heat exchanger	320
Data acquisition	Engine monitor	TBD
	Battery monitor	TBD
	Fuel cell monitor	TBD
	Fuel tank monitor	TBD
	Cooling system monitor	TBD
Post DSE design development, manufacturing and assembly	Labour hours	201,040
Materials	Engine mount materials	33.80
	Battery mount materials	58
	Firewall	13.47
Certification	Flight permit	2,728
	Registration	161
Total		**501,269.27**

Variable Costs

The variable costs consist of all costs that depend on the amount of times the SFPT is used throughout the course of its lifetime. These variable costs can be split up into two types. Namely, the maintenance costs and the operational cost.

For the operational costs, the cost of carrying out one test flight is considered. The mission profile for a test flight used for the estimation of the cost is defined as the complete flight procedure from take-off until landing including taxi.

The first and most obvious part of the operational costs are the expenses made for the fuel. This, of course, is configuration specific in the sense that cryogenic hydrogen is needed for the fuel cell configuration where electric energy is needed for the electric one.

The cost of liquid hydrogen is estimated to be around €$12/kg$ [15]. As one flight requires 3.23 €/kg of liquid hydrogen this results in a cost of €38.76 per flight.

For the cost of electric energy it is assumed that the batteries are fully charged at the start of the flight. Since each battery pack has a capacity of $11\ kWh$ the total capacity of the batteries will be $66\ kWh$. As the average price per kWh is €0.23 this amounts to a total of €15.18 per flight [16].

[14] https://wetten.overheid.nl/BWBR0023145/2021-01-01[Accessed June 2021]
[15] https://waterstof-info.nl/waterstof-auto/ [Accessed June 2021]
[16] https://pure-energie.nl/kennisbank/wat-kost-1kwh-stroom/?gclid=CjwKCAjw8cCGBhB6EiwAgORey3J0gF67oxBwzLUh5LxKSL8dAvv_1kuvWCqZxmhJsxeVk_XcRYPAfRoCq2IQAvD_BwE [Accessed June 2021]

Next to the fuel, there is also the cost of hiring a test pilot. It was found that the salary of an engineering test pilot in Amsterdam is about 28 €/hour. Assuming that the whole flight profile from start to end will take up around three hours this would results in a cost of €84. However, since this is the salary of a test pilot and not what the employer pays, a conservative safety factor of two is taken resulting in the total costs for the test pilot being €168 per flight.

The next operational cost factor to be considered are the landing costs for airfield Teuge. According to the website of international airport Teuge the landing costs for an aircraft with a MTOW below $1.500\ kg$ is €22.25. However, an additional €6.35 is added to this due to the sound of the Cessna Skymaster peaking above 80 dB. In total this amounts to the landing costs being €28.60 per flight. It should be noted that this is for flights that are during the day when it is not necessary to make use of the runway lighting.[17].

The maintenance cost were estimated to be between 10 and 45% of the operational cost [18]. Since the cost of maintenance are still very uncertain for the SFPT the upper bound of the maintenance cost is chosen, resulting in a cost of €105.91 and €95.30 for the hydrogen fuel cell and battery electric configurations respectively. The total cost of a flight then amount to €341.27 for a hydrogen powered flight and €307.08 for an electrically powered flight.

Now finally, switching out the propulsion system to be tested also introduces labour hours for the mechanics. The amount of hours necessary for this are estimated to be 160 hours. This is also based on a talk with Fred den Toom. For a standard engine change, it would take two people to work on it for one week (roughly 80 hours). However, since this is for experimental propulsion, it usually takes longer and a safety factor of two is applied. Hence, resulting in 160 labour hours. Taking the average wage for an aircraft mechanic to be 27 [19] €/hour this results in the engine replacement costs being €4320. As an engine change is not necessary for every single flight the cost of this is not included in the total flight cost but considered seperately.

Table 11.6: Overview of variable costs

Category	Specification	Estimated cost per flight in €
Operations	3.23 [kg] Cryogenic hydrogen	38.76
	66 [kWh] of electric energy	15.18
	Test pilot	168
	Landing costs	28.60
Maintenance	Hydrogen fuel cell configuration	105.91
	Battery electric configuration	95.30
Total flight cost	**Hydrogen fuel cell configuration**	**341.27**
	Battery electric configuration	**307.08**
Added cost for engine replacement	Labour cost	4,320
	Addition to cost of maintenance	1,944

11.4. Compliance matrix

In this section a compliance matrix is set up to verify the design adheres to its goals. Driving requirements are given in grey. If applicable, a value is given which shows the modified design's capability (e.g. a requirement for climb at 4m/s: the design is capable of 5m/s).

Requirements that cannot yet be checked or verified are omitted, for example MKT-PROP-2 states "The experimental propulsion system shall be able to be interchanged within 10 working days". Although interchangeability has been kept in mind throughout the design process, this specific requirement can only be verified through demonstrated once the design is complete.

Table 11.7 shows compliance to the "preserve existing design requirements". Since the existing fuel tanks are not modified, PED-1 is adhered to. The most important results of design compliance are that

[17] http://teuge-airport.nl/wp-content/uploads/2019/07/Havengelden-per-1-januari-2019.pdf [Accessed June 2021]

[18] https://www.aviationpros.com/aircraft/maintenance-providers/mro/article/10387195/aircraft-maintenance-costs-significant-but-tricky [Accessed June 2021]

[19] http://www.salaryexplorer.com/salary-survey.php?loc=152&loctype=1&job=68&jobtype=3 [Accessed June 2021]

the mass is within limits, that the front firewall was placed to seat three people, and that the c.g. is within limits through ballast.

Table 11.7: Preserve existing design requirements

Requirement ID	Requirement	✓	Value
PED-1	The existing fuel tanks shall not be reduced in size so that their capacity is less than 46 US gallons.	✓	46 USG
PED-2	The design shall respect existing mass and balance limitations.	✓	
PED-2.1	The take-off weight shall not exceed the MTOW of 2100 kg.	✓	$1923\ kg$
PED-2.2	The CG shall be within $3.50\ m - 3.63\ m$ from the nose.	✓	$28\ kg$ Ballast
PED-3	The design shall seat three people including the pilot.	✓	
PED-4	The data acquisition system shall not interfere with existing systems.	✓	

Table 11.8 shows that the aircraft meets performance requirements. For performance the aircraft was required to operate for one hour at an altitude of 5000ft. Estimates showed that the design is capable of flying for one hour and three minutes. This shows compliance to the requirement, albeit with little margin for error. A conscious effort was made to not over-design the aircraft (i.e. cruise for 1:30) as the extra fuel would have a dramatic effect on mass and volume budgets.

Furthermore, other driving requirements state that the aircraft must climb at a minimum $700 ft/min$ for obstacle clearance. In the worst case scenario (limiting part of engine envelope) the design is able to climb at $850 ft/min$. For the single front engine operative case the aircraft is required to to climb at a rate of 200ft/min to compensate for downdrafts. Analysis showed that the design is capable of achieving $350 ft/min$.

Table 11.8: Performance and propulsion system requirements

Requirement ID	Requirement	✓	Value
PROP-PERF-2.1	The experimental engine shall operate for one hour at an altitude of $5000\ ft$.	✓	1:03 hours
PROP-PERF-2.2	The aircraft shall be able to depart at MTOW with three POB.	✓	
PROP-PERF-2.2.1	The aircraft shall take off in a distance of $1199m$ at MTOW.	✓	447m
PROP-PERF-2.2.2	The aircraft shall, with all engines operative, be able to climb at a rate of $700\ ft/min$ at ISA/MSL.	✓	$850\ ft/min$
PROP-PERF-2.2.3	The aircraft shall, with single front engine operative, be able to climb at a rate of $200\ ft/min$ at ISA/MSL.	✓	$350\ ft/min$
PROP-PERF-3	The aircraft shall, with all engines operative, maintain a climb gradient of 5.0 percent.	✓	

Although Table 11.9 does not contain any driving requirements, the most important considering for data acquisition during the design process was the amount of power it required. It was found that the propulsion system is capable of supply the necessary power to the data acquisition system, namely 300W.

Table 11.9: Data acquisition requirements

Requirement ID	Requirement	✓	Value
DA	The aircraft shall have a data acquisition system.	✓	
DA-M-1.1	The sensors shall record all relevant flight performance parameters (as shown in the RDT, [1]).	✓	
DA-M-1.2	The sensors shall record engine parameters.	✓	
DA-M-1.3	The sensors shall record control parameters.	✓	
DA-M-2	The sensors shall be able to output data to the data collection system.	✓	
DA-S-1	The data collection system shall be able to store data throughout one flight.	✓	

Table 11.10 shows compliance to safety requirements. As the aircraft weight is below the original MTOW and the original front engine is unmodified, failure of the existing engine falls under certification of the existing aircraft. These requirements drove the design of mounts and the placement of an additional firewall in the fuselage.

Table 11.10: Safety and certification requirements

Requirement ID	Requirement	✓	Value
SAF-ENG-1	The design shall be able to tolerate failure of the existing engine.[20]	✓	
SAF-ENG-1.1	The non-experimental engine failure shall not cause an unsafe condition in accordance with EASA requirements.	✓	
SAF-ENG-2	The design shall be able to tolerate failure of the experimental engine.	✓	
SAF-ENG-2.1	The experimental engine failure shall not cause an unsafe condition in accordance with EASA requirements.	✓	
SAF-ENG-2.2	The design shall be able to cruise at 5000ft at max gross weight, ISA and experimental engine inoperative.	✓	
SAF-ENG-2.2.3	The design shall be controllable in accordance with CS23 with experimental engine being inoperative.	✓	C.g. limits
SAF-CRASH	The modifications shall be crash-worthy (for further breakdown EASA certification requirements are consulted).	✓	19g forward

Table 11.11 shows adherence to the market analysis requirements. The budget for the modifications and interchanging the engines, is to be determined by the research institution funding the project. In this case, this would be DEAC. However, as no budget was provided, it is not yet clear whether or not the requirements on costs are met. Therefore, the corresponding requirements are not ticked of. Furthermore, the two types of fuel are hydrogen and electric. The aircraft is capable of having external measuring equipment installed like noise estimation tools. The data acquisition system is capable of supporting and processing additional data acquisition.

[20] Although requirements SAF-ENG-1 and SAF-ENG-1.1 are already covered by the existing certification of the aircraft they are still included as modifications to the aircraft might have an effect on performance with respect to this requirement.

Table 11.11: Market analysis requirements

Requirement ID	Requirement	✓	Value
MKT-COST-1	Permanent modifications to the aircraft shall cost no more than [TBD] EUR.		€501,269.27
MKT-COST-2	Interchanging experimental propulsion system shall cost no more than [TBD] EUR.		€6,264
MKT-PROP-1	Fuel storage and distribution capabilities shall be provided for both battery- and hydrogen-powered systems.	✓	
MKT-PROP-2	The experimental propulsion system shall be able to be interchanged within 10 working days.	✓	
MKT-PROP-3	The aircraft shall be able to perform nominal flight missions within a determined envelope of engine power and mass[1].	✓	$P_{available} > 145kW$ & $m_{aircraft} < 21$
MKT-PROP-4	The aircraft shall be able to house the experimental propulsion system without damaging it under the loads specified in the flight envelope.	✓	
MKT-PROP-5	The aircraft shall provide mounting availability for external data acquisition systems	✓	

Figure 8.10 shows compliance to the specific requirements for the engine mount.

Table 11.12: Engine mount requirements

Requirement ID	Requirement	✓	Value
STRUC-MOUNT-1	The engine mount shall use the same four installation nodes as for the mounts of the Continental IO-360 engine.	✓	
STRUC-MOUNT-2	The engine mount shall be constructed from readily available materials for aircraft structures.	✓	Steel 4130
STRUC-MOUNT-4	The engine mount shall be able to sustain load cases according to CS-23.	✓	
STRUC-MOUNT-5	The engine mount shall isolate vibrations with a maximum frequency of 50Hz.	✓	>50Hz

The most important requirement in Table 11.13 is RISK-TECH-3. This drove the design of a cooling system as detailed in Chapter 7.

Table 11.13: Requirements stemming from risk

Requirement ID	Requirement	✓	Value
RISK-TECH-1	A ground test regime shall be used to verify the engine integration.	✓	
RISK-TECH-3	The fuel cells shall be cooled to prevent overheating.	✓	

Finally, Table 11.14 shows compliance to the fuel mount requirements. To prevent injury to the pilot, compliance to requirement FUEL-MNT-4 is crucial and led to an analysis of the connection between the fuel mount and the fuselage.

Table 11.14: Fuel mount requirements

Code	Requirement	✓	Value
FUEL-MNT-1	The structural mount shall weigh no more than 30kg.	✓	18.6kg
FUEL-MNT-2	The structural mount shall introduce loads into the existing structure in a way that maintains its integrity.	✓	
FUEL-MNT-3	The structural mount shall accommodate connections between the engine and fuel cells such as cabling or fuel lines.	✓	
FUEL-MNT-4	The structural mount shall prevent the fuel from moving around in the cabin.	✓	19g

Part III

Future Development

12 Future Project Development

In this chapter, the manufacturing, assembly and integration of the testbed components are described in Section 12.1, the operations and logistics concept description is detailed in Section 12.2. Finally, the future project design and development logic is shown in Section 12.3.

12.1. Manufacturing, Assembly, Integration (Production and Maintenance Plan)

Once the testing & certification phase has started, with the design then being frozen and a flight manual being produced, the implementation of the modifications can be commenced. A Production Flow Diagram has been created as is found in Figure 12.1. This graph was produced as part of the lean manufacturing design philosophy. By adhering to this flow of procedure, waste of time, materials and money can be minimised and therefore sustainability of the entire project optimised.

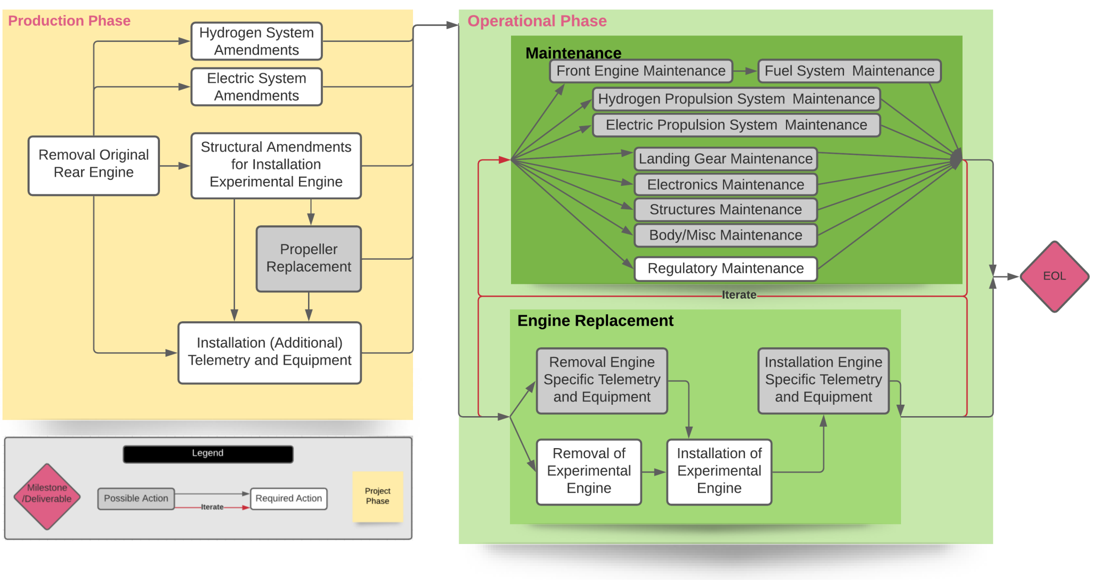

Figure 12.1: Production and Operational Flow Diagram

Production Phase

As can be seen from Figure 12.1, the different steps of the assembly of the new parts of the aircraft are interrelated. Nevertheless, many actions can be performed in parallel as they involve different parts of the aircraft. As a starting point, first the original engine needs to be removed. After this the required actions for assembly can be split into fuel systems replacement, structural modifications for the experimental engine, telemetry and equipment installation and the possible installation of new propellers. All of these actions can either be completed independent after the original engine has been removed or part of the work can be started simultaneously. The adjustments required for the engine fuel system can then be performed for both electrical and hydrogen fuel cell propulsion, for which the specific parts of the production process will be discussed in Section 8.1. Simultaneously, structural changes are then made to the aircraft, enabling the attachment of alternative propulsion systems as will be discussed in Section 8.1. The new propulsion system is integrated in the aircraft together with the necessary instrumentation equipment for data collection of this engine specifically and will be interchanged during the operational phase, as further discussed in Figure 12.1. For the rest of the aircraft, part of this installation may already be installed with regards to the front engine while other modifications are being performed. More changes to the telemetry and equipment can only be done once all other changes have been made.

Some of the aforementioned processes will require the installation of one or multiple off-the-shelf products while others will require the production of new parts. In comparison to commercial aircraft, the Skymaster Flying Propulsion Testbed (SFPT) has a short and specific manufacturing process with parts that will not be produced in bulk. As there will be minimal profit in purchasing new machinery, collaborations with (several different) manufacturing companies is beneficial. The direct collaboration of DEAC with Aircraft Maintenance Netherlands and Hangar One contributes to having the majority being supplied in a close and short supply chain. Where these two partners will not have the relevant equipment or materials, contractors can be attracted for the supply of these parts and/or materials. In line with the sustainability approach, an effort should always be made to try to resource these parts and materials as local as possible and from organisations that are known to apply lean and sustainable manufacturing.

In Section 11.3 a detailed estimation was given for the manhours and cost involved with the post-DSE activities. From this 22338 manhours were allocated to performing the modifications adding up to €201,040 euros. Next to the the material costs are estimated to be €105.27.

Engine and Fuel Mount

The engine mount, including the permanent structure and the specific sub-structure per engine, is expected to be manufactured, assembled and integrated into the Skymaster at DEAC. Advice on these procedures is detailed in the following section. The fuel mount and firewall production is also discussed.

Manufacturing - The engine mount uses the material chromoly steel (4130) for the tubes which may be welded together using either Tungsten Inert Gas (TIG) or Metal Inert Gas (MIG) (also known as 'wire' welding) processes. TIG welding uses a tungsten electrode which has a very high melting point of 3,422°. [1] During the welding process, the electrode heats up but does not melt which is known as non-consumable welding. TIG welding melts the steel of the elements to be joined. During TIG welding, it is optional to use a filler material. MIG welding uses a filler metal to join the base metal (steel 4130). The filler metal is the wire electrode and is consumed during the welding process as it is added to the base metal. For the engine mount of the SFPT, it is advised to use TIG welding as it produces higher quality welds. It is also in-line with the sustainability objective, due to it's non-consumable filament and lower production of smoke or fumes. Note that it is crucial the steel is must first be cleaned to ensure that any contaminants (including paint, oils and rust) do not mix in the join during the welding process.

The manufacturing of the fuel mount structure is very similar to that of the engine mount with the addition of the plates that are included to support the fuel. In addition, the firewall must be manufactured to fit the dimensions stated in Figure 11.1.

Assembly - The engine mount is assembled in four parts. The first part is the permanent engine mount, attached to the firewall frame. Secondly, rubber bushings are used for damping of the engine. Next, the substructure is added, this is specific to the engine being tested and is bolted to the permanent structure. Lastly, the engine itself is fitted to the sub-structure.

The fuel mount is assembled in 3 parts; the truss structure must be welded together and then the plates are added.

Integration - The permanent engine mount is installed in the aircraft by bolting it directly to the rear firewall frame using M10 bolts. For this, the same mounting hard points as for the unmodified aircraft are used. The mount must first be aligned with the mounting points and then bolted through the cabin

[1] `https://www.wolfmet.com/tungstenalloys/#:~:text=These20metals20have20similar20physical,melting20point20of20any20metal.` [Accessed June 2021]

side. It must be ensured that the bolt has sufficient clearance so that unnecessary stress concentrations do not form. In the case that the clearance is not sufficient, it is a possibility to grind the head of the bolt to fit, although this may also weaken the material. It is important that for grinding, the bolt is taken into an area away from aircraft as the grinding process emits hot steel particles that stick to aluminium. As well as metal contamination, the steel particles may rust holes into the aluminium. Once the bolt is through the firewall and mount, a washer and nut is tightened evenly over each bolt thread to secure the mount.

The fuel mount is riveted to the fuselage and three rows of fasteners are used to secure to each keel beam. For safety, it is required that an additional firewall is integrated into the fuselage, this is detailed in Figure 11.1.

Propulsion System
For the propulsion system, the system can be split into 3 categories; combustion, hydrogen and electric propulsion. For each system, the production approach varies. The combustion engine system will stay relatively unmodified with the exception of the removal of half the fuel.

Electric
The electric propulsion system consists of the battery packs, an inverter, a DC-DC converter, a power distribution system, the electric motor, a cooling system, and several cables. Where possible, off-the-shelf products are bought and integrated. However, not all products are readily available with the requested properties, especially since far higher power transmission capabilities are necessary in this system compared to existing electrical systems in aviation. Therefore, some components need to be manufactured at DEAC or custom-made by external parties.

Manufacturing - The battery packs are acquired directly from Pipistrel. In particular, six PB345V124E-L battery packs are acquired, as well as a portable charging station. In continuation, the inverter, converter and power distribution system must be manufactured. For the battery-powered system, the inverter and converter must be capable of transmitting a minimum of $271\ kW$ of power and the distribution system $280\ kW$ of power. For the hydrogen-powered system, the inverter and converter must be capable of transmitting a minimum of $245\ kW$ of power and the distribution system $250\ kW$ of power. These components do not exist as off-the-shelf products, but can be ordered from electrical engineering companies for aviation. This is likely preferable over manufacturing at DEAC when considering certification and the high degree of expertise required to make a reliable electrical system. The cables must also be custom ordered and be capable of handling the currents and voltages as outlined in Figure 7.2 and Figure 7.3. Special care should be taken to ensure that the cables and subsystem connections are compatible. Furthermore, the electric motors must be acquired. The two engines for which a detailed design is made in this report are the Emrax 348 and the Magni250.

Assembly - It is recommended to assemble the entire electrical propulsion unit (all subsystems listed above) outside of the aircraft to verify that all subsystems and cables are compatible. Other than this, no assembly is required before integration into the aircraft.

Integration - Begin by fastening the inverter and DC-DC converter to the rear firewall or the engine mount. Then, attach the electric motor to the engine mount. When connecting the Emrax 348 use at least six M8 bolts to connect the back side to the mount [33]. Once this is firmly connected, the front side of the motor can be attached to the governor using six M10 bolts [33]. For the Magni250 mounting points are also available, although exact specification on this is not disclosed online [31]. In continuation, connect the power distribution system to the starboard side of the fuselage between the new firewall and the rear firewall. Furthermore, the structural tray and battery packs must be installed. First, connect the tray to the to the keel beams of the aircraft by bolting. Once this is secure, connect the six PB345V124E-L battery packs to the tray using the mounting points. Lastly, the cables should be connected and fastened. Once all manufacturing is complete, the new firewall can also be integrated into the aircraft.

Hydrogen
The hydrogen propulsion system consists of a tank, compressor and its subsystems, and a fuel cell

Manufacturing - Most of the aforementioned parts will be off-the-shelf products that will only need assembling and installing. For example two PowerCellution P-Stack fuel cells will be used. The storage tank however will need to be specifically made to fit into the fuel mount design. The cables, the main inverter and DC-DC converter, the power distribution system and the electric motors will be re-used from the electric propulsion system.

Assembly - The hydrogen propulsion system is assembled from three main parts, being the tank, compressor and fuel cell. Other than to check for compatibility, no assembly is required before integration into the aircraft.

Integration - To integrate the fuel cell propulsion system into the aircraft, the following connections should be made. From the fuel cell cell a connection is made to the power distribution system, and from there to the main inverter and DC-DC converter, and the compressor subsystem including a small inverter and DC-DC converter. From the main inverter it than is connected to the electric motors. The cooling system of the fuel cell is connected to the radiator on the belly of the aircraft to cool the cooling fluid. The hydrogen tank is connected to the fuel cell to provide hydrogen. For the electric motors mounting points are available on the engine mount. The tank and fuel cells are integrated onto the fuel mount. The power distribution system is attached to the sidewall of the aircraft, whereas the main inverter and DC-DC converter are attached to the aft firewall.

Cooling
The cooling system consists of heat exchangers, air ducts, internal tubing, pumps and a coolant tank.

Manufacturing - The heat exchangers can be obtained from one of the many companies that produce them for the automotive industry. For the air ducts and inlets both aerospace composite materials and aluminium offer very interesting options and the material choice will likely partially drive the design itself. Such a part can be produced by most of the companies that build light aircraft structures. Now the internal tubing, pumps and coolant tank are all components that can be bought ”off the shelf” and therefore do not have to be manufactured.

Assembly - The assembly of the cooling system is a matter of connecting all components that have to be cooled to the system through the use of tubes. The coolant is then connected to the designed heat exchangers. As discussed in Section 7.4, the battery electric system is to be connected to the heat exchanger in the air duct at the back of the plane and the hydrogen system is to be connected to the auxiliary heat exchanger at the location of the belly pod. Since the fuel cell cooling system is detachable the process of mounting it on the fuselage may happen multiple times during the lifespan of SFPT.

Integration - To make space for the permanent part of the cooling system the original rear engine cooling system has to be removed. Afterwards the new cooling system can be installed. For the installation of the detachable cooling system part, the mounts for the cargo belly pod are used. If these are not present on the aircraft already, they should be installed.

Data Acquisition
For the data acquisition, many individual off-the-shelf products will be assembled together to build a remote data acquisition system.

Manufacturing - For the data acquisition, all sensors and parts will have to be bought individually. No data acquisition parts are expected to be made for this application specifically and the final assembly is expected to be consisting of already existing parts. This includes all the sensors and equipment as discussed in Chapter 9.

Assembly - For the assembly of the entire system, it is advised to consult an electronics expert. Together, the correct power and voltage certified cabling, connections and converters can be installed. As the data acquisition is involved with all the different individual parts of the (propulsion) system, but not always (inter)dependent, installation of the different data acquisition parts and assemblies can be applied on a component to component basis as can also be seen from Figure 12.1. Depending on the specific part we are looking at this can be done with the part off the aircraft (by the costumer) or on the aircraft.

Integration - Finally, once all the individual sensors and equipment has been installed it can be integrated and connected to the engine display and data storage system. With this the data of the already electronically working system can be displayed and used during and after flight.

Operational Phase

For the operational phase, as seen in Figure 12.1, work performed on the aircraft can be split into maintenance and engine replacement. Both processes are iterative and will be performed multiple times over the operational life-cycle. It should be noted that next to the required regulatory maintenance, additional maintenance can be performed favouring the durability of the aircraft.

Maintenance

The maintenance of different part will be different in their cost and time intensity as well as the frequency of maintenance that is required. The different sorts of maintenance can be split into:

1. Regulatory Maintenance - This is the periodic maintenance that is minimally required to be performed in order to be able to keep a flight permit. This type of service should be performed according to the standards of EASA.
2. Propulsion System Maintenance - This involves the maintenance of the original front engine. The maintenance of the engine itself is often done together with that of the fuel lines and/or fuel tank. For this maintenance group the fuel tank should be cleaned, fuel lines should be checked to be safely secured and free of leaks and spark plugs and fairings should be removed and cleaned. The cooling system should also be checked and refrigerant replaced.
3. Hydrogen Propulsion System Maintenance - As for the original propulsion system the hydrogen propulsion system should be checked. This includes the cleaning of the tank, fuel lines, maintenance of the humidifier and mechanics of the compressor. The fuel cell allows and requires little maintenance apart from checking and cleaning plugs and connections. Depending on when the last original engine service has been performed, the cooling system should also be checked and refrigerant replaced.
4. Electric Propulsion System Maintenance - As for the hydrogen fuel cell, batteries are hard to perform maintenance on. Nevertheless for the electric propulsion system all cabling and connections should be checked for damage and cleaned. The cooling system should also be checked and refrigerant replaced.
5. Landing Gear Maintenance - For the landing gear the tires should be checked for wear and damage and if necessary replaced. Shock struts should be lubricated and check for it air levels. Shock absorber chords should be checked for damage and in necessary replaced. All landing gear bearings and mechanical components should be checked for damage, cleaned and lubricated.
6. Electronics Maintenance - For the electronics maintenance the cables should be checked for damaged. Also it should be checked if all cabling and connections are safely secured.
7. Structures Maintenance - The structural maintenance includes checking the security of the static and dynamic parts. This includes checking if the rudder, elevators and stabilisers ares still securely attached. All these components should be cleaned and lubricated. The general body, wings and the attachments to each other should be checked for any major damage and if damage is present should be fixed. Doors and windows should be checked for visible damage and checked to be properly secured. All rivets and bolts should be checked and frequently replaced.
8. Body/Misc Maintenance - Added to the maintenance groups as described above, there is general (non-critical) body parts that should be checked from time to time. This includes seats, seat belts, air-conditioning and ventilation, internal and external lights and lenses of positions

Engine Replacement

The replacement of the engine is a process that occurs every time a (new) client wants to test a different engine. To minimise the turn around time, instrumentation sensors and electronics should be assembled with the experimental engine beforehand as much as possible. How much work can be done with the experimental off the aircraft is dependent on every particular case.

Once the previous engine has been removed and the engine specific telemetry, the new experimental engine can be attached to the engine mount as earlier described. Once the engine is all structurally secured, the engine should be electronically connected to the specific propulsion system, being either the electric battery or the hydrogen fuel cell. Finally the experimental engine specific instrumentation should be connected to the data acquisition system.

Once the whole experimental propulsion system is installed, it should be tested stationary. As before any flight, all instrumentation mechanical and dynamic parts should be tested again before departure.

12.2. Operations & logistics concept description

The operations in general are divided into two domain: the ground and the testbed operations. They are further divided into pre-flight, flight and post-flight phases.

12.2.1. Ground Operations

The ground operations can be mainly divided up into two phases; the pre-flight phase and the post-flight phase. In these phases the ground support performs work on the testbed while the testbed is inoperative. It is noted that not all pre-flight operations are ground operations, as some are performed by the testbed and are thus included in the testbed operations in Section 12.2.2. All ground operations are in the top half of the operations block diagram shown in Figure 12.2.

Pre-Flight Operations

The pre-flight ground operations are meant to prepare the aircraft for the flight and test execution. First of all, this means generating the test profile to be performed. The test profile will be determined by the educational or research institute using the SFPT for research purposes, or by any other client wanting to use the SFPT for their own research or experiments. The second step in the pre-flight operations is to determine what experimental engine is required from the test profile, and install it on the testbed. The next step is to mount the data acquisition system on board the testbed. This is required to perform in-flight measurements as is explained in Section 12.2.2. The actual measurements taken by the data acquisition system are to be determined by means of the test profile, and in accordance with the institute or client operating the testbed.

After the instrumentation has been mounted into the aircraft, the aircraft can then be refuelled or charged for its flight depending on the type of experimental propulsion system installed. In the case of a battery-electric engine combination, the aircraft should be charged well ahead of time using a charging station such as Pipistrel's SkyCharge[2] in order to ensure that the batteries do not degrade at too high a rate. In the case of a hydrogen-electric engine combination, the aircraft can simply be refuelled with the hydrogen before flight. After the experimental engine has been fuelled then the conventional engine can also be fuelled with regular avgas.

Post-Flight Operations

During the post-flight operations the aircraft undergoes maintenance and the test profile is concluded. Firstly, the data that was acquired while performing the flight and test profile is processed. This will involve transferring the flight data to an off-board storage solution before sending it to the organisation for which the test was conducted. Subsequently, the ground support begins the maintenance procedure of the aircraft. This includes regular checks of parts prone to failure, and occasional major checks of the entire aircraft. Also if necessary, repair of the experimental research engine may also be performed. Performing maintenance is extremely important to keep the SFPT flying safely and reliably. Finally, if all test profiles are executed as requested by the institute or client, the experimental engine can then be removed.

12.2.2. Testbed Operations

The testbed operations occur primarily in the pre-flight phase and the in-flight phase concerning the preparation of the aircraft flight and flight operations to conduct tests. All testbed operations can be seen in the bottom half of the operations block diagram shown in Figure 12.2.

[2] https://www.pipistrel-aircraft.com/aircraft/electric-flight/charging-infrastructure/ [Accessed June 2021]

Pre-Flight Operations
In the pre-flight stage the testbed operations are designed to be routine. First the fuel is loaded into the aircraft and the batteries are charged. Then, in correspondence with the risk mitigation strategy the experimental engine performs a ground test alongside the data acquisition system to ensure their functionality. Once the instrumentation and propulsion system are determined to be working, the testbed can begin its pre-flight check which includes the pilot's walk-around and nominal flight procedures before taxiing to the runway.

Flight Operations
In flight is where the testbed has the bulk of its operations. The flight operations begin after the pre-flight checklist has been completed. The Skymaster can then taxi to the runway before taking off, from there the aircraft climbs to the cruising altitude before performing the test profile as determined during the pre-flight stage. Here measurements can be performed and logged on-board as many times as required. Once the required tests have been completed or the aircraft must return to the airfield for example due to an experimental engine failure the aircraft will cruise to the airfield and then approach and land. This then leads to the post-flight operations conducted entirely by the ground support. During the flight phase, the testbed remains in constant contact with Air Traffic Control (ATC).

12.2.3. Logistics

As DEAC is based in Teuge, all the modification and maintenance stages of the aircraft take place in Teuge. Once the design has been finalised and completed it can be delivered to DEAC where the logistics of the project begin. The modification and maintenance of the aircraft is conducted by DEAC partners Aircraft Maintenance Netherlands (AMN) and Hangar One[3]. This modification stage comprises of the initial conversion of the Skymaster into a suitable testbed which is detailed further in Section 12.3, whereas the maintenance stages is conducted as shown in Figure 12.2 performing necessary repairs after flights as well as the installation and removal of the rear propulsion system

A key section of the logistics that is yet to be addressed is the acquisition of experimental engines, fuel and energy sources. The acquisition of the engines and energy sources is not discussed here since that is dependant on the manufacturer of the product. However, the acquisition of fuel can be considered. Regular avgas for the conventional engine is readily available to DEAC. However, hydrogen for hydrogen fuel cells would have to be sourced from nearby hydrogen production facilities in the Netherlands, one such example is Cleantech Regio partners GldH2[4]. Furthermore, charging the batteries is a relatively trivial process. As referenced in the ground pre-flight operations, a charging station will be used to charge the batteries. These are commercially available and can be used on any existing power infrastructure.

12.3. Project Design and Development Logic

The project design and development logic consists of the activities to be executed from the detailed design phase (post-DSE) onwards. The activities are divided into five phases; detailed design, testing & certification, modification implementation, operation and the end-of-life phases. Figure 12.3 gives an overview of the activity flow to be performed after the DSE.

At the end of the DSE project, the design will be partially iterated but due to the limited time frame of the exercise it will require further improvement. Further iteration is necessary for the design to compete with contemporary standards in industrial practice.

The Testing & Certification phase focuses on making sure the design works correctly and is certified. Testing the alternative propulsion systems extensively before implementation is important to reduce the probability of unnecessary engine failures whilst testing in flight. Moreover, tests should be conducted on the structural design to validate its required performance, as failure of the structure may have catastrophic implications.

The design is then frozen and a flight manual is produced as guidance for the test pilots. In order for the aircraft to be permitted to fly in Dutch airspace, it then has to be certified. The certification is a process that is highly time consuming. This consists of intensive testing of all systems.

[3] `https://deac-teuge.nl/over-ons/` [Accessed June 2021]
[4] `https://gldh2.nl/index.php` [Accessed June 2021]

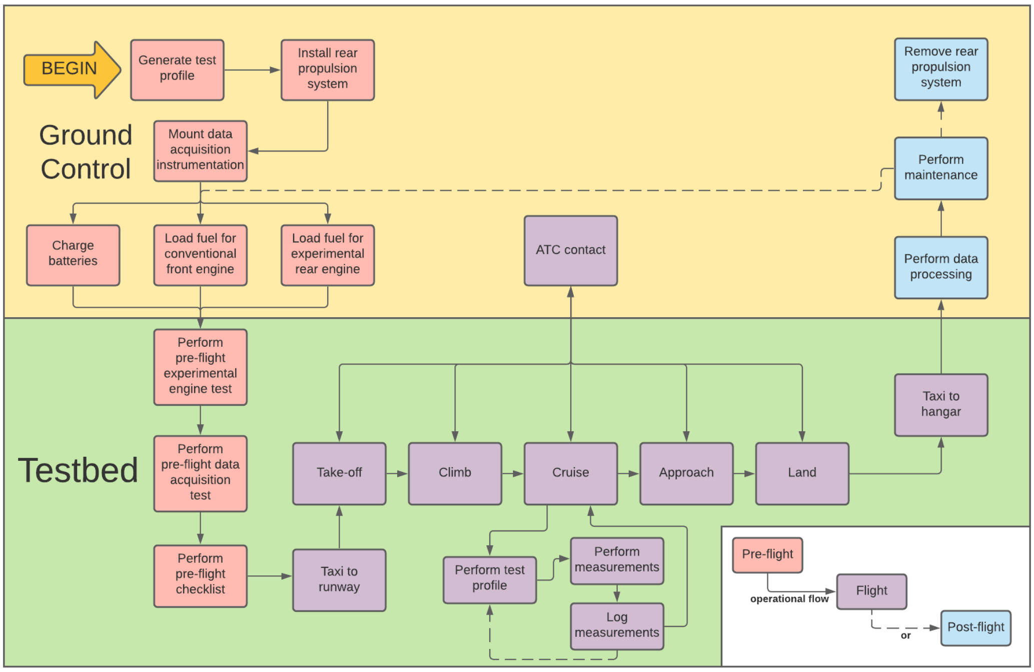

Figure 12.2: The operations block diagram of the testbed subdivided into the pre-flight, flight and post-flight stages.

The implementation of the modifications starts off by removing one of the existing engines. Structural changes are then made to the aircraft, enabling the attachment of alternative propulsion systems. The structural system is designed to be flexible in such a way that the propulsion systems are interchangeable and accessible. The new propulsion system is integrated in the aircraft together with the necessary instrumentation equipment for data collection.

The operational phase of the testbed will commence with training of test pilots for the particular aircraft modifications. Test flight are performed using the alternative propulsion system alongside the original one and data is collected for research purposes. The data can be used to do analyses on the propulsion systems. The aircraft will require constant maintenance throughout the operational phase.

The final phase is the end-of-life of the aircraft. This is most likely to occur if at some point the aircraft is either deemed unsafe to fly or there is no purpose for it anymore. The aircraft could then be disassembled where some parts can be reused and others disposed of.

Project Gantt Chart

A Project Gantt Chart is also included in Figure 12.4 with estimates of a time-frame for the post-DSE activities that will be conducted at DEAC Teuge. First, the design is iterated upon and finalised. This is estimated to take around 5 months from the completion of the detailed design. Next, the design will be frozen and the flight manual will up updated with relevant information on the modifications. The longest phase is predicted to be the certification process which will consist of intensive testing and analysis of result. The finalised design will then be implemented within the Cessna Skymaster. An exact schedule for this will be produced within a production plan at a later stage of the design process. Finally, the time for test pilot training is predicted to take around a month. The schedule is over-estimated to allow for pilot time and weather that is deemed unsafe to fly during the winter months in the Netherlands. The testbed will be completed by the beginning of April 2023.

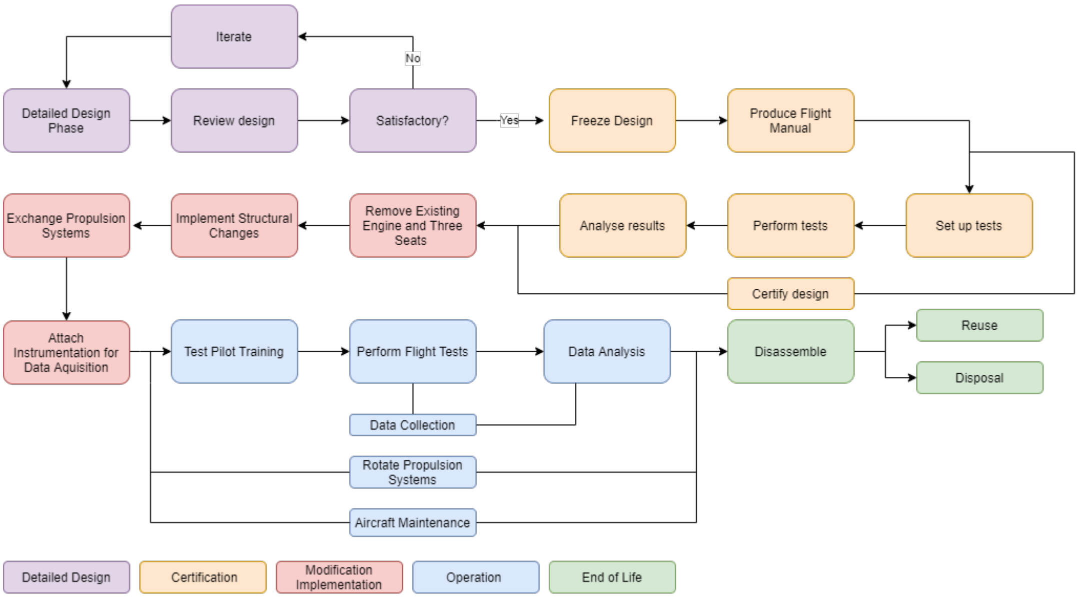

Figure 12.3: Project Design and Development

ID	Task Name	Start	Finish	Scheduled Duration
1	**Review Design**	Mon 12-7-21	Fri 10-12-21	110 days
2	Freeze Design	Mon 13-12-21	Mon 13-12-2	0 days
3	Produce Flight Manual	Mon 13-12-21	Thu 23-12-21	9 days
4	**Certification**	Mon 27-12-21	Mon 24-10-2	216 days
5	Set up Tests	Mon 27-12-21	Fri 25-3-22	65 days
6	Perform Tests	Mon 28-3-22	Fri 29-7-22	90 days
7	Analyse Results	Mon 1-8-22	Fri 28-10-22	65 days
8	**Modification Implementation**	Fri 28-10-22	Mon 13-2-23	77 days
9	Remove Existing Engines and Seats	Fri 28-10-22	Mon 7-11-22	7 days
10	Implement Structural Modifications	Mon 7-11-22	Fri 16-12-22	30 days
11	Switch Propulsion Systems	Fri 16-12-22	Thu 26-1-23	30 days
12	Attach Instrumentation for Data Acquisition	Fri 27-1-23	Thu 9-2-23	10 days
13	**Test Pilot Training**	Thu 9-2-23	Wed 29-3-23	35 days

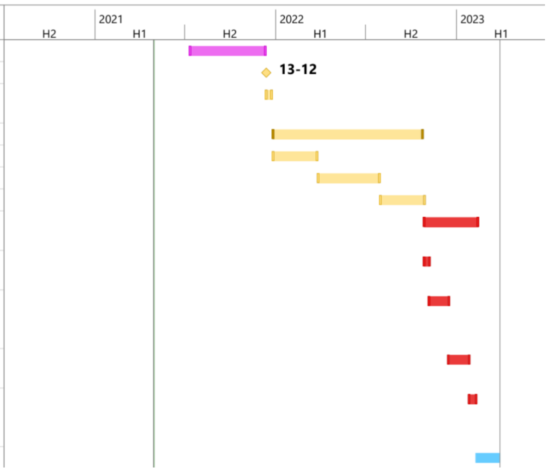

Figure 12.4: Post-DSE Gantt chart

Conclusion

The aim of this report was to design the necessary modification to the Cessna Skymaster so that it may be retrofitted with an experimental engine and data acquisition system for research into sustainable propulsion systems. To do this requirements were generated and orientated around the existing aircraft design, certification & safety, performance & propulsion, structural design, data acquisition, market analysis and risk. Below, the results of the design for these requirements are detailed.

Firstly, certification is considered and it is concluded that for the Skymaster to function as a testbed in the Netherlands, the aircraft must be re-certified by registering it in the Netherlands as an Annex-1 aircraft and use the Dutch National Aviation Authority to acquire a permit to fly.

For the technical design, to meet the requirements, the work focused on in the design of the testbed revolved around three key areas; propulsion, structures and data acquisition. The data acquisition systems are designed for both battery and hydrogen systems and weighs $11.4 kg$.

For the testbed, the two most promising designs for propulsion systems that are selected for this design are the Magni250 and the Emrax 348 due to the amount of information available and their technical readiness levels. To meet the requirements, cruise is assumed at $5000\ ft$, at $150\ mph$ with 2500 RPM propeller speed and using 75% of available front propeller power. For the battery system, it is chosen to use six PB345V124E-L Lithium-Ion battery packs, which lead to an endurance upwards of 1 hour and 3 minutes after take-off and climb to $5000\ ft$. This limits the maximum rated engine power that can be tested to $252\ kW$. For a hydrogen system, the endurance at $150\ mph$ with 2500 RPM propeller speed and using 75% of available front propeller power is exactly 1 hour after take-off and climb. The maximum rated engine power of the two selected PowerCellution P-Stack fuel cells is $220\ kW$.

To integrate the propulsion system into the aircraft, two main structural features are designed, an engine mount and a fuel mount. The engine mount consists of a permanent structure, mounted to the existing hard points in the firewall frame and sub-structures, specific to the engine being tested. The engine mount is made from steel 4130 and is a truss structure with an element diameter of $2.5\ cm$ and wall thickness $4.8\ mm$, it weighs $13.04\ kg$. The fuel mounting is analysed for a capacity of up to $450\ kg$ in the core section of the fuselage. For this, the maximum compression was found to $-218\ kPa$, occurring in the bottom of the fuselage. Tension peaked at $328\ kPa$ in the top part of the fuselage. For a fuel load of $450\ kg$ these loads did not increase since the maximum moment along the fuselage remained constant. The fuel will be mounted within a truss structure in this region with a second firewall, weighing $3.6\ kg$, being placed in front for safety. To carry the introduced loads, it is suggested to lower the manoeuvre loads in the flight profile, or to add a third keel beam in the bottom plate.

It is required that there is a minimum pilot weight of $70\ kg$, as well as $28\ kg$ of ballast being added in the tail ($x = 9m$). This may be increased in case of lighter pilot and passengers. The aerodynamics of the aircraft are analysed for the new cooling system - for the battery system there is a difference of -47 drag counts between the original and modified aircraft and for the hydrogen system a difference of $+13$ drag counts. This is an increase of 12% and is assumed to be negligible in the overall performance.

The final battery-powered system has a total mass of $1923\ kg$ (including three people) and draws $590\ W$ from the main power bus, for which $980\ W$ is available. The hydrogen-powered system has a total mass of $1593\ kg$ and draws $766\ W$ from the main power bus. Furthermore, the fixed costs required to implement all engines and propulsion systems are estimated at €$501,269$. The calculated take-off distance for the SFPT equals $447\ m$. This is sufficient for taking off at Teuge, which has a runway of $1,200\ m$, but for safety concerns it is recommended to perform preliminary flight tests at an airfield with a larger runway.

Furthermore, DEAC is recommended to begin development for a battery-powered system, a promising energy source for small-scale general aviation with readily available technology and infrastructure. However, once the infrastructure and effective cooling systems are developed for for hydrogen systems, this seems the most promising alternative due to its high specific energy. Currently the best option for this is cryogenic storage due to its low mass and volume, though cryo-compressed storage could allow even smaller volume. Also, an interesting option for a hydroge system is to lower the MTOW, as this could allow testing lower powered engines and still obtain a safe minimum rate of climb.

As for battery-powered systems, a limiting factor for the SFPT is the endurance. This can be increased by storing extra batteries in the wings, in place of the auxiliary fuel tanks. If the equivalent of two PB345V124E-L battery packs are added, this could increase endurance by approximately 24 minutes and allow $336\ kW$ of engine output power to be tested. Furthermore, DEAC is recommended to closely follow the scientific development of Lithium-Sulfur batteries, of which the specific energy is predicted to more than double in the coming years compared to Lithium-Ion batteries.

For the engine mount, it is recommended to perform a further analysis of crash loads, thermal loading of the engine mount and isolation of the engine mount, as amplitudes of vibrations are unknown. For the CATIA simulations used, it is also advised to use a finer mesh as the simulations are currently limited by computer power. Another possibility is to refine the mesh in regions of known higher stress.

References

[1] DSE Group 25. *Baseline Report Flying Testbed*. Apr. 2021.

[2] DSE Group 25. *Midterm Report Flying Testbed*. May 2021.

[3] DSE Group 25. *Project Plan Flying Testbed*. Apr. 2021.

[4] "A complete range of wire & cable solutions for aerospace applications". In: *Nexans* 9 (June 2013), pp. 30–150. URL: `https://datasheet.octopart.com/M81044-12-20-9-Nexans-datasheet-57011848.pdf`.

[5] Dr. Frank Anton. *Siemens eAircraft overview*. Sept. 2019.

[6] National Transportation Safety Board. *National Transportation Safety Board Aviation Accident Final Report Nr. ANC00FA081*.

[7] FUEL CELLS and HYDROGEN 2 JOINT UNDERTAKING. *Hydrogen-powered aviation A fact-based study of hydrogen technology, economics, and climate impact by 2050*. May 2020.

[8] The European Commission. *Commission Regulations (EU) No 748/2012*. May 2021.

[9] Cessna Aircraft Company. *Super Skymaster Owner's Manual*. 1971.

[10] M. Cooke. *Flight Dynamics Principles*. Butterworth-Heinemann, 2012.

[11] P. V. Law D. D. Whitney. "Evaporative Cooling – The Racer's Edge". In: *The Journal of the Rolls-Royce Heritage Trust* (2016).

[12] Or Dantsker and Renato Mancuso. "Flight Data Acquisition Platform Development, Integration, and Operation on Small- to Medium-Sized Unmanned Aircraft". In: Jan. 2019. DOI: `10.2514/6.2019-1262`.

[13] ATP David F. Rogers PhD. "Propeller Efficiency Rule of Thumb". In: *American Bonanza Society* (2010). Copyright©2010 David F. Roger. All rights reserved.

[14] P.L. Dhar. *Thermal System Design And Simulation*. Elsevier, 2017.

[15] "DLR's HY4 hydrogen aircraft cleared to fly". In: *Fuel Cells Bulletin* 2021.1 (2021), p. 6. ISSN: 1464-2859. DOI: `https://doi.org/10.1016/S1464-2859(21)00016-X`. URL: `https://www.sciencedirect.com/science/article/pii/S146428592100016X`.

[16] "DLRs HY4 hydrogen aircraft cleared to fly". In: *Fuel Cells Bulletin* 2021.1 (2021), p. 6. DOI: `10.1016/s1464-2859(21)00016-x`.

[17] Mark Drela. "Aerodynamics of Heat Exchangers for High-Altitude Aircraft". In: *Journal of Aircraft* 11 (Apr. 1996).

[18] W. van der Wal E. Mooij Z. Papp. *AE3212-II Simulation Verification and Validation Lecture Notes*. Feb. 2021.

[19] W. van der Wal E. Mooij Z. Papp. *Type-Certificate Data Sheet No. EASA.A.573*. Jan. 2021.

[20] EASA. *Easy Access Rules for Normal, Utility, Aerobatic and Commuter Category Aeroplanes (CS-23) (Initial issue)*. June 2018.

[21] Plastics Europe. *Environmental benefits of Fibre Reinforced Plastics (FRP)*. URL: `https://www.plasticseurope.org/download_file/force/1594/181`.

[22] S. Gudmundsson. *General aviation aircraft design : applied methods and procedures*. Butterworth-Heinemann., 2014.

[23] R. Hamann and M. van Tooren. *Systems Engineering and Technical Management Techniques*. TU Delft, 2006.

[24] HECARRUS. *State-of-the-art technologies on research and developments underway in the field of alternative propulsion architectures*. Mar. 2020.

[25] S. F. Hoerner. *Fluid-Dynamic Drag*. Hoerner Fluid Dynamics, 1965.

[26] B. von den Hoff. *Noise assessment of the Cessna Skymaster*. TU Delft, 2021.

[27] D. Scheldt J. Unruh. *Engine Induced Structural-Borne Noise in General Aviation Aircraft*. 1979.

[28] Dohoy Jung and Dennis N. Assanis. “Numerical Modeling of Cross Flow Compact Heat Exchanger with Louvered Fins using Thermal Resistance Concept”. In: *SAE Technical Paper Series* 11 (Jan. 2006).

[29] M. Keyser et al. “Thermal Evaluation and Performance of High-Power Lithium-Ion Cells”. In: *16th Electric Vehicle Conference Beijing, China* (Oct. 1999). URL: https://www.nrel.gov/docs/fy99osti/26616.pdf.

[30] Simone Pica Luca Piancastelli Leonardo Frizziero and Giampiero Donnici. “High Altitude Operations With Piston Engines Powerplant Design Optimization Part IV: Radiators Optimum Design”. In: *ARPN Journal of Engineering and Applied Sciences* 11 (May 2016).

[31] *Magni 250 Specification*. May 2021.

[32] Anna Maiorova, Aleksandr Vasil’ev, and Oganes Chelebyan. “Biofuels in Aircraft Engines”. In: *Biofuels*. Ed. by Krzysztof Biernat. Rijeka: IntechOpen, 2015. Chap. 16. DOI: 10.5772/59871. URL: https://doi.org/10.5772/59871.

[33] *Manual for EMRAX Motors / Generators Version 5.4*. Mar. 2021. URL: https://emrax.com/wp-content/uploads/2020/03/manual_for_emrax_motors_version_5.4.pdf.

[34] T.H.G. Megson. *Materials: engineering, science, processing and designs*. 6th ed. Oxford, United Kingdom: Butterworth-Heinemann, 2017.

[35] F.W. Meredith. “Note on the cooling of aircraft engines with special reference to radiators enclosed in ducts.” In: *British Aeronautical Research Committee* (1936).

[36] S. J. Miley. “Review of Liquid-Cooled Aircraft Engine Installation Aerodynamics”. In: *Journal of Aircraft* (1988).

[37] J.-K Mueller et al. “Design Considerations for the Electrical Power Supply of Future Civil Aircraft with Active High-Lift Systems”. In: *Energies* 11 (Jan. 2018), p. 179. DOI: 10.3390/en11010179.

[38] Rebecca Mumford. *The Circular Economy of Everyday Life*. 2018.

[39] Christopher Hendricks Nicholas Williard Wei He and Michael Pecht. “Lessons learned from the 787 Dreamliner issue on Lithium-Ion battery reliability”. In: *Energies* (2013).

[40] International Civil Aviation Organisation. *Convention on International Civil Aviation*. Dec. 1994.

[41] *Part AO.Om Part X: Flight Test Operations Manual*. Aug. 2016.

[42] M. B. Taylor. “Pusher Propeller Efficiency and Problems”. In: *Sport Aviation* ().

[43] J. Katz V. C. Corsiglia. *Full-Scale Wind Tunnel Study of Nacelle Shape on Cooling Drag*. Aug. 1979.

[44] G.L.M. Vonhoff. “Conceptual Design of Hydrogen Fuel Cell Aircraft: Flying on hydrogen for a more sustainable future”. MA thesis. Delft University of Technology, 2021.

[45] A. L. London W. M. Kays. *Compact Heat Exchangers*. Third Edition. Scientific International Pvt. Ltd., 2018.

[46] *Wire Gauge and Current Limits Including Skin Depth and Strength*. Apr. 2021. URL: https://www.powerstream.com/Wire_Size.htm.